OFFICIAL JOURNAL OF THE SCIENTIFIC SOCIETY OF ANATOMISTS, HISTOLOGISTS, EMBRYOLOGISTS AND TOPOGRAPHIC ANATOMISTS OF UKRAINE

DOI: 10.31393
ISSN 1818-1295
eISSN 2616-6194

ВІСНИК МОРФОЛОГІЇ
REPORTS OF MORPHOLOGY

VOL. 31, №4, 2025

Scientific peer-reviewed journal in the fields of normal and pathological anatomy, histology, cytology and embryology, topographical anatomy and operative surgery, biomedical anthropology, ecology, molecular biology, biology of development

Published since 1993
Periodicity: 4 times a year

Vinnytsya • 2025

ВІСНИК МОРФОЛОГІЇ - REPORTS OF MORPHOLOGY

Founded by the “Scientific Society of Anatomists, Histologists, Embryologists, and Topographic Anatomists of Ukraine” and National Pyrogov Memorial Medical University, Vinnytsya in 1993

Certificate of state registration КВ №9310 from 02.11.2004

Professional scientific publication of Ukraine in the field of medical sciences in specialties 221, 222, 228, 229
According to the list of professional scientific publications of Ukraine, approved by the order of the Ministry of Education and Science of Ukraine No. 1188 of 24.09.2020

Professional scientific publication of Ukraine in the field of biological sciences in specialty 091
According to the list of professional scientific publications of Ukraine, approved by the order of the Ministry of Education and Science of Ukraine No. 1471 of 26.11.2020

Approved by the Academic Council of National Pyrogov Memorial Medical University, Vinnytsya, protocol №5 from 27.11.2025.

Indexation: Scopus, CrossRef, Index Copernicus, Google Schoolar Metrics, National Library of Ukraine Vernadsky

Address editors and publisher:
Pyrogov Str. 56,
Vinnytsya, Ukraine - 21018
Tel.: +38 (0432) 553959
E-mail: nila@vnmu.edu.ua

Computer page-proofs - Slobodianiuk L.M.
Translator - Gunas V.I.
Technical support - Levenchuk S.S.
Scientific editing - editorship

The site of the magazine - https://morphology-journal.com

CONTENT

Lopatkina O. P., Zalevskyi L. L., Tykholaz V. O., Galunko G. M., Danylevych V. P., Kravets R. A.
Morphology of hindbrain neuronal complexes in human fetuses of 17-18 weeks of intrauterine development **5**

Bilash S. M., Oliinichenko Ya. O., Pronina O. M., Shostya A. M., Koptev M. M., Pirog-Zakaznikova A. V., Donchenko S. V., Oleksiienko V. V., Mamai O. V., Oliinichenko M. O., Koval Yu. P., Kopytko N. S.
Immunohistochemical characteristics of the rat ileum under impaired antioxidant defence induced by the administration of a complex of chemical food additives **12**

Shakatira M. A. M., Dmytrenko S. V., Prokopenko S. V., Golubovsky I. A., Gonchar O. O., Zverkhovska V. F., Kyselova T. M.
Features of skinfold thickness in Ukrainian men with alopecia areata **22**

Chadiuk V. O., Kotsiubynska Yu. Z., Kolev Ya. G., Fentsyk V. L., Shutak O. V., Yurak M. Z., Solodzhuk Yu. I., Kozan N. M.
Ridge and delta counts of plantar dermatoglyphics in suicide victims: sex-related specificities **29**

Pshychenko V. V., Cherno V. S., Korolyova O. V., Naidich O. V., Iovenko A. V., Brodovskyi V. A.
Topographical-anatomic features of the pineal gland in laboratory rats of the Wistar line **36**

Bezsmertnyi Y. O., Bondarenko D. V., Shevchuk V. I., Branitsky O. Y.
The role of mechanical stress and local vascular thrombosis in the formation of stress fracture of bone stump (experimental research) **42**

Islamov Sh. E., Yakubov M. Z., Alikulov A. I., Zhuraev K. D., Makhmatmuradova N. N., Kudratov R.
Morphological and immunohistochemical characteristics of the thymus of newborns in the early neonatal period **51**

Spodaruk A. L., Shinkaruk-Dykovytska M. M., Valchuk O. G., Pozur T. P., Shevchenko V. M., Tykholaz S.I., Chernysh A. V.
Regression models of parameters required for constructing an appropriate dental arch form depending on the characteristics of teleroentgenometric indices by the Schwarz method and computed tomographic tooth dimensions in Ukrainian young men and women with normal occlusion **59**

Nebesna Z. M., Kulbitska V. V., Ohinska N. V., Dovbush A. V., Lytvynyuk S. O., Rymar A. A.
Peculiarities of histological and immunohistochemical changes in the respiratory portion of the white rats' lungs in experimental colon adenocarcinoma *in situ* **69**

Matkivska R. M., Samborska I. A., Mostiuk O. M.
Features of CD20 expression in the kidney tissue of experimental rats three hours after administration of Leiurus macroctenus scorpion venom **76**

DOI: 10.31393/morphology-journal-2025-31(4)-01 Reports of Morphology, Vol. 31, №4, Pages 5-11

ISSN 1818-1295 eISSN 2616-6194

REPORTS OF MORPHOLOGY

Official Journal of the Scientific Society of Anatomists, Histologists, Embryologists and Topographic Anatomists of Ukraine

journal homepage: https://morphology-journal.com

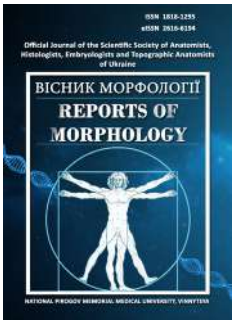

Morphology of hindbrain neuronal complexes in human fetuses of 17-18 weeks of intrauterine development

Lopatkina O. P.[1], Zalevskyi L. L.[1], Tykholaz V. O.[2], Galunko G. M.[1], Danylevych V. P.[1], Kravets R. A.[1]

[1] National Pirogov Memorial Medical University, Vinnytsya, Ukraine

[2] Shupyk National Healthcare University of Ukraine, Kyiv, Ukraine

ARTICLE INFO

Received: 19 November 2024

Accepted: 11 August 2025

UDC: 612.82:57.017.642

CORRESPONDING AUTHOR

e-mail: lopatkinaksyusha@gmail.com

Lopatkina O. P.

CONFLICT OF INTEREST

The authors have no conflicts of interest to declare.

FUNDING

Not applicable.

DATA SHARING

Data are available upon reasonable request to corresponding author.

Congenital defects of the central nervous system (CNS) are one of the most common causes of death and disability in newborns. Therefore, it is extremely important to assess the development of the fetal CNS in the intrauterine period in time to identify any changes in its development and give appropriate advice to parents on pregnancy support, offer options for fetal therapy and type of delivery, as well as postpartum treatment and prognosis. The aim of our research was to determine the morphological features of the neural complexes of the human fetal hindbrain at 17-18 weeks of fetal development, the size and area of the cranial nerve nuclei in the region of the pons and the cerebellar nuclei. In a research study we used biological material obtained from the Vinnytsia Maternity Hospital after a termination of pregnancy in a healthy women for medical reasons, due to fetal chromosomal abnormalities not related to CNS developmental defects. The material for anatomical and histological examination were human fetuses with a gestation period of 17-18 weeks. The fetus`s weighed 250.8±14.5 g, and the parieto-coccygeal length were 163.3±8.4 mm. The researched tissue samples of hindbrain were fixed in a 10 % solution of neutral formalin, and then sections of 8-9 μm thick celluloid blocks were prepared for further histological examination. The preparations were stained with hematoxylin-eosin, toluidine blue according to the Nissl modification. For the statistical analysis of digital data Microsoft Excel 2016 and Statistica 6.1 were used. The normality of the distribution was assessed using the Shapiro-Wilk test, histograms were constructed for data visualization, and the standard deviation and variance of the samples were calculated. Histograms were constructed to visualize the data, the standard deviation and sample variance were calculated. The microscopic examination of the cerebellum revealed the outer granular, molecular, inner granular, intermediate, and ventricular layers. The presence of cerebellar nuclei, which were located in the intermediate layer, was also established. On the cerebellar section, the dentate nucleus was visualized as a thin curved line with its convex side directed laterally and dorsally. The abducens nucleus is located ventrally to the dorsal surface of the pons, laterally to the medial longitudinal fascicle. The facial motor nucleus is located medially to the abducens nucleus and has an elongated shape with indistinct borders. The trigeminal motor nucleus is laterally to the facial nucleus, has indistinct borders, a rounded shape, and consists of neurons at different maturation stages. In the lateral part of the pons is the vestibular nucleus, which has an irregular oval shape; the borders of the nucleus are indistinct. Also, below the vestibular nucleus, laterally, there is a cochlear nucleus, without clear contours, oval elongated shape. Thus, in the posterior part of the brain at 17-18 weeks of fetal development, the nuclei of the abducens, trigeminal, facial, and vestibulocochlear nerves located in the pons. Dentate, globose, emboliform and fastigial nuclei also were found in the cerebellum.

Keywords: *central nervous system, fetal development, hindbrain, pons, cerebellum, neurons, nuclei.*

Introduction

CNS congenital defects are one of the most common causes of mortality and disability in newborns. Although

the frequency of detection of such defects at birth is about 1.4-1.6 per 1000 live births, among stillborns this figure is higher – 3-6% [18]. The formation of the central nervous system occurs between the 3rd and 20th week of fetal development. During this period any disorders in the development of the central nervous system can lead to birth defects [21, 23, 26]. Therefore, it is extremely important to assess the development of the fetal CNS in the intrauterine period to identify any changes in its development and give appropriate advice to parents due to pregnancy management, offer options for fetal therapy and type of delivery, as well as postpartum treatment and prognosis [2, 25, 29]. The assessment and diagnosis of CNS defects in the intrauterine period can be performed using ultrasound at any stage of pregnancy, which allows visualizing the brain and spinal cord, assessing their size, shape, and structure [10, 13, 17, 22]. Ultrasound examination makes it possible to detect most anomalies of the central nervous system in the early stages of pregnancy, starting from the first trimester and throughout the second [28]. Ultrasound can be used to identify the following defects: anencephaly – the absence of a significant part of the brain and skull, spinal hernia – a spinal defect in which part of the spinal cord or its meninx extends beyond the spinal canal, hydrocephalus – excessive accumulation of cerebrospinal fluid in the cerebral cavities, microcephaly – abnormally small size of the brain, spinal cord disruption – incomplete closure of the vertebral arches, impaired development of the brain ventricles – increase or decrease in sizes of the brain ventricles [11, 15, 27].

The hindbrain controls the most important physiological processes, such as motor activity, breathing, sleeping, and blood circulation. It also receives information and transmits multiple sensory data, including auditory, pre-cerebellar, and vestibular [8]. The development of the hindbrain is closely related to the development of the bone structures of the posterior cranial fossa. The posterior cranial fossa is characterized by a complicated anatomical structure that is formed as a result of the interaction of various tissues and structures [14]. Disruption of these complex developmental processes can cause serious defects, such as Chiari syndrome and others [20, 24]. Detailed studies of the development of the hindbrain in scientific publications are quite limited.

So *the aim* of our study was determination of morphological features of neural complexes of the human fetal hindbrain at 17-18 weeks of fetal development, size and area of cranial nerve nuclei in the pons region and cerebellar nuclei.

Materials and methods

The study was conducted using biological material obtained from the Vinnytsia Maternity Hospital after the termination of pregnancy in a healthy woman of 28 years old for medical reasons, due to fetal chromosomal abnormalities not related to CNS malformations. The material for the histological examination was a human fetus with a gestation period of 17-18 weeks. The fetus weighed 250.8±14.5 g, the parieto-coccygeal length was 163.3±8.4 mm.

The weight of the fetus and the hindbrain (pons and cerebellum) was determined using electronic scales. According to the method of Avtandilov G. G., the size of the head and the size of the hindbrain were determined using a caliper SHC-125 [1]. Tissue samples were fixed in a 10% solution of neutral formalin, and then sections of celluloid blocks 8-9 μm thick were prepared for further histological examination. The microspecimens were stained with hematoxylin-eosin, toluidine blue according to the Nissl modification. Using a MBS-9 and Euromex iScope series microscope and a camera Euromex Microscope B. V. DC. 1359 F 100, with magnifications x4, x40, x100, x400, microscopic examination was performed. Computer histometry (Toup View) was used for morphometric study.

For the statistical analysis of digital data on a personal computer, the programs Microsoft Excel 2016 and Statistica 6.1 were used. Using them the normality of the distribution of the obtained statistical data was assessed with the Shapiro-Wilk test. Histograms were constructed for data visualization, and the standard deviation and variance of the samples were also calculated.

The work was performed as part of the SRW of the Department of Human Anatomy, “Establishment of patterns of organ and histogenesis and topography of internal organs of the thoracic and abdominal cavities, as well as structures of the central nervous system of human fetuses (macroscopic, histological, immunohistochemical and ultrasound examination)”.

The study was approved at the meeting of the Biomedical Ethics Committee of the National Pirogov Memorial Medical University, Vinnytsya (Protocol No. 3 dated March 18, 2025), in compliance with the basic provisions of GCP (1996), Convention on the Protection of Human Rights and Dignity in Connection with the Application of Advances in Biology and Medicine (1996). The research materials do not contradict the basic bioethical norms of the Declaration of Helsinki on the ethical principles of conducting scientific and medical research involving human subjects, adopted by the 59th General Assembly of the World Medical Association in 2008.

Results

During examination human fetus at 17-18 weeks of gestation period, the following anthropometric parameters of the head were determined: circumference – 145.6±6.2 mm, height – 58.20±2.80 mm, transverse size – 48.60±2.51 mm, longitudinal size – 56.54±3.82 mm, longitudinal and transverse size of the anterior fontanelle – 23.00±1.10 mm and 14.10±0.81 mm, respectively, longitudinal and transverse size of the posterior fontanelle – 10.53±0.50 mm and 6.032±0.298 mm, respectively. The weight of the hindbrain was 7.914±0.401 g (Fig. 1).

At 17-18 weeks of fetal development, the human cerebellum resembles the medulla oblongata, but is distinguished by its greater thickness and the presence of massive protrusions connecting it to the cerebellum, and a distinct groove separating the cerebellum from the medulla oblongata on the anterior surface, and the stria medullaris of the fourth ventricle are defined on the posterior surface.

Fig. 1. Layer-by-layer dissection of a human fetus at 17-18 weeks of fetal development with subsequent detachment of the hindbrain. Photo by Canon EOS 1000D.

The basilar sulcus is formed on the anterior surface, and the posterior surface is involved in the formation of the upper part of the rhomboid fossa. Transverse grooves were observed on the surface of the cerebellar hemispheres and cerebellar vermis, which passed through the hemispheres and vermis, forming cerebellar folliums. Also, a deep horizontal groove was observed, which began at the point of entry into the cerebellum of the middle cerebellar peduncle connecting the pons to the cerebellum.

Macrometric measurements of the hindbrain were as follows: pons height – 7.421±0.413 mm, pons thickness – 7.242±0.403 mm, pons width – 9.100±0.502 mm, pons weight – 6.509±0.302 g, transverse cerebellar size – 18.33±0.80 mm, longitudinal cerebellar size – 11.22±0.51 mm, cerebellar height – 7.103±0.388 mm, cerebellar weight – 1.442±0.104 g.

The microscopic examination identified the following layers: outer granular, molecular, inner granular, intermediate and ventricular layers. The presence of cerebellar nuclei, which were located in the intermediate layer, was also established. In the cerebellar section, the dentate nucleus was visualized as a thin curved line with its convex side directed laterally and dorsally. In the medial direction, the configuration of the dentate nucleus is not closed; this area is called the gate of the dentate nucleus. During the morphometric study, we obtained the areas of the cerebellar nuclei: dentate – 0.240±0.100 mm^2, emboliform – 0.050±0.020 mm^2, globose – 0.033±0.010 mm^2, and fastigial – 7852±412 μm^2.

The dentate, emboliform, globose and fastigial cerebellar nuclei are represented by undifferentiated neural cells that are round and slightly oval in shape, with an area of 19.16±0.90 μm^2 for the round cells and 34.27±1.80 μm^2 for the oval cells, respectively, with a cell diameter of 5.011±0.248 μm and 5.10±10.03 μm for the oval cells (Fig. 2).

The nuclei of the abducens, trigeminal, facial and vestibulocochlear nerves are recognized in the pons region in human fetuses of 17-18 weeks of gestation period. The abducens nucleus is located ventrally to the dorsal surface of the pons, laterally to the medial longitudinal fascicle. The nucleus boundaries are indistinct, the nucleus area is 0.191±0.010 mm^2, the nucleus neurons are rounded (Fig. 3A), the neuronal area is 117.2±5.8 μm^2, the cells nuclei have almost the same diameter and area (cell nucleus area is 51.53±2.50 μm^2, diameter is 6.339±0.302 μm). The facial motor nucleus is located in the thickness of the pons, medially to the abducens nucleus; it has an elongated shape with indistinct borders (Fig. 4A), the nucleus area is 0.110±0.050 mm^2, the neuronal area is 382.5±18.6 μm^2. The nucleus cells are dome-shaped, the same size, with a nucleus area of 63.74±3.10 μm^2 and a cell diameter – 10.13±0.51 μm. The trigeminal motor nucleus is laterally to the nucleus of the facial nerve, has indistinct contours, a rounded shape and consists of neurons at different maturation stages (Fig. 3B). The nucleus area is 0.128±0.061 mm^2, neuronal area is 316.4±15.8 μm^2, cell nucleus area is 53.17±2.60 μm^2, and cell diameter is 8.069±0.404 μm.

In the lateral part of the pons, there is an irregularly oval nucleus with irregular oval shape, nucleus borders are indistinct (Fig. 4B), the nucleus area is 0.179±0.010 mm^2. One group of neurons in the vestibular nucleus is at the stage of differentiation into mature neurons, the other – has undifferentiated cells, neurons with different (from large to small) nucleus areas (Fig. 5A). The average neuronal area is 209.3±10.4 μm^2, the nucleus area – 62.15±3.50 μm^2, the cell diameter – 8.300±0.400 μm. Also, below the vestibular nucleus in the lateral region of the pons sample, there is a cochlear nucleus, which has no clear contours and with oval elongated shape (Fig. 4B), nucleus area is 0.118±0.031 mm^2. The cells of the cochlear nerve nucleus are represented by rounded neuroblasts at the stage of differentiation into mature neurons (Fig. 5B), neuronal area is 152.4±7.8 μm^2, cell nucleus area – 45.18±2.20 μm^2, cell diameter – 7.452±0.412 μm.

Discussion

Thus, in human fetuses at 17-18 weeks of gestation, the hindbrain already contains the formed cranial nerve nuclei of the pons (abducens, trigeminal, facial, vestibulocochlear) and the four main cerebellar deep nuclei (globose, emboliform, dentate, fastigial), which allowed for their quantitative

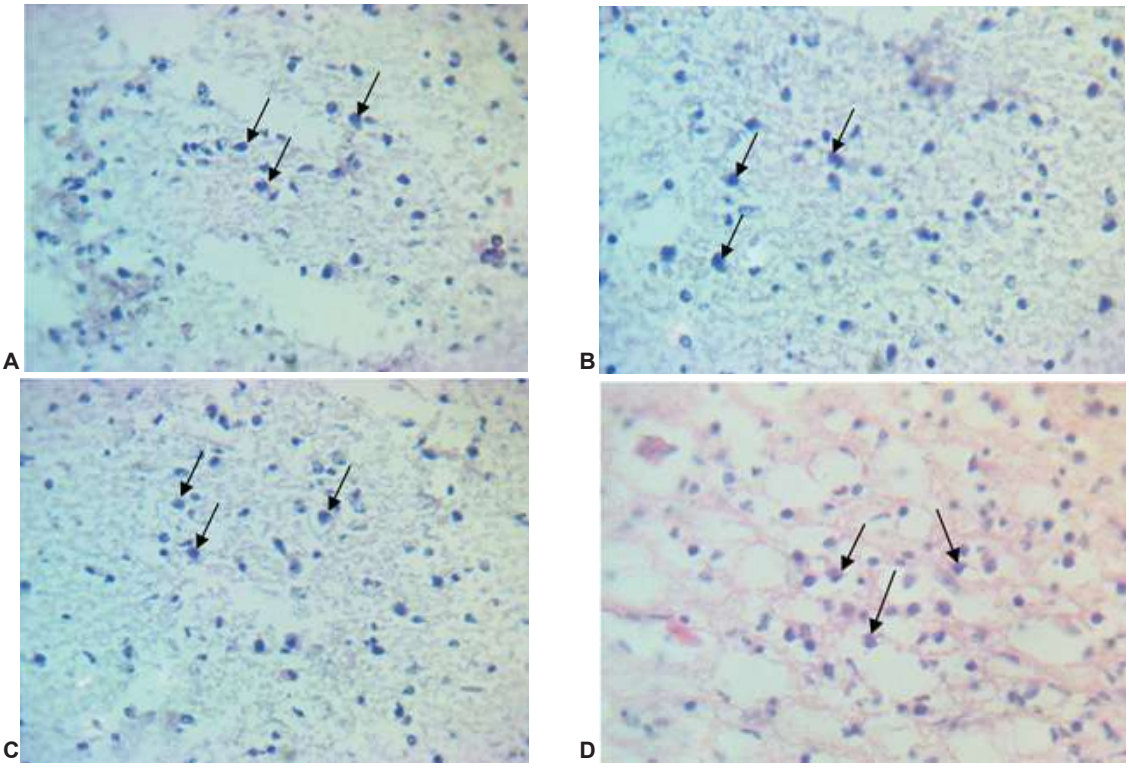

Fig. 2. Horizontal section of the cerebellum of a human fetus at 17-18 weeks of gestation period. A – undifferentiated neural cells of the globose nucleus (matched). Hematoxylin-eosin, ×400. B – undifferentiated neural cells of the fastigial nucleus (matched). Hematoxylin-eosin, ×400. C – undifferentiated neural cells of the dentate nucleus (matched). Hematoxylin-eosin, ×400. D – undifferentiated neural cells of the emboliform nucleus (matched). Hematoxylin-eosin, ×400.

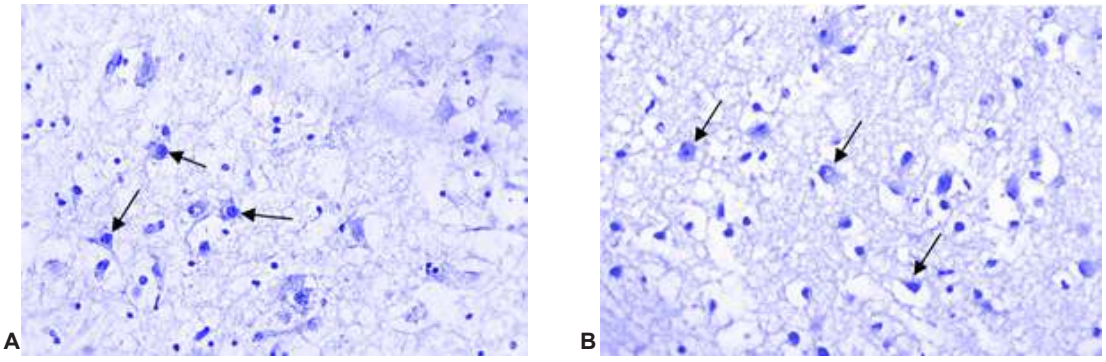

Fig. 3. Horizontal section of the pons of the human fetus at 17-18 weeks of age. A – neurons of the abducens nerve (matched). Hematoxylin-eosin, ×400. B – neurons of the trigeminal nerve (matched). Hematoxylin-eosin, ×400.

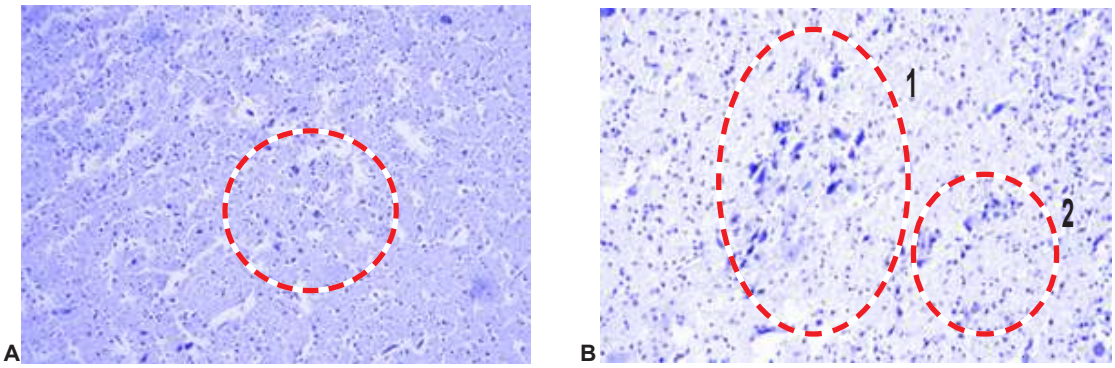

Fig. 4. Horizontal section of the pons of the human fetus at 17-18 weeks of gestation period. A – The facial motor nucleus (matched red colour). Hematoxylin-eosin, ×40. B – vestibulocochlear nerves nuclei (1 – vestibular, 2 – cochlear). Hematoxylin-eosin, ×400.

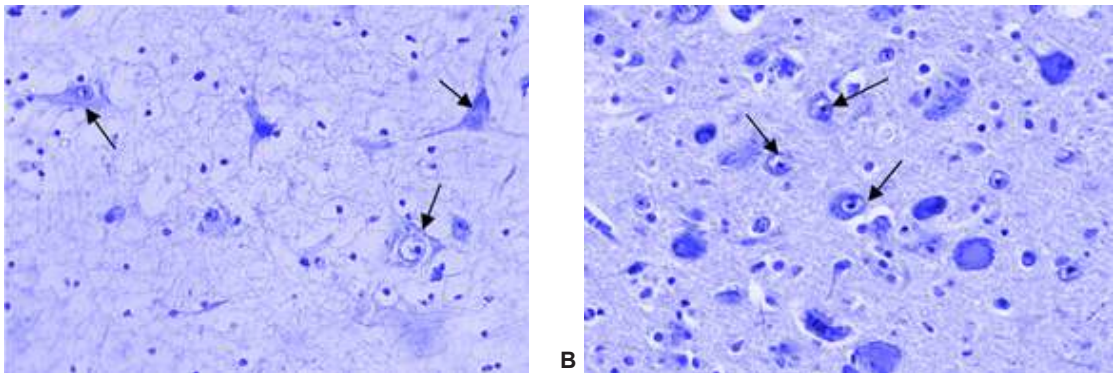

Fig. 5. Horizontal section of the human fetal pons at 17-18 weeks of gestation period. A – vestibular nuclei neurons (neurons with larger and smaller area, matched). Hematoxylin-eosin, ×400. B – cochlear nuclei neurons (matched). Hematoxylin-eosin, ×400.

assessment. The motor nuclei of the hindbrain occupy a larger total area due to the high density and number of interneurons and efferent neurons required for precise motor control. Sensory neurons have a larger area compared to motor neurons, likely reflecting their requirement for a more complex metabolism to support the processing of large volumes of sensory information.

An insignificant amount of modern scientific works are devoted to the research of the human brain at the stage of intrauterine development, especially the posterior brain region, determines the need for comprehensive and systematic studying of its histological structure and topography [5]. Our study tries to fill this gap in scientific knowledge [6, 9].

L. S. Chitty et al. [4] and T. N. Leung et al. [12] studied the fetuses' biometrics at different gestational periods. The circumference and biparietal size of the head in fetuses at 17-18 weeks of gestation period according to the study of Chitty L. S. et al. and Leung T. N. et al. coincides with the data of our study.

Three-dimensional transvaginal neurosonography of the middle brain and hindbrain of the human fetus at 14-19 weeks of fetal development was performed by Birnbaum R. et al. [3] who in their study indicated that the anterior-posterior diameter of the pons was 0.889 mm (from 0.747 mm to 0.956 mm), according to our study, the thickness of the pons at 17-18 weeks of gestation period was 7.242 mm. Differences between the results of our study and the study by Birnbaum R. et al. [3] may be explained by different methods of research: Birnbaum R. et al. conducted the study using transvaginal ultrasound diagnostics of mothers, while we used data obtained during the study of the fetal cadaver.

The development of cranial nerves in human fetuses was studied by Müller F. and O'rahilly R. [16]. In their research, they indicated that cranial nerves can be recognized at the 16th stage of intrauterine, during our study in the pons area of a human fetus at 17-18 weeks of gestation period, we identified the nuclei of the trigeminal, abducens, facial and vestibulocochlear nerves.

N. Pruthi and co-authors [19] point out that there are four pairs of nuclei in the cerebellum: dentate, emboliform, globose and fastigial nuclei. The deep nuclei of the cerebellum play a significant role in cerebellar function, as they integrate excitatory and inhibitory signals.

Fei Liu and co-authors [7] in a study of the intrauterine development of the human cerebellum between 14 and 22 weeks of gestation period using MRI, found that the dentate nucleus could normally be detected at 16 week. The dentate nucleus was outlined as a semi-circular area with low signal intensity relatively to the surrounding cerebellum. The dentate nucleus became clearly visible and had the pocket-shape after 18 weeks of fetal development. Other deep nuclei of cerebellum were not visible at time of this scientific research.

K. Yamaguchi and co-authors [30] investigated the morphometric development of human cerebellar nuclei in 9 fetuses 16-40 weeks of development. During the research of area and neuronal density nuclei three stages were observed: the primary or undifferentiated stage, which was observed from 16-20 weeks of fetal development, the secondary stage with variability at 21-32 weeks of development, and the tertiary stage with a monotonous increase in nuclei volume or a gradual decrease in neuronal density after 35 weeks of development. We found that in the period of 17-18 weeks of development the cerebellar nuclei form undifferentiated neural cells, which coincides with research of Yamaguchi K. and co-authors.

Conclusions

1. In hindbrain at 17-18 weeks of fetal development we founded the following nuclei: the pons Varolii cranial nerve nuclei – nuclei of the trigeminal, abducens, facial and vestibulocochlear nerves; the cerebellar nuclei – the dentate, emboliform, globose and fastigial nuclei.

2. Among the nuclei of the hindbrain, the dentate nucleus of the cerebellum (with an area of 0.240±0.100 mm^2) and the abducens nucleus in the pons (with an area of 0.191±0.010 mm^2) occupy the largest area. The fastigial cerebellar nucleus (with an area of 7852±412 μm^2) and the facial motor nucleus in the pons (with an area of 0.118±0.031 mm^2) occupy the smallest area.

3. The area of the motor cranial nerve nuclei in the pons is larger than the area of the sensory nuclei, but the area of the sensory neurons is larger than the area of the motor neurons.

References

[1] Avtandilov, G. G. (2002). *Основы количественной патологической анатомии* [*Basics of Quantitative Pathological Anatomy*]. M.: Медицина = M.: Medicine.

[2] Aydın, E., Tanacan, A., Büyükeren, M., Uçkan, H., Yurdakök, M., & Beksaç, M. S. (2019). Congenital central nervous system anomalies: Ten-year single center experience on a challenging issue in perinatal medicine. *Journal of the Turkish German Gynecological Association*, *20*(3), 170. doi: 10.4274/jtgga.galenos.2018.2018.0079

[3] Birnbaum, R., Barzilay, R., Brusilov, M., Acharya, P., Malinger, G., & Krajden Haratz, K. (2021). Early second-trimester three-dimensional transvaginal neurosonography of fetal midbrain and hindbrain: normative data and technical aspects. *Ultrasound in Obstetrics & Gynecology*, *59*(3), 317-324. doi: 10.1002/uog.23691

[4] Chitty, L. S., Altman, D. G., Henderson, A., & Campbell, S. (1994). Charts of fetal size: 2. Head measurements. *BJOG: An International Journal of Obstetrics & Gynaecology*, *101*(1), 35-43. doi: 10.1111/j.1471-0528.1994.tb13007.x

[5] Dall'Asta, A., Ramirez Zegarra, R., Corno, E., Mappa, I., Lu, J. L. A., Di Pasquo, E., ... & Ghi, T. (2023). Role of fetal head-circumference-to-maternal-height ratio in predicting Cesarean section for labor dystocia: prospective multicenter study. *Ultrasound in Obstetrics & Gynecology, 61*(1), 93-98. doi: 10.1002/uog.24981

[6] Dovjak, G. O., Schmidbauer, V., Brugger, P. C., Gruber, G. M., Diogo, M., Glatter, S., ... & Kasprian, G. J. (2021). Normal human brainstem development in vivo: a quantitative fetal MRI study. *Ultrasound in Obstetrics & Gynecology*, *58*(2), 254-263. doi: 10.1002/uog.22162

[7] Fei Liu, Zhonghe Zhang, Xiangtao Lin, Gaojun Teng, Haiwei Meng, Taifei Yu, … & Shuwei Liu. (2011). Development of the human fetal cerebellum in the second trimester: a post mortem magnetic resonance imaging evaluation. *J Anatomy*, *4*, *219*(5), 582-588. doi: 10.1111/j.1469-7580.2011.01418.x

[8] Frank, D., & Sela-Donenfeld, D. (2019). Hindbrain induction and patterning during early vertebrate development. *Cellular and Molecular Life Sciences, 76*(5), 941-960. doi: 10.1007/s00018-018-2974-x

[9] Ginath, S., Lerman-Sagie, T., Haratz Krajden, K., Lev, D., Cohen-Sacher, B., Bar, J., & Malinger, G. (2013). The fetal vermis, pons and brainstem: normal longitudinal development as shown by dedicated neurosonography. *The Journal of Maternal-Fetal & Neonatal Medicine*, *26*(8), 757-762. doi: 10.3109/14767058.2012.755508

[10] Guimaraes, C. V., & Dahmoush, H. M. (2022). Fetal brain anatomy. *Neuroimaging Clinics*, *32*(3), 663-681. doi: 10.1016/j.nic.2022.04.009

[11] Imbard, A., Benoist, J. F., & Blom, H. J. (2013). Neural tube defects, folic acid and methylation. *International Journal of Environmental Research and Public Health*, *10*(9), 4352-4389. doi: 10.3390/ijerph10094352

[12] Leung, T. N., Pang, M. W., Daljit, S. S., Leung, T. Y., Poon, C. F., Wong, S. M., & Lau, T. K. (2008). Fetal biometry in ethnic Chinese: biparietal diameter, head circumference, abdominal circumference and femur length. *Ultrasound in Obstetrics and Gynecology: The Official Journal of the International Society of Ultrasound in Obstetrics and Gynecology, 31*(3), 321-327. doi: 10.1002/uog.5192

[13] Milani, H. J. F., Barreto, E. Q. D. S., Araujo, E., Peixoto, A. B., Nardozza, L. M. M., & Moron, A. F. (2019). Ultrasonographic evaluation of the fetal central nervous system: review of guidelines. *Radiologia Brasileira*, *52*(3), 176-181. doi: 10.1590/0100-3984.2018.0056

[14] Miller, E., Orman, G. & Huisman, T. A. (2021). Fetal MRI assessment of posterior fossa anomalies: A review. *Journal of Neuroimaging*, *31*(4), 620-640. doi: 10.1111/jon.12871

[15] Mirlesse, V., Courtiol, C., Althuser, M., CFEF, & Duyme, M. (2010). Ultrasonography of the fetal brainstem: a biometric and anatomical, multioperator, cross-sectional study of 913 fetuses of 21-36 weeks of gestation. *Prenatal Diagnosis*, *30*(8), 739-745. doi: 10.1002/pd.2501

[16] Müller, F., & O'rahilly, R. (2011). The initial appearance of the cranial nerves and related neuronal migration in staged human embryos. *Cells Tissues Organs*, *193*(4), 215-238. doi: 10.1159/000320026

[17] Nagaraj, U. D., & Kline-Fath, B. M. (2022). Clinical applications of fetal MRI in the brain. *Diagnostics*, *12*(3), 764. doi: 10.3390/diagnostics12030764

[18] Patel, K., Shah, B. R., Nagrani, S., & Desai, M. (2022). The study of fetal central nervous system anomalies by the means of antenatal 2D ultrasound examination in varying trimesters. *International Journal of Health Sciences*, (I), 10783-10793. doi: 10.53730/ijhs.v6nS1.7592

[19] Pruthi, N., Kadri, P. A. S., & Ture, U. (2021). Fiber microdissection technique for demonstrating the deep cerebellar nuclei and cerebellar peduncles. *Operative Neurosurgery*, *20*(2), E118-E124. doi: 10.1093/ons/opaa318

[20] Raafat, M., Alalfy, M., Nagy, O., & Saraya, S. (2021). Fetal brain MRI: how it added to ultrasound diagnosis of fetal CNS anomalies-1 year experience. *Egyptian Journal of Radiology and Nuclear Medicine*, *52*, 1-7. doi: 10.1186/s43055-021-00465-6

[21] Saleem, S. N. (2014). Fetal MRI: An approach to practice: A review. *Journal of advanced research*, *5*(5), 507-523. doi: 10.1016/j.jare.2013.06.001

[22] Sezik, M., & Özkaya, M. O. (2018). Investigation of fetal magnetic resonance imaging indications. *Perinatal Journal*, *26*(1), 18-24. doi: 10.2399/prn.18.0261006

[23] Shkolnikov, V. S. (2020). Fetal anatomy of the spinal cord. *Clinical Anatomy and Operative Surgery*, *19*(3), 5-12. doi: 10.24061/1727-0847.19.3.2020.33

[24] Shoja, M. M., Ramdhan, R., Jensen, C. J., Chern, J. J., Oakes, W. J., & Tubbs, R. S. (2018). Embryology of the craniocervical junction and posterior cranial fossa, part I: development of the upper vertebrae and skull. *Clinical Anatomy*, *31*(4), 466-487. doi: 10.1002/ca.23049

[25] Struksnæs, C., Blaas, H. G. K., & Vogt, C. (2019). Autopsy findings of central nervous system anomalies in intact fetuses following termination of pregnancy after prenatal ultrasound diagnosis. *Pediatric and Developmental Pathology*, *22*(6), 546-557. doi: 10.1177/1093526619860385

[26] ten Donkelaar, H. J., Takakuwa, T., Vasung, L., Yamada, S., Shiota, K., & van der Vliet, T. (2023). Overview of the development of the human brain and spinal cord. In *Clinical neuroembryology: development and developmental disorders of the human central nervous system*. Cham: Springer International Publishing. doi: 10.1007/978-3-031-26098-8_1

[27] Ungureanu, D. R., Drăguşin, R. C., Căpitănescu, R. G., Zorilă, L., Ofiţeru, A. M. I., Marinaş, C., ... & Iliescu, D. G. (2023). First trimester ultrasound detection of fetal central nervous system anomalies. *Brain Sciences*, *13*(1), 118. doi: 10.3390/brainsci13010118

[28] Vegar-Zubovic, S., Behmen, A., Bektesevic, H., Prevljak,

S., Sefic-Pasic, I., Dzananovic, A., & Bukvic, M. (2019). Magnetic resonance imaging in the diagnosis of fetal pathology. *Acta Informatica Medica*, *27*(1), 50. doi: 10.5455/aim.2019.27.50-53

[29] Witczak, M., Ferenc, T., & Wilczyński, J. (2007). Pathogenesis and genetics of neural tube defects. *Ginekologia Polska*, *78*(12), 981-985. doi: 10.1002/wsbm.1559

[30] Yamaguchi, K., Goto, N., & Yamamoto, T. Y. (1989). Development of human cerebellar nuclei. Morphometric study. *Acta Anatomy*, *136*(1), 61-68. doi: 10.1159/000146799

МОРФОЛОГІЯ НЕЙРОННИХ КОМПЛЕКСІВ ЗАДНЬОГО МОЗКУ У ПЛОДІВ ЛЮДИНИ 17-18 ТИЖНІВ ВНУТРІШНЬОУТРОБНОГО РОЗВИТКУ

Лопаткіна О. П., Залевський Л. Л., Тихолаз В. О., Галунко Г. М., Данилевич В. П., Кравець Р. А.

Вроджені вади центральної нервової системи (ЦНС) є однією з найпоширеніших причин смертності та інвалідності новонароджених. Тому надзвичайно важливо вчасно оцінити розвиток ЦНС плода у внутрішньоутробному періоді, щоб виявити будь-які зміни в його розвитку і дати відповідні поради батькам щодо супроводу вагітності, запропонувати варіанти фетальної терапії та тип пологів, а також післяпологове лікування та прогноз. Метою наукової роботи є встановлення морфологічних особливостей нейронних комплексів заднього мозку плодів людини в терміні 17-18 тижнів внутрішньоутробного розвитку, розмірів та площі ядер черепних нервів в ділянці моста та ядер мозочка. Для проведення дослідження використовували біологічний матеріал, отриманий з Вінницького пологового будинку після переривання вагітності у здорових жінок за медичними показаннями, у зв'язку з хромосомними аномаліями плодів, які не пов'язані з вадами розвитку ЦНС. Матеріалом для анатомо-гістологічного дослідження були плоди людини терміном гестації 17-18 тижнів. Маса плодів становила 250,8±14,5 г, тім'яно-куприкова довжина – 163,3±8,4 мм. Зразки тканин заднього мозку фіксували у 10 % розчині нейтрального формаліну, згодом готували зрізи целоїдинових блоків товщиною 8-9 мкм для подальшого гістологічного дослідження. Забарвлення препаратів проводили гематоксиліном-еозином, толуїдиновим синім у модифікації Ніссля. Для статистичного аналізу цифрових даних на персональному комп'ютері використовували Microsoft Excel 2016 та Statistica 6.1, де нормальність розподілу оцінювали за допомогою тесту Шапіро-Уілка, для візуалізації даних будували гістограми, а також обчислювали стандартне відхилення та дисперсію вибірок. При мікроскопічному дослідженні мозочка було визначено зовнішній зернистий, молекулярний, внутрішній зернистий, проміжний та вентрикулярний шари. Також встановили наявність ядер мозочка, які були розміщені в проміжному шарі. На зрізі мозочка зубчасте ядро візуалізувалось у формі тонкої вигнутої лінії, що випуклою стороною направлена латерально і дорзально. Ядро відвідного нерва знаходиться вентрально від дорсальної поверхні моста, латерально від медіального поздовжнього пучка. Рухове ядро лицевого нерва розташовується медіальніше від ядра відвідного нерва і має видовжену форму з нечіткими межами. Рухове ядро трійчастого нерва займає латеральне положення відносно ядра лицевого нерва, має нечіткі контури, округлу форму і складається з нейронів, які перебувають на різних стадіях дозрівання. В латеральній ділянці моста розташовується присінкове ядро, що має неправильну овальну форму, межі ядра нечіткі. Також нижче присінкового ядра в латеральній ділянці знаходиться завиткове ядро, без чітких контурів, овальної видовженої форми. Таким чином, у задньому відділі головного мозку в терміні 17-18 тижнів внутрішньоутробного розвитку плода людини встановлено наявність ядер відвідного, трійчастого, лицевого, присінково-завиткового нервів, які розташовувались у мості та кулясте, коркоподібне, зубчасте та ядро вершини, які розташовувались у мозочку.

Ключові слова: *центральна нервова система, внутрішньоутробний розвиток, задній мозок, міст, мозочок, нейрони, ядра.*

Author's contribution

Lopatkina O. P. – research, methodology and writing of the original draft.
Zalevskyi L. L. – data visualization, formal analysis and validation.
Tykholaz V. O. – software, resources.
Galunko G. M. – conceptualization, supervision.
Danylevych V. P. – review writing and editing, project administration
Kravets R. A. – project administration.

DOI: 10.31393/morphology-journal-2025-31(4)-02 Reports of Morphology, Vol. 31, №4, Pages 12-21

ISSN 1818-1295 eISSN 2616-6194

REPORTS OF MORPHOLOGY

Official Journal of the Scientific Society of Anatomists, Histologists, Embryologists and Topographic Anatomists of Ukraine

journal homepage: https://morphology-journal.com

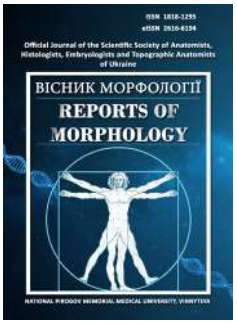

Immunohistochemical characteristics of the rat ileum under impaired antioxidant defence induced by the administration of a complex of chemical food additives

Bilash S. M.[1], Oliinichenko Ya. O.[1], Pronina O. M.[1], Shostya A. M.[2], Koptev M. M.[1], Pirog-Zakaznikova A. V.[1], Donchenko S. V.[1], Oleksiienko V. V.[1], Mamai O. V.[1], Oliinichenko M. O.[1], Koval Yu. P.[1], Kopytko N. S.[1]

[1] Poltava State Medical University, Poltava, Ukraine

[2] Poltava State Agrarian University, Poltava, Ukraine

ARTICLE INFO

Received: 17 February 2025

Accepted: 19 August 2025

UDC: 611.344:612.014.46:613.29:616-097:616-07

CORRESPONDING AUTHOR

e-mail: jarinaoliinichenko93@gmail.com

Oliinichenko Ya. O.

CONFLICT OF INTEREST

The authors have no conflicts of interest to declare.

FUNDING

Not applicable.

DATA SHARING

Data are available upon reasonable request to corresponding author.

The use of chemical food additives can cause morphofunctional changes in various internal organs. This is accompanied by disruption of both local immune and antioxidant defences. Therefore, the aim of the study was to evaluate immunohistochemical changes in the ileum of rats under conditions of impaired antioxidant defence caused by the combined administration of monosodium glutamate, sodium nitrite and Ponceau 4R dye. The study was conducted on 70 sexually mature white rats, which were divided into a control group and six experimental groups of 10 animals each. The control group received saline, while the experimental groups were administered a solution of chemical food additives for 1, 4, 8, 12, 16 and 20 weeks. At the end of each experimental period, ileal tissue was collected. Immunohistochemical studies were performed on paraffin-embedded sections. CD4, CD8, CD20 and CD68 markers were used to assess the cellular and humoral components of immunity. The state of the antioxidant system was evaluated by determining the levels of superoxide dismutase and catalase activity. Statistical analysis of the results was carried out using the "InStat" software package. In the early stages of the experiment, an increase in the number of $CD68^+$ and $CD20^+$ cells was observed, reflecting an acute tissue response to the toxic effects of the food additive complex. From weeks 4-8 onwards, a gradual decrease in the expression of $CD4^+$, $CD8^+$, $CD20^+$ and $CD68^+$ was noted, indicating the depletion of the immunoregulatory and effector components of local immunity. The lowest level of all studied cell populations was recorded at week 16. At the same time, suppression of superoxide dismutase and catalase activity was detected. Their reduction in the early stages indicates activation of lipid peroxidation processes and accumulation of reactive oxygen species, which may contribute to structural damage to the cellular components of the intestinal wall. Despite activation of the antioxidant defence system at the intermediate stages, the subsequent decline in enzyme activity after 12 weeks suggests depletion of defence mechanisms and the development of oxidative stress. Partial restoration of enzymatic activity at the end of the experiment is likely to reflect compensatory tissue responses to prolonged exposure to the damaging factor. Thus, the combined administration of monosodium glutamate, sodium nitrite and Ponceau 4R dye induces significant morphofunctional changes in the rat ileal mucosa, characterized by disruption of the cellular composition of the immune system and decreased antioxidant defence activity.

Key words: *rats, digestive tract, small intestine, ileum, food additives, microscopic changes, immunohistochemical study, CD4, CD8, CD20, CD68, superoxide dismutase, catalase, oxidative stress, monosodium glutamate, sodium nitrite, Ponceau 4R.*

Introduction

The modern food industry is characterised by the widespread use of chemical food additives aimed at improving the taste, colour and structural properties of products, as well as extending their shelf life [26]. Among

the most common are synthetic compounds such as flavour enhancers, preservatives and colourants, in particular monosodium glutamate [18], sodium nitrite [22] and Ponceau 4R [5]. Despite the permissible levels of these substances established by regulatory standards, prolonged or combined intake may have adverse effects on various organs and systems [19], especially on the digestive organs [13, 27].

The small intestine, particularly the ileum, represents the principal link in the digestive system, where nutrient absorption and maintenance of the mucosal barrier function take place. Structural alterations in its wall may lead to disturbances in microcirculation, absorption processes and local immune defence [14].

At the same time, a crucial aspect of the pathogenesis of structural and functional alterations in the intestine is the development of oxidative stress, which is accompanied by excessive formation of reactive oxygen species and depletion of the antioxidant defence systems [1, 9]. Among the enzymes that neutralise free radicals, superoxide dismutase (SOD) and catalase play a major role [11].

Immunohistochemical examination is one of the key methods for assessing the cellular components of the intestinal mucosa, as it enables the identification of distinct populations of immunocompetent cells using specific markers. Among these, CD4, CD8, CD20 and CD68 are of particular significance, as they reflect the condition of the cellular and humoral components of the immune response.

The selection of these immunohistochemical markers and antioxidant defence enzymes is based on their pivotal role in the pathogenic response of the intestinal mucosa. $CD4^+$ and $CD8^+$ T-lymphocytes are the principal effectors of cellular immunity [15, 32], and the balance between them determines the nature and direction of the immune response. $CD20^+$ B-lymphocytes represent the humoral component of immunity [2], whereas $CD68^+$ macrophages act as central regulators of local inflammatory processes and as a major source of reactive oxygen species [20]. Excessive activation of macrophages and T-cells is often accompanied by increased oxidative stress, which in turn may lead to structural damage of cellular elements and impairment of the functional integrity of the intestinal wall.

The determination of superoxide dismutase and catalase activity allows a quantitative assessment of antioxidant protection, which is essential for understanding the interrelation between immune responses and the intensity of free radical processes. A comprehensive analysis of these indicators enables characterisation of the morphofunctional alterations in the ileal mucosa under the combined influence of food additives and a reduction in the organism's antioxidant potential.

The aim of the study is to assess immunohistochemical alterations in the ileum of rats under conditions of impaired antioxidant defence induced by the combined administration of monosodium glutamate, sodium nitrite and Ponceau 4R dye.

Materials and methods

The study was carried out on 70 sexually mature white rats, which were divided into a control group and six experimental groups comprising 10 animals each. The animals in the control group received 0.5 ml of saline orally each day throughout the experiment. The rats in the experimental groups were administered a solution of chemical food additives containing monosodium glutamate (20 mg/kg), Ponceau 4R dye (5 mg/kg) and sodium nitrite (0.6 mg/kg), dissolved in 0.5 ml of distilled water. The duration of exposure was 1, 4, 8, 12, 16 and 20 weeks, respectively, depending on the group. The doses used were equivalent to half of the maximum permissible levels. Throughout the experiment, the animals had free access to standard vivarium feed and drinking water. At the end of the respective observation period, the animals were humanely euthanised by an overdose of thiopental sodium under ether anaesthesia.

The study was conducted in accordance with the requirements of the *Rules for the Use of Laboratory Experimental Animals* (2006, Appendix 4), the principles of the Helsinki Declaration on the humane treatment of animals, and the Law of Ukraine *On the Protection of Animals from Cruel Treatment* (No. 3447-IV of 21 February 2006). The experimental procedures complied with the provisions of the European Convention for the Protection of Vertebrate Animals Used for Experimental and Other Scientific Purposes (Strasbourg, 1986) and were approved by the Bioethics Commission of Poltava State Medical University (Protocol No. 208, 22 September 2022).

Immunohistochemical analysis

Fragments of the ileum were fixed in 10 % neutral buffered formalin, dehydrated, embedded in paraffin, and 3-4 μm thick histological sections were prepared using standard methods. For general morphological evaluation, the sections were stained with haematoxylin and eosin.

Immunohistochemical examination was performed on paraffin sections using the following primary antibodies: rabbit recombinant anti-CD4 (ab237722, Abcam, USA) for the identification of $CD4^+$ cells; mouse monoclonal anti-CD8 (ab33786, Abcam, USA) for the detection of $CD8^+$ cells; rabbit recombinant anti-CD20 (ab64088, Abcam, USA) for $CD20^+$ cells; and rabbit recombinant anti-CD68 (ab303565, Abcam, USA) for the detection of $CD68^+$ macrophages. The Mouse/Rabbit PolyVue™ HRP/DAB polymer detection system (Diagnostic BioSystems, USA) was used as the secondary antibody. The sections were counterstained with Mayer's haematoxylin (Biognost, Croatia).

Microphotography of selected areas was performed using a Levenhuk D740T microscope equipped with a digital camera, followed by image processing in specialised software modules. The results of the immunohistochemical reactions were evaluated by counting the number of positively stained areas, represented by brown-stained cell nuclei of varying intensity.

Biochemical analysis

The activity of SOD was determined by monitoring the kinetics of adrenaline auto-oxidation, while catalase activity was assessed using the molybdate method, both of which were previously modified and validated for use with 10 %

tissue homogenate.

Statistical analysis

Statistical processing of the results was carried out using the *InStat* software package. Differences were considered statistically significant at $p<0.05$.

Results

When assessing the immunohistochemical reactions in the rat ileum following administration of monosodium glutamate, sodium nitrite, and Ponceau 4R, it was found that CD4⁺ positive cells were predominantly localised in the lamina propria and in the walls of the vascular elements of the haemomicrocirculatory bed. Morphometric analysis revealed that their number decreased by 6.05 % after 1 week compared with the control group. After 4 weeks, no statistically significant difference was observed compared with the previous period, although the value remained 6.85 % lower than the control. After 8 weeks, the number of cells decreased by 32.47 % compared with the previous period and by 37.10 % relative to the control ($p<0.05$). At 12 weeks, the index decreased further compared with both week 8 and the control group, by 37.12 % and 60.48 %, respectively. In the histological sections, CD4⁺ positive cells (T-helper cells) were cytotopographically located within the layers of loose connective tissue between adjacent villi and occasionally in the basal regions of the villi. Goblet cells were arranged in groups, and their cytoplasm appeared oxyphilic, indicating secretion extrusion (Fig. 1A). The lowest value was observed after 16 weeks, being 2.04 % lower than in the previous period and 61.29 % lower than in the control. After 20 weeks, the number of CD4⁺ cells increased by 63.54 % compared with the previous stage but remained 36.69 % lower than the control (Fig. 2). In the histological sections, T-helper cells were visualised at the base of the crypts and within the fibrous component of the loose connective tissue surrounding them. The cytoplasm of goblet cells retained its oxyphilicity (Fig. 1B).

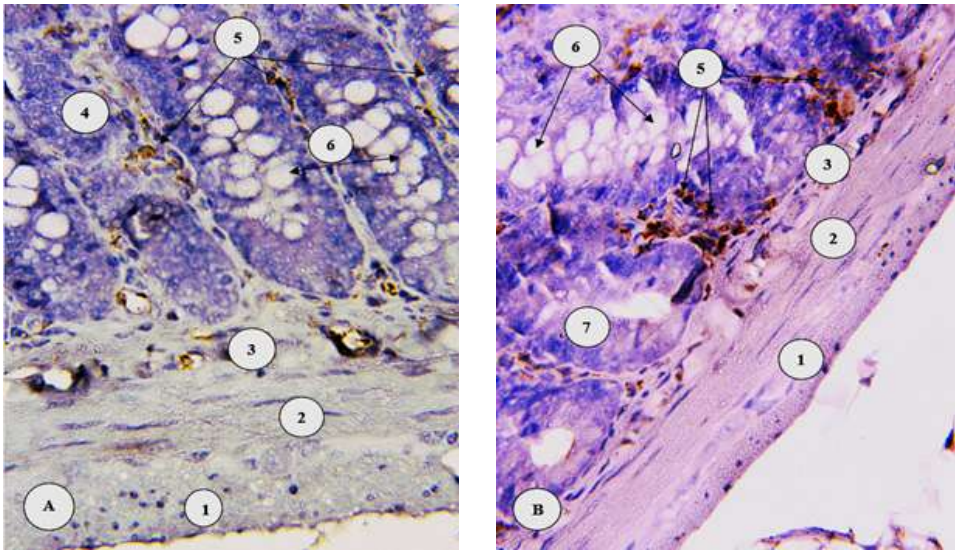

Fig. 1. Distribution of CD4⁺ immunoreactive structures in the rat ileum: A – after 12 weeks of the experimental study; B – after 20 weeks of the experimental study. 1 – serosa; 2 – muscular layer; 3 – submucosa; 4 – villi of the mucosa; 5 – T-helper cells; 6 – goblet cells at the extrusion stage; 7 – mucosal crypts. Paraffin section. Immunohistochemical staining for CD4 antigen with Mayer's haematoxylin counterstaining. ×400.

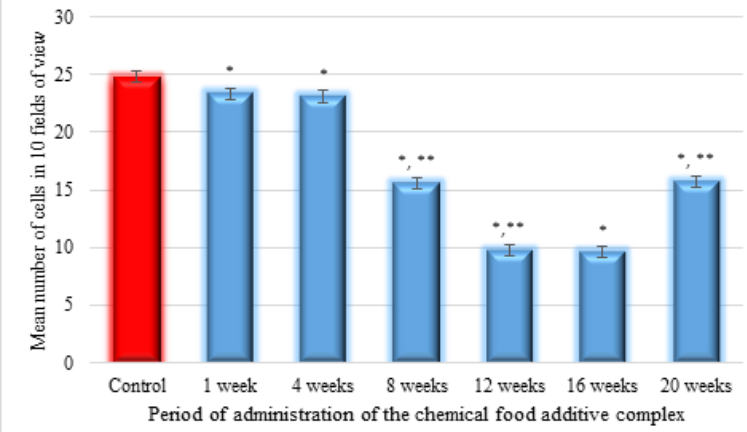

Fig. 2. Dynamics of changes in the mean number of CD4⁺-positive cells in the rat ileum at different periods of administration of the chemical food additive complex. * – statistically significant at $p<0.05$ compared with the control group; ** – statistically significant at $p<0.05$ compared with the previous observation period.

$CD8^+$ positive cells were mainly located intraepithelially and within the submucosa. Their number decreased by 13.55 % after 1 week compared with the control. Histologically, $CD8^+$ positive cells (cytotoxic T-lymphocytes) were cytotopographically distributed within the layers of loose connective tissue surrounding the crypts. Degranulated goblet cells indicated secretion extrusion (Fig. 3A). After 4 weeks, the value decreased by 19.09 % compared with the previous period and by 30.05 % relative to the control group ($p<0.05$). After 8 weeks, no statistically significant decrease was observed compared with the previous period, although the value remained 30.30 % lower than the control. After 12 weeks, the indicator increased by 24.03 % compared with the previous stage of the study, but remained 13.55 % lower than in the control group ($p<0.05$). After 16 weeks, a further decrease in the number of $CD8^+$ positive cells was observed – by 21.08 % compared with the previous period and by 31.77 % relative to the control values. At the final stage of the study, a 5.78 % increase was recorded compared with week 16, although the value did not return to control levels, remaining 27.83 % lower (Fig. 4). In the histological sections, cytotoxic T-lymphocytes were localised in the basal parts of the crypts and within the submucosa. The oxyphilicity of goblet cells was preserved, while their mean number decreased 1.4-fold (Fig. 3B).

$CD20^+$ positive cells were localised within lymphoid follicles and the lamina propria. Their number increased by 38.19 % after 1 week compared with the control. In the histological sections, $CD20^+$ positive cells (B lymphocytes) were situated around the crypts within layers of loose connective tissue. A reduction in the lumen of the crypts, which appeared elongated, was observed. Signs of goblet cell extrusion were also noted (Fig. 5A). After 4 weeks, the value decreased by 24.37 % compared with the previous period, but remained 4.51 % higher than the control. After 8 weeks, a decrease in the studied parameter was recorded

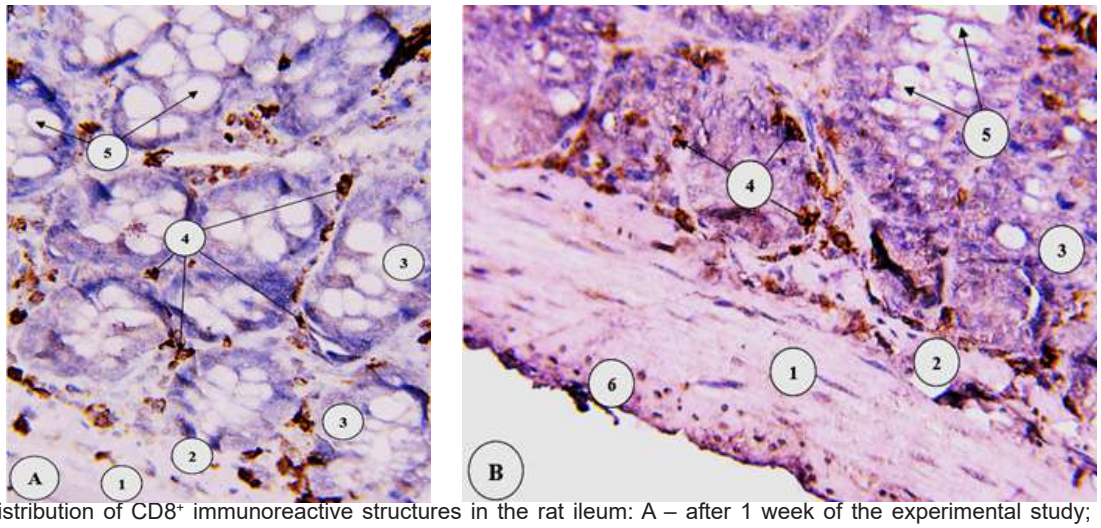

Fig. 3. Distribution of $CD8^+$ immunoreactive structures in the rat ileum: A – after 1 week of the experimental study; B – after 20 weeks of the experimental study. 1 – muscular layer; 2 – submucosa; 3 – mucosal crypts; 4 – cytotoxic T lymphocytes; 5 – degranulated goblet cells; 6 – serosa. Paraffin section. Immunohistochemical staining for CD8 antigen with Mayer's haematoxylin counterstaining. ×400.

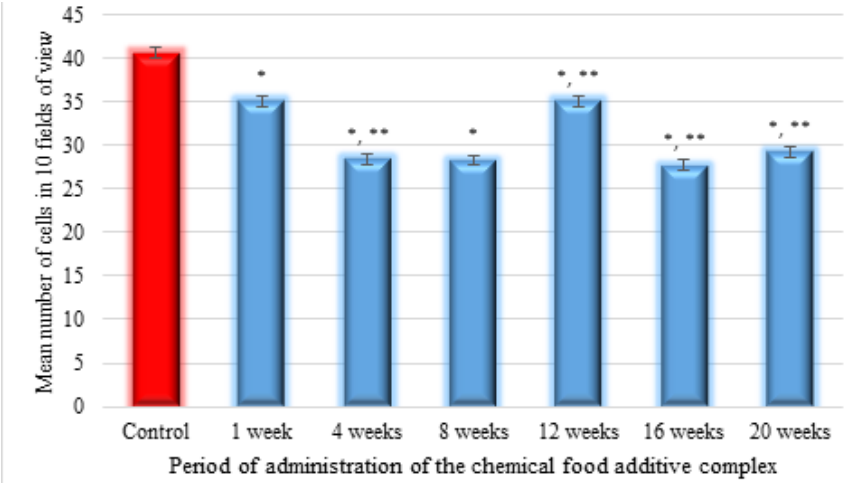

Fig. 4. Dynamics of changes in the mean number of $CD8^+$-positive cells in the rat ileum at different periods of administration of the chemical food additive complex. * – statistically significant at $p<0.05$ compared with the control group; ** – statistically significant at $p<0.05$ compared with the previous observation period.

both relative to week 4 and to the control group – by 8.97 % and 4.86 %, respectively ($p<0.05$). After 12 weeks, the number of $CD20^+$ cells increased by 20.07 % compared with the previous stage and by 14.24 % compared with the control. After 16 weeks, a reverse trend was observed, characterised by a decrease in the studied parameter relative to the previous period (by 32.83 %) and to the control (by 23.26 %). At the end of the experiment, the number of cells increased slightly compared to week 16 (by 4.98 %), but remained 19.44 % lower than the control (Fig. 6). Histological evaluation revealed a reduction in the mean number of B-lymphocytes. The crypts appeared elongated with enlarged lumens. Cytotopographically, $CD20^+$ cells were localised around the crypts. The oxyphilicity of goblet cells indicated an ongoing secretory process (Fig. 5B).

$CD68^+$ positive cells were mainly localised in the lamina propria. After 1 week of the experiment, their number increased by 34.09 %. Cytotopographically, $CD68^+$ positive cells (macrophages) were visualised within the villous lumen. Goblet cells were characterised by reduced secretion, with some appearing “empty” (Fig. 7A). After 4 weeks, the indicator decreased by 24.86 % compared to the previous period, although no statistically significant difference was observed relative to the control group. After 8 weeks, a marked decrease in the studied parameter was recorded, both compared with the previous period and with the control data, by 48.50 % and 48.11 %, respectively ($p<0.05$). After 12 weeks, no statistically significant increase in the number of $CD68^+$ positive cells was observed compared with week 8, although their number remained 47.73 % lower than in

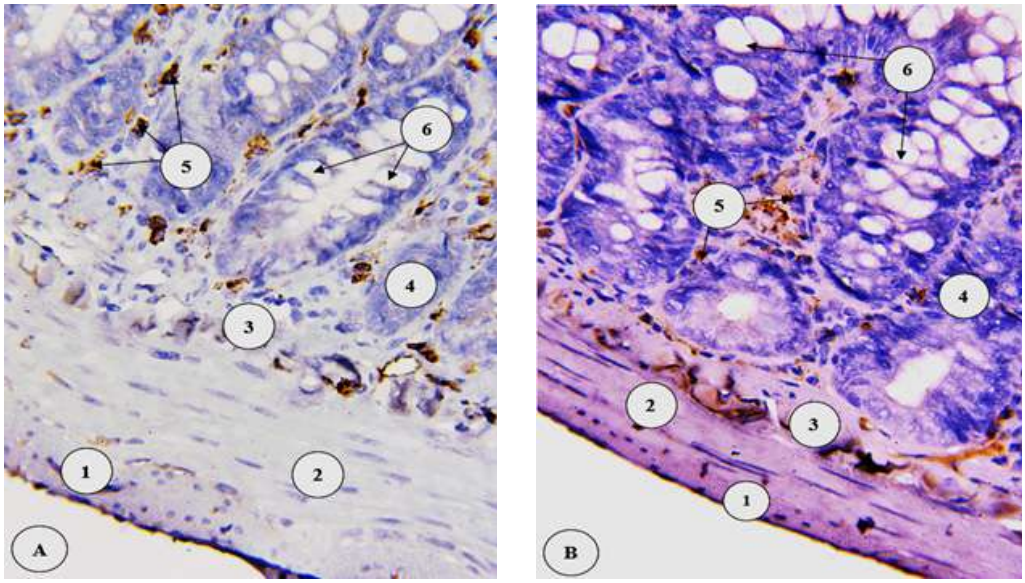

Fig. 5. Distribution of $CD20^+$ immunoreactive structures in the rat ileum: A – after 1 week of experimental study; B – after 20 weeks of experimental study. 1 – serosa; 2 – muscular layer; 3 – submucosa; 4 – mucosal crypts; 5 – B-lymphocytes; 6 – goblet cells in the stage of extrusion. Paraffin section. Immunohistochemical staining for CD20 antigen with Mayer’s haematoxylin counterstaining. ×400.

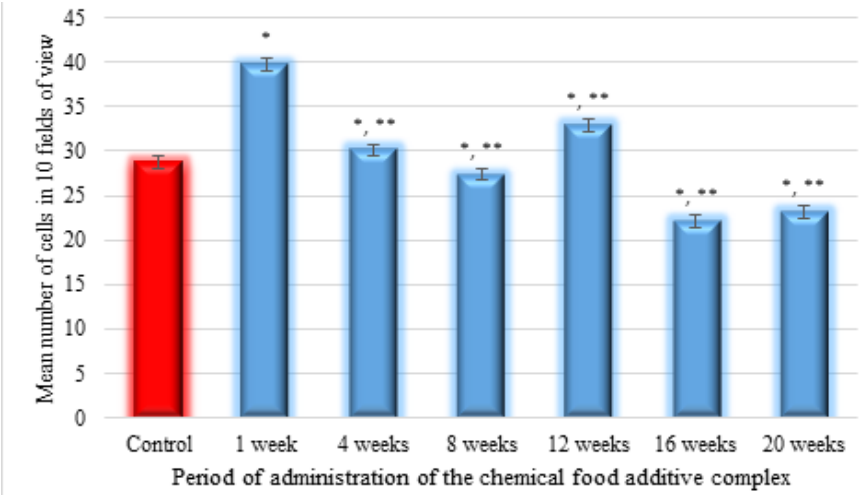

Fig. 6. Dynamics of changes in the mean number of $CD20^+$-positive cells in the rat ileum at different periods of administration of the chemical food additive complex. * – statistically significant at $p<0.05$ compared with the control group; ** – statistically significant at $p<0.05$ compared with the previous observation period.

the control. Histologically, the mean number of macrophages decreased; they were localised within the villous lumen and observed in the vessels of the capacitive segment of the haemomicrocirculatory bed. Goblet cells were arranged in groups and exhibited oxyphilic cytoplasm, indicating the preservation of the extrusion phenomenon (Fig. 7B). The lowest value was recorded after 16 weeks of the experiment, being 39.86 % lower than the previous period and 68.56 % lower than the control. At the final stage of the study, the parameter increased by 43.37 % compared with week 16 but remained 54.92 % lower than in the control group (Fig. 8).

At the next stage of the study, biochemical parameters characterising the state of antioxidant protection were assessed against the background of combined administration of monosodium glutamate, sodium nitrite, and Ponceau 4R.

When evaluating the dynamic changes in the mean superoxide dismutase (SOD) activity in ileal biopsies, it was found that this parameter decreased by 33.24 % after 1 week of the experiment ($p<0.05$). After 4 weeks, the parameter increased by 7.36 % compared with the previous stage, but remained 28.32 % lower than the control. After 8 weeks, a similar trend was observed, with the value 22.98 % higher than the previous period, yet 11.85 % lower than the control. The lowest SOD activity was recorded after 12 weeks, being 29.84 % lower than the previous stage and 38.15 % lower than the control ($p<0.05$). After 16 weeks, the parameter increased by 21.26 %, but remained 25.00 % lower than the control. At the final stage, despite a slight increase compared with the previous period (by 2.50 %), the value remained below the control by 23.12 % (Fig. 9).

Catalase activity was subsequently assessed in ileal biopsies. After 1 week of the experiment, the parameter decreased by 30.30 % compared with the control. After 4 weeks, it increased relative to the previous period (by 26.09 %), but remained 12.12 % lower than the control ($p<0.05$). After 8 weeks, a similar trend was observed: the

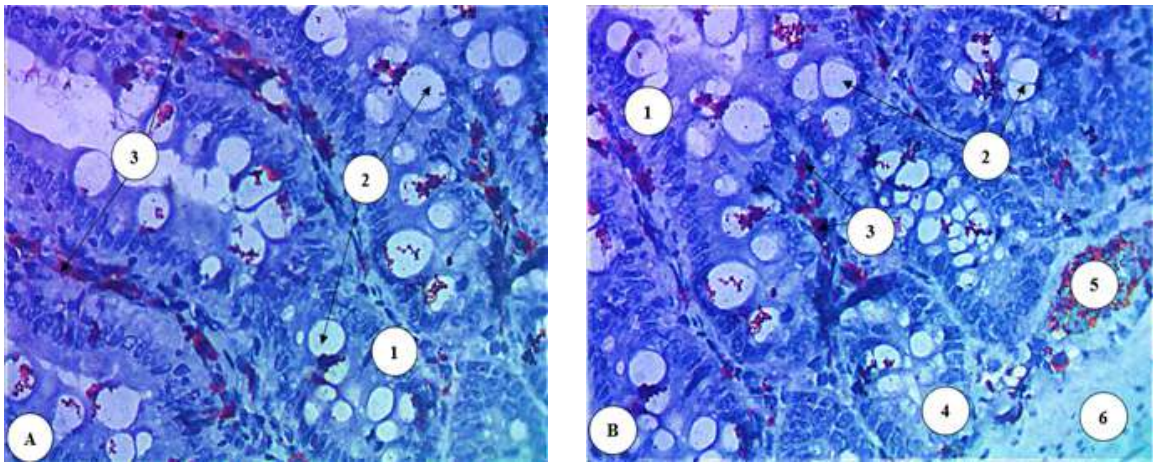

Fig. 7. Distribution of CD68$^+$ immunoreactive structures in the rat ileum: A – after 1 week of experimental study; B – after 12 weeks of experimental study. 1 – mucosal villi; 2 – degranulated goblet cells; 3 – macrophages; 4 – mucosal crypts; 5 – venule; 6 – submucosa. Paraffin section. Immunohistochemical staining for CD68 antigen with Mayer's haematoxylin counterstaining. ×400.

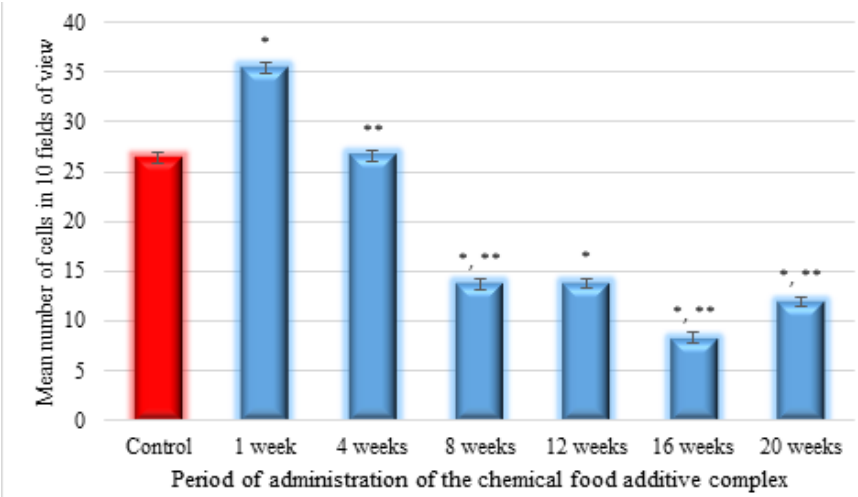

Fig. 8. Dynamics of changes in the mean number of CD68$^+$-positive cells in the rat ileum at different periods of administration of the chemical food additive complex. * – statistically significant at $p<0.05$ compared with the control group; ** – statistically significant at $p<0.05$ compared with the previous observation period.

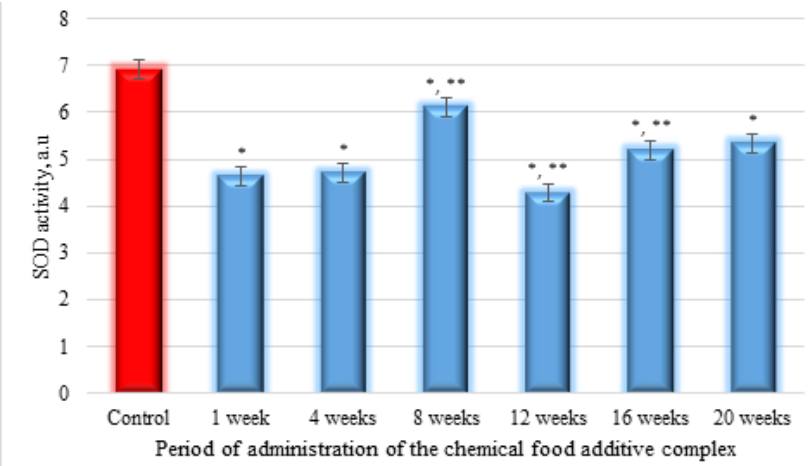

Fig. 9. Dynamics of the mean superoxide dismutase activity in ileal biopsies of rats at different periods of administration of the chemical food additive complex. * – statistically significant at p<0.05 compared with the control group; ** – statistically significant at p<0.05 compared with the previous observation period.

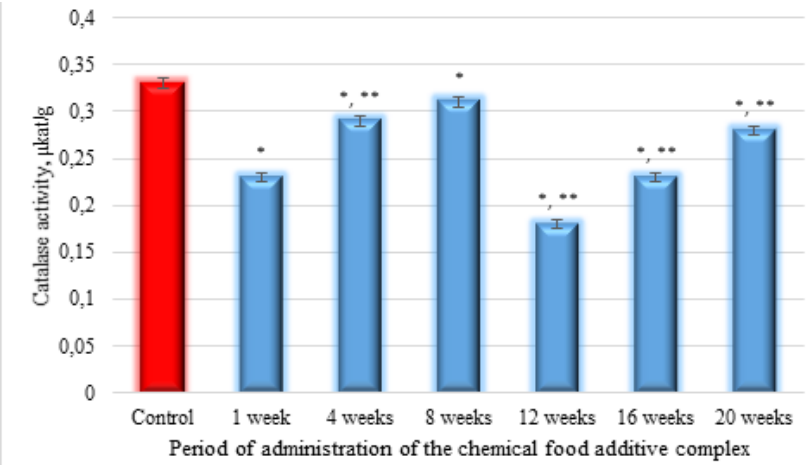

Fig. 10. Dynamics of the mean catalase activity in ileal biopsies of rats at different periods of administration of the chemical food additive complex. * – statistically significant at p<0.05 compared with the control group; ** – statistically significant at p<0.05 compared with the previous observation period.

value was 6.90 % higher than in the previous period, yet 6.06 % lower than the control. The lowest catalase activity was recorded after 12 weeks, with a 41.94 % decrease compared with week 8 and a 45.45 % decrease compared with the control (p<0.05). After 16 weeks, the parameter increased by 27.78 % compared with the previous stage, but remained 30.30 % lower than the control. At the final stage (20 weeks), despite an increase compared with the previous period (by 21.74 %), the value did not return to control levels, remaining 15.15 % lower (Fig. 10).

Discussion

The results indicate that the combined administration of monosodium glutamate, sodium nitrite, and Ponceau 4R leads to significant alterations in the structural and functional organisation of the local immune response in the ileal mucosa of rats.

In the early stages of the experiment, activation of phagocytic and humoral cells (reflected by an increase in the number of $CD68^+$ and $CD20^+$ positive cells) was observed, indicating an acute tissue response to the toxic effects of the food additive complex. Subsequently, from weeks 4-8, a gradual decrease in the expression of $CD4^+$, $CD8^+$, $CD20^+$, and $CD68^+$ cells was observed, suggesting depletion of immunoregulatory and effector components of local immunity. Despite a modest increase in the number of $CD68^+$, $CD8^+$, and $CD20^+$ positive cells at week 12, $CD4^+$ levels continued to decline. The most pronounced decrease in the number of all studied cells at week 16, and the absence of recovery to control values even at the end of the experiment, are likely associated with exhaustion of adaptive mechanisms and the limited potential of the mucosal immune response.

At the same time, the activity of key antioxidant defence enzymes – superoxide dismutase and catalase – was suppressed. Their reduction at the early stages indicates activation of lipid peroxidation processes and accumulation of reactive oxygen species, contributing to structural damage of the cellular components of the intestinal wall. A gradual

increase in enzyme activity during the intermediate stages of the experiment reflects activation of the antioxidant defence system, whereas a subsequent sharp decrease at week 12 indicates exhaustion of defence mechanisms and the development of oxidative stress. Partial restoration of enzymatic activity at the end of the experiment reflects compensatory tissue responses to prolonged exposure to a damaging factor.

Thus, the combined administration of chemical food additives adversely affects the local immune defence of the ileal mucosa, accompanied by disruption of antioxidant homeostasis with partial compensation at the later stages of observation.

The selected immunohistochemical markers allowed assessment of changes in both the cellular and humoral components of regional immunity. CD4 is a marker of T-helper lymphocytes, which play a central role in regulating immune responses by stimulating the differentiation and activation of other immune cells [17]. CD8 identifies cytotoxic T-lymphocytes, whose primary function is the elimination of cells infected by viruses or altered by pathological processes [12]. CD20 is a specific marker of B-lymphocytes and reflects the activity of the humoral immune response, as these cells are responsible for antibody synthesis [10]. CD68 is a marker of macrophages involved in phagocytosis, antigen presentation, and regulation of the inflammatory response [4].

Changes in the quantitative composition of these cell subpopulations can occur under the influence of both exogenous and endogenous factors, particularly in the mucosa of the small intestine, a crucial component of the body's natural barrier that supports immune function [6, 30]. Assessment of immune cell proliferation is important for the accurate diagnosis of inflammatory bowel diseases [28, 31] and irritable bowel syndrome [3]. In addition, macrophages play a key role in local inflammatory processes [8, 23, 25] and in tissue repair [7, 24, 29].

Disruption of the antioxidant defence in the small intestine can be observed after laparotomy in the context of a lipopolysaccharide-induced systemic inflammatory response [21], as well as in post-traumatic stress disorder [16].

The data obtained indicate a link between disruption of antioxidant homeostasis and alterations in the cellular composition of the ileal mucosal immune system, which may represent an important pathogenetic mechanism in the development of inflammatory and degenerative processes in the intestine.

Conclusions

1. Combined administration of monosodium glutamate, sodium nitrite, and Ponceau 4R leads to significant morphofunctional changes in the ileal mucosa of rats, characterised by disruption of the cellular composition of local immune defence and a decrease in the activity of the antioxidant system.

2. In the early stages of the experiment, activation of the phagocytic and humoral arms of immunity (increased expression of $CD68^+$ and $CD20^+$) was observed, reflecting an acute adaptive response to the toxic effects of the food additive complex. Subsequently, a decrease in the expression of $CD4^+$, $CD8^+$, $CD20^+$, and $CD68^+$ was observed, indicating depletion of the immunoregulatory and effector components of local immunity.

3. Suppression of superoxide dismutase and catalase activity, particularly at weeks 12-16, indicates the development of oxidative stress, which may contribute to structural damage of the mucosa. Partial restoration of enzymatic activity at the end of the experiment reflects activation of compensatory mechanisms; however, the indicators do not fully return to control values, suggesting exhaustion of the tissue's adaptive potential.

4. The results confirm the relationship between disruption of antioxidant homeostasis and imbalance of immune cells in the ileal mucosa, which occurs following chronic intake of chemical food additives.

References

[1] Akimov, O. Y., & Kostenko, V. O. (2016). Functioning of nitric oxide cycle in gastric mucosa of rats under excessive combined intake of sodium nitrate and fluoride. *Ukr Biochem J*, *88*(6), 70-5. doi: 10.15407/ubj88.06.070

[2] Boross, P., & Leusen, J. H. (2012). Mechanisms of action of CD20 antibodies. *Am J Cancer Res*, 2(6), 676-90. PMID: 23226614

[3] Burns, G. L., Talley, N. J., & Keely, S. (2022). Immune responses in the irritable bowel syndromes: time to consider the small intestine. *BMC Med*, *20*(1), 115. doi: 10.1186/s12916-022-02301-8

[4] Chen, B., Li, R., Kubota, A., Alex, L., & Frangogiannis, N. G. (2022). Identification of macrophages in normal and injured mouse tissues using reporter lines and antibodies. *Sci Rep*, *12*(1), 4542. doi: 10.1038/s41598-022-08278-x

[5] Chen, Y., Sun, Y., Pang, X., Wang, R., Waterhouse, G. I. N., & Xu, Z. (2023). Three-dimensional dual-network magnetic conductive hydrogel for the highly sensitive electrochemical detection of ponceau 4R in foods. *Biosens Bioelectron, 241,* 115698. doi: 10.1016/j.bios.2023.115698

[6] Gu, W., Eke, C., Gonzalez Santiago, E., Olaloye, O., & Konnikova, L. (2024). Single-cell atlas of the small intestine throughout the human lifespan demonstrates unique features of fetal immune cells. *Mucosal Immunol*, *17*(4), 599-617. doi: 10.1016/j.mucimm.2024.03.011

[7] Kierdorf, K., Prinz, M., Geissmann, F., & Gomez Perdiguero, E. (2015). Development and function of tissue resident macrophages in mice. *Semin Immunol*, *27*(6), 369-78. doi: 10.1016/j.smim.2016.03.017

[8] Klinge, U., Dievernich, A., Tolba, R., Klosterhalfen, B., & Davies, L. (2020). CD68+ macrophages as crucial components of the foreign body reaction demonstrate an unconventional pattern of functional markers quantified by analysis with double fluorescence staining. *J Biomed Mater Res B Appl Biomater*, *108*(8), 3134-3146. doi: 10.1002/jbm.b.34639

[9] Kostenko, V., Akimov, O., Gutnik, O., Kostenko, H., Kostenko, V., Romantseva, T., … & Taran, O. (2023). Modulation of redox-sensitive transcription factors with polyphenols

as pathogenetically grounded approach in therapy of systemic inflammatory response. *Heliyon*, *9*(5), e15551. doi: 10.1016/j.heliyon.2023.e15551

[10] Lee, A. Y. S. (2022). CD20+ T cells: an emerging T cell subset in human pathology. *Inflamm Res*, *71*(10-11), 1181-1189. doi: 10.1007/s00011-022-01622-x

[11] Li, Y., Li, X., Cui, Z., He, F., Zong, W., & Liu, R. (2023). Probing the toxic effect of quinoline to catalase and superoxide dismutase by multispectral method. *Spectrochim Acta A Mol Biomol Spectrosc*, *293*, 122449. doi: 10.1016/j.saa.2023.122449

[12] Lin, Y. H., Duong, H. G., Limary, A. E., Kim, E. S., Hsu, P., Patel, S. A., … & Chang, J. T. (2023). Small intestine and colon tissue-resident memory CD8+ T cells exhibit molecular heterogeneity and differential dependence on Eomes. *Immunity*, *56*(1), 207-223.e8. doi: 10.1016/j.immuni.2022.12.007

[13] Marsh, A., Chachay, V., Banks, M., Okano, S., Hartel, G., & Radford-Smith, G. (2024). A pilot randomized controlled trial investigating the effects of an anti-inflammatory dietary pattern on disease activity, symptoms and microbiota profile in adults with inflammatory bowel disease. *Eur J Clin Nutr*, *78*(12), 1072-1081. doi: 10.1038/s41430-024-01487-9

[14] Pereira, J. N. B., Murata, G. M., Sato, F. T., Marosti, A. R., Carvalho, C. R. O., & Curi, R. (2021). Small intestine remodeling in male Goto-Kakizaki rats. *Physiol Rep*, *9*(3), e14755. doi: 10.14814/phy2.14755

[15] Preglej, T., & Ellmeier, W. (2022). CD4+ Cytotoxic T cells - Phenotype, Function and Transcriptional Networks Controlling Their Differentiation Pathways. *Immunol Lett*, *247*, 27-42. doi: 10.1016/j.imlet.2022.05.001

[16] Riabushko, R. M., & Kostenko, V. O. (2024). Джерела супероксидного аніон-радикала в тканинах тонкої кишки щурів за умов хірургічної травми, відтвореної на тлі експериментальної моделі посттравматичного стресового розладу [Sources of superoxide anion radical in small intestine tissues in rats subjected to surgical trauma simulated under experimental model of posttraumatic stress disorder]. Актуальні проблеми сучасної медицини*:* Вісник Української медичної стоматологічної академії=*Actual Problems of the Modern Medicine: Bulletin of Ukrainian Medical Stomatological Academy*, *24*(2), 137-141. doi: 10.31718/2077-1096.24.2.137

[17] Ruterbusch, M., Pruner, K. B., Shehata, L., & Pepper, M. (2020). In Vivo CD4+ T Cell Differentiation and Function: Revisiting the Th1/Th2 Paradigm. *Annu Rev Immunol*, *38*, 705-725. doi: 10.1146/annurev-immunol-103019-085803

[18] Shastri, M., Raval, D. M., & Rathod, V. M. (2023). Monosodium Glutamate (MSG) Symptom Complex (Chinese Restaurant Syndrome): Nightmare of Chinese Food Lovers! *J Assoc Physicians India*, *71*(6), 11-12. doi: 10.5005/japi-11001-0264

[19] Shevchenko, K. V., Yeroshenko, G. A., Donets, I. M., Grygorenko, A. S., Klepets, O.V., Sokolenko, V.M., & Sharlay, N. M. (2024). Restructuring of the lung alveolar apparatus under the impact of the complex of food additives. Світ медицини та біології=*World of Medicine and Biology, 1*(87), 246-251. doi: 10.26724/2079-8334-2024-1-87-246-251

[20] Stetsuk, E. V., Shepitko, V. I., Solovyova, N. V., & Akimov, O. E. (2021). Роль рецептора CD68+ у змінах активності маркерних ферментів поляризації макрофагів в сім'яниках щурів при тривалій блокаді синтезу лютеїнізуючого гормону трипторелін [The role CD68+ receptor on changes in the activity of marker enzymes macrophage polarization in rat testes after long central deprivation of luteinizing hormone]. Вісник проблем біології *і* медицини=*Bulletin of problems in biology and medicine*, *3*(161), 277-281. doi: 10.29254/2077-4214-2021-3-161-277-281

[21] Taran, O. V., & Solovyova, N. V. (2022). Вплив модуляторів транскрипційних чинників NF-капа B і NRF2 на показники оксидативно-нітрозативного стресу в тканинах тонкої кишки щурів після лапаратомії на тлі ліпополісахарид-індукованої системної запальної відповіді [Effect of transcription factor modulators on oxidative-nitrosative stress indicators in tissues of the small intestine of rats after laparatomy under lipopolysaccharide-induced systemic inflammatory response]. Актуальні проблеми сучасної медицини*:* Вісник Української медичної стоматологічної академії=*Actual Problems of the Modern Medicine: Bulletin of Ukrainian Medical Stomatological Academy*, *22*(2), 76-1. doi: 10.31718/2077–1096.22.2.76

[22] Vodovar, D., & Megarbane, B. (2022). Are sodium nitrite exposures increasing in the United States? *Clin Toxicol (Phila)*, *60*(3), 416-417. doi: 10.1080/15563650.2021.1948560

[23] Watanabe, S., Alexander, M., Misharin, A. V., & Budinger, G. R. S. (2019). The role of macrophages in the resolution of inflammation. *J Clin Invest*, *129*(7), 2619-2628. doi: 10.1172/JCI124615

[24] Wculek, S. K., Dunphy, G., Heras-Murillo, I., Mastrangelo, A., & Sancho, D. (2022). Metabolism of tissue macrophages in homeostasis and pathology. *Cell Mol Immunol*, *19*(3), 384-408. doi: 10.1038/s41423-021-00791-9

[25] Weinberger, T., Esfandyari, D., Messerer, D., Percin, G., Schleifer, C., Thaler, R., … & Schulz, C. (2020). Ontogeny of arterial macrophages defines their functions in homeostasis and inflammation. *Nat Commun*, *11(1)*, 4549. doi: 10.1038/s41467-020-18287-x

[26] Wu, L., Zhang, C., Long, Y., Chen, Q., Zhang, W., & Liu, G. (2022). Food additives: From functions to analytical methods. *Crit Rev Food Sci Nutr*, *62*(30), 8497-8517. doi: 10.1080/10408398.2021.1929823

[27] Yeroshenko, G.A., Grygorenko, A.S., Shevchenko, K.V., Lysachenko, O.D., Maksymenko, N.T., Vatsenko, A.V., & Klepets, O.V. (2022). The features of the normal ultrastructure of the rat duodenum and under the combined effect of the food additives complex. *Wiad Lek, 75*(6), 1466-1470. doi: 10.36740/WLek202206107

[28] Yoo, J. W., Jo, S. I., Shin, D. W., Park, J. W., Kim, S. E., Lim, H., … & Soh, J. S. (2023). Clinical Usefulness of Immune Profiling for Differential Diagnosis between Crohn's Disease, Intestinal Tuberculosis, and Behcet's Disease. *Diagnostics (Basel)*, *13*(18), 2904. doi: 10.3390/diagnostics13182904

[29] Zhang, C., Yang, M., & Ericsson, A. C. (2021). Function of Macrophages in Disease: Current Understanding on Molecular Mechanisms. *Front Immunol*, *12*, 620510. doi: 10.3389/fimmu.2021.620510

[30] Zhang, Q., Cui, Y., Yu, S. J., Huang, Y. F., Pan, Y. Y., & Bai, Z. C. (2022). Immune cells in the small intestinal mucosa of newborn yaks. *Folia Morphol (Warsz)*, *81*(1), 91-100. doi: 10.5603/FM.a2021.0102

[31] Zheng, M., & Zhu, J. (2022). Innate Lymphoid Cells and Intestinal Inflammatory Disorders. *Int J Mol Sci*, *23*(3), 1856. doi: 10.3390/ijms23031856

[32] Zheng, Y., Wang, X., & Huang, M. (2022). Metabolic Regulation of CD8+ T Cells: From Mechanism to Therapy. *Antioxid Redox Signal*, *37*(16-18), 1234-1253. doi: 10.1089/ars.2022.0040

ІМУНОГІСТОХІМІЧНА ХАРАКТЕРИСТИКА КЛУБОВОЇ КИШКИ ЩУРІВ НА ТЛІ ПОРУШЕННЯ АНТИОКСИДАНТНОГО ЗАХИСТУ ПРИ ВВЕДЕННІ КОМПЛЕКСУ ХІМІЧНИХ ХАРЧОВИХ ДОБАВОК

Білаш С. М., Олійніченко Я. О., Проніна О. М., Шостя А. М., Коптев М. М., Пирог-Заказникова А. В., Донченко С. В., Олексієнко В. В., Мамай О. В., Олійніченко М. О., Коваль Ю. П., Копитько Н. С.

Застосування хімічних харчових добавок може бути причиною виникнення морфофункціональних змін різних внутрішніх органів. Це супроводжується порушенням як місцевого імунного, так і антиоксидантного захисту. Тому метою дослідження було провести оцінку імуногістохімічних змін у клубовій кишці щурів за умов порушення антиоксидантного захисту, викликаного комбінованим введенням глутамату натрію, нітриту натрію та барвника Понсо 4R. Дослідження виконано на 70 статевозрілих білих щурах, яких розподілили на контрольну та шість експериментальних груп по 10 тварин у кожній. Контрольна група отримувала фізіологічний розчин, а експериментальні – розчин хімічних харчових добавок протягом 1, 4, 8, 12, 16 та 20 тижнів. По завершенню відповідного терміну, проводили забір біоматеріалу (клубової кишки). Імуногістохімічне дослідження проводили на парафінових зрізах. Для оцінки клітинної та гуморальної ланок імунітету використано CD4, CD8, CD20 та CD68 маркери. Стан антиоксидантної системи оцінювали шляхом визначення рівня активності супероксиддисмутази та каталази. Статистичний аналіз результатів дослідження проводили з використанням програмного пакета «InStat». У ранні терміни експерименту відзначалося підвищення кількості $CD68^+$ та $CD20^+$ позитивних клітин, що відображало гостру реакцію тканини на токсичний вплив комплексу харчових добавок. Починаючи з 4-8 тижня, спостерігалося поступове зниження експресії $CD4^+$, $CD8^+$, $CD20^+$ та $CD68^+$, що свідчить про виснаження імунорегуляторних та ефекторних компонентів місцевого імунітету. Найнижчий показник всіх досліджуваних клітин було встановлено на 16 тижні. Водночас виявлено пригнічення активності супероксиддисмутази та каталази. Їх зниження на ранніх етапах свідчить про активацію процесів перекисного окиснення ліпідів і накопичення активних форм кисню, що могло сприяти структурним ушкодженням клітинних компонентів кишкової стінки. Незважаючи на активацію системи антиоксидантного захисту на проміжних термінах, зниження активності ферментів після 12 тижня свідчить про виснаження захисних механізмів і розвиток оксидативного стресу. Часткове відновлення ферментативної активності наприкінці експерименту, ймовірно, є проявом компенсаторних реакцій тканини у відповідь на тривалий вплив ушкоджуючого чинника. Таким чином, комбіноване введення глутамату натрію, нітриту натрію та барвника Понсо 4R викликає суттєві морфофункціональні зміни у слизовій оболонці клубової кишки щурів, що характеризується порушенням клітинного складу імунної системи та зниженням активності антиоксидантного захисту.

Ключові слова: *щури, травна трубка, тонка кишка, клубова кишка, харчові добавки, мікроскопічні зміни, імуногістохімічне дослідження, CD4, CD8, CD20, CD68, супероксиддисмутаза, каталаза, оксидативний стрес, глутамат натрію, нітрит натрію, Понсо 4R.*

Author's contribution

Bilash S. M. – conceptualization, research, review writing and editing.
Oliinichenko Ya. O. – research, methodology and writing of the original draft, data visualization.
Pronina O. M. – scientific management, project administration.
Shostya A.M. – project administration, conceptualization.
Koptev M. M. – formal analysis and validation.
Pirog-Zakaznikova A. V. – data visualization.
Donchenko S. V. – software, resources.
Oleksiienko V. V. – formal analysis and validation, resources.
Mamai O. V. – software, conceptualization.
Oliinichenko M. O. – formal analysis and validation, resources.
Koval Yu. P. – conceptualization, resources.
Kopytko N. S. – software, resources.

DOI: 10.31393/morphology-journal-2025-31(4)-03 Reports of Morphology, Vol. 31, №4, Pages 22-28

ISSN 1818-1295 eISSN 2616-6194

REPORTS OF MORPHOLOGY

Official Journal of the Scientific Society of Anatomists, Histologists, Embryologists and Topographic Anatomists of Ukraine

journal homepage: https://morphology-journal.com

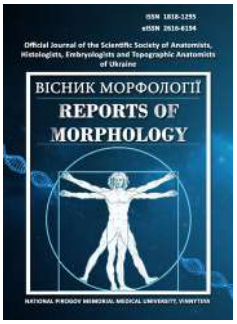

Features of skinfold thickness in Ukrainian men with alopecia areata

Shakatira M. A. M., Dmytrenko S. V., Prokopenko S. V., Golubovsky I. A., Gonchar O. O., Zverkhovska V. F., Kyselova T. M.

National Pirogov Memorial Medical University, Vinnytsya, Ukraine

ARTICLE INFO

Received: 10 February 2025

Accepted: 25 August 2025

UDC: 616.594.14:572.087

CORRESPONDING AUTHOR

e-mail: mohammedshakhatren00@gmail.com

Shakatira M. A. M.

CONFLICT OF INTEREST

The authors have no conflicts of interest to declare.

FUNDING

Not applicable.

DATA SHARING

Data are available upon reasonable request to corresponding author.

Alopecia areata is believed to be an isolated dermatological disease and also a potential marker of systematic diseases, particularly changes in body fat distribution as well as metabolic risk. An analysis of the thickness of skin-fat folds in men with alopecia areata in Ukraine makes it possible to expand our understanding of pathogenetic mechanisms of this disease and to approach more deeply its early diagnosis, and individual therapy. The aim of the study was to determine the features of skinfold thickness (SFT) in young adult Ukrainian men with alopecia areata. A clinical and instrumental examination (using an ARAMO ASW 300 dermatoscope-trichoscope) and an anthropological assessment (measurement of SFT in accordance with the recommendations of P. P. Shaparenko) were performed in 81 young adult Ukrainian men with alopecia areata. The severity of alopecia areata was determined according to I. V. Shutskiy. As a control group, we used SFT indicators of 82 apparently healthy Ukrainian men of the same age group from the database of the Research Center of Vinnytsia National Pirogov Memorial Medical University. Statistical processing of the results was carried out using the licensed software package Statistica 6.0, applying nonparametric evaluation methods. Significantly higher values of SFT were found in Ukrainian men with alopecia areata overall and at different degrees of severity, compared with practically healthy men, on the posterior (by 13.42-22.11 %), anterior surface of the arm (by 47.16-66.90 %), forearm (by 35.56-47.78 %), chest (by 70.59-87.86 %), and flank (by 21.77-31.63 %), and significantly lower SFT values on the thigh (by 15.73-20.98 %) and under the inferior angle of the scapula (by 36.13-47.59 %). Between groups of Ukrainian men with alopecia areata of different severity, only significantly lower SFT values on the posterior (by 9.31 % and 14.08 %) and anterior (by 9.73 % and 13.42 %) surfaces of the arm in patients with grade I severity compared with patients with grades II and III were established. The identified oppositely directed changes in SFT on the upper limb and thigh, as well as under the inferior angle of the scapula versus on the chest and flank in Ukrainian men with alopecia areata overall and at different degrees of severity, are manifestations of a "subpathological" constitutional type in this disease.

Keywords: *skin diseases, alopecia areata, practically healthy and sick Ukrainian men, anthropometry, skinfold thickness.*

Introduction

Alopecia areata (AA) is among the most prevalent autoimmune non-scarring alopecias, marked by abrupt hair loss on the scalp and other body sites and having a tendency to a relapsing course. Based on classic population-based studies and systematic reviews, the estimated lifetime prevalence of AA is about 2 % in the general population, with data from the Rochester Epidemiology Project showing a cumulative incidence of 2.1 %. The global burden of disease attributable to AA is estimated to exceed 1.3 million years lived with disability (DALYs), which highlights the substantial medical and social impact of what may initially appear to be a purely "skin condition" [11, 24, 30].

A meta-analysis by Lee H. H. et al. [11] demonstrated that the prevalence of AA on a worldwide scale is approximately 2.11 % in health-care-based samples, close to 0.75 % in population-based samples, and exceeds 3 % in clinical

samples, which may be influenced by both methodological differences and healthcare-seeking behavior. There has been a noticeable change in prevalence over time, with rates around 1.0 % reported before 2000 and more than 3.2 % after 2009, particularly higher in children than in adults. An earlier systematic review by Villasante Fricke A. C. and Miteva M. [24] underlined, on the one hand, the high worldwide prevalence of AA and, on the other, a wide spectrum of comorbid mental disorders together with reduced quality of life (QoL) in more than 50 % of patients; together, these observations enhance our perception of the burden of AA as a major medical problem. Furthermore, a recent systematic review with a pharmacoeconomic focus demonstrated large differences in estimates: point prevalence of AA in the general population ranged from 0.04 % to 6.7 %, period prevalence (0-5 years) from 0.42 % to 4.95 %, and lifetime prevalence from 2.5% to 13.8 %, which may be explained by heterogeneity in study designs, registries and diagnostic criteria [25].

Recent global model-based research improves our understanding of AA epidemiology, but also reveals substantial discrepancies in the currently available data. In a systematic review and Bayesian hierarchical model-based meta-analysis, Jeon J. J. et al. [9] analyzed 88 studies from 28 countries and noted that recorded incidence is higher among individuals aged 19-50 years, with Asia showing a higher prevalence than Africa. Lifetime prevalence of physician-diagnosed AA has been estimated at approximately 0.10 % in the general population (0.12 % in adults and 0.03 % in children), yet almost half of the regions mapped by the Global Burden of Disease project lack robust epidemiological data. Comparable conclusions regarding an absolute increase in the number of AA cases and AA-related years lived with disability, alongside only marginally fluctuating age-standardized incidence and prevalence rates, were reported by Wang H. et al. [26], consistent with recent analyses of the global burden of AA and related disorders from 1990 to 2021 [30].

Large national studies show distinct ethnic, social and age-related patterns of AA within populations, with the total number of affected individuals reaching many millions worldwide. In the UK, Harries M. et al. [7] reported an overall incidence rate of 0.26 per 1000 person-years and a point prevalence of 0.58 % in adults in primary care in 2018, with increased risks among non-European (particularly Asian) individuals, urban residents and people living in socioeconomically deprived areas, based on a primary-care database of more than 4.1 million individuals. In South Korea, nationwide insurance database studies showed low but gradually increasing prevalence and incidence rates of AA over 2006-2015, with a predominance of limited forms in young adult patients [12]. In Saudi Arabia, a tertiary-centre clinical study found that AA affected 2.3 % of dermatology clinic attendees and showed a predilection for children, with close associations with atopic conditions and other comorbidities [2]. Analysis of a large US dataset of employed, insured individuals demonstrated a rising trend in both prevalence and incidence of AA, alopecia totalis and alopecia universalis among adults and children in recent years, reflecting not only a true increase in case numbers but also improved case detection due to heightened diagnostic awareness [17, 25].

The review by Lintzeri D. A. et al. [15] presents the up-to-date concept of AA as a chronic multifactorial autoimmune disease that represents one of the most common dermatoses, with an estimated lifetime risk of approximately 2 %, and is significantly associated with other autoimmune, atopic, metabolic and psychiatric disorders. In the context of emerging targeted therapies (particularly JAK inhibitors) and growing interest in the systemic metabolic and neuropsychiatric implications of AA, issues related to accurate estimation of its prevalence and risk factors in different populations are becoming increasingly important. At the same time, global modelling work highlights the under-representation of middle- and low-income countries (including those of Eastern Europe) in large epidemiological datasets [7, 9, 26, 30]. This underscores the need for regional studies that not only refine the prevalence of alopecia areata but also clarify its relationship with somatotypological and anthropometric characteristics, particularly the distribution of subcutaneous fat, which forms the rationale for our study on the peculiarities of skinfold thickness in Ukrainian men with alopecia areata.

The aim of the study is to determine the characteristics of skinfold thickness in young Ukrainian men with alopecia areata.

Materials and methods

A clinical and instrumental as well as anthropological examination (in accordance with the recommendations of Shaparenko P. P. [20]) was performed in 81 young adult Ukrainian men (25-44 years according to the WHO age classification, 2015) with alopecia areata. The Committee on Bioethics of National Pirogov Memorial Medical University, Vinnytsya (protocol No. 4 from 18.03.2023) concluded that the study does not contradict the basic bioethical standards of the Declaration of Helsinki, the Council of Europe Convention on Human Rights and Biomedicine (1977), the relevant WHO regulations and the laws of Ukraine.

The diagnosis of alopecia areata was established using an ARAMO ASW 300 (Korea) dermatoscope-trichoscope, which makes it possible to assess hair density, hair thickness, the condition of the cuticle, scalp keratin and scalp capillary vessels. According to the severity of alopecia areata by Shutskiy I. V. [16], the following distribution of male patients was established: 35 patients with grade I severity, 33 patients with grade II severity, and 12 patients with grade III severity.

Skinfold thickness (SFT) on the extremities and trunk was measured with a caliper (mm). The skinfold was firmly grasped between the index finger and thumb, or with three fingers, in such a way that both the skin and the subcutaneous fat layer were included in the fold. The caliper

branches were applied so that the distance from the crest of the fold to the measurement point approximately equaled the thickness of the fold itself.

As a control group, we used SFT indices of 82 apparently healthy Ukrainian men of the same age group, obtained from the database of the Research Center of Vinnytsia National Pirogov Memorial Medical University. Statistical processing of the results was carried out using the licensed software package "Statistica 6.0", applying nonparametric evaluation methods. The mean values and standard deviations were calculated for each variable. The significance of differences between independent quantitative variables was determined using the Mann-Whitney U-test.

Results

It was found that SFT on the posterior surface of the arm in Ukrainian men with alopecia areata overall (8.901±1.751 mm), and in those with grade II (9.182±1.590 mm) and grade III (9.583±1.084 mm) severity, was significantly higher ($p<0.05$-0.01) than in apparently healthy Ukrainian men (7.848±2.914 mm) (Fig. 1A). When comparing this parameter among Ukrainian men with alopecia areata of different severity, significantly lower values ($p<0.05$ in both cases) were found in patients with grade I severity (8.400±1.988 mm) compared with patients with grades II and III severity (see Fig. 1A).

SFT on the anterior surface of the arm in Ukrainian men with alopecia areata, both overall (8.716±1.919 mm) and in patients with different degrees of severity (grade I – 8.229±1.987 mm, grade II – 9.030±1.976 mm, and grade III – 9.333±1.303 mm, respectively), was significantly higher ($p<0.001$ in all cases) than in apparently healthy Ukrainian men (5.592±2.132 mm) (Fig. 1B). When comparing this parameter among Ukrainian men with alopecia areata of different severity, significantly lower values ($p<0.05$ in both cases) were found in patients with grade I severity compared with those with grades II and III severity (see Fig. 1B).

SFT on the forearm in Ukrainian men with alopecia areata, both overall (5.926±1.439 mm) and in patients with different degrees of severity (grade I – 5.657±1.392 mm, grade II – 6.121±1.495 mm, and grade III – 6.167±1.467 mm, respectively), was significantly higher ($p<0.001$ in all cases) than in apparently healthy Ukrainian men (4.173±1.621 mm) (Fig. 1C). When comparing forearm SFT among Ukrainian men with alopecia areata of different severity, no significant differences or even trends toward differences in this parameter were found (see Fig. 1C).

SFT under the inferior angle of the scapula in Ukrainian men with alopecia areata, both overall (9.593±1.745 mm) and in patients with different degrees of severity (grade I – 9.429±1.668 mm, grade II – 9.939±1.983 mm, and grade III – 9.167±1.193 mm, respectively), was significantly lower ($p<0.001$ in all cases) than in apparently healthy Ukrainian men (13.53±3.92 mm) (Fig. 2A). When comparing SFT under the inferior angle of the scapula among Ukrainian men with

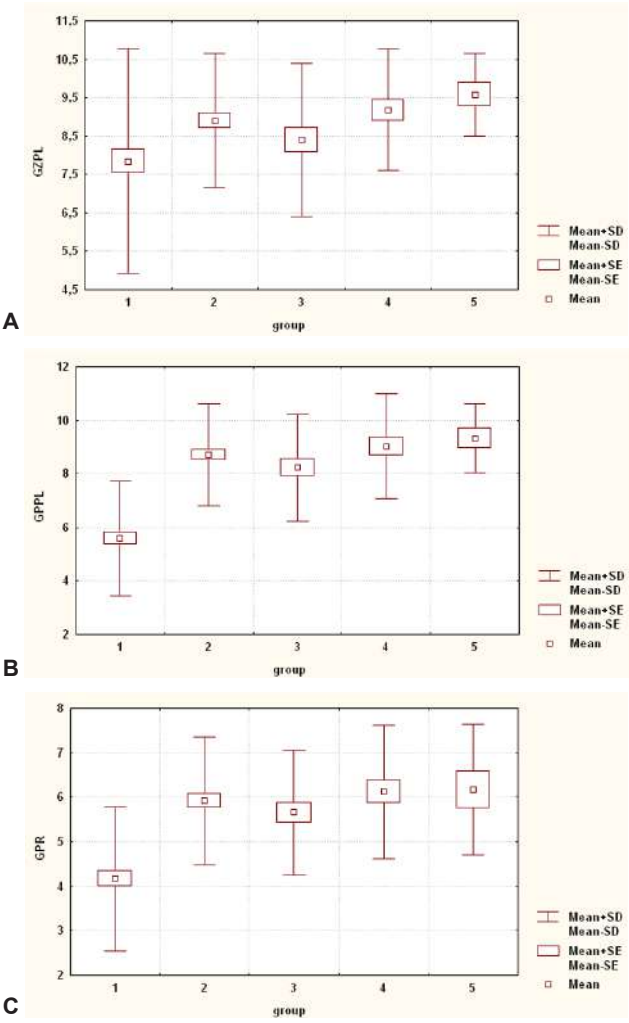

Fig. 1. Features of SFT on the upper limbs in Ukrainian men with alopecia areata of different severity. A – SFT on the posterior surface of the arm (GZPL); B – SFT on the anterior surface of the arm (GPPL); C – SFT on the forearm (GPR). In this and the following figure: 1 – apparently healthy men; 2 – all men with alopecia areata; 3 – men with alopecia areata of grade I severity; 4 – men with alopecia areata of grade II severity; 5 – men with alopecia areata of grade III severity. group – corresponding groups of the examined men; Mean – mean value; Mean±SE – mean value ± standard error of the mean; Mean±SD – mean value ± standard deviation.

alopecia areata of different severity, no significant differences or trends toward differences in this parameter were found (see Fig. 2A).

SFT on the chest in Ukrainian men with alopecia areata, both overall (8.864±1.752 mm) and in patients with different degrees of severity (grade I – 8.400±1.897 mm, grade II – 9.182±1.722 mm, and grade III – 9.250±1.138 mm, respectively), was significantly higher ($p<0.001$ in all cases) than in apparently healthy Ukrainian men (4.924±1.729 mm) (Fig. 2B). When comparing chest SFT among Ukrainian men with alopecia areata of different severity, a trend ($p=0.064$) and a slight trend ($p=0.099$) towards lower values of this parameter

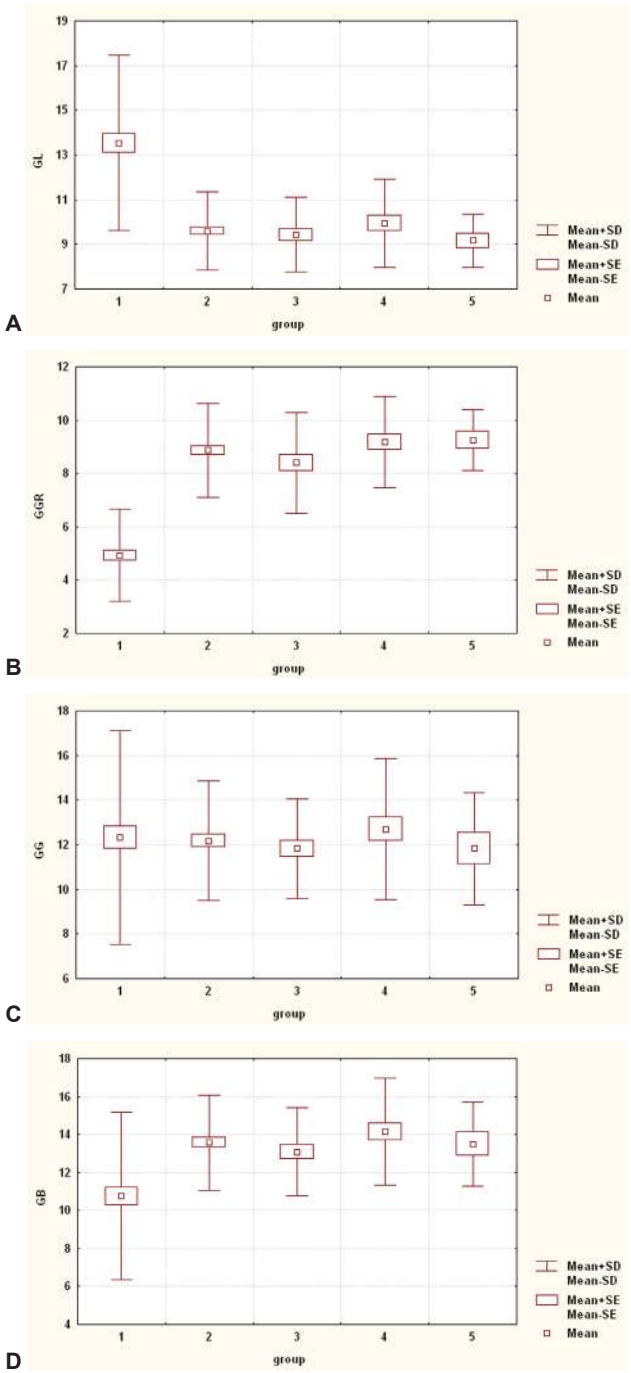

Fig. 2. Features of SFT on the trunk in Ukrainian men with alopecia areata of different severity. **A** – SFT under the inferior angle of the scapula (GL); **B** – SFT on the chest (GGR); **C** – SFT on the abdomen (GG); **D** – SFT on the flank (GB).

was found in patients with grade I severity compared with those with grades II and III severity (see Fig. 2B).

When comparing abdominal SFT between apparently healthy and Ukrainian men with alopecia areata, as well as among patients with different degrees of severity, no significant differences or trends towards differences in this parameter were found (Fig. 2C).

SFT on the flank in Ukrainian men with alopecia areata, both overall (13.57±2.53 mm) and in patients with different degrees of severity (grade I – 13.09±2.33 mm, grade II – 14.15±2.81 mm, and grade III – 13.50±2.20 mm, respectively), was significantly higher (p<0.01-0.001) than in apparently healthy Ukrainian men (10.75±4.41 mm) (Fig. 2D). When comparing flank SFT among Ukrainian men with alopecia areata of different severity, no significant differences or trends towards differences in this parameter were found (see Fig. 2D).

SFT on the thigh in Ukrainian men with alopecia areata, both overall (10.81±1.21 mm) and in patients with different degrees of severity (grade I – 10.69±1.28 mm, grade II – 11.06±1.25 mm, and grade III – 10.58±0.79 mm, respectively), was significantly lower (p<0.05-0.001) than in apparently healthy Ukrainian men (12.80±3.85 mm) (Fig. 3A). When comparing thigh SFT among Ukrainian men with alopecia areata of different severity, no significant differences or trends towards differences in this parameter were found (see Fig. 3A).

SFT on the shin in Ukrainian men with alopecia areata overall (9.111±1.118 mm) and in those with grade II severity (9.273±1.098 mm) showed only slight trends toward higher values (p=0.082 and p=0.088, respectively) compared with apparently healthy Ukrainian men (8.982±2.691 mm) (Fig. 3B). When comparing shin SFT among Ukrainian men with alopecia areata of different severity, no significant differences or trends toward differences in this parameter were found (see Fig. 3B).

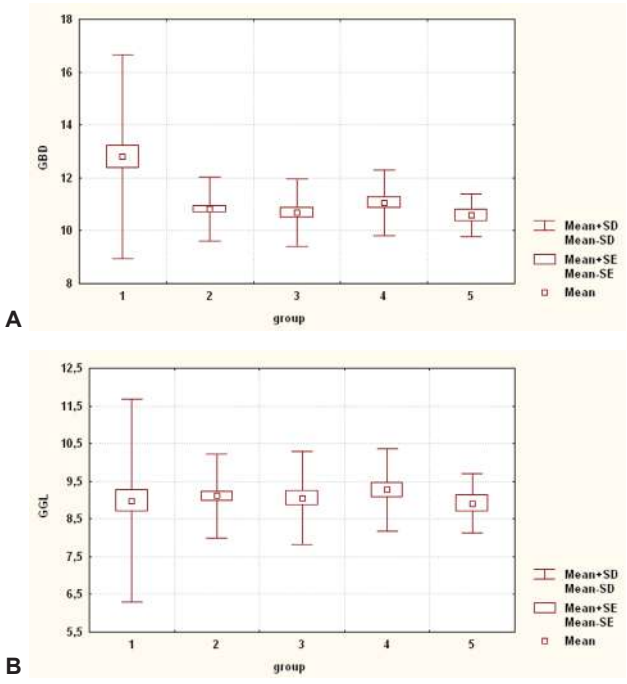

Fig. 3. Features of SFT on the lower limb in Ukrainian men with alopecia areata of different severity. **A** – SFT on the thigh (GBD); **B** – SFT on the shin (GGL).

Discussion

Thus, when comparing SFT between apparently healthy and Ukrainian men with alopecia areata overall and with different degrees of severity, the following was established: significantly higher values ($p<0.05$-0.001) or slight trends toward higher values ($p=0.081$ and $p=0.088$) in patients for SFT on the posterior (by 13.42 %–17.00 %–22.11 %, except in patients with grade I severity) and anterior surface of the arm (by 55.87 %–47.16 %–61.48 %–66.90 %), on the forearm (by 42.01 %–35.56 %–46.68 %–47.78 %), on the shin (only trends of 1.44 % and 3.24 % in patients overall and with grade II severity), on the chest (by 80.02 %–70.59 %–86.47 %–87.86 %), and on the flank (by 26.23 %–21.77 %–31.63 %–25.58 %). At the same time, significantly lower SFT values ($p<0.05$-0.001) were found in patients on the thigh (by 18.41 %–19.74 %–15.73 %–20.98 %) and under the inferior angle of the scapula (by 41.04 %–43.49 %–36.13 %–47.59 %). The oppositely directed changes in SFT on the upper limb and thigh, as well as under the inferior angle of the scapula versus on the chest and flank in Ukrainian men with alopecia areata compared with apparently healthy men, are manifestations of a "subpathological" constitutional type in this disease [18].

When comparing SFT among Ukrainian men with alopecia areata of different severity, only significantly lower values ($p<0.05$) or trends ($p=0.064$ and $p=0.099$) toward lower values were found in patients with grade I severity compared with those with grades II and III severity for SFT on the posterior (by 9.31 % and 14.08 %) and anterior (by 9.73 % and 13.42 %) surfaces of the arm and on the chest (by 9.31 % and 10.12 %).

C. Lie et al. [14] systematic review revealed that AA and AGA are both often related to metabolic syndrome (MetS) components, such as abdominal obesity, arterial hypertension, dyslipidemia and insulin resistance. A meta-analysis and systematic review by Qiu Q. I. U. et al. [29] confirmed these findings using both unadjusted and adjusted estimates: the pooled OR for AGA in the presence of MetS was 3.46 (95 % CI 2.38-5.05; $p<0.001$), and AGA patients had a worse profile with respect to BMI, waist circumference, fasting blood glucose, lipids and blood pressure than individuals without alopecia. A number of primary case–control studies have shown a greater prevalence of MetS and central obesity among men with AGA than in controls. In the investigation by Gopinath H. and Upadya G. M. [5], MetS was noted in 22.4 % of AGA patients compared with 9.4 % of the comparison group ($p=0.021$), i.e. more than twice as often. M. M. Devi et al. [4] found even more striking disparities in an Indian population: MetS was detected in 60 % of AGA patients and 24 % of controls ($p=0.0002$); abdominal obesity by waist circumference was present in 68.4 % versus 18.4 %, and hypertriglyceridaemia in 51 % versus 22 %, respectively.

In the studies by Swaroop et al. M. R. [22], Taheri A. R. et al. [23] and Qureshi H. F. et al. [19], early-onset or severe AGA in men was associated with a significantly higher frequency of MetS, insulin resistance (by HOMA-IR) and elevated blood pressure ($p<0.05$), further supporting the concept of AGA as a marker of cardiometabolic risk. A biochemical study by Hamed A. M. et al. [6] showed that in patients with AGA and MetS, circulating levels of the peptide alarin were significantly higher and correlated with waist circumference, triglycerides and insulin resistance, suggesting the involvement of adipokines in the pathogenic link between obesity and hair loss. At the same time, some studies, such as that by Danesh-Shakiba M. et al. [3], did not confirm clear differences in BMI or waist-to-height ratio between AGA and controls, given similar proportions of individuals with WHtR>0.5, emphasizing that not all anthropometric indices are equally sensitive for risk detection.

The evidence regarding AA as an autoimmune non-scarring type of alopecia is more heterogeneous. In a recent case–control study conducted by Abdollahimajd F. et al. [1], MetS was reported in 11.67 % (7 of 60) of patients with AA versus 6.67 % (4 of 60) in age- and sex-matched control subjects, with no statistically significant difference between the two groups ($p=0.34$). Meanwhile, the authors also demonstrated that MetS was strongly correlated with abdominal circumference (OR 1.10, 95 % CI 1.02-1.19), emphasizing the role of fat distribution rather than BMI alone. Similar results were reported by Singdia H. et al. [21] in north-western India: the prevalence of MetS among cases (7.54 %) and controls (8.47 %) was comparable ($p=1.0$), but all patients with AA who had MetS also had an increased waist circumference, and low HDL-C was the only component observed significantly more frequently in cases than in controls. A Ukrainian study conducted by Horda I. I. and Vozianova S. V. [8] revealed that, among AA patients with MetS, dyslipidemia and insulin resistance were predictors of a more progressive and recurrent course.

Other investigations expand on these findings by focusing on body weight, obesity and prediabetes. In a retrospective study analyzing 257 AA patients, Lee Y. B. and Lee W. S. [13] described the distribution of BMI categories across clinical subtypes and age at onset; they suggested that overweight and obesity are common comorbidities, but could not demonstrate a clear association with AA severity. However, in a large population-based cohort study by Wohl Y. et al. [27] involving 33,401 patients with AA and 66,802 controls, the prevalence of prediabetes (26.3 % vs 18.1 %; OR 1.62) and obesity (17.2 % vs 13 %; OR 1.35) was substantially higher in the patient group; furthermore, individuals with AA aged ≥40 years had approximately a twofold increased risk of developing prediabetes. A prospective cohort of 2.16 million Korean children analyzed by Kim S. R. et al. [10] showed that childhood obesity significantly increases the risk of immune-mediated skin diseases, including AA: a total of 4,878 cases of AA were registered, and the trend of increasing risk with rising BMI was statistically significant ($p<0.01$).

The study by Wróblewska-Kończalik K. et al. [28] did not reveal statistically significant differences in BMI or mean WHtR between patients and controls (0.49 and 0.51, respectively), and the proportion of individuals with

WHtR>0.5 was even higher among controls [28]. There was, however, a high prevalence of vitamin D deficiency (64.86 %) and low ferritin (48.65 %) in the patient group, as well as hypertriglyceridemia (27.2 %), corresponding to the findings of Lie C. et al. [14] on the involvement of dyslipidemia, micronutrient deficiencies and hormonal disturbances in determining the "metabolic phenotype" of alopecic subjects.

Our finding of regional patterns of SFT in young Ukrainian men with AA, characterized by high levels of SFT on the upper limb, chest and flank together with low levels of SFT on the thigh and under the inferior angle of the scapula, fits well into the concept of a "subpathological" constitutional adipose pattern associated with cardiometabolic risk. In contrast to the majority of investigations that report only global indices (BMI, waist circumference, WHtR) and the presence/absence of MetS [14, 19, 22, 23], our study describes in more detail the topography of subcutaneous fatty tissue. The opposite-direction changes in SFT on the upper limb, trunk and thigh may represent early constitutional shifts in fat distribution, consistent with studies of AGA and AA in combination with abdominal obesity, prediabetes, dyslipidemia and vitamin D deficiency [8, 10, 14].

Conclusions

1. The higher SFT values on the upper limb, chest and flank, together with lower SFT values on the thigh and under the inferior angle of the scapula in Ukrainian men with alopecia areata overall and at different degrees of severity compared with apparently healthy men, indicate the presence of a "subpathological" constitutional type in this disease.

2. Among groups of Ukrainian men with alopecia areata of different severity, only isolated differences in SFT were found, predominantly on the upper limb.

References

[1] Abdollahimajd, F., Niknezhad, N., Bahreini, N., Younespour, S., & Namazi, N. (2021). Metabolic syndrome in patients with alopecia areata: a case-control study. *Dermatologic Therapy*, *34*(4), e14979. doi: 10.1111/dth.14979

[2] Alshahrani, A. A., Al-Tuwaijri, R., Abuoliat, Z. A., Alyabsi, M., AlJasser, M. I., & Alkhodair, R. (2020). Prevalence and clinical characteristics of alopecia areata at a tertiary care center in Saudi Arabia. *Dermatology research and practice*, *2020*(1), 7194270. doi: 10.1155/2020/7194270

[3] Danesh-Shakiba, M., Poorolajal, J., & Alirezaei, P. (2020). Androgenetic alopecia: relationship to anthropometric indices, blood pressure and life-style habits. *Clinical, cosmetic and investigational dermatology*, 137-143. doi: 10.2147/CCID.S231940

[4] Devi, M. M., Raju, P. K., Gopal, K. V. T., & Rao, T. N. (2018). Study of prevalence of metabolic syndrome in androgenetic alopecia. *Int J Res Dermatol*, *4*, 522-526. doi: 10.18203/issn.2455-4529.IntJResDermatol20184454

[5] Gopinath, H., & Upadya, G. M. (2016). Metabolic syndrome in androgenic alopecia. *Indian journal of dermatology, venereology and leprology*, *82*, 404-408. doi: 10.4103/0378-6323.174421

[6] Hamed, A. M., Fatah, M. A., & Shams, G. M. (2022). Androgenetic alopecia and metabolic syndrome: is Alarin a missing link?. *The Journal of clinical and aesthetic dermatology*, *15*(7), 32-37. PMID: 35942015

[7] Harries, M., Macbeth, A. E., Holmes, S., Chiu, W. S., Gallardo, W. R., Nijher, M., ... & Messenger, A. G. (2022). The epidemiology of alopecia areata: a population-based cohort study in UK primary care. *British journal of dermatology*, *186*(2), 257-265. doi: 10.1111/bjd.20628

[8] Horda, I. I., & Vozianova, S. V. (2021). Effect of dyslipidaemia and insulin resistance on the course of alopecia areata associated with metabolic syndrome. *Dermatology and venereology,* (1), 18-22. doi: 10.33743/2308-1066-2021-1-18-22

[9] Jeon, J. J., Jung, S. W., Kim, Y. H., Parisi, R., Lee, J. Y., Kim, M. H., ... & Lee, S. (2024). Global, regional and national epidemiology of alopecia areata: a systematic review and modelling study. *British Journal of Dermatology*, *191*(3), 325-335. doi: 10.1093/bjd/ljae058

[10] Kim, S. R., Koh, S. J., & Park, H. (2024). Childhood obesity, weight change, and pediatric immune-mediated skin diseases. *Journal of Investigative Dermatology*, *144*(9), 1975-1984. doi: 10.1016/j.jid.2024.01.037

[11] Lee, H. H., Gwillim, E., Patel, K. R., Hua, T., Rastogi, S., Ibler, E., & Silverberg, J. I. (2020). Epidemiology of alopecia areata, ophiasis, totalis, and universalis: a systematic review and meta-analysis. *Journal of the American Academy of Dermatology*, *82*(3), 675-682. doi: 10.1016/j.jaad.2019.08.032

[12] Lee, J. H., Kim, H. J., Han, K. D., Han, J. H., Bang, C. H., Park, Y. M., ... & Lee, Y. B. (2019). Incidence and prevalence of alopecia areata according to subtype: a nationwide, population-based study in South Korea (2006–2015). *British Journal of Dermatology*, *181*(5), 1092-1093. doi: 10.1111/bjd.18145

[13] Lee, Y. B., & Lee, W. S. (2022). Alopecia areata and body mass index: A retrospective analysis of 257 cases. *Annals of Dermatology*, *34*(4), 305-308. doi: 10.5021/ad.20.084

[14] Lie, C., Liew, C. F., & Oon, H. H. (2018). Alopecia and the metabolic syndrome. *Clinics in dermatology*, *36*(1), 54-61. doi: 10.1016/j.clindermatol.2017.09.009

[15] Lintzeri, D. A., Constantinou, A., Hillmann, K., Ghoreschi, K., Vogt, A., & Blume-Peytavi, U. (2022). Alopecia areata–Current understanding and management. *JDDG: Journal der Deutschen Dermatologischen Gesellschaft, 20*(1), 59-90. doi: 10.1111/ddg.14689

[16] Mavrov, I. I., Bolotnaia, L. A., & Serbyna, I. M. (2007). *Основы диагностики и лечения в дерматологии и венерологи: руководство для врачей, интернов, студентов* [*Basics of diagnostics and treatment in dermatology and venereology: a guide for doctors, interns, students*]. Харьков: Факт=Kharkiv: Fact.

[17] Mostaghimi, A., Gao, W., Ray, M., Bartolome, L., Wang, T., Carley, C., ... & Swallow, E. (2023). Trends in prevalence and incidence of alopecia areata, alopecia totalis, and alopecia universalis among adults and children in a US employer-sponsored insured population. *JAMA dermatology*, *159*(4), 411-418. doi: 10.1001/jamadermatol.2023.0002

[18] Nykytiuk, B. A., Moroz, V. M., & Nykytiuk, D. B. (1998). *Теория и практика интегративной антропологии. Очерки* [*Theory and Practice of Integrative Anthropology. Essays*]. Киев-Винница: Здоров'я=Kyiv-Vinnitsa: Zdorovia.

[19] Qureshi, H. F., Akhtar, A., Kakar, A., Sakina, S., Irum, S., & Nasr, N. (2024). Association of Androgenetic Alopecia with Metabolic Syndrome. *Journal of the College of Physicians and Surgeons--Pakistan: JCPSP*, *34*(10), 1245-1248.

doi: 10.29271/jcpsp.2024.10.1245
[20] Shaparenko, P. P. (2000). Антропометрія [*Anthropometry*]. Вінниця: ВДМУ ім. М. І. Пирогова=Vinnytsia: VDMU im. M. I. Pyrogova.
[21] Singdia, H., Bhargava, P., Nijhawan, S., & Mathur, D. K. (2023). A Study of Correlation of Alopecia Areata and Metabolic Syndrome in Northwest Indian Population: A Case–Control Study. *International Journal of Trichology*, *15*(2), 63-69. doi: 10.4103/ijt.ijt_89_21
[22] Swaroop, M. R., Kumar, B. M., Sathyanarayana, B. D., Yogesh, D., Raghavendra, J. C., & Kumari, P. (2019). The association of metabolic syndrome and insulin resistance in early-onset androgenetic alopecia in males: A case–control study. *Indian journal of dermatology*, *64*(1), 23-27. doi: 10.4103/ijd.IJD_724_16
[23] Taheri, A. R., Afkhamizadeh, M., Sabourirad, S., Hassani, O., & Ghanizadeh, S. (2020). The association of androgenetic alopecia with metabolic syndrome: a case control study on Iranian population. *Iranian Journal of Dermatology*, *22*(4), 129-132. doi: 10.22034/ijd.2020.104819
[24] Villasante Fricke, A. C., & Miteva, M. (2015). Epidemiology and burden of alopecia areata: a systematic review. *Clinical, cosmetic and investigational dermatology*, 397-403. doi: 10.2147/CCID.S53985
[25] Vu, B. K., Tuson, H., Harricharan, S., Law, E., Wosik, K., Tran, H., ... & Neary, M. P. (2022). EPH57 Epidemiology of Alopecia Areata Across Global Regions–A Systematic Literature Review. *Value in Health*, *25*(12), S202. doi: 10.1016/j.jval.2022.09.979
[26] Wang, H., Pan, L., & Wu, Y. (2022). Epidemiological trends in alopecia areata at the global, regional, and national levels. *Frontiers in immunology*, *13*, 874677. doi: 10.3389/fimmu.2022.874677
[27] Wohl, Y., Mashiah, J., Noy, O., Drutin, Y., Vered, S., & Ben-Tov, A. (2025). Alopecia Areata Is Associated with an Increased Risk for Prediabetes and Obesity: A Nationwide Case–Control Study. *Journal of Personalized Medicine*, *15*(1), 16. doi: 10.3390/jpm15010016
[28] Wróblewska-Kończalik, K., Pawlaczyk, M., Kolasiński, J., Kolenda, M., Miechowicz, I., Seraszek-Jaros, A., ... & Gornowicz-Porowska, J. (2024). Non-cicatricial alopecia and its association with anthropometric measurements and nutritional laboratory markers. *Life*, *14*(5), 609. doi: 10.3390/life14050609
[29] Yueqi, Q. I. U., Xingyu, Z. H. O. U., Siqi, F. U., Shuaihantian, L. U. O., & Yaping, L. I. (2022). Systematic review and meta-analysis of the association between metabolic syndrome and androgenetic alopecia. *Acta dermato-venereologica*, *102*, 1012. doi: 10.2340/actadv.v101.1012
[30] Zhou, J., Liang, L., Zhang, H., Liu, M., Zhu, Z., Leng, L., & Li, J. (2025). Global burden of alopecia areata and associated diseases: a trend analysis from 1990 to 2021. *Journal of cosmetic dermatology*, *24*(3), e70076. doi: 10.1111/jocd.70076

ОСОБЛИВОСТІ ТОВЩИНИ ШКІРНО-ЖИРОВИХ СКЛАДОК У ХВОРИХ НА ГНІЗДОВУ АЛОПЕЦІЮ УКРАЇНСЬКИХ ЧОЛОВІКІВ

Шакатіра М. А. М., Дмитренко С. В., Прокопенко С. В., Голубовський І. А., Гончар О. О., Зверховська В. Ф., Кисельова Т. М.
Гніздову алопецію розглядають не лише як ізольоване дерматологічне захворювання, але й як потенційний маркер системних порушень, зокрема змін розподілу жирової тканини в організмі та метаболічного ризику. Аналіз товщини шкірно-жирових складок у чоловіків з гніздовою алопецією в Україні дає змогу розширити розуміння патогенетичних механізмів цього захворювання та поглибити підходи до його ранньої діагностики й індивідуалізованої терапії. Мета дослідження – встановлення особливостей товщини шкірно-жирових складок (ТШЖС) у хворих на гніздову алопецію українських чоловіків молодого віку. Проведено клініко-інструментальне (за допомогою дерматоскопу-трихоскопу ARAMO ASW 300) та антропологічне (визначення ТШЖС у відповідності до рекомендацій Шапаренка П. П.) обстеження 81 хворих на гніздову алопецію українських чоловіків молодого віку. Визначення тяжкості гніздової алопеції проводили за Шуцьким І. В. В якості контрольної групи використані показники ТШЖС 82 практично здорових українських чоловіків аналогічної вікової групи з банку даних науково-дослідного центру Вінницького національного медичного університету ім. М. І. Пирогова. Статистична обробка отриманих результатів проведена у ліцензійному пакеті «Statistica 6.0» з використанням непараметричних методів оцінки. Встановлені достовірно більші значення у хворих на гніздову алопецію українських чоловіків загалом і різного ступеня тяжкості, ніж у практично здорових чоловіків, ТШЖС на задній (на 13,42-22,11 %), передній поверхні плеча (на 47,16-66,90 %), на передпліччі (на 35,56-47,78 %), на грудях (на 70,59-87,86 %) і на боку (на 21,77-31,63 %) та достовірно менші значення ТШЖС на стегні (на 15,73-20,98 %) і під нижнім кутом лопатки (на 36,13-47,59 %). Між групами хворих на гніздову алопецію з різним ступенем тяжкості українських чоловіків встановлені лише достовірно менші значення ТШЖС на задній (на 9,31 % і 14,08 %) і передній (на 9,73 % і 13,42 %) поверхні плеча у хворих 1-го ступеня тяжкості порівняно з хворими 2-го та 3-го ступеня тяжкості. Встановлена різнонаправленість змін ТШЖС на верхній кінцівці та стегні, а також під нижнім кутом лопакти та на грудях і боку у хворих на гніздову алопецію українських чоловіків загалом і різного ступеня тяжкості є проявами «субпатологічного» конституціонального типу при даному захворюванні.
Ключові слова: *шкірні захворювання, гніздова алопеція, практично здорові та хворі українськи чоловіки, антропометрія, товщина шкірно-жирових складок.*

Author's contribution
Shakatira M. A. M. – research, data visualization, methodology and writing of the original draft.
Dmytrenko S. V. – conceptualization, project administration.
Prokopenko S. V. – formal analysis and validation.
Golubovsky I. A. – review writing and editing.
Gonchar O. O. – review writing and editing.
Zverkhovska V. F. – software.
Kyselova T. M. – supervision.

DOI: 10.31393/morphology-journal-2025-31(4)-04 Reports of Morphology, Vol. 31, №4, Pages 29-35

ISSN 1818-1295 eISSN 2616-6194

REPORTS OF MORPHOLOGY

Official Journal of the Scientific Society of Anatomists, Histologists, Embryologists and Topographic Anatomists of Ukraine

journal homepage: https://morphology-journal.com

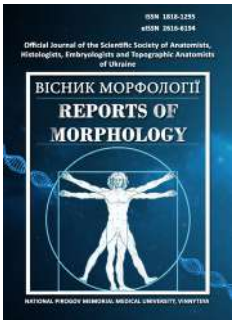

Ridge and delta counts of plantar dermatoglyphics in suicide victims: sex-related specificities

Chadiuk V. O.[1], Kotsiubynska Yu. Z.[1], Kolev Ya. G.[2], Fentsyk V. L.[3], Shutak O. V.[1], Yurak M. Z.[1], Solodzhuk Yu. I.[1], Kozan N. M.[1]

[1] Ivano-Frankivsk National Medical University, Ivano-Frankivsk, Ukraine

[2] Medical University, Pleven, Bulgaria

[3] Uzhhorod National University, Uzhhorod, Ukraine

ARTICLE INFO

Received: 15 January 2025

Accepted: 29 August 2025

UDC: 572.781.084:616-058.55:304.3-055.2/.3

CORRESPONDING AUTHOR

e-mail: nkozan@ifnmu.edu.ua

Kozan N. M.

CONFLICT OF INTEREST

The authors have no conflicts of interest to declare.

FUNDING

Not applicable.

DATA SHARING

Data are available upon reasonable request to corresponding author.

The problem of identifying morphological markers of susceptibility to suicidal behavior remains relevant both in forensic medicine and in psychobiology, particularly in view of the rising suicide rates in modern society. The dermatoglyphic characteristics of the plantar surfaces of the human feet – ridge counts and delta counts – are stable, embryogenetically determined traits that form at 13-19 weeks of intrauterine development simultaneously with the central nervous system and may be associated with psychophysiological features of an individual. The aim of the study was to determine gender-specific features of plantar skin patterns in individuals who died by suicide and to evaluate the feasibility of their application in forensic practice for identification and risk assessment. The study material included plantar prints of 52 individuals who died by suicide (37 males and 15 females), aged 18 to 59 years, and 50 individuals in the control group (25 males and 25 females). Dermatoglyphs were documented by photography followed by image processing using specialized software. Ridge and delta counts were measured on the distal phalanges of the toes, as well as in the plantar thenar, hypothenar, and subdigital areas. Statistical analysis included tests of distribution normality (Shapiro-Wilk and Kolmogorov-Smirnov tests) and the non-parametric Mann-Whitney U test to evaluate between-group differences at $p<0.05$. Statistically significant gender differences in dermatoglyphic parameters were identified: male suicide victims demonstrated significantly higher ridge counts on the first toe (radial areas) of both feet ($p=0.017$; $p=0.006$), which may indicate a more complex organization of epidermal ridges. Female suicide victims exhibited significantly higher delta counts in the subdigital areas of both the left ($p=0.018$) and right foot ($p=0.010$), suggesting morphogenetic features potentially associated with neuropsychic vulnerability. No significant gender differences were found for the plantar hypothenar areas, confirming their lower diagnostic value. The identified patterns demonstrate the high potential of plantar dermatoglyphic analysis as an additional tool for forensic identification and as an objective marker for assessing the risk of suicidal behavior, with possible practical applications in forensic expert work.

Keywords: *plantar dermatoglyphics, suicidal behavior, ridge count, delta count, gender differences, forensic identification.*

Introduction

Dermatoglyphics – the science that examines the ridge patterns of the skin on fingers, palms, and soles – is one of the most stable morphogenetic markers reflecting hereditary and prenatal factors of human development [1]. Over recent decades, its application has markedly expanded: from anthropological and forensic examinations to diagnostic and prognostic tools in behavioral, neurological, and psychiatric sciences [5, 6].

One of the most compelling avenues of modern forensic medicine is the investigation of dermatoglyphic correlates of suicidal behavior [27, 29]. Several studies support the hypothesis that specific features of papillary ridge patterns, the number of ridges and triradii, as well as degrees of asymmetry, may serve as morphological markers of susceptibility to suicidal acts [4, 14, 18]. Prior research has demonstrated alterations in dermatoglyphic configurations

among suicide victims compared with control groups, suggesting neurodevelopmental instability associated with the formation of suicidal behavior [7].

Gender differences play an important role, manifesting both in suicidal behavior and in dermatoglyphic structures [15, 22, 26]. According to multiple authors, males tend to exhibit lower ridge counts and greater pattern asymmetry, whereas females typically demonstrate higher stability of patterns and elevated triradial counts [5, 10, 19, 21]. This sexual dimorphism is particularly pronounced in plantar dermatoglyphics, which, although less studied than digital or palmar patterns, may serve as informative indicators of neuroendocrine and behavioral characteristics [11, 20].

Recent investigations conducted across various ethnic groups – including Indian, Chinese, Korean, and African populations – underscore the value of analyzing plantar ridge and triradial counts for detecting gender-specific morphological traits associated with suicidal behavior [16, 24]. Moreover, dermatoglyphic markers have shown correlations with psychological characteristics such as impulsivity, aggression, and emotional instability – factors known to elevate suicide risk [2, 3].

Given the multifactorial nature of suicide and the potential of dermatoglyphic parameters to reflect biological predisposition, the present study focuses on analyzing gender-specific features of plantar ridge and triradial counts in individuals who died by suicide. The findings may be valuable both for improving the precision of forensic identification and for deepening the understanding of the biopsychosocial mechanisms underlying suicidal behavior [23, 25].

Thus, the examination of plantar dermatoglyphics in the context of suicidal behavior represents a highly relevant research direction that integrates anthropological, forensic, and psychosocial approaches. Studying gender-specific differences in this domain may provide new tools for identifying individual risk factors and for developing preventive strategies.

Aim of the study: to analyze the gender-specific characteristics of plantar ridge and triradial counts in individuals who died by suicide and to evaluate their potential application in forensic medical practice.

Materials and methods

The object of the study comprised dermatoglyphic features – specifically, the ridge count and triradial (delta) count – of the distal phalanges of the toes and the plantar digital pads, obtained from 52 individuals, including 37 males and 15 females, aged 18 to 59 years, who died by suicide, as well as 50 individuals in the control group (25 males and 25 females).

To determine group assignment, the following inclusion factors were considered: the commission of a suicidal act; authorization from the investigative officer in charge of the respective criminal case; absence of genetic disorders, endocrine system pathology, or musculoskeletal abnormalities; age between 18 and 59 years.

Exclusion criteria included: presence of psychiatric or genetic disorders, endocrine pathology, or musculoskeletal abnormalities; age younger than 18 or older than 59 years; lack of investigator's permission to conduct the study.

To examine dermatoglyphic characteristics, we employed digital photography of plantar dermatoglyphics, followed by image processing using specialized graphic software, including the Fingerprint Identification Algorithm (FIA).

Ridge and triradial counts were determined according to standardized dermatoglyphic methodology.

A combination of descriptive and nonparametric statistical methods was used to compare plantar dermatoglyphic indicators (ridge and triradial counts) between men and women who died by suicide. For preliminary assessment of the distribution of quantitative variables, the following tests were utilized:

• Shapiro-Wilk test – the primary method for evaluating conformity to the normal distribution;

• Kolmogorov-Smirnov test with Lilliefors correction – an auxiliary test to confirm or refute normality for larger samples;

• Graphical methods (histograms, density plots) – for visual assessment of distribution shape and detection of asymmetry or multimodality.

Since, in most cases, the distribution of examined variables deviated from normality ($p < 0.05$), the use of nonparametric tests for further analysis was justified.

To compare dermatoglyphic parameters between two independent groups (males and females), the Mann-Whitney U test – a nonparametric analogue of Student's t-test – was applied, enabling comparison of medians between samples independently of distribution type.

For all quantitative variables, core descriptive statistics were calculated: mean (Mean), median (Median), minimum and maximum values (Min, Max), standard deviation (SD), and standard error of the mean (SE). All statistical analyses were performed using licensed software packages IBM SPSS Statistics v.27 and Microsoft Excel 2019. Statistical significance was set at $p<0.05$.

The volume and methods of the study complied with the ethical principles of the Helsinki Declaration on Biomedical Research (1974), adapted at the 41st International Assembly in Hong Kong (September 1989), governing research involving human subjects. The study adhered to fundamental principles of respect for the individual, informed consent, and assessment of risk versus benefit. Compliance with bioethical requirements was confirmed by the Ethics Committee of Ivano-Frankivsk National Medical University (protocol No. 153/25 dated 18.06.2025).

Results

During the study, an assessment of the normality of distribution of the examined parameters was performed. The Shapiro-Wilk test values for the ridge counts of the distal phalanges of the toes in male and female suicide victims indicated a deviation from the normal distribution, which was additionally confirmed by the Kolmogorov-Smirnov test (criterion: $p\geq0.20$). The results of normality assessment were further verified using graphical methods, which supported the hypothesis that the distribution of triradial (delta) counts of the distal phalanges also deviated from normality.

The mean statistical values of the ridge counts of the distal phalanges of the toes in individuals who died by suicide are presented in Table 1.

Table 1. Statistical indicators of ridge counts of the distal phalanges of the toes in suicide victims.

Indicators	Sex	N	Median	Min	Max	Mean	Std. Error	Std. Deviation
RC1LF_U	male	37	10	7	18	10.49	0.32	1.94
	female	15	11	9	11	10.40	0.21	0.83
RC2LF_U	male	37	9	4	11	8.649	0.255	1.549
	female	15	9	8	10	8.800	0.200	0.775
RC3LF_U	male	37	8	5	12	8.324	0.254	1.547
	female	15	8	7	9	7.800	0.200	0.775
RC4LF_U	male	37	7	5	11	7.541	0.244	1.483
	female	15	8	6	10	8.000	0.378	1.464
RC5LF_U	male	37	7	4	10	6.865	0.252	1.530
	female	15	7	6	10	7.200	0.393	1.521
RC1LF_R	male	37	10	5	17	10.70	0.47	2.88
	female	15	9	8	10	9.000	0.239	0.926
RC2LF_R	male	37	8	4	11	8.027	0.281	1.708
	female	15	9	7	10	8.400	0.321	1.242
RC3LF_R	male	37	7	5	11	7.595	0.250	1.518
	female	15	8	6	9	7.600	0.273	1.056
RC4LF_R	male	37	7	4	12	6.946	0.260	1.580
	female	15	6	5	8	6.400	0.273	1.056
RC5LF_R	male	37	7	4	9	6.487	0.238	1.446
	female	15	5	4	8	5.800	0.393	1.521
RC1RF_U	male	37	10	6	17	10.43	0.37	2.24
	female	15	11	9	12	10.60	0.27	1.06
RC2RF_U	male	37	8	5	12	8.487	0.270	1.644
	female	15	9	8	10	8.800	0.200	0.775
RC3RF_U	male	37	7	5	11	7.919	0.278	1.689
	female	15	8	7	10	8.000	0.293	1.134
RC4RF_U	male	37	7	4	12	7.514	0.297	1.805
	female	15	8	5	10	7.800	0.460	1.781
RC5RF_U	male	37	7	5	13	7.270	0.302	1.836
	female	15	7	5	9	7.000	0.378	1.464
RC1RF_R	male	37	11	6	19	10.84	0.39	2.37
	female	15	10	7	10	9.200	0.312	1.207
RC2RF_R	male	37	8	4	13	8.243	0.294	1.786
	female	15	8	7	10	8.200	0.262	1.014
RC3RF_R	male	37	7	5	11	7.460	0.211	1.282
	female	15	7	6	11	7.600	0.466	1.805
RC4RF_R	male	37	7	5	11	7.054	0.236	1.433
	female	15	7	6	7	6.600	0.131	0.507
RC5RF_R	male	37	6	4	11	6.297	0.265	1.614
	female	15	7	5	8	6.800	0.312	1.207

Notes: In this and the following tables: RC1-5LN_U – ridge counts (number of papillary ridges between the triradius and the pattern core) of the distal phalanges of toes 1-5 of the left foot with an ulnar (U) pattern type; RC1-5LN_R – ridge counts of the distal phalanges of toes 1-5 of the left foot with a radial (R) pattern type; RC1-5RN_U – ridge counts of the distal phalanges of toes 1-5 of the right foot with an ulnar (U) pattern type; RC1-5RN_R – ridge counts of the distal phalanges of toes 1-5 of the right foot with a radial (R) pattern type.

Since the distribution of ridge-count values of the distal phalanges of the toes did not meet the criteria of normality, a nonparametric Mann-Whitney U test was applied to perform a comparative analysis of potential differences between male and female subjects (Table 2).

As demonstrated by the results of the comparative analysis using the nonparametric Mann-Whitney U test, the triradial (delta) counts of the distal phalanges (ulnar and radial patterns) of the toes of male and female suicide victims did not differ significantly, except for the 1st toe with a radial pattern (ULF: U=162.0, p=0.017; URF: U=145.5, p=0.006).

The mean statistical values of the ridge counts of the thenar, hypothenar, and plantar digital areas of the feet in suicide victims showed that the Shapiro-Wilk test for these indicators in males ranged from 0.708 to 0.895, indicating that the distributions of ridge counts in the thenar, hypothenar, and plantar digital regions in male suicide victims deviated from normality. In female suicide victims, the Shapiro-Wilk test with the auxiliary Kolmogorov-Smirnov consistency test indicated deviation from normality in 75.00 % of cases. Graphical assessment further confirmed the hypothesis that the distribution of triradial count variables of the distal phalanges of the toes deviated from a normal distribution.

The mean statistical values of ridge counts in the thenar, hypothenar, and plantar digital regions of the feet in suicide victims are presented in Table 3.

Since the distribution of ridge-count values in the thenar, hypothenar, and plantar digital regions of the feet did not conform to a normal distribution, a nonparametric Mann-Whitney U test was applied to perform a comparative analysis of potential differences between male and female subjects (Table 4).

According to the results of the comparative analysis using the nonparametric Mann-Whitney U test, the ridge counts of the thenar regions of the feet in male and female suicide victims differed significantly only on the left foot for ulnar loops (U=175.5, p=0.038). Statistically significant differences were also observed in the plantar digital areas of both feet for ulnar (U=163.5, p=0.018) and radial (U=151.5, p=0.010) loops. No statistically significant differences were identified between male and female suicide victims for ridge counts of the hypothenar regions of the feet.

Similar results were obtained for the total triradial (delta) count of the toes of the left and right feet in males and females who died by suicide.

Since the probability value P (Sig.) according to both the

Table 2. Results of the comparative analysis of ridge counts of the distal phalanges of the toes in female and male suicide victims.

	RC1LF_U	RC2LF_U	RC3LF_U	RC4LF_U	RC5LF_U	RC1LF_R	RC2LF_R	RC3LF_R	RC4LF_R	RC5LF_R
Female suicide victims										
Mann-Whitney U	273.0	273.0	219.0	226.5	259.5	162.0	241.5	264.0	225.0	211.5
Wilcoxon W	976.0	976.0	339.0	929.5	962.5	282.0	944.5	967.0	345.0	331.5
Z	-0.094	-0.094	-1.222	-1.057	-0.371	-2.380	-0.746	-0.279	-1.109	-1.369
Asymp. Sig. (2-tailed)	0.925	0.925	0.222	0.291	0.710	0.017	0.456	0.780	0.268	0.171
Male suicide victims										
Mann-Whitney U	231.0	231.0	256.5	240.0	262.5	145.5	262.5	246.0	237.0	207.0
Wilcoxon W	934.0	934.0	959.5	943.0	382.5	265.5	965.5	366.0	357.0	910.0
Z	-0.957	-0.969	-0.436	-0.771	-0.309	-2.735	-0.312	-0.662	-0.856	-1.455
Asymp. Sig. (2-tailed)	0.338	0.333	0.663	0.441	0.757	0.006	0.755	0.508	0.392	0.146

Table 3. Statistical indicators of ridge counts in the thenar, hypothenar, and plantar digital regions of the feet in suicide victims.

Indicators	Sex	N	Median	Min	Max	Mean	Std. Error	Std. Deviation
RCT_LF_U	male	15	14	9	23	14.65	0.60	3.64
	female	37	12	8	18	12.40	0.87	3.38
RCT_LF_R	male	15	14	8	24	14.43	0.57	3.49
	female	37	14	10	21	14.20	1.03	4.00
RCT_RF_U	male	15	14	9	23	14.84	0.59	3.56
	female	37	14	12	18	14.60	0.67	2.59
RCT_RF_R	male	15	13	3	21	13.27	0.55	3.36
	female	37	15	10	18	14.00	0.81	3.14
RCH_LF_U	male	15	12	8	18	12.62	0.42	2.53
	female	37	12	9	17	12.60	0.73	2.82
RCH_LF_R	male	15	12	7	24	12.49	0.53	3.21
	female	37	12	11	15	12.20	0.39	1.52
RCH_RF_U	male	15	12	9	18	12.59	0.37	2.28
	female	37	13	10	15	12.60	0.50	1.92
RCH_RF_R	male	15	12	8	19	12.46	0.35	2.12
	female	37	11	10	15	12.20	0.52	2.01
RCPZ_LF_U	male	15	11	8	17	11.73	0.33	2.00
	female	37	11	8	14	11.20	0.57	2.21
RCPZ_LF_R	male	15	11	7	16	11.43	0.38	2.29
	female	37	10	9	16	11.20	0.71	2.73
RCPZ_RF_U	male	15	11	7	20	11.92	0.40	2.41
	female	37	10	9	12	10.40	0.27	1.06
RCPZ_RF_ R	male	15	12	7	19	11.76	0.50	3.06
	female	37	9	7	12	9.400	0.434	1.682

Notes: RCT_LF_U – ridge counts of the thenar region of the left foot with an ulnar (U) pattern type; RCT_LF_R – ridge counts of the thenar region of the left foot with a radial (R) pattern type; RCT_RF_U – ridge counts of the thenar region of the right foot with an ulnar (U) pattern type; RCT_RF_R – ridge counts of the thenar region of the right foot with a radial (R) pattern type; RCH_LF_U – ridge counts of the hypothenar region of the left foot with an ulnar (U) pattern type; RCH_LF_R – ridge counts of the hypothenar region of the left foot with a radial (R) pattern type; RCH_RF_U – ridge counts of the hypothenar region of the right foot with an ulnar (U) pattern type; RCH_RF_R – ridge counts of the hypothenar region of the right foot with a radial (R) pattern type; RCPZ_LF_U – ridge counts of the plantar digital area of the left foot with an ulnar (U) pattern type; RCPZ_LF_R – ridge counts of the plantar digital area of the left foot with a radial (R) pattern type; RCPZ_RF_U – ridge counts of the plantar digital area of the right foot with an ulnar (U) pattern type; RCPZ_RF_R – ridge counts of the plantar digital area of the right foot with a radial (R) pattern type.

Shapiro-Wilk and Kolmogorov-Smirnov tests was less than 0.05 for each parameter, we accepted that the distribution of these variables deviated from normality. Distribution plots were additionally used to support the assessment of normality.

The statistical calculations for the total triradial (delta) counts of the toes of both feet in suicide victims are presented in Table 5.

To compare data that did not follow a normal distribution, the Mann-Whitney U test was applied (Table 6).

According to the results of the comparative analysis using the nonparametric Mann-Whitney U test (Table 7), the triradial (delta) counts of the toes on both feet did not differ between male and female suicide victims, in contrast to the triradial counts of the plantar zones, which showed statistically significant differences for both feet (left foot: U=159.5, p=0.007; right foot: U=171.0, p=0.014).

Table 4. Results of the comparative analysis of ridge counts of the thenar, hypothenar, and plantar digital regions of the feet in female and male suicide victims.

Indicators	Groups	N	Mean Rank	Sum of Ranks
Thenar LF_U	Female suicide victims	15	19.70	295,5
	Male suicide victims	37	29.26	1083
Thenar LF _R	Female suicide victims	15	25.00	375.0
	Male suicide victims	37	27.11	1003
Thenar RF _U	Female suicide victims	15	25.80	387.0
	Male suicide victims	37	26.78	991.0
Thenar RF _R	Female suicide victims	15	28.30	424.5
	Male suicide victims	37	25.77	953.5
Hypothenar LF_U	Female suicide victims	15	26.30	394.5
	Male suicide victims	37	26.58	983.5
Hypothenar LF _R	Female suicide victims	15	26.80	402.0
	Male suicide victims	37	26.38	976.0
Hypothenar RF _U	Female suicide victims	15	27.00	405.0
	Male suicide victims	37	26.30	973.0
Hypothenar RF _R	Female suicide victims	15	25.40	381.0
	Male suicide victims	37	26.95	997.0
DPALF_U	Female suicide victims	15	24.40	366.0
	Male suicide victims	37	27.35	1012
DPALF _R	Female suicide victims	15	24.10	361.5
	Male suicide victims	37	27.47	1017
DPARF _U	Female suicide victims	15	18.90	283.5
	Male suicide victims	37	29.58	1095
DPARF _R	Female suicide victims	15	18.10	271.5
	Male suicide victims	37	29.91	1107

Table 5. Statistical indicators of the total triradial (delta) count of the toes in suicide victims.

Indicators	Sex	N	Median	Min	Max	Mean	Std. Error	Std. Deviation
TRC_LF	male	15	5	5	8	5.512	0.143	0.870
	female	37	5	5	7	5.267	0.153	0.594
TRC_RF	male	15	5	5	13	5.703	0.242	1.469
	female	37	5	5	6	5.400	0.131	0.507
TTRC_PZ_LF	male	15	3	3	4	3.432	0.083	0.502
	female	37	4	3	6	4.000	0.195	0.756
TTRC_PZ_RF	male	15	3	3	12	3.568	0.247	1.501
	female	37	4	3	5	3.800	0.145	0.561

Notes: TRC_LF – triradial (delta) count of the toes of the left foot; TRC_RF – triradial (delta) count of the toes of the right foot; TTRC_PZ_LF – total triradial (delta) count of the plantar zone of the left foot; TTRC_PZ_RF – total triradial (delta) count of the plantar zone of the right foot.

Table 6. Results of the comparative analysis of triradial (delta) counts of the toes and plantar zones of the feet in suicide victims.

Indicators	Groups	N	Mean Rank	Sum of Ranks
TRC_LF	Female suicide victims	15	24.03	360.5
	Male suicide victims	37	27.50	1017
TRC_RF	Female suicide victims	15	26.20	393.0
	Male suicide victims	37	26.62	985.0
TTRC_PZ_LF	Female suicide victims	15	34.37	515.5
	Male suicide victims	37	23.31	862.5
TTRC_PZ_RF	Female suicide victims	15	33.60	504.0
	Male suicide victims	37	23.62	874.0

Note: TRC_LF – triradial (delta) count of the toes of the left foot; TRC_RF – triradial (delta) count of the toes of the right foot; TTRC_PZ_LF – total triradial (delta) count of the plantar zone of the left foot; TTRC_PZ_RF – total triradial (delta) count of the plantar zone of the right foot.

Table 7. Results of the comparative analysis of triradial (delta) counts of the toes and plantar zones using the nonparametric Mann-Whitney U test.

	TRC_LF	TRC_RF	TTRC_PZ_LF	TTRC_PZ_RF
Mann-Whitney U	240.5	273.0	159.5	171.0
Wilcoxon W	360.5	393.0	862.5	874.0
Z	-0.938	-0.106	-2.704	-2.454
Asymp. Sig. (2-tailed)	0.348	0.915	0.007	0.014

Discussion

The obtained results demonstrate pronounced and statistically significant gender-specific differences in plantar dermatoglyphic parameters among individuals who died by suicide. This finding supports the interpretation of plantar dermatoglyphic structures as potential biomarkers of neuropsychological vulnerability and as indicators of embryogenetic stability, correlating with the risk of suicidal behavior. Such an approach aligns with modern concepts regarding phenotypic markers of psychopathology, described in research on affective and depressive disorders [11, 20].

Male suicide victims exhibited significantly higher ridge counts on the 1st radial toe of both the left and right foot ($p=0.017$; $p=0.006$). Increased ridge counts are traditionally associated with a more complex organization of epidermal ridges and enhanced transverse differentiation of ectodermal structures. Similar associations have been reported in studies of individuals with psychiatric disorders, particularly in depressive states and impairments of affective regulation [14, 20], as well as in populations demonstrating altered overall dermatoglyphic symmetry [13, 19]. Our findings are consistent with a systematic review of minor physical anomalies and dermatoglyphic markers in affective disorders, which identified a higher frequency of morphogenetic variations in patients with psychiatric conditions [4].

Gender differences in triradial (delta) counts, specifically the significantly higher values in the plantar digital zones of female subjects ($p = 0.018$; $p = 0.010$), may indicate disturbances in early morphogenetic stability formed between the 13th and 19th gestational weeks. This developmental period coincides with the simultaneous formation of cortical brain structures; therefore, plantar dermatoglyphics may reflect the emergence of neurobehavioral traits. Comparable changes have been reported in studies of patients with schizophrenia, where increased delta counts and disorganization of epidermal ridges were observed in plantar regions [21].

Moreover, women generally exhibit a different neurobiological risk profile for suicidal behavior, which is reflected in studies analyzing gender-specific patterns among adolescents and adults [11, 15, 26]. Our findings confirm this trend at the morphological level, which may have practical value for forensic identification and the reconstruction of biobehavioral characteristics in postmortem analysis.

In the context of plantar dermatoglyphics, the subdigital area is particularly informative, as it demonstrated the most pronounced sex differences. Similar observations appear in studies focusing on dermatoglyphic markers in affective and neurobiological disorders [24, 27], where authors emphasize the diagnostic usefulness of these regions. Conversely, the absence of significant differences in the hypothenar areas is consistent with previous anatomical research, where hypothenar patterns showed lower correlations with psychiatric pathology [4, 26].

The forensic context is also essential. An increased delta count in specific plantar zones may be valuable in cases where standard identification methods are unavailable, such as in complex suicides, mass disasters, or military conflict settings [3, 10, 25]. This aligns with reports highlighting the growing role of morphological markers in postmortem identification under contemporary conditions [8, 12].

Our results also reflect broader trends in the study of biomarkers of suicidal behavior. Evidence accumulated in recent years indicates the importance of a multidisciplinary approach: integrating genetic, behavioral, neurobiological, and morphological indicators provides a more comprehensive model of suicide risk [7, 17, 28].

At the same time, this study has several limitations: a small sample size; lack of stratification by psychiatric diagnoses; possible influence of external factors (stressful events, intoxications, socioeconomic status); and the need for comparison with normative population dermatoglyphic databases [16, 19].

Future research perspectives include expanding the sample with consideration of age, ethnic background, and psychiatric history; conducting genetic analyses of developmental stability; integrating plantar dermatoglyphics with digital identification methods that have demonstrated effectiveness in forensic models [5, 21, 29]; and applying machine-learning techniques to develop predictive risk models.

Thus, the findings of this study broaden current understanding of morphological markers of suicidal behavior and confirm the relevance of plantar dermatoglyphics as a potential tool for forensic identification and expert assessment of psychobiological risk.

Conclusions

1. The study established that the ridge counts and delta counts of plantar skin patterns show gender-related variability in individuals who died by suicide. The most pronounced differences were identified in the ridge count values of the distal phalanges of the first toe on both feet (radial zones), as well as in the delta count of the subdigital areas, where women demonstrated a statistically significant increase in the number of elements compared with men. This may indicate differences in embryogenesis and support the role of dermatoglyphics as a marker of neuropsychic instability.

2. The results demonstrate the potential applicability of plantar skin patterns in forensic practice, particularly for refining the personal profile of unidentified individuals and for analyzing vulnerability to suicidal behavior. The use of non-parametric statistical methods proved appropriate due to the non-normal distribution of most of the studied variables.

References

[1] Aiartzaguena, M., & Morentin, B. (2022). Risk factors for completed suicide in young people and middle-aged adults: Population forensic study. *Spanish Journal of Legal Medicine,* 48(2), 53-59. doi: 10.1016/j.remle.2021.09.002

[2] Al-Halabí, S., & Fonseca-Pedrero, E. (2021). Suicidal behavior prevention: The time to act is now. *Clínica y Salud*, 32(2), 89-92. doi: 10.5093/clysa2021a17

[3] Austin, A. E., & Byard, R. W. (2013). Skin messages in suicide – An unusual occurrence. *Journal of Forensic and Legal Medicine*, 20(6), 618-620. doi: 10.1016/j.jflm.2013.03.017

[4] Berecz, H., Csábi, G., Herold, R., Trixler, D., Fekete, J., & Tényi, T. (2017). Minor physical anomalies and dermatoglyphic signs in affective disorders: A systematic review. *Psychiatr Hung*, 32(1), 108-127.

[5] Bhuvaneshwari, S., Chand, S., Chaudhari, D., Manohar, B., Buyan, L., & Srinivasan, S. (2023). Dactoscopy in Human Identification: A Retrospective Study in Bhubaneswar City. Journal of Pharmacy and Bioallied Sciences, 15(Suppl 1), S326-S329. doi: 10.4103/jpbs.jpbs_526_22

[6] Bose, P. K., Kushal, S. A., & Arafat, S. Y. (2023). *Forensic and legal aspects of suicide in Bangladesh. In Suicide in Bangladesh: Epidemiology, Risk Factors, and Prevention.* Singapore: Springer Nature Singapore. doi: 10.1007/978-981-99-0289-7_2

[7] Carretta, R. F., McKee, S. A., & Rhee, T. G. (2023). Gender differences in risks of suicide and suicidal behaviors in the USA: A narrative review. *Current psychiatry reports*, 25(12), 809-824. doi: 10.1007/s11920-023-01473-1

[8] De Simone, S., Alfieri, L., Bosco, M. A., Cantatore, S., Carpinteri, M., Cipolloni, L., & Neri, M. (2024). The forensic aspects of suicide and neurotrophin factors: a research study. *Frontiers in Pharmacology*, 15, 1392832. doi: 10.3389/fphar.2024.1392832

[9] Dunayev, O., Gunas, I., Popadynets, O., Kozoviy, R., & Kindrativ, E. (2021). Theoretical justification of the dermatoglyphics use as basic identification method. *Galician Medical Journal*, 28(1), E202116. doi: 10.21802/gmj.2021.1.6

[10] Galante, N., Gentile, G., Tambuzzi, S., & Zoja, R. (2022). Suicide pacts in the Milan district (Italy): A retrospective autopsy-based study with literature review. *Journal of Forensic and Legal Medicine*, 86, 102319. doi: 10.1016/j.jflm.2022.102319

[11] Grossberg, A., & Rice, T. (2023). Depression and suicidal behavior in adolescents. *Medical Clinics*, 107(1), 169-182. doi: 10.1016/j.mcna.2022.04.005

[12] Gualtieri, S., Lombardo, S., Sacco, M. A., Verrina, M. C., Tarallo, A. P., Carbone, A., ... & Aquila, I. (2025). Suicide in Italy: Epidemiological Trends, Contributing Factors, and the Forensic Pathologist's Role in Prevention and Investigation. *Journal of Clinical Medicine*, 14(4), 1186. doi: 10.3390/jcm14041186

[13] Gunas, V. I. (2019). Correlations of indices of personality traits with indexes of finger and palmar dermatoglyphics of practically healthy Ukrainian men. *Biomedical and Biosocial Anthropology*, (34), 20-25. doi: 10.31393/bba34-2019-03

[14] Hemasankar, C., Rao, S. R., Balaji, K., Yeturu, S. S., Ragavendra, M. P., & Krishnan, M. (2023). Fingerprint patterns in neuropsychological disorder depression among south Indian population. *Bioinformation*, 19(3), 266-271. doi: 10.6026/97320630019266

[15] Hua, L. L., Lee, J., Rahmandar, M. H., Sigel, E. J., Committee on Adolescence, & Council on Injury, Violence, and Poison Prevention. (2024). Suicide and suicide risk in adolescents. Pediatrics, 153(1), e2023064800. doi: 10.1542/peds.2023-064800

[16] Ibeh, O. O. (2025). Evaluation of Digital Dermatoglyphic Patterns and Sex Distribution among the Ikot Obong Otoro Population of Akwa Ibom State, Nigeria. *Tropical Journal of Science and Technology*, 6(1), 30-37. doi: 10.47524/tjst.v6i1.31

[17] Johnston, J. N., Campbell, D., Caruncho, H. J., Henter, I. D., Ballard, E. D., & Zarate Jr, C. A. (2022). Suicide biomarkers to predict risk, classify diagnostic subtypes, and identify novel therapeutic targets: 5 years of promising research. I*nternational Journal of Neuropsychopharmacology*, 25(3), 197-214. doi: 10.1093/ijnp/pyab083

[18] Kaur, M., & Sharma, K. (2016). Dermal digital ridge density of a penal population: Analysis of association and individualization. *Journal of Forensic and Legal Medicine*, 44, 143-149. doi: 10.1016/j.jflm.2016.10.011

[19] Li, G., Sun, Z., Li, Z., Cheng, H., & Liu, M. (2025). Investigation and analysis of hand characteristics of Chinese Han youth in Shandong province: A cross-sectional study. *Medicine*, 104(26), e43189. doi: 10.1097/MD.0000000000043189

[20] Maciejewski, D. F., Renteria, M. E., Abdellaoui, A., Medland, S. E., Few, L. R., Gordon, S. D., ... & Verweij, K. J. (2017). The association of genetic predisposition to depressive symptoms with non-suicidal and suicidal self-injuries. *Behavior genetics*, 47(1), 3-10. doi: 10.1007/s10519-016-9809-z

[21] Majeed, N. S., Arko-Boham, B., Fiagbe, D. K., Adutwum-Ofosu, K. K., Koney, N. K. K., Hottor, B. A., ... & Ahenkorah, J. (2023). Digital-palmar dermatoglyphics characteristics of patients living with schizophrenia in Ghana. *All Life*, 16(1), 2224937. doi: 10.1080/26895293.2023.2224937

[22] Mamun, M. A., Siddique, A. B., Sikder, M. T., & Griffiths, M. D. (2022). Student suicide risk and gender: a retrospective study from Bangladeshi press reports. *International Journal of Mental Health and Addiction*, 20(3), 1438-1445. doi: 10.1007/s11469-020-00267-3

[23] Murakami, R., Kamikubo, A., Morioka, D., & Kuroki, H. (2024). Forensic analysis of suicide deaths: comparing forensic information with public information and investigating factors contributing to psychiatric consultations. *Psychiatry and Clinical Neurosciences Reports*, 3(2), e194. doi: 10.1002/pcn5.194

[24] Pal, A. K., Ray, S., & Bhattacharya, J. (2021). Use of dermatoglyphic parameters as possible markers in bipolar affective disorder. *International Journal of Health Sciences and Research*, 11(7), 509-515. doi: 10.52403/ijhsr.20210753

[25] Pallocci, M., Passalacqua, P., Zanovello, C., Coppeta, L., Ferrari, C., Milano, F., ... & Treglia, M. (2024). Forensic characterisation of complex suicides: a literature review. *Forensic Sciences*, 4(3), 277-288. doi: 10.3390/forensicsci4030020

[26] Ramchand, R., Schuler, M. S., Schoenbaum, M., Colpe, L., & Ayer, L. (2022). Suicidality among sexual minority adults: Gender, age, and race/ethnicity differences. American Journal of Preventive Medicine, 62(2), 193-202. doi: 10.1016/j.amepre.2021.07.012

[27] Ray, A. K., Duari, R. K., & Gole, S. N. (2015). Dermatoglyphics: A method of sex differentiation - A study. *Journal of Evolution of Medical and Dental Sciences*, 4(49), 8461-8465. doi: 10.14260/jemds/2015/1227

[28] Sudol, K., & Mann, J. J. (2017). Biomarkers of suicide at-

tempt behavior: towards a biological model of risk. *Current Psychiatry Reports*, 19(6), 31. doi: 10.1007/s11920-017-0781-y

[29] Vasan, M. D., & Thakar, B. R. (2019). Predictive Digital Forensic Model to Track Antisocial Behavior Based on Dermatoglyphics. In: Peng, SL., Dey, N., Bundele, M. (eds) Computing and Network Sustainability. *Lecture Notes in Networks and Systems, vol 75. Springer, Singapore*. doi: 10.1007/978-981-13-7150-9_37

ГРЕБІНЦЕВІ Й ДЕЛЬТОВІ РАХУНКИ ШКІРНИХ ВІЗЕРУНКІВ ПІДОШВИ У САМОГУБЦІВ: ГЕНДЕРНІ ОСОБЛИВОСТІ

Чадюк В. О., Коцюбинська Ю. З., Колев Я.Г., Фенцик В. Л., Шутак О. В., Юрак М. З., Солоджук Ю. І., Козань Н. М.

Проблема вивчення морфологічних маркерів схильності до суїцидальної поведінки залишається актуальною як у судово-медичному, так і в психобіологічному контексті, особливо з огляду на зростання рівня самогубств у сучасному суспільстві. Дерматогліфічні характеристики підошвових поверхонь стоп людини – гребінцеві та дельтові рахунки – є стабільними ембріогенетично детермінованими ознаками, які формуються на 13-19 тижні внутрішньоутробного розвитку одночасно з центральною нервовою системою і можуть бути пов'язані з психофізіологічними особливостями особи. Метою дослідження стало виявлення гендерних особливостей шкірних візерунків підошви у самогубців та оцінка можливості їх застосування в судово-медичній практиці для ідентифікації та прогнозування ризиків. Матеріал дослідження включав відбитки підошов 52 осіб, які вчинили самогубство (37 чоловіків, 15 жінок), віком від 18 до 59 років та 50 осіб контрольної групи (25 чоловіків та 25 жінок). Використовували метод фотографування дерматогліфів з подальшою обробкою зображень за допомогою спеціалізованого програмного забезпечення. Вимірювали гребінцеві та дельтові рахунки дистальних фаланг пальців ніг, а також зон тенара, гіпотенара і підпальцевої ділянки стоп. Статистичний аналіз передбачав перевірку нормальності розподілу (критерії Шапіро-Вілка, Колмогорова-Смірнова) та застосування непараметричного критерію Манна-Уїтні для оцінки міжгрупових відмінностей при p<0,05. Встановлено статистично значущі гендерні відмінності в дерматогліфічних показниках: у чоловіків-самогубців виявлено вірогідно вищі значення гребінцевого рахунку 1-го пальця (радіальні зони) обох ніг (p=0,017; p=0,006), що може вказувати на складнішу організацію епідермальних гребенів. У жінок-самогубців зафіксовано достовірно вищі значення дельтового рахунку в підпальцевих зонах як лівої (p=0,018), так і правої ноги (p=0,010), що свідчить про морфогенетичні особливості та можливу асоціацію з нейропсихічною вразливістю. Для гіпотенарів стоп значущих гендерних відмінностей не виявлено, що підтверджує їх меншу діагностичну цінність. Виявлені закономірності демонструють високий потенціал дерматогліфічного аналізу підошви як додаткового інструмента судово-медичної ідентифікації осіб та об'єктивного маркера оцінки ризику суїцидальної поведінки з можливістю практичного застосування в експертній діяльності.

Ключові слова: *дерматогліфіка стопи, суїцидальна поведінка, гребінцевий рахунок, дельтовий рахунок, гендерні відмінності, судово-медична ідентифікація.*

Author's contributions

Chadiuk V. O. – conceptualization, writing – original draft.
Kotsiubynska Yu. Z. – data curation, validation, formal analysis.
Kolev Ya. G. – methodology, resources.
Fentsyk V. L. – investigation, literature search.
Shutak O. V. – project administration.
Yurak M. Z. – project administration.
Solodzhuk Yu. I. – methodology.
Kozan N. M. – supervision, scientific guidance.

DOI: 10.31393/morphology-journal-2025-31(4)-05 Reports of Morphology, Vol. 31, №4, Pages 36-41

ISSN 1818-1295 eISSN 2616-6194

REPORTS OF MORPHOLOGY

Official Journal of the Scientific Society of Anatomists, Histologists, Embryologists and Topographic Anatomists of Ukraine

journal homepage: https://morphology-journal.com

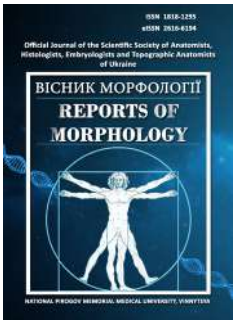

Topographical-anatomic features of the pineal gland in laboratory rats of the Wistar line

Pshychenko V. V.[1,2], Cherno V. S.[1], Korolyova O. V.[1,2], Naidich O. V.[2], Iovenko A. V.[2], Brodovskyi V. A.[2]

[1] Petro Mohyla Black Sea National University, Mykolaiv, Ukraine

[2] Mykolaiv National Agrarian University, Mykolaiv, Ukraine

ARTICLE INFO

Received: 21 January 2025

Accepted: 5 September 2025

UDC: 591.481.3

CORRESPONDING AUTHOR

e-mail: pshychenko85@gmail.com

Pshychenko V. V.

CONFLICT OF INTEREST

The authors have no conflicts of interest to declare.

FUNDING

Not applicable.

DATA SHARING

Data are available upon reasonable request to corresponding author.

The pineal gland is an organ of the central endocrine system that coordinates the activity of peripheral endocrine glands, immune and nervous systems, regulates biological rhythms, ensures adaptation processes and triggers the stress response. The pineal gland is inherent in almost all vertebrates, but there are different variations in the shape and location of the pineal gland in the brain of animals even within the same species. Most often, laboratory rats of the Wistar line are use for laboratory research, and for the correct interpretation of the results obtained, species-specific anatomical features and possible individual variations in the location of the pineal gland in normal laboratory rats should be taken into account. The aim of the work was to study the features of the anatomical structure and topography of the pineal gland in white laboratory rats of the Wistar line. The pineal glands of 24 sexually mature male Wistar laboratory rats were examine. Morphological, morphometric and statistical research methods were use. During the study, individual variations in the topography, shape, and blood supply of the pineal gland in laboratory rats were identify. It has been establish that in some animals the pineal gland was located in the groove between the posterior edges of the occipital lobes of the cerebral hemispheres, was richly supply with blood by a large number of blood vessels, and had either an oval or a conical shape. In other animals, the pineal gland was located in the groove between the upper anterior corpora quadrigemina. In this case, the pineal gland was supply with blood by a small number of blood vessels, and the shape of the pineal gland with such localization in the brain was rounded. Individual variations in the linear dimensions of the epiphysis have been establish. When studying morphometric parameters, it was found that the transverse size of the pineal glands was the most stable, while the vertical size was more labile, which probably caused individual differences in the volumes of the pineal glands in the studied rats. Thus, the obtained results of the study on individual variations in the anatomical, topographic and morphometric structure of the pineal gland in intact laboratory Wistar rats can be the basis for assessing pathological changes in the organ when conducting experimental studies in medical and biological fields.

Keywords: *brain, pineal gland, anatomy, topography, laboratory rats, individual variations.*

Introduction

The pineal gland, or epiphysis cerebri, is an organ of the central endocrine system that has close morpho-functional connections with the central nervous system and coordinates the activities of peripheral endocrine glands, the immune and nervous systems. [12, 25]. It is known that the pineal gland is inherent in almost all vertebrates, but in different classes of animals, there are peculiarities of its structure, which is associated not only with the climatic conditions of residence, lifestyle, and weight of animals, but also with evolutionary changes, from the photoreceptor organ in fish to the neuroendocrine organ in mammals [18, 22, 30, 31]. In all animal species, the main functions of the pineal gland are the regulation of biological rhythms, in particular the sleep-wake cycle, reproductive cycles, triggering the neuroendocrine response to stress of various origins, and ensuring adaptive processes in the body [4, 8, 16].

In recent years, a very large number of scientific publications by both Ukrainian researchers and scientists from other countries have been devoted to the structure and functions of the pineal gland [28]. Increased interest in the pineal gland is due primarily to the wide spectrum of biological action of the hormone it synthesizes - melatonin and its successful use in various areas of medicine for the purpose of correction and prevention of diseases of various genesis [3, 20, 24, 29]. In addition, the pineal gland is a source of such important biological substances as tryptophan and serotonin, which regulate vital processes occurring in the body [15, 27]. At the same time, it should be noted that the pineal gland is the least studied endocrine gland, which is due to the small size of the organ and topographic features that complicate its atraumatic removal [4, 9, 19]. In this regard, the morphological features of the pineal gland of various animal species are still poor described in literary sources. In addition, according to literature data, there are different variations in the shape and location of the pineal gland in the brain of vertebrates, even within the same species [10]. Considering the fact that animals, especially laboratory rats, are objects that are most often used for experimental research in biological and medical fields, which is due to the similarity of the structural organization of human and animal organs, for the correct interpretation of the obtained research results, one should take into account not only the species-specific features of the anatomical structure of this organ, but also possible individual variations of its location in laboratory rats of the Wistar line in the norm.

The purpose of the study was to study the features of the anatomical structure and topography of the pineal gland in white laboratory rats of the Wistar line.

Materials and methods

The results of this work are a fragment of the research topic of the Department of Morphology and Public Health of the Petro Mohyla Black Sea National University of the Ministry of Education and Science of Ukraine “The influence of environmentally hazardous factors on the mechanisms of development of civilization diseases and their correction with physiologically active substances”, state registration number 0124U002163.

An anatomical and experimental study was conducted on 24 intact male laboratory Wistar rats weighing 180-220 g, who had reached sexual maturity. The choice of males for the study was due to the lack of fluctuations in the level of melatonin in the blood plasma compared to females, in which the concentration of the melatonin hormone, the morphological and functional state of the pineal gland are determined by the phase of the sexual cycle. All experimental animals were kept in standard vivarium conditions and had free access to food and drinking water. Artificial light sources not used in the vivarium, since the pineal gland responds to changes in light levels with morpho-functional restructuring. The study was carried out under natural lighting typical during the autumn-winter period.

The object of the study was the pineal gland. In order to remove the pineal gland, laboratory rats were fixed on a dissecting board using special straps [13]. After fixation, the animals were removed from the experiment by single-step decapitation under intraperitoneal thiopentane anesthesia at a rate of 25 mg/kg body weight. Excess wool on the animals’ heads was removed at the incision site using scissors [9]. After completion of the decapitation procedure, the skull of the animals was scalped with subsequent removal of the cranial vault along with the dura mater. Then the brain, along with the pia mater, was separated from the base of the skull and the pineal gland was isolated. Next, the isolated pineal glands was subjected to morphometric measurements, namely, the length and width of the organ (mm) were determined. Caliper were used to conduct organometric measurements of the sizes of the studied glands (mm). Then, the pineal gland was fixed in a 10 % neutral formalin solution. After fixation, dehydration was performed in alcohols of increasing concentration, after which the studied material was embedded in paraffin and sections 4-5 μm thick were made on a semi-automatic rotary microtome “Microm” type (Germany). The histological specimens thus obtained were stained with hematoxylin and eosin according to standard methods. After embedding the specimens in Canadian balsam, histological preparations of the pineal gland were studied at a magnification of eyepiece ×10 and objectives ×4, ×10 of a microscope of the “Carl Zeiss” brand (Germany). Photo documentation of the research results was performed using a Canon digital SLR camera.

All stages of the study were carried out in accordance with the current requirements of the general principles of work with experimental animals in accordance with the following standards: Council of Europe Convention on Bioethics (1997); European Convention for the Protection of Vertebrate Animals Used for Experimental and Other Scientific Purposes, General Ethical Principles of Experiments on Animals, approved by the First National Congress of Ukraine on Bioethics (2001); Law of Ukraine “On the Protection of Animals from Cruelty” (2006) and other international treaties and current national legislation in the field of biomedical research. The study was conducted according to a protocol approved by the Bioethics Commission of the Petro Mohyla Black Sea State University (Protocol No. 4 dated June 24, 2024).

We entered the determined quantitative morphometric data characterizing the linear dimensions of the pineal glands into the electronic research journal and subjected it to statistical analysis. For all indicators, arithmetic means, standard mistakes of the arithmetic mean, and standard deviation were calculated. Statistical calculations were performed on a personal computer using standard software “STATISTICA 6” for computers with the Windows operating system.

Results

The pineal gland in animals belonging to the mammalian

class is located in the median plane between the upper anterior corpora quadrigemina. According to the results of our morphological studies, it was found that the shape and location of the pineal gland in the brain in laboratory Wistar rats had some individual variations. Thus, in most experimental animals, the narrowed apex of the pineal gland was located in the groove between the posterior edges of the occipital lobes of the cerebral hemispheres, above and caudal to the cerebellum and in direct contact with the tissue of the third ventricle of the brain. The other, opposite part of the pineal gland was directed towards the cerebral hemispheres. Therefore, we divided the pineal gland into three conditional parts. We designated the distal pole, directed towards the cerebral hemispheres, as the base, and the proximal pole, which faces the third ventricle, as the apex. The middle part of the organ, located between the poles, was called the body. With the described variant of location in the brain, two possible forms of the pineal gland were encountered on longitudinal sections made through the center of the studied organ. Thus, in some animals, the pineal gland appeared as a light red formation and had an elongated oval shape with two pointed edges (Fig. 1).

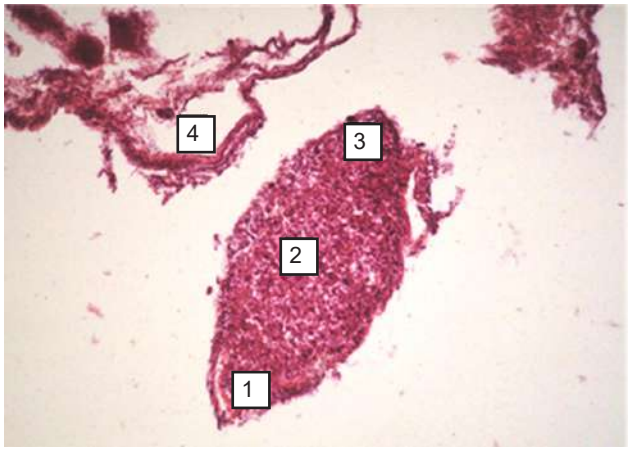

Fig. 1. Microphotograph of the pineal gland of laboratory Wistar rats. Oval shape of the pineal gland. 1 – narrowed apex; 2 – body; 3 – base of the epiphysis; 4 – extraorgan blood vessels. Hematoxylin and eosin staining. ×40.

In other laboratory animals, the pineal gland had a cone-shaped shape. At the same time, one of the ends of the studied organ, which faced the third ventricle, was pointed, while the opposite end, facing the cerebral hemispheres, was thickened and rounded (Fig. 2).

With this placement in the brain, it was noted that the pineal gland was surrounded by a large number of blood vessels of large and small caliber and had a red-gray color, which distinguished it from other parts of the brain. The detected vascular plexuses were a direct continuation of the vascular plexus of the third ventricle of the brain and in most animals penetrated into the studied organ. However, it should be noted that the upper surface of the pineal gland was free and had no contact with blood vessels.

In the other part of the laboratory rats studied, the apical

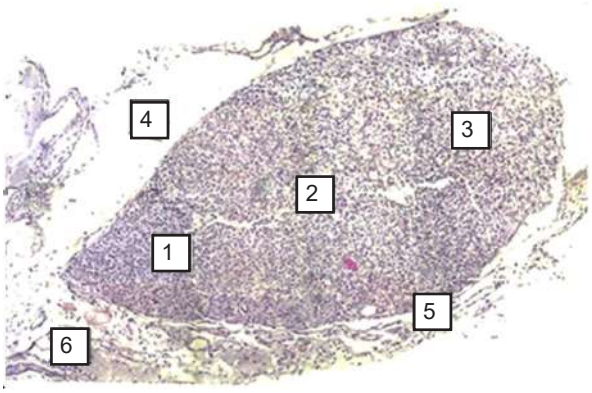

Fig. 2. Micrograph of the pineal gland of laboratory Wistar rats. Cone-shaped shape of the pineal gland. 1 – narrowed apex; 2 – body; 3 – rounded base; 4 – expanded subarachnoid space; 5 – narrowed subarachnoid space; 6 – extraorgan blood vessels. Hematoxylin and eosin staining. ×100.

part of the pineal gland was not identified in the sulcus between the occipital lobes of the cerebral hemispheres. In these cases, the pineal gland was found in the groove between the upper anterior corpora quadrigemina. At the same time, visualization of the pineal gland was complicated, since to detect it, it was necessary to lower the cerebellum and elevate the occipital lobes of the cerebral hemispheres. In some animals, the pineal gland was connected by a plate of the pia mater to the lower surface of the cerebral hemispheres. It should be noted that with such a topography of the pineal gland, there was no close connection with the vascular plexus, and the color of the pineal gland was light gray, which is explained by the smaller number of blood vessels in contact with this organ. It was found that one, at most two blood vessels approached the pineal gland, which tightly surrounded it, branched and penetrated the organ. It was established that the source of blood supply to the organ in this case was the vascular plexus located under the cover of the third ventricle of the brain. It should be noted that the shape of the pineal gland with this placement was rounded (Fig. 3).

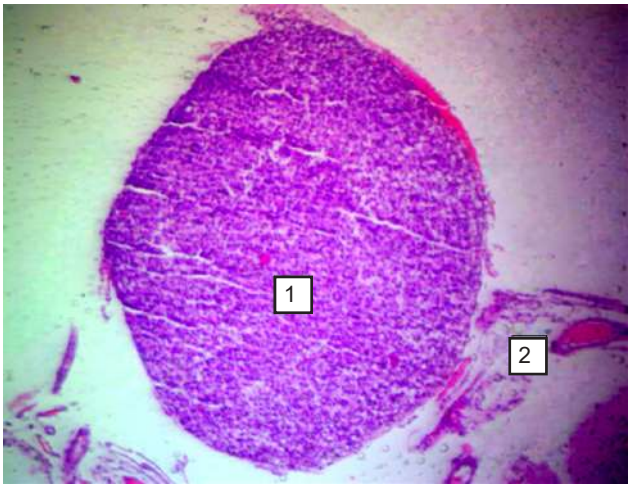

Fig. 3. Micrograph of the pineal gland of Wistar laboratory rats. Rounded shape of the pineal gland. 1 – pineal gland; 2 – extraorgan blood vessels. Hematoxylin and eosin staining. ×100.

It was found that the outer surface of the pineal gland was surrounded by a continuation of the pia mater and arachnoid membrane of the brain. At the same time, it was noted that the subarachnoid space in the apex region was the widest, but when moving to the main part, it gradually narrowed (see Fig. 2). It can be assumed that the width of the subarachnoid space varies depending on individual fluctuations in the size of the organ itself or on the degree of filling it with cerebrospinal fluid. On the outside, the pineal gland was covered by a thin capsule formed by connective tissue. The capsule was tightly attached to the pineal gland and contained blood vessels. In places, connective tissue membranes extended from the capsule into the organ, dividing the parenchyma into lobes of various sizes. The intercellular membranes contained numerous blood vessels and nerve fibers.

During further anatomical studies, variations in the linear dimensions of the pineal gland in experimental animals were established. Thus, in rats whose pineal gland had a conical shape, the average length was 1.141±0.912 mm, and the width in the widest part was 0.884±0.382 mm. For animals whose pineal gland was oval shape, the following average linear dimensions were characteristic: length was 1.263±0.722 mm, and width was 0.812±0.294 mm. With a rounded shape of the pineal gland, its average length was 1.023±0.872 mm, and its width was 0.911±0.363 mm. As the obtained digital data showed, the transverse size of the pineal glands was the most stable, while the vertical size was more labile, which probably determines the individual differences in the glands volumes.

Discussion

The presented study was aimed at supplementing data on the topographic and anatomical features of the pineal gland in laboratory Wistar line rats, since information on possible variations in the location of the pineal gland in the domestic and foreign literary sources we reviewed is sparse.

According to these literature sources, the pineal gland in different classes and species of animals has anatomical and physiological features that are determined by a number of factors, including climatic conditions of residence, lifestyle, animal's weight, circadian and seasonal rhythms [13]. In addition, significant sexual differences in the linear dimensions of the pineal gland within the species are noted [7, 11]. The results of our study indicate that the topography, shape, and size of the pineal gland in Wistar line rats differ and have individual anatomical variations within the species, which is consistent with the data of other authors' research results [10]. Morphological studies have shown that there are two main types of pineal gland localization in the rat brain [10]. It was found that in some laboratory rats, the pineal gland was located in the groove between the posterior edges of the occipital lobes of the cerebral hemispheres. A similar variant of the pineal gland location has been observed in other vertebrates [1, 2]. With this placement, the pineal gland had an oval or cone-shaped shape and a close connection with the choroid plexus of the third ventricle [12, 14, 17, 30]. At the same time, the blood supply to the organ was intensive, as it occurred due to a large number of blood vessels [25]. It should be noted that the intensive blood supply also affected the color of the pineal gland, which manifested itself as a red-gray formation [10]. In other animals, the pineal gland was located in the groove between the upper anterior corpora quadrigemina and was characterized by a rounded shape [14. 21, 26]. With such topographic features, a small number of blood vessels approached the pineal gland, which branched and penetrated into the organ parenchyma. With the described variant of the pineal gland's location in the brain, its color was light gray. It is also necessary to note the fact that with all the identified variations in the location of the pineal gland, there was always a connection with the vascular plexus of the third ventricle of the brain, which is also indicated by the data of studies by other authors [10, 23]. Differences in the color of the pineal gland in different placement options may be associated with a different number of blood vessels that contact the pineal gland and penetrate its parenchyma, as well as with the intensity of blood supply to the organ under study [14].

Externally, the pineal gland was surrounded by the soft meninges of the brain and was washed by cerebrospinal fluid [6]. A thin connective tissue capsule, which contained a large number of blood vessels, was tightly attached to the pineal gland [14]. Connective tissue membranes extended from the capsule into the organ, dividing the parenchyma into lobules. In general, the described histological features of the pineal gland were typical for this organ and corresponded to the literature data on the structure of the pineal gland in rats and other vertebrates [12, 14].

Depending on the shape of the pineal gland, we also detected changes in its linear indicators. Thus, in the oval and conical shape, the length of the pineal glands exceeded the length of the pineal glands, which were characterized by a rounded shape. Instead, the width of the round-shaped pineal glands was greater. It should be noted that the shape of the pineal gland and its linear dimensions influenced the volume of the subarachnoid space, which was wide in the apex and narrowed as it moved towards the main part. The linear dimensions of the pineal glands we have established correlate with the data of other researchers and are within the physiological norm for rodents [12, 13].

Thus, our morphological and morphometric analysis of macropreparations and histological sections of the pineal gland of laboratory Wistar rats allowed us to characterize in detail its possible individual topographic and anatomical features.

This experimental article differs from those published in this field in that it is the first to describe and analyze possible individual variations in the location of the pineal gland in laboratory Wistar rats. The morphological analysis performed allowed us to systematize the obtained experimental data and present a comparative topographic and anatomical characteristic of the pineal gland in animals that are most often used in experimental studies.

Conclusions

1. The anatomical features of the pineal gland in laboratory rats of the Wistar strain have certain species and individual variations, which are determined by the peculiarities of the topography, shape, and blood supply of the organ, which must be taken into account when conducting experimental studies and interpreting the results obtained.

2. Two variants of the pineal gland location in the brain of laboratory rats have been established. In some animals, the pineal gland was located in the groove between the posterior edges of the occipital lobes of the cerebral hemispheres, was richly supplied with blood by a large number of blood vessels, and had either an oval shape with two pointed edges or a cone-shaped shape. In other animals, the epiphysis was located in the groove between the upper anterior corpora quadrigemina, blood supply was provided by a small number of blood vessels and the shape of the epiphysis with such localization was rounded.

3. The morphometric data obtained as result of the study on the linear dimensions of the epiphyses in intact laboratory Wistar rats can be the basis for assessing pathological changes in the organ in the experiment.

References

[1] Barcelos, R. P., Filadelpho, A. L., Baroni, S., & Graça, W. J. (2015). The morphology of the pineal gland of the Magellanic penguin (Spheniscus magellanicus Forster, 1781). *Journal of Morphological Sciences, 32*(3), 149-156. doi: 10.4322/jms.081814

[2] Beheiry, R., & Moselhy, A. A. A. (2016). Macro and microscopical studies on the pineal gland of camel with immunohistochemical localization to pinealocytes and glia cells markers. *International Journal of Advanced Research, 4*(8), 1154-1163. doi: 10.21474/IJAR01/1317

[3] Berzin, O. V., & Kondratiuk, V. E. (2023). Фармакологічна дія мелатоніну та можливість його застосування при лікуванні подагри та супутніх захворювань [Pharmacological effects of melatonin and its potential application in therapy of gout and associated diseases]. *Актуальні проблеми сучасної медицини: Вісник Української медичної стоматологічної академії=Actual problems of modern medicine: Bulletin of the Ukrainian Medical Stomatological Academy, 24*(86), 284-292. doi: 10.31718/2077–1096.24.2.284

[4] Bruno, F., Arrigoni, F., Maggialetti, N., Natella, R., Reginelli, A., Cesare, E. Di., … & Giovagnoni, A. (2019). Neuroimaging in emergency: a review of possible role of pineal gland disease. *Gland Surgery, 8*(2), 133-140. doi: 10.21037/gs.2019.01.02

[5] Câmara, F. V., Lopes, I. R., de Oliveira, G. B., Bezerra, F. V., de Oliveira, R. E., Oliveira Júnior, C. M., … & de Oliveira, M. F. (2015). The morphology of the pineal gland of the yellow-toothed cavy (Galea Spixii Wagler, 1831) and red-rumped agouti (Dasyprocta leporina linnaeus, 1758). *Microscopy Research and Technique, 78*(8), 660-666. doi: 10.1002/jemt.22519

[6] Contreras-De La Hoz, D. L., Viracacha-López, G. C., Sarmiento-Palma, J. V., Gutierrez, L. L., Mantilla-Pardo, J. C., Blanco-Fernandez, G. A., … & Caicedo-Lozada, R. A. (2021). Recent descriptions on physiological concepts of the pineal gland: what's new? *Romanian Neurosurgery, 35*(4), 518-525. doi: 10.33962/roneuro-2021-089

[7] Diaz, M. D. W., Reátegui, A. H. C., & Zamora, M. B. N. (2022). Macro and microscopic study of the pineal gland of the adult alpaca (Vicugna pacos). *Revista de Investigaciones Veterinarias del Perú, 33*(4), e233-38. doi: 10.15381/rivep.v33i4.23338

[8] Favero, G., Bonomini, F., & Rezzani, R. (2021). Pineal Gland Tumors: A Review. *Cancers (Basel), 13*(7), 1547. doi: 10.3390/cancers13071547

[9] Gallo, C. C., Nishino, F. A., Gaspar do Amaral, F., & Cipolla-Neto, J. (2022). Pinealectomy in Rats. *Methods in molecular biology, 2550*, 45-51. doi: 10.1007/978-1-0716-2593-4_7.0

[10] Gheban, B. A., Rosca, I. A., & Crisan, M. (2019). The morphological and functional characteristics of the pineal gland. *Medicine and Pharmacy Reports, 92*(3), 226-234. doi: 10.15386/mpr-1235

[11] Han, Q., Li, Y., Wang, J., & Zhao, X. (2018). Sex Difference in the Morphology of Pineal Gland in Adults Based on Brain Magnetic Resonance Imaging. *Journal of Craniofacial Surgery, 29*(5), e509-e513. doi: 10.1097/SCS.0000000000004558

[12] Hryntsova, N. (2022). Реадаптаційні перебудови епіфіза статевозрілих щурів після впливу на організм клітинного зневоднення [Readaptational adjustments of mature rat's epiphysis after influence on the cellular dehydration]. *Екологічні науки=Ecological Sciences, 1*(40), 50-54. doi: 10.32846/2306-9716/2022.eco.1-40.9

[13] Hryntsova, N. B., & Romaniuk, A. M. (2020). *Спосіб ідентифікації і атравматичного вилучення епіфіза у щурів [Method of identification and atraumatic extraction of pineal gland in rats].* UA. Patent No. 142276 U. Суми: Міністерство розвитку економіки, торгівлі та сільського господарства України=Sumy: Ministry of Economy, Environment and Agriculture of Ukraine.

[14] Hussain, M., Kausar, R., Qureshi, A. S. & Jamil, H. (2023). Age-Related Gross and Histomorphometrical Dynamics of Pineal Gland (Epiphysis cereberi) Associated with Melatonin Profile in Beetal Goat (Capra aegagrus hircus) of Pakistan. *Pakistan Veterinary Journal, 43*(3), 531-536. doi: 10.29261/pakvetj/2023.051

[15] Kanova, M., & Kohout, P. (2021). Serotonin - Its Synthesis and Roles in the Healthy and the Critically Ill Int. *International Journal of Molecular Sciences. 22*(9), 4837. doi: 10.3390/ijms22094837

[16] Kumar, S., Meshram, B., Joshi, H., Saran, D., Parmar, N., & Singh, G. (2020). Gross Anatomy and Morphometry of the Brain in Guinea Fowl (Numida meleagris). *International Journal of Livestock Research, 10*(11), 79-84. doi: 10.5455/ijlr.2019071104234

[17] Lomakina, Yu. V., & Bulyk, R. E. (2016). Морфофункціональний стан шишкоподібної залози за стандартного режиму освітлення у старих щурів [Morphological and functional state of the pineal gland with standard mode of light in old rats]. *Клінічна анатомія та оперативна хірургія=Clinical Anatomy and Operative Surgery, 15*(2), 50-54. doi: 10.24061/1727-0847.15.2.2016.40

[18] Mascarenhas, L. J. S., Pereira, D. K. S., Pereira, K. F., Pagliarin, L. G., Franzo, V. S., & Vulcani, V. A. S. (2022). Morphological study of the pineal gland of Alouatta belzebul [Estudo morfológico da glândula pineal de Alouatta belzebul]. V*eterinary Medicine. Arquivo Brasileiro de Medicina*

*Veterinaria e Zootecnia, 74(*4), 617-625. doi: 10.1590/1678-4162-12638
[19] Mohammadi, S., & Zahmatkesh, M. (2023). A surgical modification in the technique of rat pinealectomy. *Anatomical Science International, 98*(2), 164-175. doi: 10.1007/s12565-022-00683-6
[20] Munmun, F., & Witt-Enderby, P. A. (2021). Melatonin effects on bone: Implications for use as a therapy for managing bone loss. *Journal of Pineal Research, 71*(1), e12749. doi: 10.1111/jpi.12749
[21] Olopade, J. O., Igado, O. O., Adesina, M. A., Folarin, R. O., & Obasa, A. A. (2023). Pinealocytes and Glia Cells in the Pineal Gland of the African Straw-Coloured Fruit Bat (Eidolon helvum). *Folia Veterinaria, 67*(3), 39-48. doi: 10.2478/fv-2023-0026
[22] Örğı, E., & Oğuz, A. R. (2022). Anatomical and histological investigation of the pineal gland in the lake van fish (Alburnus tarichi (Güldenstädt, 1814)). *Anatomia, Histologia, Embryologia, 51*(4), 427-434. doi: 10.1111/ahe.12802
[23] Peruri, A., Morgan, A., D'Souza, A., Mellon, B., Hung, C. W., Kayal, G., … & Nguyen, K. (2022). Pineal gland from the cell culture to animal models: a review. *Life (Basel), 12*(7), 1057. doi: 10.3390/life12071057
[24] Pishak, V. P., Kryvchanska, M. I., Riznichuk, M. O., Bulyk, O. R., & Lukan, Y. R. (2022). Мелатонін: Біологічна роль та оптимізація його застосування [Melatonin: biological role and optimization of its application]. *Буковинський медичний вісник=Bukovinian Medical Herald, 26*(102) 86-90. doi: 10.24061/24130737.XXVI.2.102.2022.16
[25] Polakovičová, S., Líška, J., Varga, I., & Gálfiová, P. (2024). Morphology of the Human Pineal Gland Studied by Freeze-Fracturing in Scanning Electron Microscopy. *Life*, *14*(12), 1617. doi: 10.3390/life14121617
[26] Savka, R. F., & Berbets, A. M. (2022). Шишкоподібна залоза і прееклампсія – сучасний погляд на проблему (огляд літератури) [Pineal gland and preeclampsia – a modern view of the problem (literature review)]. *Клінічна анатомія та оперативна хірургія=Clinical Anatomy and Operative Surgery, 21*(2), 73-79. doi: 10.24061/1727-0847.21.2.2022.28
[27] Semenenko, S. B., Slobodian, K. V., Dzhuriak, V. S., Chernei, N. Ya., & Rudan, K. V. (2024). Шишкоподібна залоза: історичний екскурс та сучасні наукові факти (огляд літератури) [Pineal gland: historical excursion and current scientific facts (literature review)]. *Клінічна та експериментальна патологія=Clinical & Experimental pathology, 2*(88), 109-114. doi: 10.24061/1727-4338.XXIII.2.88.2024. 17
[28] Şen, E., Sever, S. N., & Turhan, B. (2024). Scientific Research on the Pineal Gland: A Bibliometric Analysis from Its First Publication. *Endocrinology Research & Practice, 28*(2), 65-70. doi: 10.5152/erp.2024.23410
[29] Serhiyenko, O. O., Sehin, V. B., Kuznets, V. O., & Serhiyenko, V. O. (2024). Мелатонін і артеріальний тиск: наративний огляд [Melatonin and blood pressure: a narrative review]. *Міжнародний ендокринологічний журнал=The International Journal of Endocrinology, 20*(3), 218-224. doi: 10.22141/2224-0721.20.3.2024.1393
[30] Zaccagna, F., Brown, F. S., Allinson, K. S. J., Devadass, A., Kapadia, A., Massoud, T. F., & Matys, T. (2022). In and around the pineal gland: a neuroimaging review. *Clinical Radiology, 77*(2), e107-e119. doi: 10.1016/j.crad.2021.09.020
[31] Zheng, J., Song, W., Zhou, Y., Li, X., Wang, M., & Zhang, C. (2024). Cross-species single-cell landscape of vertebrate pineal gland. *Journal of Pineal Research, 76*(1), e12927. doi: 10.1111/jpi.12927

ТОПОГРАФО-АНАТОМІЧНІ ОСОБЛИВОСТІ ЕПІФІЗУ У ЛАБОРАТОРНИХ ЩУРІВ ЛІНІЇ ВІСТАР

Пшиченко В. В., Черно В. С., Корольова О. В., Найдіч О. В., Іовенко А. В., Бродовський В. А.

Епіфіз – орган центральної ендокринної системи, який координує діяльність периферичних ендокринних залоз, імунної та нервової систем, регулює біологічні ритми, забезпечує процеси адаптації та запуск стрес-реакції. Епіфіз притаманний практично всім хребетним тваринам, але існують різні варіації форми та розташування епіфізу у головному мозку тварин навіть у межах одного виду. Найчастіше, для проведення лабораторних досліджень залучаються лабораторні щури лінії Wistar і для правильної інтерпретації отриманих результатів слід враховувати видові особливості анатомічної будови та можливі індивідуальні варіації розташування епіфізу у лабораторних щурів у нормі. Метою роботи було вивчення особливостей анатомічної будови та топографії епіфізу у білих лабораторних щурів лінії Wistar. Були досліджені епіфізи 24 статевозрілих самців лабораторних щурів лінії Wistar. Використовували морфологічні, морфометричні та статистичні методи дослідження. В ході проведення дослідження були виявлені індивідуальні варіації топографії, форми та кровопостачання епіфізу у лабораторних щурів. Встановлено, що в одних тварин епіфіз розташовувався у борозні між задніми краями потиличних часток півкуль головного мозку, рясно кровопостачався великою кількістю кровоносних судин та мав овальну або конусоподібну форму. В інших тварин епіфіз розташовувався у борозні між верхніми зоровими горбками чотиригорбикового тіла. При цьому кропопостачання епіфізу відбувалося невеликою кількістю кровоносних судин, а форма епіфізу при такій локалізації була округлою. Встановлені індивідуальні варіації лінійних розмірів епіфізу. При вивченні морфометричних параметрів було встановлено, що найбільш стабільним був поперечний розмір епіфізів, а вертикальний розмір був більш лабільним, що, вірогідно, і обумовило індивідуальні відмінності об'ємів епіфізів у досліджуваних щурів. Таким чином, отримані результати дослідження щодо індивідуальних варіацій анатомічної, топографічної та морфометричної будови епіфізу в інтактних лабораторних щурів лінії Вістар можуть бути основою при оцінці патологічних змін органу при проведенні експериментальних досліджень у медичних та біологічних науках.

Ключові слова: *головний мозок, епіфіз, анатомія, топографія, лабораторні шури, індивідуальні варіації.*

Author contribution
Pshychenko V. V. – data visualization, methodology and original project writing, resources.
Cherno V. S. – research, conceptualization.
Korolyova O. V. – project administration, software.
Naidich O. V. – formal analysis and verification.
Iovenko A. V. – writing and editing a review.
Brodovskyi V. A. – resources.

DOI: 10.31393/morphology-journal-2025-31(4)-06 Reports of Morphology, Vol. 31, №4, Pages 42-50

ISSN 1818-1295 eISSN 2616-6194

REPORTS OF MORPHOLOGY

Official Journal of the Scientific Society of Anatomists, Histologists, Embryologists and Topographic Anatomists of Ukraine

journal homepage: https://morphology-journal.com

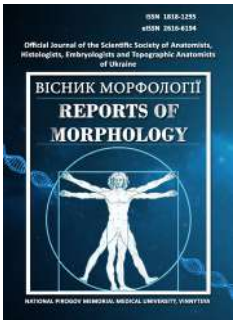

The role of mechanical stress and local vascular thrombosis in the formation of stress fracture of bone stump (experimental research)

Bezsmertnyi Y. O., Bondarenko D. V., Shevchuk V. I., Branitsky O. Y.

National Pirogov Memorial Medical University, Vinnytsya, Ukraine

ARTICLE INFO

Received: 10 April 2025

Accepted: 17 September 2025

UDC: 617.57:616.151.5

CORRESPONDING AUTHOR

e-mail: shevchukndiri@gmail.com

Shevchuk V. I.

CONFLICT OF INTEREST

The authors have no conflicts of interest to declare.

FUNDING

The study was conducted within the framework of the research work “To develop reconstructive and restorative operations on lower limb residual limb stumps after amputations as a result of mine blast injuries” (registration number 0123U100169), funded by the Ministry of Health of Ukraine with the state budget.

DATA SHARING

Data are available upon reasonable request to corresponding author.

Amputation of a limb leads to impaired remodeling of the bone stump, which often results in its functional failure and the need for re-amputation. Until now, the generally accepted explanation for the development of stress fractures has been the accumulation of fatigue microdamage in the compact bone layer. The involvement of other tissues in the formation of stress fractures has not been studied. In the course of experimental research on stress fractures after amputations, in some cases a clear pattern was observed of the occurrence of local microthromboses in the vessels of the muscles, bone and bone marrow, with subsequent ischemic necrosis and the formation of stress fractures of the bone stump. The aim of the study was to investigate the role of local changes in vessels and muscles in the development of stress fractures of the bones of an amputation stump under mechanical loading. The experimental material consisted of 42 rabbits in which stress fractures of the femoral bone stump were induced by graded pneumatic compression (30 mmHg) of the soft tissues and a focused shock wave directed at the terminal surface with an energy of 0.5 mJ/mm², frequency 2 Hz, delivering 400 impulses per session under anaesthesia daily. The research method was histological, with injection of the vessels using an India ink–gelatin mixture. Morphological examination of the bone included the study of histotopographic and routine histological sections of bone tissue. The state of the microcirculatory network of the bone and muscles was assessed. The density of vessel distribution and their diameter were taken into account (without special quantitative measurements). In the muscles, the amount of fibrous tissue was evaluated morphometrically. On micrographs at magnifications ×200 and ×400, the diameter of individual muscle fibres was measured. Statistical differences between groups were assessed using the non-parametric Kruskal-Wallis test and the Mann-Whitney U test. As a result, along with the traditional pattern of stress fracture development, microthromboses of the vessels of the surrounding muscles, bone and bone marrow were identified, which led to ischemic necrosis of these structures and the formation of stress fractures. In the compact bone above and below the fracture site, dystrophic and necrotic processes occurred, characterised by osteocyte lysis, necrosis of the contents of central canals, impoverishment of Haversian canals and the development of osteoporosis-like rarefaction. Marked rarefaction was accompanied by a decrease in the number and thickness of bony trabeculae and cellular elements. The base of the fracture gap was formed by necrotised bone marrow. Subsequently, the fracture gap became filled with fibrous tissue and trabeculae of endosteal bone formation. Fracture healing occurred through both fibrous and bone tissue. Thus, we established that cyclic loading of the bone stump combined with muscle compression, in addition to bone fatigue, also causes fatigue of the soft tissues, leading to the formation of microthromboses in the vessels of the soft tissues, bone and bone marrow, with ischemic necrosis of these tissues and the development of a stress fracture.

Keywords: *rabbits, amputation, mechanical stress, soft tissue fatigue, microthrombosis, stress fractures, morphological changes, regeneration.*

Introduction

Stress fractures account for up to 10-20 % of all injuries in sports medicine and among military recruits [8]. These are usually fatigue fractures that occur when abnormal and repetitive stress is applied to normal bone. As a result, the remodelling process is disrupted, leading to microdamage and fractures. Fatigue fractures should be differentiated from insufficiency fractures, which are the result of normal stress on a pathological bone [2, 19]. During stress, the bone deforms, and when the stress is removed, it returns to its original state. Outside the elastic range, tension remains in the cortical bone, creating microcracks and permanent plastic deformation. Inadequate recovery and accumulated damage with osteoclast activity predominating over osteoblast activity leads to a stress fracture.

The aetiology of stress fractures is multifactorial and includes numerous external and internal factors that may indicate individual susceptibility.

External factors include nutritional deficiencies, eating disorders, type and frequency of activity, footwear quality, and environmental factors [10, 24].

Internal factors include structural changes in bone, female gender, BMI, body composition, bone mineral density, biomechanics, and bone malalignment [1, 31]. The vast majority of reports focus on bone. However, bone is not isolated. It is surrounded by skin, muscles, blood vessels, and nerves, which also perceive mechanical loads. Unfortunately, the role of these components of the musculoskeletal system in the occurrence of stress fractures has not been studied. Amputation increases the stiffness of arteries, especially medium and small calibre ones. Acute changes occur in the arterial system [22], which are a sign of adaptation to the new arterial environment. They undergo neurohormonal transformations related to blood volume, arterial pressure, cardiac output, vascular remodelling, vascular tone and blood flow distribution. A decrease in blood flow in an artery leads to a decrease in its diameter and possible secondary changes in its wall. Vascular changes after amputation cannot fully compensate for tissue blood supply, which causes negative effects [22]. Amputation and prolonged immobility or sudden increase in load increase the risk of venous thrombosis [26, 27]. At the same time, minor injuries to the stump are also associated with this risk [26, 27, 32]. At the molecular level, there are several possible mechanisms: hypoxemia, activated blood clotting factors, and inflammatory response [25]. There is a considerable amount of literature devoted to the study of muscles in the amputation stump [7, 9, 12]. The vast majority of these studies have found a decrease in strength, muscle thickness and muscle fibre atrophy in the amputated limb compared to the intact limb. Muscle fibre splitting, atrophy, a decrease in the area and length of the cross-section of fibres, and fatty degeneration have been observed [29]. It should be noted that some researchers [15] expressed the opinion that, along with bone fatigue, muscle fatigue and decreased muscle strength can lead to a decrease in bone protection from physical stress and an increased risk of fatigue fractures. The authors agree with them, who believe that cyclic bone loading leads to muscle exhaustion [3, 5], bone resorption, temporary local hypoxia, and the risk of stress fractures. Another study [1, 31] raised the controversial question of what causes stress fractures: the contractile force of the muscles acting on the bone or increased fatigue of the supporting structures.

In this regard, there was a need to study and clarify the possible role of the muscular and vascular systems in the occurrence of stress fractures.

Aim: to investigate the role of local changes in blood vessels and muscles in the occurrence and healing of stress fractures of amputation stump bones under mechanical stress.

Materials and methods

The experiments were conducted on 42 sexually mature rabbits of the White Giant breed weighing 2.5-3 kg. All procedures for laboratory animals were performed in accordance with the European Convention for the Protection of Vertebrate Animals (Strasbourg, 1986) and Directive 2010/63 EU on the protection of animals used for scientific purposes (2010). The research was conducted in accordance with the recommendations of the Bioethics Commission of the National Pirogov Memorial Medical University, Vinnytsya (Protocol No. 10 dated 16 July 2024). The rabbits were kept on a standard vivarium diet. The animals underwent amputation of the thigh at the middle third and muscle plastic surgery. Four weeks after the amputation, shock wave therapy was performed to induce stress fractures, focusing on the end surface of the stump with a shock wave energy of 0.5 mJ/mm², a frequency of 2 Hz, and 300 pulses per session. Before this, the stump was placed in a pneumatic cuff, in which a pressure of 30 mm Hg was created. A total of 15 sessions were performed once a day. For pain relief before the mechanical loading procedure, the animals were intramuscularly injected with a combination of ketamine (40 mg/kg) and xylazine (5 mg/kg). The combination provided adequate sedation and analgesia for about 30 minutes, which allowed the mechanical loading session to be performed without stress and pain reactions from the animals. The rabbits were removed from the experiment on days 7, 14 and 30 after the completion of the mechanical loading course.

Methodology for examining bone stumps

Before removal from the experiment, the animal was administered 3000 IU of heparin in physiological solution intra-arterially. After 15 minutes, a lethal dose (0.5 ml) of hexenal was rapidly administered intravenously and the abdominal aorta was ligated. Below the ligature, a cannula from the intra-arterial injection system was inserted, fixing it in the lumen of the vessel, and 10 % gelatin mixture was poured in. After 24 hours, the femur was isolated in the hip joint. A visual assessment of the relationship between the soft tissues and the bone was made, after which the femoral stump was freed from the soft tissues, leaving them only on the end surface. The specimen was fixed in a 12 % formalin solution and decalcified using a 15 % nitric acid solution. A sagittal section was made through the middle of the bone, which was poured into a block of celloidin. Sections 15-

30 μm thick were stained with haematoxylin and eosin and according to Van Gieson. Clear sections were also made. The morphological study included microscopic examination of histotopographic and conventional histological sections of bone tissue. The condition of the microcirculatory network of bone and muscle filled with a gelatin mixture was assessed, taking into account (without special measurements) the density of the vessels and their diameter.

The stump muscles were fixed in a 10 % formalin solution diluted in phosphate buffer (pH 7.4). The fixation time was 24 hours at a temperature of 4 °C. The muscle samples were washed from formalin, dehydrated in isopropanol (from 70 % to 99.8 %) and embedded in paraffin. Sections 5 μm thick were made from the paraffin-embedded samples. They were stained with haematoxylin and eosin and embedded in a synthetic medium. The micro-preparations were examined under an OlympusBX51 microscope (Olympus Corporation, Japan).

The amount of fibrous tissue in the muscles was assessed morphometrically. Images of micro-preparations, taken at ×40 magnification, were divided according to localisations that differed in specific staining. Micro-preparations stained with picrosirius red contained areas with a specific red reaction to collagen, and the muscles were stained yellow. Using CarlZeiss software, areas that differed in colour were separated. Areas stained red with picrosirius were assessed as zones of collagenogenesis. They were quantified and then the ratio of these areas to the total area of the studied micro-preparations was obtained. The numerical measurements obtained were then averaged and the result was presented as the relative amount of connective tissue in relation to muscle necrosis (%).

For morphometric analysis of diameter changes in micrographs at ×200 and ×400 magnification, the diameter of individual muscle fibres was measured. Two measurements were obtained from each unit – for the larger and smaller fibre diameters. Next, the numerical measurements (μm) were averaged for each sample and statistically processed.

Statistical analysis

The statistical differences between the groups were assessed using the non-parametric Kruskal-Wallis test. This test was used to check for statistical differences between three independent groups, without assuming normality of data distribution. Data from each group were combined and ranked. After ranking, the sum of ranks was calculated for each group, which became the basis for further calculations. The resulting *H statistic* was compared with the critical value from the chi-square table, taking into account the number of degrees of freedom κ-*1* (where κ is the number of groups). If the *p-value* of the test was less than the significance level (α=0.05), the null hypothesis was rejected. If the null hypothesis was rejected, a posthoc analysis was performed to determine which groups differed from each other. For this purpose, the Mann-Whitney U test was used, which allowed comparing pairs of groups and determining between which groups there were statistically significant differences [13].

Results

In the early stages after the fracture, stasis of individual capillaries and pathological changes in medium-calibre muscle vessels were observed, consisting of necrosis of their wall cells, the appearance of thrombi and cellular debris in the lumen (Fig. 1). Significant aggregation of platelets and erythrocytes was observed in the lumen of the vessels. Such aggregates occupied the lumen of the vessels, forming light red thrombi that blocked the vessel (Fig. 2a, b). Local thrombosis of the periosteal vessels and limited necrosis of compact bone tissue were noted (Fig. 3). Thrombosis also occurred in the bone marrow vessels (Fig. 2c). Perivascular infiltration, tissue debris and a significant number of fibroblasts and leukocytes were detected in the paravascular connective tissue.

Parosally, against the background of wide areas of transverse sections of muscle fibres, foci of swelling and delamination of myofibrils were observed. In the surrounding muscles, there were foci of haemorrhages with destroyed blood cells and fibrin threads. Fragmentation and destruction of the muscle fibres surrounding the vessels were noted, as well as the absence of transverse striations and nuclei in them. Inflammatory cell infiltrates formed, and there was haemorrhagic impregnation and tissue detritus. Activated fibroblasts, lymphocytes and macrophages were found between the thin fibres.

In the area of necrobiotically altered compact bone against the background of dilated vascular channels with pronounced osteoclastic resorption and cavity formation, microcracks, avascular and osteocyte-free areas, and disruption of vascular

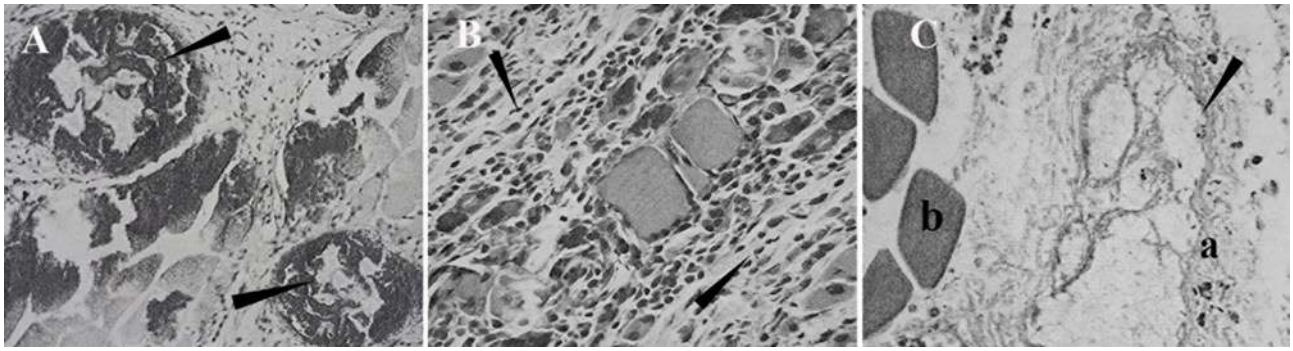

Fig. 1. Areas of muscle necrosis and vein wall necrosis. A, B – necrosis of muscle fibres with infiltration. C – necrosis of the vein wall (arrow) with absence of cell nuclei and presence of cellular debris (a) in the paravasal connective tissue, muscle fibres (b).

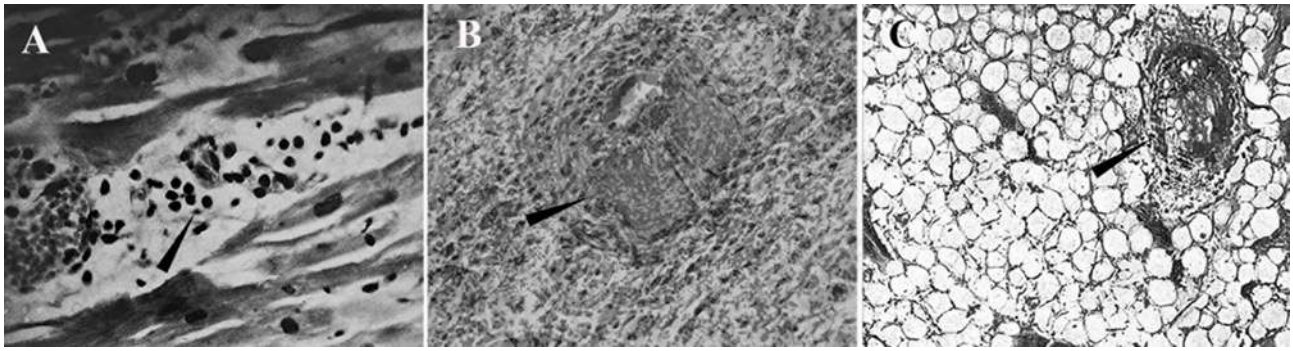

Fig. 2. The process of vascular thrombosis formation under mechanical stress. A – aggregation of formed elements in capillaries (arrow). B – organised thrombus in an artery (arrow). C – venous thrombosis (arrow). Haematoxylin and eosin. A, B – ×400, C – × 200.

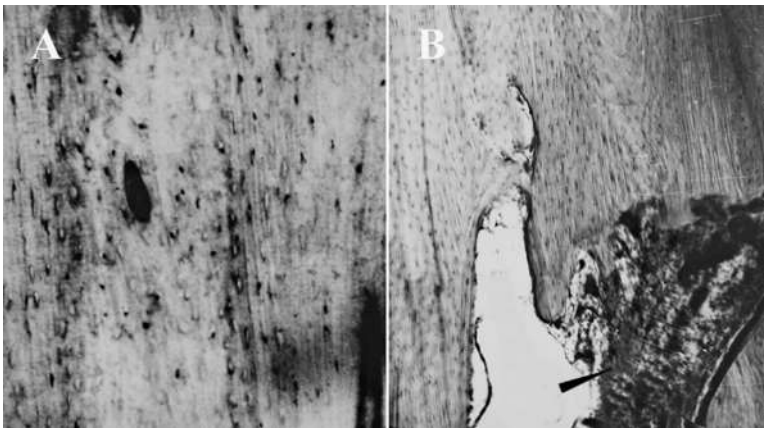

Fig. 3. Formation of a stress fracture in necrotic bone. A – necrosis of compact bone tissue, B – fracture gap (arrow). Haematoxylin and eosin. ×120.

continuity in the area of necrosis were observed. Microcracks spread mainly along the fusion and resorption lines. As a result of the fusion of microcracks, a fracture of the cortical diaphyseal layer occurred (Fig. 4). In the fracture gap zone, remnants of haematoma, proliferation of osteogenic cells, their ingrowth into fibrin accumulations, avascularity, pronounced necrobiotic changes, areas of bone tissue necrosis and pronounced osteoclastic resorption were observed. On lighted preparations, the compact bone showed disruption of vascular continuity and capillary growth. Continuity was observed only in large vessels. The bone marrow at the bottom of the gap was avascular. Massive necrosis of its cellular elements was observed. Against the background of pronounced oedema, unevenly dilated veins, sinusoids, and capillaries filled with blood cells and plasma were observed. Anastomoses formed between the bone marrow vessels and the periosteum. Bone tissue resorption (intracortical resorption) began with the periosteum and was replaced by newly formed bone tissue on the endosteal surface (Fig. 5). The inter-beam spaces and resorption cavities were occupied by fibroreticular tissue with chains of osteoblasts and osteoclasts located along the contours of the beams, indicating the formation of basic multicellular units. In the bone marrow canal, starting from the end in the proximal direction over a considerable length, there is loose, edematous fibrous tissue with a significant number of sinusoids, large tissue cysts, and thin-walled vessels of large diameter filled with ink. There was a discharge of carcass into the perivascular space. Opposite the stress fracture in the medullary canal, diffusely located macrophages, lymphoid and plasma cells, a significant number of sinusoids and tissue cysts associated with the microvascular bed were identified in the edematous fibrous tissue. The bone walls of the Haversian and Volkmann's canals were enlarged, with uneven surfaces and cracking of the bone tissue. The canals are filled with fibroreticular tissue, indicating the onset of remodelling of the cortical layer bone tissue. Subsequently, in the outer layers of the cortical diaphyseal plate, at a distance of 1 cm from the fracture line, vessels appeared, passing through the enlarged transverse bone canals from the soft tissues and periosteum. Revascularisation improved due to the maximum development and inclusion of anastomosing vessels and the existing microcirculatory bed of bone tissue with preservation of collateral blood supply in the future. New bone beams formed in the thickened osteoblastic tissue of the periosteum, forming a layer of periosteal bone formation. The gap between the fragments was filled with cellular-fibrous tissue with tissue cysts, hyaline cartilage and an area of enchondral ossification (Fig. 6). Tissue cysts and extravasates were found in the medullary canal. At a distance from the fracture, a dense network of immature bone beams was determined on the endosteal surface of the cortical layer. Fibrous-cartilaginous tissue formed periosteally was formed on

the proximal fragment. The peripheral fragment was avascular. Subsequently, immature bone beams appeared on the central fragment. Dense fibrous tissue with large areas of cartilage was detected in the fracture gap. Endosteal and periosteal bone formation occurred at the ends of the fragments. The inter-beam spaces were filled with sinusoidal vessels and tissue cysts. The bone tissue was osteocyte-free. After a month, bone formation in the form of a dense network of bone beams occurred in the fracture gap on the basis of cartilage tissue. Mature beams were found at the ends of the fragments on the periosteal and endosteal surfaces. Subsequently, the fracture gap was filled with bone beams of varying maturity (Fig. 7). Cartilage and fibrous tissue were minimal. In the long term, further remodelling of bone tissue and the vascular system continued.

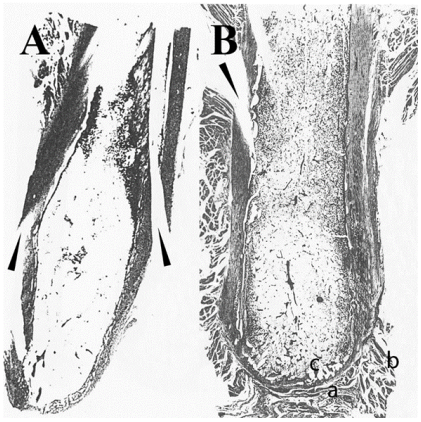

Fig. 4. Histotopograms stumps with stress fractures of the cortical diaphyseal plate. A – bilateral stress fractures (arrow) of the cortical diaphyseal plate. B – stress fracture of the cortical diaphyseal plate: a – fibrous tissue around the bone closure plate; b – muscles adjacent to the plate; c – endostal beams. Haematoxylin and eosin. ×2.5.

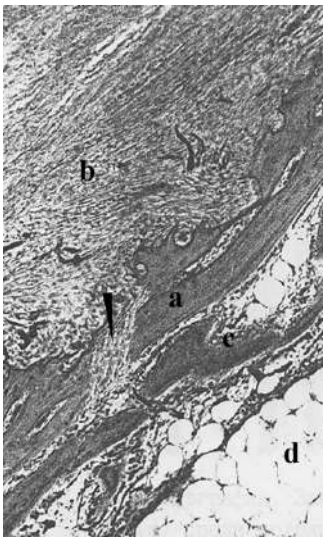

Fig. 5. Structure of the cortical diaphyseal plate at the fracture site. Significant resorption of the cortical diaphyseal plate: a – remnants of compact bone; b – dense fibrous tissue at the site of the resorbed plate; c – newly formed endosteal beams; d – bone marrow; arrow – fracture line (arrow). Haematoxylin and eosin. ×78.

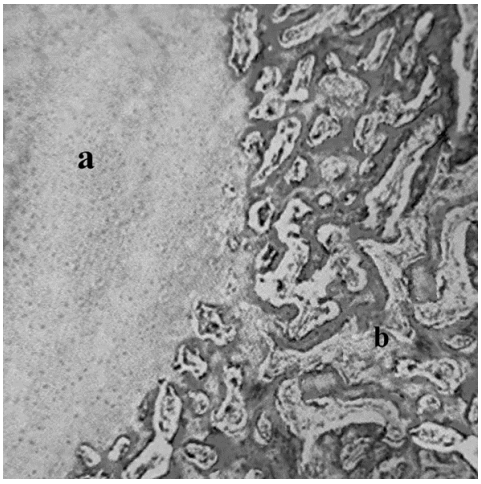

Fig. 6. Process of healing of a stress fracture of the bone stump by enchondral osteogenesis. Hyaline cartilage (a) with enchondral ossification (b). Haematoxylin and eosin. ×80.

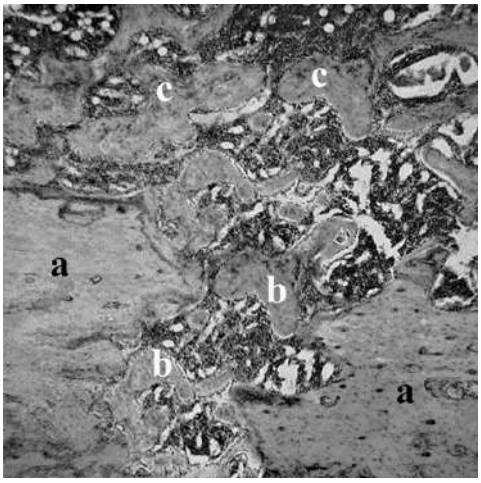

Fig. 7. Area of partial bone fusion: a – ends of fragments; b – beams of endosteal regenerate; c – beams of periosteal bone formation. Haematoxylin and eosin. ×5.

During the healing process of the stress fracture, changes occurred in the vessels and muscles of the stump. An increase in vascular density was observed. In the lumen of some of them, unchanged blood cells were already visible, indicating the restoration of blood supply. Proliferation of smooth muscle elements was noted. Muscle fibres were deformed, some of them necrotic, others thinned and less intensely stained. Transverse striations were absent. Fibroblasts and macrophages, a large amount of connective tissue, and cell-free areas with collagen were observed in the interstitial space.

In preparations with healed stress fractures (Fig. 8), restoration of the patency of arterial and venous vessels was noted. Cell nuclei and tissue formed elements appeared in their walls. Part of the muscle tissue was replaced by connective tissue. The activity of its formation was reduced. The thickness of muscle fibres decreased. Muscle fibres with nuclei in the centre and periphery of the fibre were found,

indicating active reparative processes. Foci of adipocytes were found.

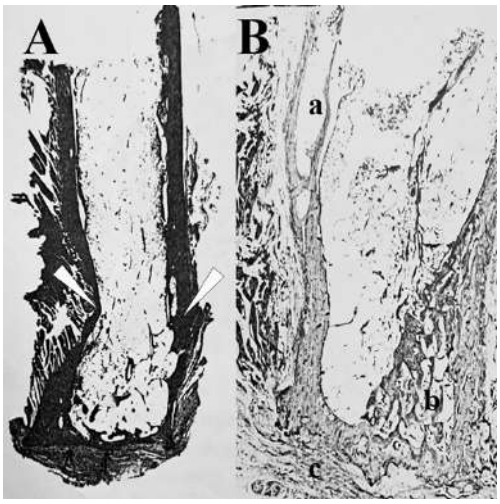

Fig. 8. Histotopograms of a deformed stumps with reconstruction of the cortical diaphyseal plate in the area of the previous fracture. A – curvature of the remodeled cortical diaphyseal plate (arrow). Van Gieson staining. ×2. B – rebuilt after a fracture: a – cortical diaphyseal plate remodeled after fracture; b – endosteal segment where the regenerate is located; c – fibrous tissue surrounding the end of the stump. Haematoxylin and eosin. ×2.5.

The participation of the muscles surrounding the bone in regeneration consisted in the proliferation of perimysium cells. At the fracture site, fibrous tissue developed after 4 weeks, which subsequently acquired the structure of the periosteum.

Since the main morphological changes in the muscles involved were the development of connective tissue and hypotrophy of muscle fibres, we determined the relative density of connective tissue and the average diameter of muscle fibres.

Table 1 shows the morphometrically determined percentage of muscle tissue destruction (necrosis, atrophy, and fibrotic changes) at different time points after detection. According to the data obtained, the relative density of collagen in intact rabbits is 5.06±0.44 %. As can be seen from the table, the percentage of relative density of collagen-positive muscle areas increased depending on the duration.

Table 1. Relative collagen density (%) in muscle samples at different time periods after modelling a stress fracture.

Group	Research period		
	7 days	14 days	30 days
Control	5.06±0.44		
Research groups	48.18±1.58*	56.83±2.83*#	71.83±2.33*#^

Note: H Kruskal-Wallis test statistics – 10.38, p-value – 0.015; * – significantly different from control (p<0.05); # – significantly different from 7 days (p<0.05); ^ – significantly different from 14 days (p<0.05).

Table 2 shows data on the diameter of muscle fibres that were not in a state of necrosis and decay. In the control group, it was 81.83±1.27 μm. The diameter of fibres that were not in a state of necrosis and decay was assessed. The diameter of muscle fibres was significantly smaller at all observation times compared to the control group. At 7 days, it was slightly higher than at 30 days of observation, which is explained by oedema. In general, muscle hypotrophy developed gradually.

Table 2. Results of muscle fibre morphometry (diameter, μm).

Group	Research period		
	7 days	14 days	30 days
Control	81.83±1.27		
Research groups	56.73±2.47*	61.43±2.05*#	53.87±1.41*#^

Note: H Kruskal-Wallis test statistics – 9.97, p-value – 0.018; * – significantly different from control (p<0.05); # – significantly different from 7 days (p<0.05); ^ – significantly different from 14 days (p<0.05).

Discussion

Amputation leads to a sharp disruption of homeostasis in the bone, destruction of microcirculatory connections between adjacent blood supply basins, and damage to vascular connections between the bone and surrounding soft tissues.

The selected model of dosed pneumatic compression of soft tissues and focused on the end surface of the shock wave maximally imitated the process of using a prosthesis. The study showed that mechanical stress on the stump leads to fatigue not only of bone tissue, but also of the muscles surrounding the bone, with blockage of the microcirculatory bed. Local spasm with vasoconstriction occurs at the site of damage. The endothelial membrane is damaged and the extracellular matrix in this area is exposed to blood components [20, 23]. The extracellular matrix releases cytokines and inflammatory markers, which leads to platelet adhesion and aggregation at this site, forming a seal over the defect. Platelet adhesion is mediated by interactions between various receptors and proteins. This is followed by platelet activation with the release of ADP, thromboxane A2, serotonin and other activation factors. Activated platelets bind to each other and to the damaged area of the endothelium, forming a primary clot. As a result of complex activations and transformations, a stabilised clot forms – a thrombus with impaired anatomical patency due to intravascular blood clotting and the formation of antigen-antibody reaction products. In the area of excluded blood supply, ischemic necrosis of vessels, muscles, periosteum, bone and bone marrow occurs with destruction and melting of the stroma under the influence of proteases secreted from the lysosomes of damaged cell elements [20]. The accumulated waste products contribute to inflammation with sequestration of necrotic bone areas. The structure of microvessels is influenced by biomechanical forces, including shear stress and biochemical signals (hormones, growth factors, cytokines, chemokines, nitric oxide). According to Seymour R. S. et al. [28], microvessels are subject to significantly increased wall shear stress and tangential force acting on the vessel walls as a result of blood flow, as their

size decreases. The average shear stress values in arterioles significantly exceed those in arteries. Unlike thrombosis in large arteries, thrombosis in microvessels leads to more diffuse perfusion impairment and widespread avascularity.

The condition of muscles after reperfusion depends not only on their direct damage, but also on metabolic dysfunction. Muscle ischaemia stimulates the hyperproduction of cytotoxic lactate, superoxide anion and creatine phosphokinase, which are manifestations of lactic acidosis and ischaemic damage [11]. Hypoxia causes inhibition of electrons in the mitochondrial respiratory chain and limits the formation of macroergic compounds (ATP, creatine phosphate) in the cells of damaged tissues [6]. Disrupts the sodium-potassium pump, membrane depolarisation and intracellular Ca^{2}+ accumulation, resulting in mitochondrial dysfunction, hyperproduction of free radicals, lipid peroxidation of biological membranes, cell necrosis and inflammation [4]. Reperfusion exacerbates damage to ischaemic tissues. Active forms of oxygen, products of lipid and protein peroxidation play a leading role in this process [33]. This causes endogenous activation of the antioxidant defence enzyme system. The activity of superoxide dismutase and catalase increases [34], while that of glutathione peroxidase decreases. According to Li Y. at al. [21], this enzyme is activated in the presence of low amounts of peroxide and lipoperoxides, while catalase is activated at high concentrations of hydrogen peroxide. Its activation and accumulation of peroxides is evidence that, in addition to direct muscle damage, secondary damage to muscle tissue develops. Thus, cyclic bone loading combined with muscle compression causes not only hypotrophy and tissue deformation, but also necrosis of muscle fibres, a decrease in muscle tissue and microcirculation disorders in skeletal muscles. This is evidenced by cell necrosis in the walls of blood vessels, haemorrhages, and thrombosis in the vessels. Interstitial oedema and haemorrhagic infiltration of the affected muscle tissue were the result of necrosis of the walls of blood vessels. Secondary microcirculatory disorders arose as a result of oedema, which increased the intra-tissue pressure inside the closed fascial space of the muscle [17, 18]. Subsequently, the oedema processes intensified, regional ischaemia and accumulation of cytotoxic metabolites in the tissues occurred [30]. Increased blood flow during reperfusion causes haemorrhagic infarction of muscle and bone, as the structural integrity and metabolic activity of ischaemically damaged vessels are impaired [16].

A significant number of plasma capillaries appear in the bone tissue, vascular permeability increases with the accumulation of plasma fluid in the perivascular spaces of the Haversian and Volkmann's systems. Dystrophic changes, focal avascularity, inflammation, oedema, necrosis of the fatty bone marrow, and its replacement by fibrous tissue occur. In the area of mechanical stress concentration, bone resorption occurs through vascular channels, leading to spongiosis and porosity. Continued mechanical stress leads to a stress fracture of the necrotic cortical diaphyseal layer of the bone. The size of the fracture gap depends on the location and extent of the area of ischaemic necrosis caused by decompensated blood supply disruption. There is widespread blockage of the microcirculatory bed of bone fragments, and their further fate depends on the aforementioned redistributive compensation for the disrupted blood supply. With complete primary compensation, which ensures rapid and sufficient restoration of blood supply, viable bone marrow is separated from the exudate by granulation tissue and inflammation does not spread to the bone marrow. Blood flow slows down in bone fragments and intraosseous pressure increases, which enhances plasma exudation and the migration of cellular elements into the fracture gap. With incomplete primary compensation of the impaired blood supply, there is a slow recovery of weakened blood flow. At the same time, in one or both bone fragments, hypoxia leads to ischaemic damage to cellular elements and changes in the cellular composition of the bone marrow. Cells with low energy metabolism are preserved. The spread of the reparative reaction to the ends of the fragments slows down. Fibroblastic differentiation of osteogenic tissue cell elements prevails here, the production of connective fibrous tissue intensifies, but the conditions for reparative bone formation deteriorate. In these cases, fibrous-chondroid fusion occurred. Sometimes, decompensation of the impaired blood supply to bone fragments and bone marrow occurs, creating unfavourable conditions for the development of a reparative reaction in the bone marrow. Revascularisation and replacement of the necrotic area begins at the site where the blood supply and cellular composition of the bone marrow are preserved. The endosteal proliferative reaction ensures slow replacement and revascularisation of the area of ischaemic necrosis with a predominance of fibrous connective tissue neoplasm. The periosteal reaction begins several days later than in compensated blood supply disorders, but then becomes pronounced. As resorption processes intensify, the periosteal vessels form periosteal-medullary anastomoses.

Studies show that the muscles and vessels surrounding the bone are directly involved in the formation of stress fractures during dosed muscle compression and mechanical loading of the bone stump. Of course, the basis is the impact on the bone remnant, but the data obtained indicate the participation of surrounding tissues in this process, and they must be taken into account in further studies, since they also participate in the healing of the fracture.

There are some limitations to this study that must be acknowledged. The results are based on a limited number of histomorphological observations of local microthrombosis in modelling stress fractures. In the future, it would be useful to study metabolic changes in ischaemic muscles and stump bone in order to develop possible methods for their prevention and treatment. All experiments were conducted under the same mechanical load. In the future, it would probably be advisable to study the role of microthrombosis in muscle and bone vessels under different mechanical loads. This would allow establishing threshold and subthreshold

loads, some of which could be used to determine the optimal option for bone impact. It would be necessary to study haemostasis indicators, the effect of microthrombosis on the thrombosis factor, cytokines, neutrophil extracellular traps, and complements. Separate studies should be planned for this purpose.

Conclusions

1. Prosthesis-like dosed compression of soft tissues with cyclic loading of the bone stump due to compression and shear deformation leads to local ischaemia, thrombosis and necrosis of muscles, bone and bone marrow tissues with the formation of a stress fracture.

2. Due to necrotic processes, stress fractures healed on the basis of cartilage through enchondral ossification.

3. Blood supply to the stress fracture area was provided by anastomoses from the vessels of intact muscles, periosteum, bone marrow, and juxta-vascular sources – tissue cysts and sinusoids. During fracture healing, restoration of patency of arterial and venous vessels affected by thrombosis was observed.

4. In the area of former necrosis, muscle tissue was replaced by scar tissue. The surrounding muscles underwent atrophy, with some of the fibres being replaced by fibrous tissue.

References

[1] Abe, K., Hashiguchi, H., Sonoki, K., Iwashita, S., & Takai, S. (2019). Tarsal navicular stress fracture in a young athlete: A case report. *J Nippon Med Sch*, 86(2), 122-125. doi: 10.1272/jnms.JNMS.2019_86-208

[2] Armstrong III, D. W., Rue, J. P., Wilckens, J. H., & Frassica, F. J. (2004). Stress fracture injury in young military men and women. *Bone*, *35*(3), 806-816. doi: 10.1016/j.bone.2004.05.014

[3] Asano, L. Y., Duarte, A. Jr., & Silva, A. P. (2014). Stress fractures in the foot and ankle of athletes. *Rev Assoc Med Bras (1992)*, *60*(6), 512-517. doi: 10.1590/1806-9282.60.06.006

[4] Barnig, C., Lutzweiler, G., Giannini, M., Lejay, A., Charles, A. L., Meyer, A., & Geny, B. (2022). Resolution of inflammation after skeletal muscle ischemia-reperfusion injury: A focus on the lipid mediators lipoxins, resolvins, protectins and maresins. *Antioxidants (Basel)*, *11*(6), 1213. doi: 10.3390/antiox11061213

[5] Behrens, S. B., Deren, M. E., Matson, A., Fadale, P. D., & Fadale, K. O. (2013). Stress fractures of the pelvis and legs in athletes: A review. *Sports Health*, *5*(2), 165-174. doi: 10.1177/1941738112467423

[6] Canfora, I., Tarantino, N., & Pierno, S. (2022). Metabolic pathways and ion channels involved in skeletal muscle atrophy: A starting point for potential therapeutic strategies. *Cells*, *11*(16), 2566. doi: 10.3390/cells11162566

[7] Cho, H., Park, J., Kim, B., Han, K., Choi, H. L., & Shin, D. W. (2024). Increased risk of fracture after traumatic amputation: A nationwide retrospective cohort study. *Healthcare (Basel)*, *12*(13), 1362. doi: 10.3390/healthcare12131362

[8] da Rocha Lemos Costa, T. M., Borba, V. Z. C., Correa, R. G. P., & Moreira, C. A. (2022). Stress fractures. *Arch Endocrinol Metab*, *66*(5), 765-773. doi: 10.20945/2359-3997000000562

[9] De Silva, G. S., Saffaf, K., Sanchez, L. A., & Zayed, M. A. (2018). Amputation stump perfusion is predictive of postoperative necrotic eschar formation. *Am J Surg*, *216*(3), 540-546. doi: 10.1016/j.amjsurg.2018.05.007

[10] Dixon, S., Nunns, M., House, C., Rice, H., Mostazir, M., Stiles, V., … Allsopp, A. (2019). Prospective study of biomechanical risk factors for second and third metatarsal stress fractures in military recruits. *J Sci Med Sport*, *22*, 135-139. doi: 10.1016/j.jsams.2018.06.015

[11] Finco, M. G., Kim, S., Ngo, W., & Menegaz, R. A. (2022). A review of musculoskeletal adaptations in individuals following major lower-limb amputation. *J Musculoskelet Neuronal Interact*, *22*(2), 269-283. PMID: 35642706

[12] Graser, M., Day, S., & Buis, A. (2020). Exploring the role of transtibial prosthetic use in deep tissue injury development: A scoping review. *BMC Biomed Eng*, *2*, 2. doi: 10.1186/s42490-020-0036-6

[13] Grjibovski, A. M., Ivanov, S. V., & Gorbatova, M. A. (2016). Описательная статистика с использованием пакетов статистических программ Statistica и SPSS [Descriptive statistics using Statistica and SPSS software]. *Наука и здравоохранение=Nauka i Zdravookhranenie, 1,* 7-23.

[14] Grjibovski, A. M., Ivanov, S. V., & Gorbatova, M. A. (2016). Analysis of quantitative data in two independent samples using Statistica and SPSS software: Parametric and non-parametric tests. *Science & Healthcare*, *2*, 5-28. doi: 10.34689/SH.2016.18.2.001

[15] Gürbüz, A., & Gür, M. (2022). Bilateral tibial stress fractures and osteoporosis in a young patient. *Sports Health*, *14*(3), 440-443. doi: 10.1177/19417381211032127

[16] Ikebe, K., Kato, T., Yamaga, M., Hirose, J., Tsuchida, T., & Takagi, K. (2001). Increased ischemia-reperfusion blood flow impairs skeletal muscle contractile function. *J Surg Res*, *99*(1), 1-6. doi: 10.1006/jsre.2001.6134

[17] Kim, J. G., Lee, J., Roe, J., Tromberg, B. J., Brenner, M., & Walters, T. J. (2009). Hemodynamic changes in rat leg muscles during tourniquet-induced ischemia-reperfusion injury observed by near-infrared spectroscopy. *Physiol Meas*, *30*(7), 529-540. doi: 10.1088/0967-3334/30/7/001

[18] Kim, S. J., Kim, E. K., Kim, S. J., & Song, D. H. (2018). Effects of bone marrow aspirate concentrate and platelet-rich plasma on patients with partial tear of the rotator cuff tendon. *J Orthop Surg Res*, *13*(1), 1. doi: 10.1186/s13018-017-0693-x

[19] Knapik, J., Montain, S. J., McGraw, S., Grier, T., Ely, M., & Jones, B. H. (2012). Stress fracture risk factors in basic combat training. *Int J Sports Med*, *33*, 940-946. doi: 10.1055/s-0032-1311583

[20] LaPelusa, A., & Dave, H. D. (2025). *Physiology, Hemostasis*. In *StatPearls* (Internet). Treasure Island (FL): StatPearls Publishing.

[21] Li, Y., Jiang, J., Tong, L., Gao, T., Bai, L., Xue, Q., & Sun, Z. (2020). Bilobalide protects against ischemia/reperfusion-induced oxidative stress and inflammatory responses via MAPK/NF-κB pathways in rats. *BMC Musculoskelet Disord*, *21*(1), 449. doi: 10.1186/s12891-020-03479-9

[22] Obeid, H., Bikia, V., Segers, P., Pare, M., Boutouyrie, P., Stergiopulos, N., & Agharazii, M. (2024). Impact of arterial system alterations due to amputation on arterial stiffness

and hemodynamics: A numerical study. *Sci Rep*, *14*(1), 24852. doi: 10.1038/s41598-024-75881-5
[23] Paniccia, R., Priora, R., Liotta, A. A., & Abbate, R. (2015). Platelet function tests: A comparative review. *Vasc Health Risk Manag*, *11*, 133-148. doi: 10.2147/VHRM.S44469
[24] Pihlajamäki, H., Parviainen, M., Kyröläinen, H., Kautiainen, H., & Kiviranta, I. (2019). Regular physical exercise before entering military service may protect young adult men from fatigue fractures. *BMC Musculoskelet Disord*, *20*, 126. doi: 10.1186/s12891-019-2513-4
[25] Schulman, S., Makatsariya, A., Khizroeva, J., Bitsadze, V., & Kapanadze, D. (2024). The basic principles of pathophysiology of venous thrombosis. *Int J Mol Sci*, *25*(21), 11447. doi: 10.3390/ijms252111447
[26] Schultz, D. J., Brasel, K. J., Washington, L., Goodman, L. R., Quickel, R. R., Lipchik, R. J., … & Weigelt, J. (2004). Incidence of asymptomatic pulmonary embolism in moderately to severely injured trauma patients. *J Trauma*, *56*(4), 727-731. doi: 10.1097/01.ta.0000119687.23542.ec
[27] Serchan, P., Shorten, G., Maher, M., & Power, S. P. (2019). Pulmonary embolism occurring early after major trauma. *BMJ Case Rep*, *12*(9), e228783. doi: 10.1136/bcr-2018-228783
[28] Seymour, R. S., Hu, Q., Snelling, E. P., & White, C. R. (2019). Interspecific scaling of blood flow rates and arterial sizes in mammals. *J Exp Biol*, *222*, 1-10. doi: 10.1242/jeb.199554
[29] Sibley, A. R., Strike, S, Moudy, S. C., & Tillin, N. A. (2020). The effects of long-term muscle disuse on neuromuscular function in unilateral transtibial amputees. *Exp Physiol*, *105*(3), 408-418. doi: 10.1113/EP088087
[30] Singh, D. P., Barani Lonbani, Z., Woodruff, M. A., Parker, T. J., Steck, R., & Peake, J. M. (2017). Effects of topical icing on inflammation, angiogenesis, revascularization, and myofiber regeneration in skeletal muscle following contusion injury. *Front Physiol*, *8*, 93. doi: 10.3389/fphys.2017.00093
[31] Stein, C. J., Sugimoto, D., Slick, N. R., Lanois, C. J., Dahlberg, B. W., Zwicker, R. L., & Micheli, L. J. (2019). Hallux sesamoid fractures in young athletes. *Phys Sportsmed*, *47*(4), 441-447. doi: 10.1080/00913847.2019.1622246
[32] van Stralen, K. J., Rosendaal, F. R., & Doggen, C. J. (2008). Minor injuries as a risk factor for venous thrombosis. *Arch Intern Med*, *168*(1), 21-26. doi: 10.1001/archinternmed.2007.5
[33] Zamorano, M., Castillo, R. L., Beltran, J. F., Herrera, L., Farias, J. A., Antileo, C., & Farias, J. G. (2021). Tackling ischemic reperfusion injury with the aid of stem cells and tissue engineering. *Front Physiol*, *12*, 705256. doi: 10.3389/fphys.2021.705256
[34] Zhou, T., Prather, E. R., Garrison, D. E., & Zuo, L. (2018). Interplay between ROS and antioxidants during ischemia-reperfusion injuries in cardiac and skeletal muscle. *Int J Mol Sci*, *19*(2), 417. doi: 10.3390/ijms19020417

РОЛЬ МЕХАНІЧНОГО НАВАНТАЖЕННЯ ТА ЛОКАЛЬНОГО ТРОМБОЗУ СУДИН У ФОРМУВАННІ СТРЕСОВОГО ПЕРЕЛОМУ КУКСИ КІСТКИ (ЕКСПЕРИМЕНТАЛЬНЕ ДОСЛІДЖЕННЯ)

Безсмертний Ю. О., Бондаренко Д. В., Шевчук В. І., Браніцький О. Ю.

Ампутація кінцівки призводить до порушення ремоделювання кукси кістки, яке часто завершується її функціональною неспроможністю і необхідністю реампутацій. До сьогодні загальноприйнятним поясненням формування стресових переломів є накопичення втомних мікропошкоджень в компактному шарі кістки. Участь інших тканин у формуванні стресових переломів не вивчалась. В процесі експериментальних досліджень стресових переломів після ампутацій в частині випадків простежувалась чітка лінія виникнення локальних мікротромбозів судин м'язів, кістки, кісткового мозку з їх ішемічним некрозом та формуванням стресових переломів кукси кістки. Мета роботи: дослідити роль локальних змін судин і м'язів у виникненні стресового перелому кісток ампутаційної кукси при механічному навантаженні. Матеріалом для експерименту були 42 кролі, у яких формували стресові переломи кукси стегнової кістки шляхом дозованої пневматичної компресії (30 мм рт. ст.) м'яких тканин і сфокусованої на торцеву поверхню ударної хвилі з енергією 0,5 мДж/мм², частотою 2 Гц з подачею 400 імпульсів за сеанс під знеболенням щоденно. Метод дослідження гістологічний з наливкою судин туш-желатиновою сумішшю. Морфологічне дослідження кістки включало вивчення гістотопографічних і звичайних гістологічних зрізів кісткової тканини. Оцінювали стан мікроциркуляторної мережі кістки та м'язів. Враховували (без спеціальних вимірювань) щільність розташування судин та їх діаметр. В м'язах морфометрично оцінювали кількість фіброзної тканини. На мікрофотографіях при збільшеннях ×200 та ×400 вимірювали діаметр окремого м'язового волокна. Оцінку статистичних відмінностей між групами проводили за допомогою непараметричного тесту Краскала-Волліса та U-тесту Манна-Уітні. В результаті поряд з традиційним розвитком стресових переломів виявлені мікротромбози судин оточуючих м'язів, кістки і кісткового мозку, що призвели до ішемічного некрозу цих структур і формування стресових переломів. В компактній кістці вище і нижче перелому наступали дистрофічні та некротичні процеси, які характеризувались лізисом остеоцитів, некрозом вмісту центральних каналів, бідністю гаверсових каналів, розвитком остеопорозу. Виразна рарефікація супроводжувалась зменшенням кількості і товщини кісткових балок та клітинних елементів. Дном щілини перелому був некротизований кістковий мозок. В подальшому спостерігалось заповнення щілини перелому фіброзною тканиною та балками ендостального кісткоутворення. Загоєння переломів проходило за рахунок фіброзної та кісткової тканин. Таким чином, нами встановлено, що циклічне навантаження кукси кістки, поєднане з компресією м'язів, поряд з втомою кістки викликає втому м'яких тканин з формуванням мікротромбозів в судинах м'яких тканин, кістки і кісткового мозку з ішемічним некрозом цих тканин і стресовим переломом.

Ключові слова: *кролі, ампутація, механічне навантаження, втома м'яких тканин, мікротромбоз, стресові переломи, морфологічні зміни, регенерація.*

Author's contribution

Bezsmertnyi Y. O. – data visualization, formal analysis and validation.
Bondarenko D. V. – software, resources.
Shevchuk V. I. – research, methodology and writing of the original draft.
Branitsky O. Y. – conceptualization, supervision.

DOI: 10.31393/morphology-journal-2025-31(4)-07 Reports of Morphology, Vol. 31, №4, Pages 51-58

ISSN 1818-1295 eISSN 2616-6194

REPORTS OF MORPHOLOGY

Official Journal of the Scientific Society of Anatomists, Histologists, Embryologists and Topographic Anatomists of Ukraine

journal homepage: https://morphology-journal.com

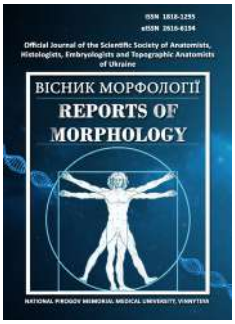

Morphological and immunohistochemical characteristics of the thymus of newborns in the early neonatal period

Islamov Sh. E.[1], Yakubov M. Z.[1], Alikulov A. I.[2], Zhuraev K. D.[1], Makhmatmuradova N. N.[1], Kudratov R.[2]

[1] Samarkand State Medical University, Samarkand, Uzbekistan

[2] Samarkand State University of Veterinary Medicine, Samarkand, Uzbekistan

ARTICLE INFO

Received: 23 January 2025

Accepted: 17 September 2025

UDC: 616-007.15

CORRESPONDING AUTHOR

e-mail: shavkat.islamov.1972@mail.ru

Islamov Sh. E.

CONFLICT OF INTEREST

The authors have no conflicts of interest to declare.

FUNDING

Not applicable.

DATA SHARING

Data are available upon reasonable request to corresponding author.

The fetal immune system develops and functions under complex conditions. While it maintains internal fetal homeostasis, it must quickly adapt and respond to maternal antigens. The aim of this study was to examine the pathological and immunohistochemical characteristics of thymus tissue in infants who died in the early neonatal period. The morphological and immunohistochemical characteristics of the thymus were analyzed in 30 infants born to mothers with preeclampsia and eclampsia who died in the early neonatal period. Thymus fragments were obtained at autopsy, fixed in 10 % neutral formalin, and then subjected to standard processing and paraffin embedding. Subsequent histological and immunohistochemical analysis was performed using CD3, CD4, and Ki-67 markers. Statistical analysis of the obtained results was performed using STATISTICA for Windows and MS Excel, employing variation statistics methods. It was established that the statistically significant changes in the integral ratio between the adrenal and thymus masses morphologically indicate the development of premature glucocorticoid-associated thymus involution. Morphologically, a marked increase in the glandular epithelium of the enterochromaffin cells of the zona fasciculata of the adrenal cortex, a sharp increase in the number of lipid inclusions in their cytoplasm, and signs of vascular plethora are noted. The thymus is characterized by a fibrous capsule of variable thickness, a convoluted surface, interstitial edema in the capsule wall, thickening and disorganization of fibrous structures, as well as numerous Hassall's corpuscles and signs of active apoptosis. Morphological changes in the thymus in neonates born to mothers with preeclampsia and eclampsia and those who died in the early neonatal period are accompanied by signs of premature involution and secondary immunodeficiency. High expression of the Ki-67 marker reflects increased proliferative activity of lymphocytes, while low positive expression of CD3+ and CD4+ indicates impaired differentiation of T-lymphocytes and insufficient production of T-helpers, which leads to decreased resistance to infections and the development of immunodeficiency states.

Keywords: *newborns, thymus, morphology, immunohistochemistry, signs, involution, immunodeficiency.*

Introduction

Currently, the prevention of early neonatal mortality of newborns born to mothers with preeclampsia and eclampsia is one of the pressing problems of modern neonatology, since the introduction into practice of criteria for live and stillbirths developed and recommended by the WHO has led to an increase in the number of registered newborns with a body weight of 500 to 999 g [6]. Globally, the average incidence of preeclampsia and eclampsia in pregnant women is 35-65 per 100,000 pregnancies. Despite a relatively small proportion (0.2-2 %) of all newborns, extremely premature infants account for 45-55 % of all births and 60-70 % of all cases of early neonatal death [13, 24, 25].

The effectiveness of nursing children with very low birth weight depends on the morphofunctional maturity of the hypothalamic-pituitary-adrenal and immune systems, which ensure the postnatal adaptation of children [7, 16, 22, 27].

The fetal immune system develops and functions under complex conditions. On the one hand, it maintains internal fetal homeostasis, while on the other, when exposed to antigenic influences from the mother's body, it must quickly

adapt and respond [3, 10, 21, 30]. It has been established that immune system processes such as proliferation, differentiation, migration, cooperation, and apoptosis are genetically determined [20, 28].

Despite significant advances in medicine in the study of the thymus gland, the significance of thymomegaly and thymus hypoplasia remains unclear, necessitating various studies to determine the etiology, pathogenesis, clinical, functional, morphological significance, consequences and prognosis of its diseases.

The aim of the study was to investigate the pathomorphological and immunohistochemical characteristics of thymus tissue in children who died in the early neonatal period.

Materials and methods

The morphological and immunohistochemical characteristics of the thymus were studied in 30 infants born to mothers with preeclampsia and eclampsia, and those who died in the early neonatal period. The study was approved by the Bioethics Committee of Samarkand State Medical University (Protocol № 3 dated November 6, 2024).

Thymus tissue samples obtained during autopsy were fixed in 10 % neutral formalin for 72 hours, rinsed in running water for 3-4 hours, then dehydrated in 70, 80, 90, 96, and 100 % alcohol and chloroform, and embedded in paraffin to prepare blocks. Sections of 3-5 μm thickness were prepared from the paraffin blocks on rotary microtomes. The paraffin was removed from the sections by melting them with xylene in an incubator at 57 °C, after which they were stained with hematoxylin and eosin solutions to examine the general histological condition of the thymus tissue.

To study profound morphological changes in the thymus gland of children who died in the neonatal period, the IHC markers CD-3, CD-4, and Ki-67 were used. These markers allow the expression and identification of various types of lymphocytes in the thymus at different stages of development.

The paraffin-embedded biopsy material was subjected to immunohistochemistry using monoclonal antibodies using standard methods. 4-μm-thick sections were prepared from the paraffin blocks, placed on glass slides, and dried at room temperature for 24 hours. Before staining, sections were placed vertically in a thermostat at 55 °C for 60 minutes. They were then deparaffinized in orthoxylene (10 minutes each in two-volume batteries), rehydrated in decreasing concentrations of ethyl alcohol (3 minutes each in three-volume batteries), and rinsed in distilled water. The slide containing the section was heated, placed in unmasking buffer, and placed in a water bath at 98 °C for 30-40 minutes.

After cooling to room temperature, the slides are washed in Tris-buffered saline (pH 7.5). To block endogenous peroxidase, sections are treated with 3 % H_2O_2 solution for 15 minutes. To reduce nonspecific binding and limit background staining, slides are treated with Protein Block (X0909) (DAKO) for 10 minutes. Before adding antibodies, sections were immersed in a special diluting solution to preserve the reagents and prevent leakage. Incubation with primary antibodies was carried out for 60-120 minutes at room temperature. The LSAB2 universal imaging kit (DAKO) was used with a minimum exposure time of 40 minutes.

Paraffin in the sections was removed by melting it with xylene in a thermostat at a temperature of 57 °C, after which the general histological condition of the lymph node tissue was studied using immunohistochemical markers.

In this study, the CD+3, CD+4, and Ki-67 markers were used. The CD+3 marker is a coreceptor for a multiprotein complex on the membrane of T lymphocytes present in the thymic cortex and binds to this receptor to identify T lymphocytes. Morphologically, it ranges in color from golden yellow to light brown. It is primarily used to quantify T lymphocytes in the paracortical region. CD+4 is a coreceptor for a protein on the B-lymphocyte membrane that binds to this receptor and stains the T-lymphocyte a golden-yellow-brown color. To do this, the prepared blocks are placed on a special adhesive slide and the material is cut using a microtome. The material is then incubated in hematoxylin solution for 2 minutes.

Using a special automated device (DAKO), CD+3 and CD+4 are applied to a glass slide surface labeled with a QR code. After 20 minutes, they are rinsed with distilled water. The slide surfaces are covered with a cover slip. To verify the accuracy of our work, when examining the slide under a microscope for reactions with the above-mentioned markers, we see golden-yellow-brown cells in the biopsy specimens. Thus, our methodology was implemented correctly. When the above markers react with a special protein on the lymphocyte membrane, a change in the indicator's color is considered an indication of a «+» expression level (Table 1). In this case, we consider the markers to be expressed by name.

Table 1. Immunohistochemical staining intensity scale.

Evaluation criteria	Note	Color index scale
«-»	No reaction	
«+»	Low expression	
«++»	Moderate expression	
«+++»	High expression	

The intensity of cell staining (or their nuclei for Ki-67 protein, estrogen receptors, and progesterone receptors) was assessed visually on a scale from 0 to 3 (negative, weak, moderately stained), and the percentage of positively stained cells was calculated. Each indicator was calculated as an intensity value (minimum for 500 epithelial and 500 stromal endometrial cells in 10 fields of view at a microscope magnification of ×400).

Statistical analysis was performed using MS Office Excel 2007 and STATISTICA for Windows 10. The significance level of differences was set at $p<0.05$. The Student's t-test was used to determine the distribution norm and to examine dynamics within groups and between populations.

Results

Our study examined morphological changes in the thymus in infants born to mothers with preeclampsia and eclampsia who died in the neonatal period. We selected infants who died in the early neonatal period (0-7 days).

The average thymus mass in children born in the early neonatal period was 7.163±1.121 g, while in the control group this figure was 13.46±1.82 g. It was found that the adrenal gland mass in children born during this period was 7.752±0.024 g, while in the control group this figure was 4.110±0.171 g. This means that the adrenal gland mass in children born against the background of preeclampsia increased by 1.71 – 1.88 times.

As a result, the presence of statistically significant differences in the integral ratio between adrenal and thymus tissue indicates, from a morphological perspective, the development of premature glucocorticoid-associated thymic involution. Morphologically, it was established that the glandular epithelium of the enterochromaffin cells of the fasciculate layer of the adrenal cortex is significantly enlarged, with a sharp increase in the number of lipid inclusions in its cytoplasm, and signs of vascular congestion. Morphologically, the thymus is characterized by a fibrous capsule of varying thickness, a tortuous surface, signs of plethora, the formation of interstitial edema in the capsule wall, the appearance of thickenings and disorganization of fibrous structures.

The epithelial cells (mother cells) in the subcapsular region were oval in shape, with pale eosinophilic cytoplasm, surrounded by a few prethymocytes, numerous macrophages located along the perimeter, coarse fibrous structures were observed in the intermediate stroma, and signs of plethora of varying intensity were observed in the small-caliber vessels of the cortical layer (Fig. 1, 2).

The density of cortical epithelial cells is sharply reduced, and the stroma contains ruptured areas resembling pore spaces. No hypercellularity is observed in the general background at 100-fold magnification. Along the perimeter of the lobules, longitudinally compressed epithelial growths with surrounding punctate spaces are visible in the blood-thymic barrier. Endothelial cells are unchanged, trabecular structures are thickened, the number of sparse fibrous

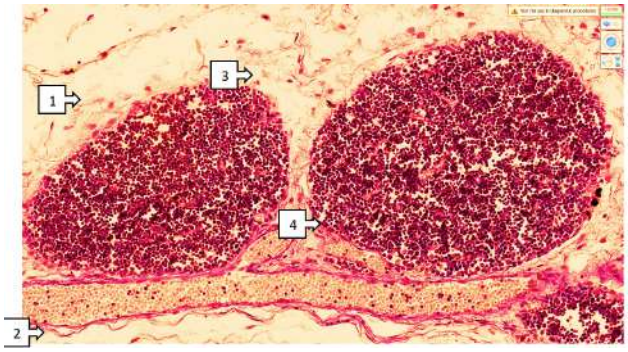

Fig. 1. Early neonatal period. Newborn, 5 days old. Thymus lobule, intermediate edema in its capsule (1), pronounced vascular congestion (2), disorganization of rare fibrous structures in the capsule (3). Hassall's corpuscles of varying size are revealed (4), the trabecular meshwork of the cortex extends into the medulla, and edema forms in the interstitium. Exposed stromal fragments are determined in the medulla. Vascular congestion is revealed in all layers. Hematoxylin-eosin staining, ×100.

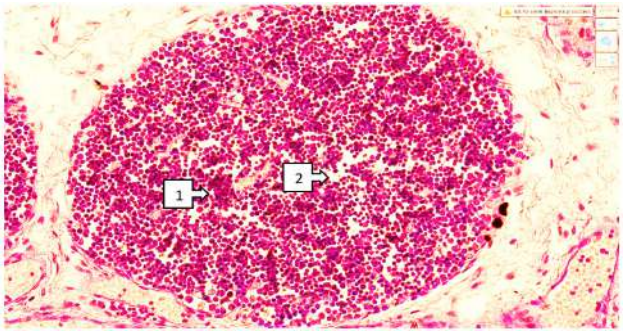

Fig. 2. Early neonatal period. 7-day-old newborn. Increased apoptosis of small lymphocytes was detected in the cortex of the gland (1), and pronounced exposure and disorganization of fibrous structures were detected in the stroma (2). Hematoxylin-eosin staining, ×40.

structures is increased, trabecular blood vessels are markedly congested, and proliferatively active foci of fibroblasts are visible along their perimeter. Specifically, around the foci of actively proliferating fibroblasts, proliferation of sparse fibrous connective tissue is observed, trabeculae of varying thickness appear, and the fibrous tissue surrounding the thymus lobules thickens.

In the medulla, numerous endothelial cells with high cytoplasm are reduced in size, metaplasia into normal endothelial cells is observed, and foci of interstitial edema and randomly distributed fibrous structures are seen around postcapillary venules. The detection of a large number of epithelial cells within Hassall's corpuscles confirms the rapid development of new corpuscles. The presence of intertwined cellular branches, separated and dissociated from each other, as well as the presence of homogeneous, loosely arranged cellular fragments in the form of various corpuscles, indicates the rapid development of apoptosis (Figs. 3, 4).

A relatively significant increase in the number of macrophages containing homogeneous inclusions of varying

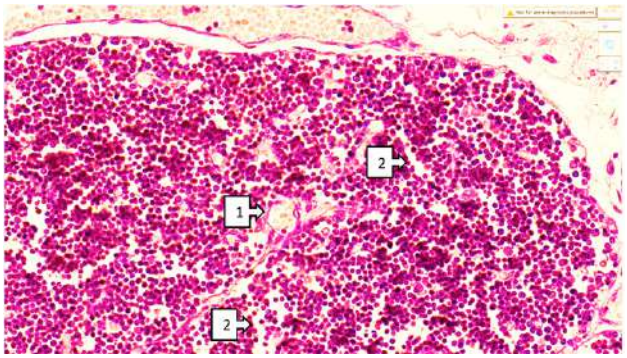

Fig. 3. Early neonatal period. 7-day-old newborn. It was established that plethora, occurring even in small capillaries (1), leads to the formation of plasma congestion in the thymus parenchyma and foci of disorganization in the stromal connective tissue with the presence of spaces (2). Hematoxylin-eosin staining, ×40.

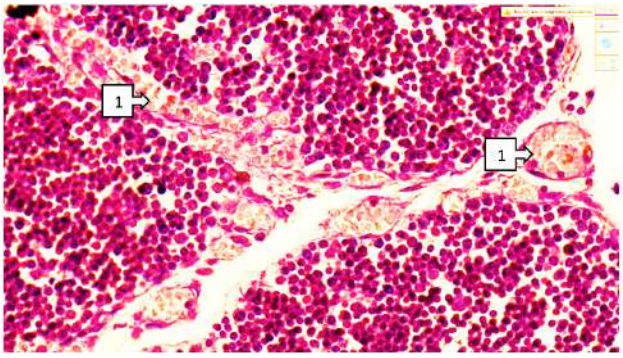

Fig. 4. Early neonatal period. 7-day-old newborn. Space between glandular lobules. In the cortex, disruption of the anastomoses of small-caliber venous vessels and a sludge phenomenon in erythrocytes were detected (1). Hematoxylin-eosin staining, ×400.

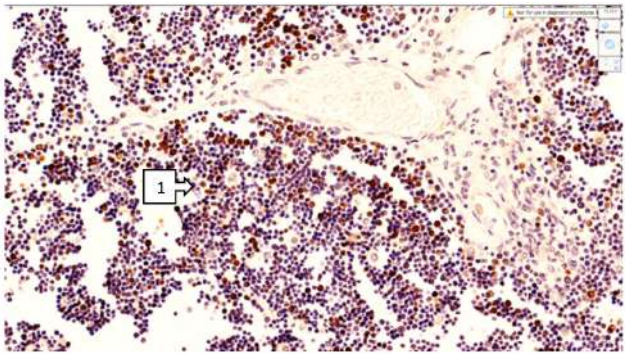

Fig. 5. Thymus tissue from a newborn who died on day 4 of the early neonatal period. High positive expression of the Ki-67 marker in the thymus tissue (1). Scanning with QuPath-0.4.0.ink and determination of expression levels. Expressed cells are dark brown. Dab chromogen staining, ×40.

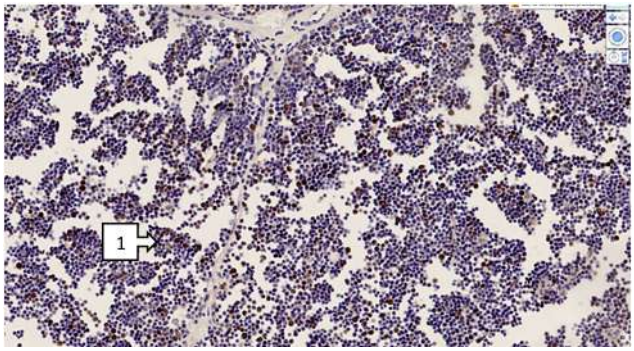

Fig. 6. Thymus tissue from a newborn who died on day 6 of the early neonatal period. Moderately positive expression of the Ki-67 marker in the thymus tissue (1). Scanning with QuPath-0.4.0.ink and determination of the expression level. Expressed cells are dark brown. Dab chromogen staining, ×40.

intensity in the cytoplasm around Hassall's bodies and postcapillary venules indicates an increase in the phagocytic process during apoptosis and confirms the development of thymus involution in children with severe preeclampsia and eclampsia, as well as in those who died in the early neonatal period from diseases of various origins.

In the early neonatal period, on days 0-7, a high level of proliferation with a high level of positive expression of the Ki-67 marker is observed in the organs of the immune system, which is maintained as the degree of differentiation increases.

In our study, among those who died in the early neonatal period, 80.0 % (24 patients) had high positive expression of the Ki-67 marker, with an average of 26.1 % and higher. Moderate positive expression was detected in 15.1 % of the examined individuals, which amounted to 16.7 % (5 patients), while in 3.3 % (1 patient), the expression level was less than 10 %. In our material, high expression was observed in 4/5 patients, which can be considered a highly positive indicator indicating a high response of the Ki-67 marker (Figs. 5, 6).

The study found that the CD3+ marker was primarily used as a marker characterizing T-lymphocytes. This confirms that T-lymphocyte cellular immunity in newborns is not fully developed, as the low positive expression of the CD3+ marker, which predominantly stains macrophages, is due to the sharp decrease in the number of T-lymphocytes in the thymic cortex, most of which undergo induced apoptosis.

In our study, 83.3 % of participants had low positive expression, and 16.7 % had negative expression. This means that lymphocytes with the CD3+ marker were very few (Figs. 7, 8).

One of the main changes in the thymus during autopsy of those who died in the early neonatal period was revealed by simple morphological studies, which manifested itself in an accidental transformation of the thymus and a decrease in immunocompetent cells. Immunohistochemical studies performed to identify the T-helper lymphocyte subpopulation using the CD4+ marker revealed a very low level of positive expression, which is due to the extremely low number of T-helper cells in the thymic cortex and medulla, which produce immunostimulatory factors that activate killer T-cells. The absence of autologous tissue confirms the lack of differentiation toward tolerance. Therefore, from a clinical and morphological perspective, this manifestation is considered a type of immunodeficiency (Figs. 9, 10).

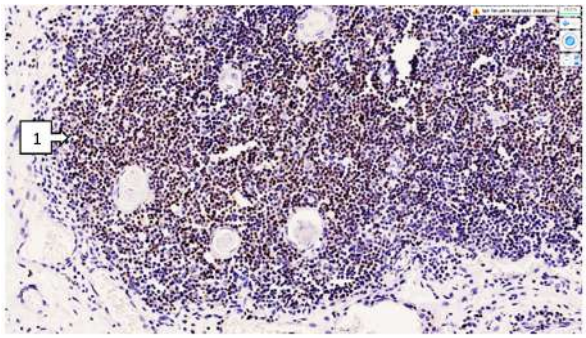

Fig. 7. Thymus tissue from a child who died on day 3 of the early neonatal period. High levels of CD3 marker expression in the thymus tissue (1). Scanning was performed using QuPath-0.4.0.ink, and the expression level was determined. Cells that do not express most of the red dye are shown in red. Dab chromogen staining, ×40.

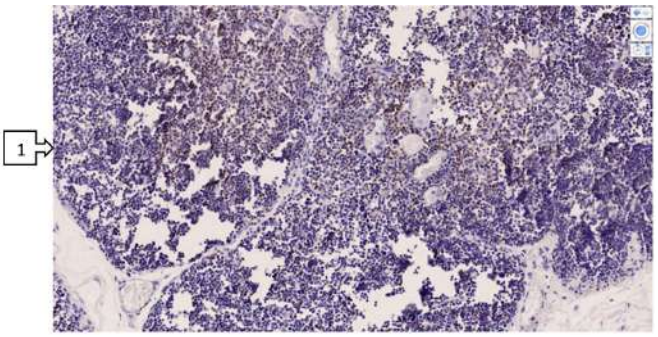

Fig. 8. Thymus tissue from a newborn who died on day 4 of the early neonatal period. High levels of positive expression of the CD3 marker in the thymus tissue (1). Scanning with QuPath-0.4.0.ink and determination of expression levels. Non-expressing cells are dark brown. Dab chromogen staining, ×40.

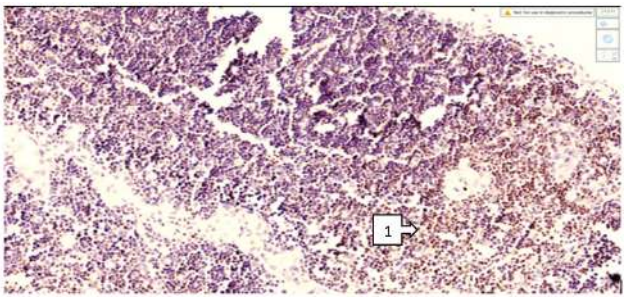

Fig. 9. Thymus tissue from a newborn who died on day 7 of the early neonatal period. Moderately positive expression of the CD4 marker in the thymus tissue (1). QuPath-0.4.0.ink. The program was used for scanning and determining the expression level. Expressed cells are dark brown. Dab chromogen staining, ×40.

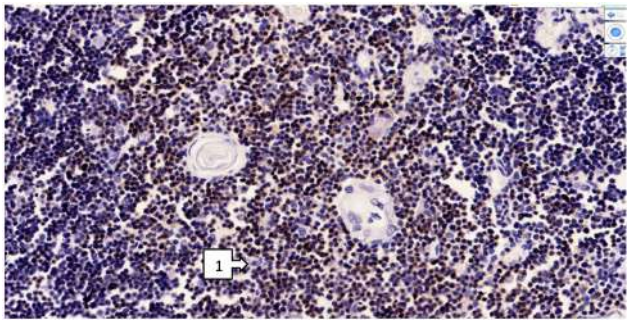

Fig. 10. Thymus tissue from a newborn who died on day 5 of the early neonatal period. Low levels of positive expression of the CD4 marker in the thymus tissue (1). Expressed cells are dark brown. Dab chromogen staining, ×40.

Thymic marker and CD4+ expression was also very low and scattered, mainly in macrophages, as relatively large and elongated cells around postcapillaries.

Discussion

In children who died on the 7th day, morphologically, the thymus had branched bundles of fibrous tissue in the stroma, which were more clearly developed compared to those in children 3-5 days old, which indicates a significant disruption of the boundaries of the cortical, corticomedullary and medullary parts of the thymus. In particular, it has been established that the thymus capsule is rich in fuchsinophilic fibers of varying thickness with an uneven trajectory of location along the perimeter, which leads to deformation of the thymus surface, and as a result of compression of the parenchyma, to atrophic changes, which causes a decrease in mass from an organometric point of view [4, 5, 11, 14].

As a result of increased formation of lymphocytes present in the parenchyma of the fully formed thymus, that is, the primary immune organ, a positive expression of the Ki-67 marker is determined, which is 200 times higher than in the control group and amounts to an average of 26.1 %. In the early neonatal period, damage caused by various infections leads to the release of profilogenic inflammatory mediators through the blood and lymphatic vessels in large quantities, leading to increased cytokine and lymphokine production. This leads to increased hyperfunctional activity of the primary immune organs. As a result, a large number of small lymphocytes are detected in the thymic cortex in the early neonatal period [23, 29].

In our study, this is mainly due to the low number of immature small lymphocytes in the thymic cortex and incomplete differentiation of CD3+ lymphocytes to the autologous antigen, which is manifested by the presence of lymphocytes, but the absence of their coreceptors, which do not give positive immunohistochemical reactions. At the same time, the morphologically greater number of T-lymphocytes than the number, and the morphofunctionally greater ability of dendritic cells to recognize autologous tolerance receptors on the lymphocyte membrane, their preservation in the form of prothymocytes and the absence of binding to the CD3+ marker we used, confirm the above data [12, 19].

According to an immunohistochemical study conducted to identify the T-helper lymphocyte subpopulation using the CD4+ marker, the level of positive expression was extremely low, and the extremely low number of T-helper cells producing immunostimulating factors that activate T-killer cells in the thymic cortex and medulla confirms the absence of differentiation toward autologous tissue tolerance. Moreover, from a clinical and morphological perspective,

this manifestation is considered a type of immunodeficiency [17, 18].

Thus, low positive expression of CD3+ and CD4+ markers in the examined thymus tissue indicates impaired differentiation of CD3+ lymphocytes and low formation of T-helper cells with CD4+ markers, which in turn leads to a sharp decrease in immunodeficiency and resistance to infection. This was confirmed in all patients who died from sepsis and septicemia that developed as a result of infection in the postnatal period, as was formed in the clinical and anamnestic data of children who died in the early neonatal period [6, 9].

It has been established that factors influencing the ontogenesis of the thymus in children born in the early neonatal period, against the background of preeclampsia and eclampsia, creating conditions for the development of involution of the gland, premature formation of Hassall's bodies, expansion and sclerosis of the interstitial barriers, uniform distribution of reticuloepithelial cells in all zones, the practical absence of epithelioid cells rich in secretory granules, accidental transformation of the thymus, a sharp decrease in lymphocytes, persistent vascular congestion and the development of interstitial edema lead to premature involution of the thymus and the development of secondary immunodeficiency [12, 15].

This directly confirms the partial detachment of a normally located placenta in preeclampsia and eclampsia, as well as increased stress factors caused by impaired fetoplacental circulation and fetal hypoxia. The thymus of newborns in the early neonatal period is characterized by incomplete formation of morphofunctionally active zones of immune organs and a decrease in the size of reticuloepithelial cells of the cortical layer, a decrease in the number of lymphocytes developing around it, a decrease in the area of proliferatively active lymphocytes, an increase in apoptotic bodies and the presence of homogeneous pink cellular components [26].

Morphologically, this was manifested in the form of clear signs of involution in the thymus, as well as a sharp change in the ratio of the cortical and medulla layers [1, 2, 8].

The obtained results highlight the importance of timely prevention and correction of immune system disorders in high-risk newborns, as well as the need for further research aimed at clarifying the mechanisms of hormonal and immune regulation of the thymus under conditions of perinatal stress and hypoxia.

Conclusions

1. Factors influencing the ontogenesis of thymus development in children born in the early neonatal period against the background of preeclampsia and eclampsia are conditions that promote the involution of the glands, the premature formation of Hassall's corpuscles, the expansion of the interlobular septa, their sclerosis and the uniform distribution of reticuloepithelial cells throughout all areas.

2. The almost complete absence of epithelioid cells rich in secretory granules, accidental transformation of the thymus, a sharp decrease in the number of lymphocytes, persistent vascular congestion and the development of interstitial edema contribute to premature involution of the thymus and the development of secondary immunodeficiency.

3. Low positive expression of CD3+ and CD4+ markers in thymus tissue indicates impaired differentiation of CD3+ lymphocytes and low production of CD4+ T-helpers, which indicates immunodeficiency and a sharp decrease in resistance to infection.

References

[1] Abaeva, T., Muratov, Z., Tukhvatshin, R., Abdullaeva, Z., Seitova, A., Tursunova, V., ... & Alimbekova, A. (2020). Morphological Characteristics of Thymus in the Newborns in Different Climatic and Geographical Conditions of Kyrgyzstan. International Journal of Medical Physics, Clinical Engineering and Radiation Oncology, 9(4), 178-185. doi: 10.4236/ijmpcero.2020.94016

[2] Abaeva, T., Tuhvatshin, R., Satybaldiev, M., Ergeshova, A., Toichieva, Z., & Bakytova, S. (2023). Stages of the evolution of thymus atrophy in children in different cities of Kyrgyzstan. Biomedicine, 43(01), 364-367. doi: 10.51248/.v43i01.2655

[3] Cowan, J. E., Takahama, Y., Bhandoola, A., & Ohigashi, I. (2020). Postnatal involution and counter-involution of the thymus. Front Immunol, 11, 897. doi: 10.3389/fimmu.2020.00897

[4] D'Attilio, L., Santucci, N., Bongiovanni, B., Bay, M. L., & Bottasso, O. (2018). Tuberculosis, the disrupted immune-endocrine response and the potential thymic repercussion as a contributing factor to disease physiopathology. Front Endocrinol (Lausanne), 9(214), 1-9. doi: 10.3389/fendo.2018.00214

[5] Fahy, G. M., Brooke, R. T., Watson, J. P., Good, Z., Vasanawala, S. S., Maecker, H., … & Horvath, S. (2019). Reversal of epigenetic aging and immunosenescent trends in humans. Aging Cell, 18(6), e13028. doi: 10.1111/acel.13028

[6] Geenen, V. (2012). Presentation of neuroendocrine self in the thymus: a necessity for integrated evolution of the immune and neuroendocrine systems. Ann N Y Acad Sci, 1261(1), 42-48. doi: 10.1111/j.1749-6632.2012.06624.x

[7] Halawani, A. Z., Alharbi, M. A., Alkhuraym, Y. Y., Alharthi, A. H., Alqahtani, S. F. M., Al-Qahtani, M. M. A., ... & Alghamd, A. S. (2023). Low Birth Weight and Preterm Infants Nursing Care: an Updated Review. International journal of health sciences, 7(S1), 3779-3794. doi: 10.53730/ijhs.v7nS1.15387

[8] Hale, L. P., Neff, J., Cheatham, L., Cardona, D., Markert, M. L., & Kurtzberg, J. (2020). Histopathologic assessment of cultured human thymus. PLoS One, 15(3), e0230668. doi: 10.1371/journal.pone.0230668

[9] Hirokawa, K., Utsuyama, M., & Kikuchi, Y. (2016). Trade off situation between thymus and growth hormone: age-related decline of growth hormone is a cause of thymic involution but favorable for elongation of lifespan. Biogerontology, 17(1), 55-59. doi: 10.1007/s10522-015-9590-z

[10] Hossain, Z., Reza, A. M., Qasem, W. A., Friel, J. K., & Omri, A. (2022). Development of the immune system in the human embryo. Pediatric research, 92(4), 951-955. doi: 10.1038/s41390-022-01940-0

[11] Hryhorieva, O. A., Masenko, V. L., & Tkachenko, T. M. (2017).

Peculiarities of lymphocyte emigration from the thymus of newborns. Pathologia, 14(1), 76-80. doi: 10.14739/2310-1237.2017.3.118765

[12] Israilov, R., Isoev, G., & Numanov, K. (2016). Сепсис у новорожденных и морфологическое состояние тимуса [Sepsis in newborns and the morphological state of the thymus]. Журнал проблемы биологии и медицины=Journal of Problems of Biology and Medicine, 3(89), 29-31.

[13] Khan, B., Yar, R. A., khan Khakwani, A., Karim, S., & Ali, H. A. (2022). Preeclampsia Incidence and Its Maternal and Neonatal Outcomes With Associated Risk Factors. Cureus, 14(11), e31143. doi: 10.7759/cureus.31143

[14] Korjavov, S O., Ismoilov, O. I., & Otamurodova, K. B. (2023). Morphological characteristics of thymus gland in young children. Research Focus, 2(9), 99-103. doi: 10.5281/zenodo.8343017

[15] Korzhavov, Sh., Tukhtamurodov, Kh., Farukhova, M., & Kuvondikov, G. (2022). Антропометрические и физиологические особенности вилковой железы у новорожденных и детей раннего возраста (обзор литературы) [Anthropometric and physiological features of the thymus gland in newborns and young children (literature review)]. Евроазийский журнал медицинских и естественных наук=Eurasian Journal of Medical and Health Sciences, 2(6), 118-130.

[16] Lins, M. P., Vieira, L. F. D. A., Rosa, A. A. M., & Smaniotto, S. (2016). Growth hormone in the presence of laminin modulates interaction of human thymic epithelial cells and thymocytes in vitro. Biological research, 49, 1-9. doi: 10.1186/s40659-016-0097-0

[17] Lins, M. P., Viana, I. M. M. N., Smaniotto, S., & Reis, M. D. D. S. (2020). Interactions between thymic endothelial cells and thymocytes are influenced by growth hormone. Growth Factors, 38(3-4), 177-188. doi: 10.1080/08977194.2021.1924699

[18] Lio, C. W., & Hsieh, C. S. (2011). Becoming self-aware: the thymic education of regulatory T cells. Curr Opin Immunol, 23(2), 213-219. doi: 10.1016/j.coi.2010.11.010

[19] Majumdar, S., Deobagkar-Lele, M., Adiga, V., Raghavan, A., Wadhwa, N., Ahmed, S. M., … & Nandi, D. (2017). Differential susceptibility and maturation of thymocyte subsets during Salmonella Typhimurium infection: insights on the roles of glucocorticoids and Interferon-gamma. Sci Rep, 16(7), 40793. doi: 10.1038/srep40793

[20] Mendes-da-Cruz, D. A., Lemos, J. P., Passos, G. A., & Savino, W. (2018). Abnormal T-Cell development in the thymus of non-obese diabetic mice: possible relationship with the pathogenesis of type 1 autoimmune diabetes. Front Endocrinol (Lausanne), 9, 381. doi: 10.3389/fendo.2018.00381

[21] Morelli, S. S., Mandal, M., Goldsmith, L. T., Kashani, B. N., & Ponzio, N. M. (2015). The maternal immune system during pregnancy and its influence on fetal development. Research and Reports in Biology, 171-189. doi: 10.2147/RRB.S80652

[22] Olin, A., Henckel, E., Chen, Y., Lakshmikanth, T., Pou, C., Mikes, J., ... & Brodin, P. (2018). Stereotypic immune system development in newborn children. Cell, 174(5), 1277-1292. doi: 10.1016/j.cell.2018.06.045

[23] Pérez, A. R., Morrot, A., Carvalho, V. F., de Meis, J., & Savino, W. (2018). Role of hormonal circuitry upon T cell development in chagas disease: possible implications on T cell dysfunctions. Front Endocrinol (Lausanne), 9, 334. doi: 10.3389/fendo.2018.00334

[24] Robillard, P. Y., Dekker, G., Chaouat, G., Elliot, M. G., & Scioscia, M. (2019). High incidence of early onset preeclampsia is probably the rule and not the exception worldwide. 20th anniversary of the reunion workshop. A summary. Journal of Reproductive Immunology, 133, 30-36. doi: 10.1016/j.jri.2019.05.003

[25] Savino, W., Mendes-da-Cruz, D. A., Lepletier, A., & Dardenne, M. (2016). Hormonal control of T-cell development in health and disease. Nat Rev Endocrinol, 12(2), 77-89. doi: 10.1038/nrendo.2015.168

[26] Sikandar, A., & Ullah, N. (2020). Microarchitecture of the Thymus Gland; Its Age and Disease-Associated Morphological Alterations, and Possible Means to Prolong Its Physiological Activity. In Thymus. IntechOpen. doi: 10.5772/intechopen.88480

[27] Stras, S. F., Werner, L., Toothaker, J. M., Olaloye, O. O., Oldham, A. L., McCourt, C. C., ... & Konnikova, L. (2019). Maturation of the human intestinal immune system occurs early in fetal development. Developmental cell, 51(3), 357-373. doi: 10.1016/j.devcel.2019.09.008

[28] Sun, D. P., Jin, H., Ding, C. Y., Liang, J. H., Wang, L., Fan, L., … & Li, J. Y. (2016). Thymic hyperplasia after chemotherapy in adults with mature B cell lymphoma and its influence on thymic output and CD4(+) T-cells repopulation. Oncoimmunology, 5(5), e1137417. doi: 10.1080/2162402X.2015.1137417

[29] Tacconelli, A., Farina, A. R., Cappabianca, L., Cea, G., Panella, S., Chioda, A., … & Mackay, A. R. (2007). The alternative TrkaIII splice variant is expressed by murine and human thymus. J Neuroimmunol, 183(1-2), 151-61. doi: 10.1016/j.jneuroim

[30] Zmora, N., Bashiardes, S., Levy, M., & Elinav, E. (2017). The role of the immune system in metabolic health and disease. Cell metabolism, 25(3), 506-521. doi: 10.1016/j.cmet.2017.02.006

МОРФОЛОГІЧНІ ТА ІМУНОГІСТОХІМІЧНІ ХАРАКТЕРИСТИКИ ТИМУСА НОВОНАРОДЖЕНИХ У РАННІЙ НЕОНАТАЛЬНИЙ ПЕРІОД

Ісламов Ш. Е., Якубов М. З., Алікулов А. І., Жураєв К. Д., Махматмурадова Н. Н., Кудратов Р.

Імунна система плода розвивається та функціонує в складних умовах. З одного боку, вона підтримує внутрішній гомеостаз плода, а з іншого – зазнаючи антигенного впливу з боку материнського організму, має швидко адаптуватися й реагувати на цей вплив. Метою роботи було вивчення патоморфологічних та імуногістохімічних характеристик тканини тимуса у дітей, які померли в ранньому неонатальному періоді. Досліджено морфологічні та імуногістохімічні особливості тимуса 30 дітей, народжених від матерів з прееклампсією та еклампсією і померлих у ранньому неонатальному періоді. Фрагменти тимуса були отримані під час аутопсії, фіксовані в 10 % нейтральному формаліні, надалі піддані стандартній проводці та заливці в парафін з подальшим гістологічним та імуногістохімічним дослідженням із використанням маркерів CD3, CD4 і Ki-67. Статистичний аналіз отриманих результатів виконували з використанням пакета STATISTICA for Windows та MS Excel із застосуванням методів варіаційної статистики. Встановлено, що виявлені статистично значущі зміни інтегрального співвідношення між масою наднирників і тимуса морфологічно свідчать про розвиток передчасної

глюкокортикоїд-асоційованої інволюції тимуса. Морфологічно відзначається виражене збільшення залозистого епітелію ентерохромафінних клітин пучкової зони кори наднирників, різке зростання кількості ліпідних включень у їх цитоплазмі та ознаки плетори судин. Тимус характеризується фіброзною капсулою різної товщини, звивистою поверхнею, інтерстиціальним набряком у стінці капсули, потовщенням і дезорганізацією фіброзних структур, а також численними тільцями Гассаля й ознаками активного апоптозу. Морфологічні зміни тимуса у новонароджених, народжених від матерів із прееклампсією та еклампсією і померлих у ранньому неонатальному періоді, супроводжуються ознаками передчасної інволюції та вторинного імунодефіциту. Висока експресія маркера Ki-67 відображає посилену проліферативну активність лімфоцитів, тоді як низька позитивна експресія CD3+ і CD4+ свідчить про порушення диференціації Т-лімфоцитів і недостатню продукцію Т-хелперів, що призводить до зниження резистентності до інфекцій і розвитку імунодефіцитних станів.

Ключові слова: *новонароджені, тимус, морфологія, імуногістохімія, ознаки, інволюція, імунодефіцит.*

Author's contribution
Islamov Sh. E. – data collection, writing of the manuscript.
Yakubov M. Z. – scientific editing of the manuscript.
Alikulov A. I. – review and approval of the final version of the manuscript.
Zhuraev K. D. – data collection, writing of the manuscript.
Makhmatmuradova N. N. – scientific editing of the manuscript.
Kudratov R. – review and approval of the final version of the manuscript.

DOI: 10.31393/morphology-journal-2025-31(4)-08 Reports of Morphology, Vol. 31, №4, Pages 59-68

ISSN 1818-1295 eISSN 2616-6194

REPORTS OF MORPHOLOGY

Official Journal of the Scientific Society of Anatomists, Histologists, Embryologists and Topographic Anatomists of Ukraine

journal homepage: https://morphology-journal.com

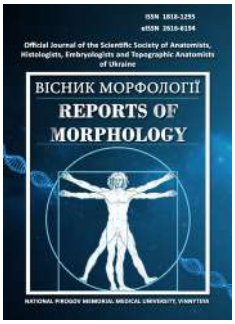

Regression models of parameters required for constructing an appropriate dental arch form depending on the characteristics of teleroentgenometric indices by the Schwarz method and computed tomographic tooth dimensions in Ukrainian young men and women with normal occlusion

Spodaruk A. L., Shinkaruk-Dykovytska M. M., Valchuk O. G., Pozur T. P., Shevchenko V. M., Tykholaz S.I., Chernysh A. V.

National Pirogov Memorial Medical University, Vinnytsya, Ukraine

ARTICLE INFO

Received: 3 April 2025

Accepted: 23 September 2025

UDC: 616.31-053

CORRESPONDING AUTHOR

e-mail: spodaruk-nastya@ukr.net

Spodaruk A. L.

CONFLICT OF INTEREST

The authors have no conflicts of interest to declare.

FUNDING

Not applicable.

DATA SHARING

Data are available upon reasonable request to corresponding author.

Malocclusions and discrepancies in dental arch form remain highly prevalent among children and adolescents worldwide, significantly affecting oral health, facial aesthetics and quality of life. Accurate, population-specific prediction of individual dental arch parameters based on cephalometric and odontometric characteristics is therefore essential for personalized planning of orthodontic and orthognathic treatment in young patients with normal occlusion. The aim of the study is to construct and analyze regression models of the dimensions required for constructing the correct dental arch form in Ukrainian young men and women with physiological occlusion depending on teleroentgenometric indices according to the Schwarz method and computed-tomographic tooth dimensions. In the OnyxCeph³™ application, 3DPro version (Image Instruments GmbH, Germany) teleroentgenometric indices according to the Schwarz method were performed on conventionally obtained lateral teleroentgenograms and on teleroentgenograms created in the 3D Slicer v5.4.0 software with points marked on 3D objects in 41 Ukrainian young men and 68 young women with physiological occlusion. Also, in these young men and women, using the software applications i-Dixel One Volume Viewer (Ver.1.5.0) J Morita Mfg. Cor and Planmeca Romexis Viewer (ver. 3.8.3.R 15.12.14) Planmeca OY, measurements of the dimensions of the teeth of the maxilla and mandible and the linear parameters of the dental arches were performed on computed tomograms. Using the licensed software package "Statistica 6.0" regression models were constructed for the parameters of the correct dental arch form depending on the characteristics of the cephalometric parameters and computed-tomographic tooth dimensions. It was established that in young men all 18 possible significant models with a coefficient of determination greater than 0.6 were constructed (R2=0.680-0.893, p<0.001); and in young women only 6 significant models with a coefficient of determination greater than 0.6 were constructed (R2=0.611-0.800, p<0.001). In the analysis of the frequency with which computed-tomographic tooth dimensions and teleroentgenometric indices entered the regression equations it was established: in young men the variables most frequently included in the models are crown width in the vestibulo-oral and mesio-distal planes, cephalometric parameters and tooth length; and in young women cephalometric parameters and crown width in the mesio-distal and vestibulo-oral planes. In the analysis of the frequency with which individual teeth entered the regression equations it was established that in young men the teeth most frequently included in the models are maxillary incisors, mandibular incisors, maxillary premolars, mandibular premolars and maxillary canines; and in young women maxillary incisors, mandibular incisors, mandibular canines and mandibular premolars.

Keywords: *dentistry, teleroentgenometry by the Schwarz method, computed tomographic dimensions of teeth and dental arches, regression analysis, Ukrainian young men and women with normal occlusion.*

Introduction

Pathology of the dentoalveolar system occupies one of the leading positions in the structure of dental morbidity in children, and its incidence tends to increase in most countries. The global distribution of the main occlusal classes in permanent dentition is approximately 74.7 % for class I, 19.6 % for class II and 5.9 % for class III, as reported by Alhammadi M. S. et al., which demonstrates that the overall burden of malocclusion is high [3]. Another systematic review on the prevalence of malocclusion in children and adolescents revealed that the proportion of individuals with various types of malocclusion generally ranges from about 40 % to more than 90 % in different regions, which indicates not only extremely high variability but also the mass character of this pathology as a worldwide public health problem [8].

Regional studies corroborate the high prevalence of malocclusions in schoolchildren in countries with diverse socio-economic conditions. A high prevalence of malocclusions and a high percentage of children in need of orthodontic treatment have been recorded in the northern regions of Saudi Arabia, which is attributed both to the characteristics of craniofacial growth and to limited access to specialized services [1]. Studies in Turkey and in major cities of China (Shanghai, Xi'an) have demonstrated that various types of malocclusion are found in a significant proportion of children aged 10-12 years and in the mixed dentition stage, with the structure of anomalies differing considerably according to age, sex and place of residence [4, 29, 30].

In view of their high prevalence, malocclusions have not only medical but also pronounced social and psycho-emotional importance, affecting the quality of life of children and adolescents. Brazilian studies have shown an association between orthodontic treatment need and oral health-related quality of life, demonstrating that a considerable number of adolescents require some type of orthodontic treatment according to public health criteria, and that the presence of severe dentoalveolar anomalies is related to worse OHRQoL, impaired self-esteem and reduced satisfaction with appearance [7]. In a study of 8-12-year-old schoolchildren it was demonstrated that the presence of moderate and severe malocclusion has a significant negative impact on functional aspects and on emotional and social well-being related to oral health, which supports the societal benefits of early orthodontic intervention at an age when disturbances in dental arch form can be detected and corrected [28].

The morphology and shape of the dental arches are key components in the development of occlusal relationships and in maintaining stability after orthodontic treatment. Recent studies indicate that children with normal occlusion and those with various types of malocclusion differ significantly in dental arch form and dimensions, and that deviations of transversal and sagittal arch parameters are associated with the development of dentoalveolar anomalies [12]. Certain groups of patients, for example children with cleft lip and/or palate, show marked changes in dentoalveolar arch morphology and a high percentage of anomalies in the position and shape of individual teeth, which emphasizes the role of individual dental arch parameters in the development of complex dentoalveolar conditions [24].

Despite a wide range of studies on the prevalence of malocclusion and its impact on quality of life, several important issues remain insufficiently resolved, including the quantitative description of dental arch form and the construction of regression models aimed at linking linear characteristics of the dentitions with cephalometric data and odontometric indices, especially in adolescents. One probable reason is that most existing studies on different types of anomalies focus primarily on the frequency and qualitative characteristics of malocclusion types and do not consider individual craniofacial morphology or spatial tooth dimensions, although precisely these approaches could potentially be used to predict the optimal dental arch form and to individualize orthodontic care. Given the global and local significance of dentoalveolar pathology and its proven relationship with arch morphology, which contributes to the formation of malocclusions, research on regression models of parameters necessary for designing an adequate dental arch form in healthy young men and women with normal occlusion acquires scientific and practical relevance [3, 8, 12].

The aim of the study is to construct and analyze regression models of the dimensions required for constructing the correct dental arch form in Ukrainian young men and women with physiological occlusion depending on cephalometric parameters according to the Schwarz method and computed-tomographic tooth dimensions.

Materials and methods

From the database of the Department of Pediatric Dentistry and the Research Center of National Pirogov Memorial Medical University, Vinnytsya primary computed tomograms of 41 Ukrainian young men (aged from 17 to 21 years) and 68 Ukrainian young women (aged from 16 to 20 years) with physiological occlusion were obtained. All teleroentgenographic (using the dental cone-beam tomograph Veraviewepocs 3D Morita, Japan) and computed-tomographic (using the dental cone-beam tomograph Planmeca ProMax 3D Mid, Finland) examinations were carried out on the basis of the principle of voluntary informed consent in the private dental clinic "Vinintermed" and in the "Center for Maxillofacial Diagnostics Planmeca 3D". Committee on Bioethics of National Pirogov Memorial Medical University, Vinnytsya (protocol № 8 From 9.09.2025) found that the studies do not contradict the basic bioethical standards of the Declaration of Helsinki, the Council of Europe Convention on Human Rights and Biomedicine (1977), the relevant WHO regulations and laws of Ukraine.

On conventionally obtained lateral cephalograms and cephalograms created in the 3D Slicer v5.4.0 software with points marked on 3D objects, measurements according to the method of Schwarz A. M. [26, 27] were performed in the OnyxCeph³™ application, 3DPro version, Image Instruments GmbH (Germany).

In accordance with the Schwarz method the following craniometric (Fig. 1), gnathometric indices (Figs. 2, 3) and soft tissue profile indices (Fig. 4) were determined: angle **F** (°) – facial angle, formed by the lines Se-N and N-A and defining the position of the anterior contour of the maxilla in the sagittal plane relative to the cranial base; angle **H** (°) – the angle formed by the lines Po-Or (Frankfurt plane (Fp)) and Pn ((nasal perpendicular, the perpendicular line from point N' (cutaneous nasion) to the line Se-N)), defining the inclination of the Frankfurt plane to the cranial base; angle **I** (°) – inclination angle, defining the angle of inclination of the maxilla (spinal plane) to the nasal perpendicular, the angle formed by the line ANS-PNS and Pn (nasal perpendicular, the perpendicular line from point N' to the line Se-N); angle **T** (°) – profile angle T, formed by the lines Sn-Pog' and Pn (nasal perpendicular); angle **B** (°) – basal angle, indicating the angle between the maxilla and mandible, formed by the lines ANS-PNS (palatal plane SpP) and Im-Me (mandibular plane MPS according to Schwarz); distance **N-Se** (mm) – distance from point Se to point N, or the length of the anterior part of the cranial base; distance **Max** (mm) – maxillary length, the distance from the projection of point A onto the line ANS-PNS to point PNS; angle **Max1-SpP** (°) – formed by the lines Ap1u-Is1u (inclination of the central axis of the maxillary central incisor) and ANS-PNS (palatal plane, SpP); angle **II** (°) – interincisal angle, formed by the lines Ap1u-Is1u (central axis of the maxillary central incisor) and Ap1L-Is1L (central axis of the mandibular central incisor); angle **G** (°) – gonial angle, mandibular angle, formed by the lines ppCond-MT2 and MT1-Me, which intersect at point tGoS; distance **L-Mand** (length of mandible) (mm) – mandibular length; the distance from the projection of point Pog onto the line MT1-Me to point tGoS; distance **R.asc.** (mm) – ramus length; the distance from the constructed point R.asc to the constructed point tGoS; angle **Mand1-MP** (°) – formed by the lines Ap1L-Is1L and Me-Im and defining the position of the axes of the mandibular incisors relative to the mandibular plane according to Schwarz; angle **MM** (°) – maxillo-mandibular angle, defining the angle at which the maxilla is positioned relative to the mandible in the sagittal plane, formed by the lines A-B and ANS-PNS; distance **Sn-Pn** (mm) – defining the position of point Sn relative to the perpendicular Pn; distance **Pog'-Por** (mm) – distance from point Pog' to the orbital perpendicular Por, defining the position of the chin relative to the perpendicular to the Frankfurt plane drawn through the orbit; angle **Gl'LsPog'** (°) – formed by the lines Gl'-Ls and LsPog', defining facial convexity; angle **SnPog'-Pn** (°) – formed by the lines SnPog' and the perpendicular Pn; distance **Li-SnPog'** (mm) – defining the position of point Li relative to the line SnPog'.

For the morphometric study of the teeth of the maxilla and mandible and the dimensions of the dental arches the software applications i-Dixel One Volume Viewer (Ver.1.5.0) J Morita Mfg. Cor and Planmeca Romexis Viewer (ver. 3.8.3.R 15.12.14) Planmeca OY were used.

For the anterior group of teeth, namely for the incisors and canines of the maxilla and mandible, crown width and the width of the dentinoenamel junction of the tooth were determined in

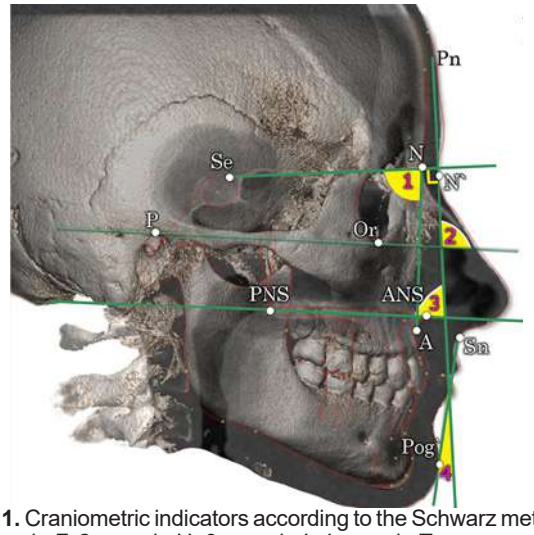

Fig. 1. Craniometric indicators according to the Schwarz method. 1 – angle F, 2 – angle H, 3 – angle I, 4 – angle T.

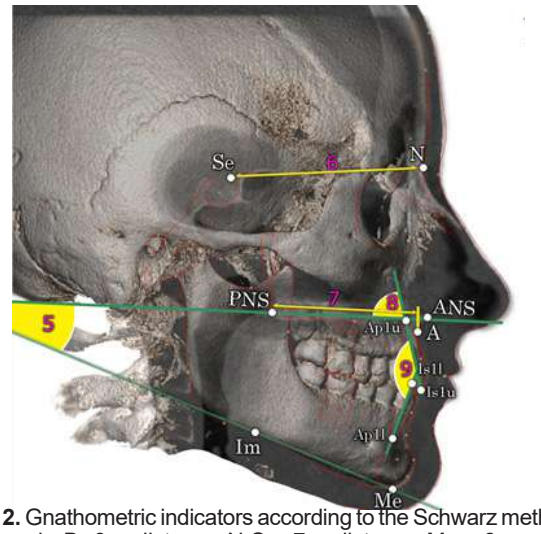

Fig. 2. Gnathometric indicators according to the Schwarz method. 5 – angle B, 6 – distance N-Se, 7 – distance Max, 8 – angle Max1-SpP, 9 – angle II.

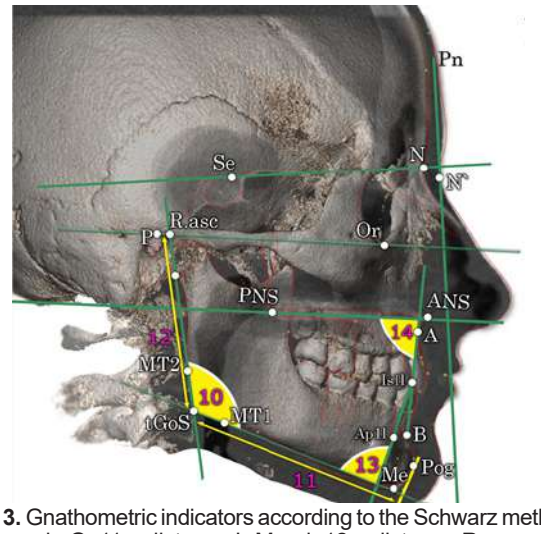

Fig. 3. Gnathometric indicators according to the Schwarz method. 10 – angle G, 11 – distance L-Mand, 12 – distance R.asc., 13 – angle Mand1-MP, 14 – angle MM

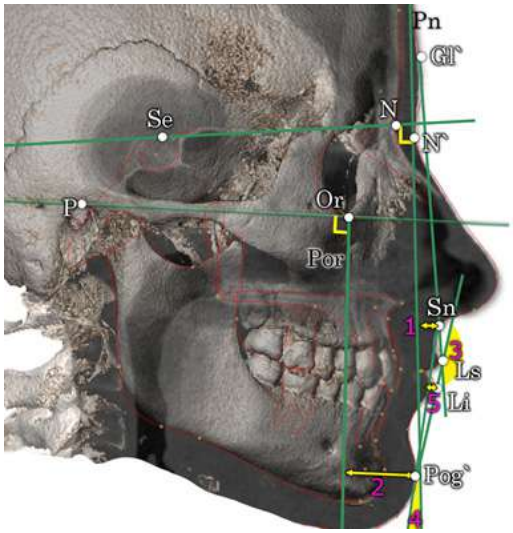

Fig. 4. Soft tissue profile indicators according to the Schwarz method. 1– Sn-Pn distance; 2 – Pog'-Por distance; 3 – Gl'LsPog' angle; 4 – SnPog'-Pn angle; 5 – Li-SnPog' distance.

the mesiodistal (MdK and MdC, respectively) and vestibulo-oral (VoK and VoC) projections, the length of the whole tooth (MdLD – identical in both projections), as well as crown height (MdLK and VoLK) and root length (MdLR and VoLR) relative to the cervical line in the corresponding projections.

For the premolars of the maxilla and mandible the crown width was determined in the mesiodistal and vestibulo-oral projections, as well as tooth length, which was measured between the cusp tip of the buccal cusp and the root apex in the vestibulo-oral projection (if the premolar had two roots tooth length was determined to the apex of the buccal root).

For the first molars of the maxilla and mandible the crown width was determined in the mesiodistal and vestibulo-oral projections.

Since in previous studies [17], when comparing computed-tomographic dimensions of corresponding teeth on the right and left sides, no significant differences or trends toward differences were found, we used mean values of the corresponding teeth in the maxilla and mandible: 11 or 41 – maxillary or mandibular central incisors, 12 or 42 – maxillary or mandibular lateral incisors, 13 or 43 – maxillary or mandibular canines, 14 or 44 – maxillary or mandibular first premolars, 15 or 45 – maxillary or mandibular second premolars, 16 or 46 – maxillary or mandibular first molars.

The parameters of the dental arches were determined in three cranial planes. In the axial plane the following distances were measured: between the cusp tips (13_23Bugr and 33_43Bugr) and root apices (13_23Apx and 33_43Apx) of the maxillary and mandibular canines (Fig. 5); distances between the apices of the mesiobuccal (napx_6), palatal (mapex_6), distobuccal roots (dapx_6) and the buccal cusps (VestBM) of the maxillary first molars (Fig. 6) and the apices of the mesial (mapx_46) and distal (dapx_46) roots of the mandibular first molars; the distance between the premolar (PonPr) and molar (PonM) Pont's points in the maxilla, and in the sagittal plane the distances were measured between the incisal edges of the central incisors and the lines connecting the canine cusps (DL_C), the premolar (DL_F) and molar (DL_S) Pont's points in the maxilla (Fig. 7). In the vertical plane distances were measured that characterize the position of the occlusal plane at the level of the canines (GL_1), first premolars (GL_2) and molars (GL_3) relative to the hard palate (Fig. 8).

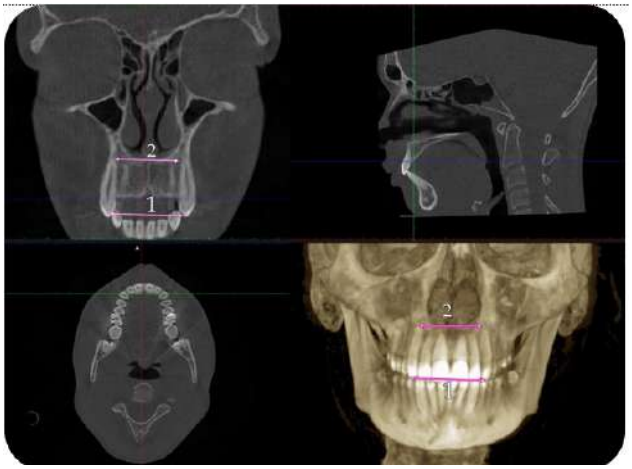

Fig. 5. Determination of the distance between the cusp tips (1) and root apices (2) of the maxillary canines.

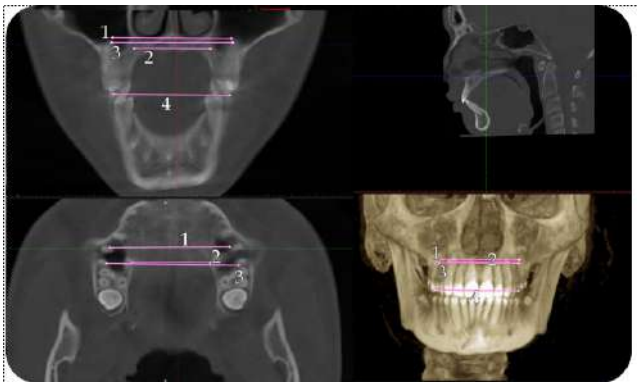

Fig. 6. Determination of the distances between the apices of the mesiobuccal (1), palatal (2) and distobuccal roots (3) and the buccal cusps (4) of the maxillary first molars.

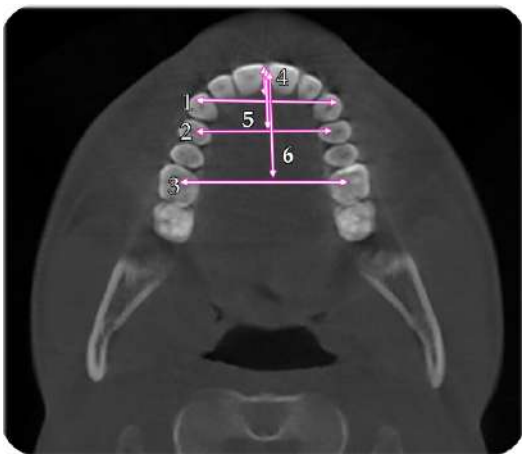

Fig. 7. Determination of the distances between the canine cusps (1), the premolar (2) and molar (3) Pont's points, and the distances between the incisal point and the canine (4), premolar (5) and molar (6) lines in the maxilla.

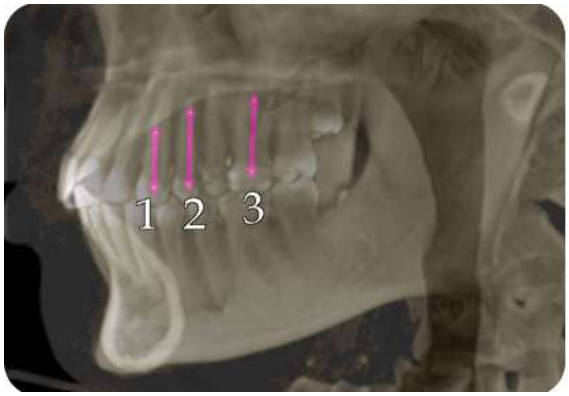

Fig. 8. Determination of the distances that characterize the position of the occlusal plane relative to the hard palate at the level of the canine (1), premolar (2) and molar (3) lines.

Using the "Statistica 6.0" license package, regression models were built (using the stepwise regression analysis method) of the dental arch parameters depending on the characteristics of teleradiometric indicators and computed tomography dimensions of the teeth.

Results

In Ukrainian *young men* with physiological occlusion the following significant regression models (with a coefficient of determination $R^2>0.60$) of the linear dimensions required for constructing the correct dental arch form depending on the characteristics of cephalometric parameters according to the Schwarz method and computed-tomographic tooth dimensions were constructed:

distance DL_C (young men)= -14.89 + 0.814×MdK11 + 1.323×VoK41 + 0.081×MM - 0.403×VoLK41 + 0.744×MdC11 + 0.381MdLK13 - 0.155VoLR13 (R^2=0.849, $F_{(7.33)}$=26.45, p<0.001, Std.Error of estimate=0.575);

distance DL_F (young men)= -9.443 + 1.570×MdK11 + 1.240×VoK15 - 0.381×VoLK42 - 0.590×VoK45 + 1.248×VoC42 - 0.323×MdLR42 + 0.166×MdLR41 + 0.032×Gl'LsPog' (R^2=0.849, $F_{(8.32)}$=22.51, p<0.001, Std.Error of estimate=0.669);

distance DL_S (young men)= 6.145 + 1.905×MdK11 + 1.548×VoK15 + 0.861×VoK46 - 0.071×Mand1-MP - 0.857×VoK45 - 0.336×MdLR12 + 0.370×VoK14 (R^2=0.893, $F_{(7.33)}$=39.35, p<0.001, Std.Error of estimate=0.675);

distance GL_1 (young men)= 17.66 + 0.201×Max1-SpP - 2.482×MdK46 + 1.333×VoK15 - 0.255×H + 0.122×Max + 2.087×VoC42 - 0.581×MdLR12 + 0.325×MdLD13 (R^2=0.727, $F_{(8.32)}$=10.63, p<0.001, Std.Error of estimate=1.417);

distance GL_2 (young men)= -2.572 + 0.173×Max1-SpP + 0.683×VoLR13 - 0.980×MdLD45 + 2.864×VoK12 + 0.773×MdLK13 - 0.654×MdLD41 + 0.477×MdLK11 (R^2=0.680, $F_{(7.33)}$=10.00, p<0.001, Std.Error of estimate=1.641);

distance GL_3 (young men)= -0.775 + 0.120×Gl'LsPog' - 1.127×MdLD45 + 0.910×MdLD11 + 0.065×L-Mand - 1.920×MdK16 + 1.002×VoK15 + 1.726×MdK14 (R^2=0.753, $F_{(7.33)}$=14.40, p<0.001, Std.Error of estimate=1.141);

distance PonPr (young men)= 5.701 + 1.366×MdK12 + 1.573×MdK15 - 0.478×MdLR12 + 2.217×MdK45 + 2.042×MdK41 - 0.319×MdLD14 (R^2=0.801, $F_{(6.34)}$=22.80, p<0.001, Std.Error of estimate=1.002);

distance PonM (young men)= 35.38 + 2.544×VoK15 + 0.751×MdLD44 - 0.494×MdLD14 - 0.124×G - 0.157×Sn-Pn - 1.808×VoK42 + 1.453×VoK43 (R^2=0.758, $F_{(7.33)}$=14.75, p<0.001, Std.Error of estimate=1.392);

distance VestBM (young men)= 48.12 + 2.526×VoK15 + 1.282×MdLD44 - 0.569×MdLD42 - 0.625×MdLD45 - 0.122×G - 0.074×Max (R^2=0.786, $F_{(6.34)}$=20.87, p<0.001, Std.Error of estimate=1.326);

distance 13_23Bugr (young men)= 7.992 + 2.502×MdK12 + 1.849×MdK13 - 0.487×VoLR12 - 0.913×VoK14 + 1.396×MdK41 + 1.171×MdC41 (R^2=0.764, $F_{(6.34)}$=18.34, p<0.001, Std.Error of estimate=1.058);

distance 13_23Apx (young men)= 38.82 + 0.205×Max1-SpP + 0.322×Li-SnPog' - 1.357×VoK16 + 2.037×VoK45 - 2.229×VoK13 + 1.742×MdK12 + 0.450×MdLD14 - 2.237×MdK13 - 0.072×L-Mand - 0.124×B (R^2=0.771, $F_{(10.29)}$=9.14, p<0.001, Std.Error of estimate=1.270);

distance napx_6 (young men)= 37.58 + 3.061×MdC42 - 2.737×VoK16 + 4.664×MdK12 - 0.732×VoLR13 + 0.762×MdLD45 - 0.800×VoLR11 - 0.097×Max (R^2=0.715, $F_{(7.33)}$=11.84, p<0.001, Std.Error of estimate=1.876);

distance dapx_6 (young men)= -23.49 + 2.973×VoK15 + 3.030×MdK46 - 5.057×MdC13 + 1.121×VoLK13 + 2.296×MdK12 + 3.452×MdK15 + 2.377×VoC13 - 1.996×MdK16 (R^2=0.764, $F_{(8.32)}$=12.95, p<0.001, Std.Error of estimate=2.374);

distance mapex_6 (young men)= -44.74 + 3.792×MdK45 + 4.363×MdK15 + 3.178×MdK12 + 0.309×H + 1.630×MdC41 - 0.567×MdLR42 - 1.567×VoK15 + 1.476×VoK12 (R^2=0.872, $F_{(8.32)}$=27.14, p<0.001, Std.Error of estimate=1.328);

distance 33_43Bugr (young men)= -0.244 + 1.476×MdK12 + 2.401×MdK42 - 0.420×MdLR11 + 0.376×MdLD43 - 0.243×VoLR13 + 0.202×MdLR42 (R^2=0.704, $F_{(6.34)}$=13.45, p<0.001, Std.Error of estimate=0.871);

distance 33_43Apx (young men)= 22.05 + 0.884×MdLD43 - 0.124×Max + 4.785×VoK43 - 2.772×VoC43 - 1.923×VoK42 - 0.468×MdLD45 - 1.865×MdK15 (R^2=0.751, $F_{(7.33)}$=14.21, p<0.001, Std.Error of estimate=1.273);

distance mapx_46 (young men)= 13.14 + 1.487×MdLK12 + 2.458×MdK45 + 2.978×VoK16 - 0.664×MdLD45 - 2.050×VoK46 - 0.083×R.asc. + 2.985×MdK42 (R^2=0.782, $F_{(7.32)}$=16.43, p<0.001, Std.Error of estimate=1.401);

distance dapx_46 (young men)= 23.21 + 0.143×Mand1-MP - 0.169×Max + 1.552×VoK16 + 1.910×MdC12 - 2.452×VoK12 + 1.978×VoK15 (R^2=0.747, $F_{(6.33)}$=16.26, p<0.001, Std.Error of estimate=1.551);

where, here and in the following equations, R^2 – coefficient of determination; $F_{(!)}$=! – critical $_{(!)}$ and obtained (!) Fisher's test value; p – confidence level; Std.Error of estimate – standard error of estimate.

In Ukrainian young women with physiological occlusion the following significant regression models (with a coefficient of determination $R^2>0.60$) of the linear dimensions required

for constructing the correct dental arch form depending on the characteristics of cephalometric parameters according to the Schwarz method and computed-tomographic tooth dimensions were constructed:

distance DL_F (young women)= 1.379 + 1.202×MdK11 + 0.141×Li-SnPog' + 0.879×VoK12 + 0.101×Sn-Pn - 0.043×Mand1-MP + 0.186×VoLR11 (R^2=0.680, $F_{(6.61)}$=21.59, p<0.001, Std.Error of estimate=0.817);

distance DL_S (young women)= 7.206 + 1.201×MdK11 + 0.211×Li-SnPog' + 0.706×VoK12 + 0.351×MdLK11 - 0.068×Mand1-MP + 0.627×MdK16 + 0.239×MdLD41 (R^2=0.800, $F_{(7.60)}$=34.29, p<0.001, Std.Error of estimate=0.776);

distance GL_2 (young women)= 4.175 + 0.368×MdLK42 + 0.193×Max1-SpP + 1.600×MdK46 - 1.610×VoLK43 - 0.259×I + 1.161×VoLK41 + 1.128×VoK46 - 1.464×MdK16 + 1.133×MdK45 (R^2=0.635, $F_{(9.58)}$=11.20, p<0.001, Std.Error of estimate=1.557);

distance 13_23Bugr (young women)= -12.68 + 1.122×MdK11 + 0.132×Gl'LsPog' - 0.039×MdC43 + 0.882×MdK43 + 0.352×VoLK11 + 0.290×MdLK42 + 0.820×VoC12 (R^2=0.632, $F_{(7.60)}$=14.71, p<0.001, Std.Error of estimate=1.090);

distance mapx_46 (young women)= 25.26 + 1.640×MdK16 - 0.066×MdC43 - 0.190×T + 1.096×MdLK13 - 0.368×Li-SnPog' + 1.938×MdK15 - 1.215×VoK44 (R^2=0.611, $F_{(7.54)}$=12.13, p<0.001, Std.Error of estimate=1.820);

distance dapx_46 (young women)= 17.87 - 0.197×T + 0.954×MdLD45 - 0.455×VoLK11 + 2.311×MdC12 + 0.152×Gl'LsPog' - 0.444×MdLR41 - 0.841×VoK44 (R^2=0.698, $F_{(7.54)}$=17.81, p<0.001, Std.Error of estimate=1.886).

Since, in *young women* in the constructed reliable distance models, *DL_C*, *GL_1*, *GL_3*, *PonPr*, *PonM*, *VestBM*, *13_23Apx*, *napx_6*, *dapx_6*, *mapex_6*, *33_43Bugr* and *33_43Apx* the coefficient of determination of the regression equations is from 0.340 to 0.594, these models do not have important practical significance for dentists.

Discussion

Thus, in Ukrainian young men with physiological occlusion all 18 possible significant (p<0.001 in all cases) models of the linear parameters of the dental arches depending on the characteristics of cephalometric parameters according to the Schwarz method and computed-tomographic tooth dimensions were constructed with a coefficient of determination greater than 0.6 (R^2= from 0.680 to 0.893).

As a result of the analysis of the frequency with which cephalometric parameters according to the Schwarz method and computed-tomographic tooth dimensions entered the regression equations in young men the following percentage of inclusion of these parameters in the models was established: crown width in the vestibulo-oral (22.66 %) and mesio-distal plane (21.88 %), cephalometric parameters according to the Schwarz method (17.97 %), tooth length (13.28 %), root portion length in the mesio-distal (6.25 %) and vestibulo-oral plane (4.69 %), cervical portion width in the mesio-distal (4.69 %) and vestibulo-oral plane (3.13 %), and crown portion length in the mesio-distal (3.13 %) and vestibulo-oral plane (2.34 %).

As a result of the analysis of the frequency with which the corresponding teeth entered the regression equations in young men the following percentage of inclusion of these parameters in the models was established: 22.86 % maxillary incisors (of which 15.24 % lateral and 7.62 % central), 19.05 % mandibular incisors (of which 11.43 % lateral and 7.62 % central), 18.09 % maxillary premolars (of which 12.38 % second and 5.71 % first), 13.33 % mandibular premolars (of which 11.43 % second and 1.90 % first), 12.38 % maxillary canines, 5.71 % maxillary first molars, 4.76 % mandibular canines and 3.81 % mandibular first molars.

In Ukrainian young women with physiological occlusion, of 18 possible models only 6 significant (p<0.001 in all cases) models of the linear parameters of the dental arches depending on the characteristics of cephalometric parameters according to the Schwarz method and computed-tomographic tooth dimensions were constructed with a coefficient of determination greater than 0.6 (R^2= from 0.611 to 0.800).

As a result of the analysis of the frequency with which cephalometric parameters according to the Schwarz method and computed-tomographic tooth dimensions entered the regression equations in young women the following percentage of inclusion of these parameters in the models was established: cephalometric parameters according to the Schwarz method (27.91 %), crown portion width in the mesio-distal (23.26 %) and vestibulo-oral plane (11.63 %), crown portion length in the mesio-distal and vestibulo-oral plane (9.30 % each), cervical portion width in the mesio-distal (6.98 %) and vestibulo-oral plane (2.33 %), tooth length (4.65 %), and root portion length in the mesio-distal and vestibulo-oral plane (2.33 % each).

As a result of the analysis of the frequency with which the corresponding teeth entered the regression equations in young women the following percentage of inclusion of these parameters in the models was established: 35.48 % maxillary incisors (of which 22.58 % central and 12.90 % lateral), 16.13 % mandibular incisors (of which 9.68 % central and 6.45 % lateral), 12.90 % mandibular canines, 12.90 % mandibular premolars (of which 6.45 % first and 6.45 % second), 9.68 % maxillary first molars, 6.45 % mandibular first molars, 3.23 % maxillary canines and 3.23 % maxillary second premolars.

Our findings support the feasibility of formulating sex-specific regression models of the linear variables of the dental arches that include both cephalometric indicators according to Schwarz and computed-tomographic odontometric features. In Ukrainian young men with physiological occlusion, it was possible to construct all 18 significant models, with R^2 values ranging from 0.680 to 0.893 (p<0.001), whereas in young women only 6 models with R^2 values from 0.611 to 0.800 (p<0.001) were obtained [16, 20, 21, 22].

Among the correlations between CT-derived measurements of the dental arches and jaws, the most numerous are those involving mesiodistal crown dimensions (53.5 %) and buccolingual crown dimensions (50.7 %), as well as the width of the dentinoenamel junction in the buccolingual direction (54.2 %) [14]. This is consistent with the fact that in our models for young men the frequency of inclusion of crown width in the vestibulo-oral and mesiodistal planes was 22.66 % and 21.88 %, respectively, while tooth length was included in 13.28 % of cases, that is, these parameters constitute the “core” of predictability for the linear dimensions of the dental arches. Similarly, in young women the largest proportion of predictors was represented by cephalometric characteristics (27.91 %) and by crown width in the mesiodistal (23.26 %) and vestibulo-oral planes (11.63 %), which mirrors the structure of relationships described in the studies by Marchenko A. V. on different craniofacial types [14, 15].

Our findings also agree with the conclusions of the review by Ryabov T. V., based on multiple studies of tooth size versus cranial parameters, which suggests that most correlations between tooth dimensions and cranial factors have moderate or greater strength (often $r>0.4$-0.5, $p<0.05$) and should be considered separately for different sexes, age-related stages of development and facial patterns [25].

In the works of Brotskyi N. O. and co-authors regression models of the linear dimensions required for the formation of a correct dental arch shape were constructed on the basis of teleradiography according to Ricketts and computed-tomographic tooth dimensions in boys and girls with wide and very wide facial types; high coefficients of determination were obtained, and mesiodistal and vestibulo-oral crown diameters were identified as particularly important predictors [5, 6].

In research conducted by Prokopenko O. S. in young men and women with various facial profiles, regression models were constructed for teleradiographic indicators of tooth position and soft tissue facial profile according to Schwarz; these models showed high sensitivity to sex and profile type [20]. A similar principle was applied in the study by Marchenko A. V. et al., where mathematical modeling of cephalometric values according to Schwarz was based on basic craniometric indices, and in the study by Nesterenko Y. A. et al., where COGS parameters were modeled in young women with a broad facial type [16, 18]. The approach presented by Dmitriev M. O. for modeling COGS parameters, with subdivision of indices into three groups, reflects the idea that not all indices contribute equally to the formation of dental arch form and occlusal relationships, emphasizing that only part of the indicators makes a substantial contribution to the variability of arch morphology and occlusion [10, 18].

From a methodological point of view, the justification for the use of computed tomography for combined cephalo- and odontometric assessment is particularly important. In the study by Devanna R. a three-dimensional CBCT-based cephalometric analysis was developed, which made it possible to determine 3D cephalometric norms with good reproducibility of measurements compared with conventional two-dimensional methods [9]. The study by Lin Y. et al. in children with operated unilateral cleft lip and palate showed that CBCT-reconstructed lateral cephalograms allow detection of differences in craniofacial structures between clinical groups and are not less informative than the traditional method [11]. In the systematic review by Raj G. and colleagues the diagnostic accuracy and reproducibility of CBCT-synthesized lateral cephalograms were found to be equivalent to those of conventional lateral cephalograms in 20 included studies, and in four studies even higher accuracy of CSLC was reported [23]. Taken together, these data support the use of CBCT as a high-precision source of odontometric and cephalometric measurements and verify our methodological approach, which further develops teleradiography according to Schwarz by adding detailed three-dimensional characterization of tooth dimensions.

Given the current discussion regarding the predictability of classical indices (particularly Pont) with respect to dental arch width in various populations, our findings gain special interest. In the Malay sample studied by Alam M. K. and co-authors using CBCT it was shown that predictions based on Pont’s index often failed to correspond to the actual interpremolar and intermolar widths, which raises questions about the universality of classical formulas [2]. More recently, much more rigorous conclusions were reached by Mahmood T. M. A. et al., who demonstrated in a Kurdish sample that actual arch width differed significantly from the calculated values and that only weak positive correlations between them were observed; the authors explicitly call for the development of alternative formulas based on scan-derived data [13]. The models we constructed, with high R^2 values based on real computed-tomographic tooth dimensions and cephalometric indicators, in fact implement this approach for Ukrainian young men and women with physiological occlusion, offering a personalized rather than a “universal” forecast of dental arch form [2, 5, 6, 13].

A. Potapchuk and co-authors studied dental arch forms and their correlations with morphotopogeometric facial parameters and reported that the shape and dimensions of the dental arches exert a considerable influence on the morphotopogeometric characteristics of the face and therefore can be regarded as one of the significant factors in achieving harmonious aesthetic proportions [19].

Conclusions

1. In Ukrainian young men and women with physiological occlusion without taking facial type into account significant regression models of the linear parameters of the dental arches depending on the characteristics of cephalometric parameters according to the Schwarz method and computed-tomographic tooth dimensions with a coefficient of determination greater than 0.6 were constructed (in young men all 18 possible models, R^2= from 0.680 to 0.893; in young women only 6, R^2= from 0.611 to 0.800).

2. In the analysis of the frequency with which cephalometric

parameters according to the Schwarz method and computed-tomographic tooth dimensions entered the models in young men the variables most frequently included in the models are crown width in the vestibulo-oral (22.66 %) and mesio-distal plane (21.88 %), cephalometric parameters (17.97 %) and tooth length (13.28 %); and in young women cephalometric parameters (27.91 %) and crown width in the mesio-distal (23.26 %) and vestibulo-oral plane (11.63 %).

3. In the analysis of the frequency with which the corresponding teeth entered the models in young men the teeth most frequently included in the models are maxillary incisors (22.86 %), mandibular incisors (19.05 %), maxillary premolars (18.09 %), mandibular premolars (13.33 %) and maxillary canines (12.38 %); and in young women maxillary incisors (35.48 %), mandibular incisors (16.13 %), mandibular canines and mandibular premolars (12.90 % each).

References

[1] Alajlan, S. S., Alsaleh, M. K., Alshammari, A. F., Alharbi, S. M., Alshammari, A. K., & Alshammari, R. R. (2019). The prevalence of malocclusion and orthodontic treatment need of school children in Northern Saudi Arabia. *Journal of orthodontic science*, *8*(1), 10. doi: 10.4103/jos.JOS_104_18

[2] Alam, M. K., Shahid, F., Purmal, K., & Khamis, M. F. (2015). Cone-beam computed tomography evaluation of Pont's index predictability for Malay population in orthodontics. *Journal of natural science, biology, and medicine*, *6*(Suppl 1), S113-S117. doi: 10.4103/0976-9668.166106

[3] Alhammadi, M. S., Halboub, E., Fayed, M. S., Labib, A., & El-Saaidi, C. (2018). Global distribution of malocclusion traits: A systematic review. *Dental press journal of orthodontics*, *23*(06), 40-e1. doi: 10.1590/2177-6709.23.6.40.e1-10.onl

[4] Atasever İşler, A. A., Hezenci, Y., & Bulut, M. (2025). Prevalence of orthodontic malocclusion in children aged 10–12: an epidemiological study. *BMC Oral Health*, *25*(1), 249. doi: 10.1186/s12903-025-05650-x

[5] Brotskyi, N. O., Dmitriev, M. O., Karliychuk, M. A., Ocheretna, N. P., & Shevchuk, Y. G. (2025). Regression models of the dimensions of the dental arch shape in girls with a physiological bite and a very wide facial type depending on the features of telerontgenometric indicators by the Ricketts method and computed tomographic dimensions of the teeth. *Світ медицини та біології=World of Medicine and Biology, 2*(92), 35-39. doi: 10.26724/2079-8334-2025-2-92-35-39

[6] Brotskyi, N. O., Dmitriev, M. O., Arshynnikov, R. S., Drachuk, N. V., Popova, O. I., Moskalenko, V. B., & Ruban, M. M. (2024). Models of linear dimensions necessary for constructing the correct shape of the dental arch in boys and girls with a wide face type depending on the characteristics of teleradiometric indicators. *Вісник Вінницького національного медичного університету=Reports of Vinnytsia National Medical University*, *28*(4), 613-619. doi: 10.31393/reports-vnmedical-2024-28(4)-06

[7] de Freitas, C. V., Souza, J. G. S., Mendes, D. C., Pordeus, I. A., Jones, K. M., & de Barros Lima, A. M. E. (2015). Need for orthodontic treatment among Brazilian adolescents: evaluation based on public health. *Revista Paulista de Pediatria (English Edition)*, *33*(2), 204-210. doi: 10.1016/S2359-3482(15)30052-X

[8] De Ridder, L., Aleksieva, A., Willems, G., Declerck, D., & Cadenas de Llano-Pérula, M. (2022). Prevalence of orthodontic malocclusions in healthy children and adolescents: a systematic review. *International journal of environmental research and public health*, *19*(12), 7446. doi: 10.3390/ijerph19127446

[9] Devanna, R. (2015). Two-dimensional to three-dimensional: A new three-dimensional cone-beam computed tomography cephalometric analysis. *Journal of Orthodontic Research*, *3*(1), 30. doi: 10.4103/2321-3825.146356

[10] Dmitriev, M. O., Gunas, I. V., Dzevulska, I. V., & Zhulkevych, I. V. (2018). Determination of individual cephalometric characteristics of the occlusal plane in Ukrainian young men and young women with orthognatic bite. *Biomedical and Biosocial Anthropology*, (33), 5-11. doi: 10.31393/bba33-2018-1

[11] Lin, Y., Fu, Z., Ma, L., & Li, W. (2016). Cone-beam computed tomography–synthesized cephalometric study of operated unilateral cleft lip and palate and noncleft children with Class III skeletal relationship. *American Journal of Orthodontics and Dentofacial Orthopedics*, *150*(5), 802-810. doi: 10.1016/j.ajodo.2016.03.031

[12] Luo, J., Liu, T., Wang, Y., & Li, X. (2024). The association between dental and dentoalveolar arch forms of children with normal occlusion and malocclusion: a cross-sectional study. *BMC Oral Health*, *24*(1), 731. doi: 10.1186/s12903-024-04515-z

[13] Mahmood, T. M. A., Noori, A. J., Aziz, Z. H., Rauf, A. M., & Kareem, F. A. (2023). Scan aided Dental Arch Width Prediction via internationally recognized formulas and indices in a sample of kurdish Population/Iraq. *Diagnostics*, *13*(11), 1900. doi: 10.3390/diagnostics13111900

[14] Marchenko, A. V. (2018). Connections of transversal volumes of the upper and lower jaw and sagittal characteristics of the dental arch with odontometric and cephalometric indicators of youth brachycephals with orthognathic bite. *Світ медицини та біології=World of Medicine and Biology*, *1*(63), 47-52. doi: 10.26724/2079-8334-2018-1-63-47-52

[15] Marchenko, A. V. (2018). Relationships of linear dimensions necessary for constructing the correct form of the dental arch with odontometric and cephalometric indicators in mesocephalic girls with orthognathic bite. *Klinichna Stomatolohiia (Clinical Dentistry)*, *1*, 50-59. doi: 10.11603/2311-9624.2018.1.8582

[16] Marchenko, A. V., Prokopenko, O. S., Dzevulska, I. V., Zakalata, T. R., & Gunas, I. V. (2021). Mathematical modeling of teleroentgenographic parameters according to the method of Schwarz am depending on the basic cephalometric parameters in ukrainian young men and young women with different face types. *Wiadomosci lekarskie (Warsaw, Poland: 1960)*, *74*(6), 1488-1492. PMID: 34159943

[17] Marchenko, A. V., Gunas, I. V., Petrushanko, T. O., Serebrennikova, O. A., & Trofimenko, Yu. Yu. (2017). Computer-tomographic characteristics of root length incisors and canines of the upper and lower jaws in boys and girls with different craniotypes and physiological bite. *Wiadomosci Lekarskie (Warsaw, Poland: 1960)*, *70*(3 pt 1), 499-502. PMID: 28711896

[18] Nesterenko, Ye. A., Shevchuk, Yu. G., Shinkaruk-Dykovytska, M. M., Lysenko, S. **A**., & Chugu, T. V. (2023). Simulation of individual teleradiographic indicators using the "Cephelometrics for orthognathic surgery" method in

Ukrainian young women with a very broad face type. *Світ медицини та біології=World of Medicine and Biology*, *2*(84), 119-123. doi: 10.26724/2079-8334-2023-2-84-119-123

[19] Potapchuk, A., Almashi, V., Horzov, A., & Kostenko, S. (2024). Comparative analysis of the influence of the shapes and dimensions of dental arches on the morphotopogeometric characteristics of the facial area. *Polski Merkuriusz Lekarski: Organ Polskiego Towarzystwa Lekarskiego*, *52*(3), 356-362. doi: 10.36740/Merkur202403113

[20] Prokopenko, O. S. (2021). Regression models of teleradiographic indicators of the position of teeth and the profile of face soft tissues in Ukrainian young men and young women with different face profiles according to Schwarz AM. *Вісник Вінницького національного медичного університету=Reports of Vinnytsia National Medical University*, *25*(2), 208-214. doi: 10.31393/reports-vnmedical-2021-25(2)-05

[21] Prokopenko, O. S., Beliaiev, E. V., Gulmen, M. K., Popova, O. I., & Cherkasova L. A. (2020). Features of t teleroentgenographic parameters of the upper and lower jaws in Ukrainian young men and young women with orthognathic occlusion and with different types and profiles of the face according to Schwarz A. M.. *Biomedical and Biosocial Anthropology*, (39), 62-69. doi: 10.31393/bba39-2020-10

[22] Prokopenko, O. S., Polishchuk, S. S., Prokopenko, S. V., Gunko, I. P., & Haiduk, O. A. (2023). Correlations of teleroentgenographic parameters of the jaws with basic craniometric parameters in juvenile men and juvenile women with orthognathic bite and different facial types according to Schwarz A. M.. *Світ медицини та біології=World of Medicine and Biology, 2*(84), 124-128. doi: 10.26724/2079-8334-2023-2-84-124-128

[23] Raj, G., Raj, M., & Saigo, L. (2024). Accuracy of conventional versus cone-beam CT-synthesised lateral cephalograms for cephalometric analysis: A systematic review. *Journal of Orthodontics*, *51*(2), 160-176. doi: 10.1177/14653125231178038

[24] Rullo, R., Festa, V. M., Rullo, R., Addabbo, F., Chiodini, P., Vitale, M., & Perillo, L. (2015). Prevalence of dental anomalies in children with cleft lip and unilateral and bilateral cleft lip and palate. *Eur J Paediatr Dent*, *16*(3), 229-232. PMID: 26418927

[25] Ryabov, T. V. (2022). Relationship of odontometric and cephalometric indicators: Review of literary sources. *Вісник Вінницького національного медичного університету=Reports of Vinnytsia National Medical University, 26*(4), 687-691. doi: 10.31393/reports-vnmedical-2022-26(4)-29

[26] Schwarz, A. M. (1960). *Röntgenostatics; Practical Evaluation of the Tele-X-ray-photo (study-head-plate) (Vol. 1)*. Leo L. Bruder.

[27] Schwarz, A. M. (1961). Roentgenostatics: a practical evaluation of the x-ray headplate. *American Journal of Orthodontics*, *47*(8), 561-585. doi: 10.1016/0002-9416(61)90001-X

[28] Simões, R. C., Goettems, M. L., Schuch, H. S., Torriani, D. D., & Demarco, F. F. (2017). Impact of malocclusion on oral health-related quality of life of 8-12 years old schoolchildren in Southern Brazil. *Brazilian Dental Journal*, *28*, 105-112. doi: 10.1590/0103-6440201701278

[29] Yin, J., Zhang, H., Zeng, X., Yu, J., Wang, H., Jiang, Y., ... & Zhang, Y. (2023). Prevalence and influencing factors of malocclusion in adolescents in Shanghai, China. *BMC Oral Health*, *23*(1), 590. doi: 10.1186/s12903-023-03187-5

[30] Zhou, Z., Liu, F., Shen, S., Shang, L., Shang, L., & Wang, X. (2016). Prevalence of and factors affecting malocclusion in primary dentition among children in Xi'an, China. *BMC Oral Health*, *16*(1), 91. doi: 10.1186/s12903-016-0285-x

РЕГРЕСІЙНІ МОДЕЛІ ПАРАМЕТРІВ НЕОБХІДНИХ ДЛЯ ПОБУДОВИ КОРЕКТНОЇ ФОРМИ ЗУБНОЇ ДУГИ В ЗАЛЕЖНОСТІ ВІД ОСОБЛИВОСТЕЙ ТЕЛЕРЕНТГЕНОМЕТРИЧНИХ ПОКАЗНИКІВ ЗА МЕТОДОМ SCHWARZ І КОМП'ЮТЕРНО-ТОМОГРАФІЧНИХ РОЗМІРІВ ЗУБІВ В УКРАЇНСЬКИХ ЮНАКІВ І ДІВЧАТ ІЗ ФІЗІОЛОГІЧНИМ ПРИКУСОМ

Сподарук А. Л., Шінкарук-Диковицька М. М., Вальчук О. Г., Позур Т. П., Шевченко В. М., Тихолаз С.І., Черниш А. В.

Аномалії прикусу та розбіжності у формі зубних дуг залишаються дуже поширеними серед дітей та підлітків у всьому світі, суттєво впливаючи на здоров'я порожнини рота, естетику обличчя та якість життя. Тому точне, специфічне для популяції прогнозування індивідуальних параметрів зубних дуг на основі цефалометричних та одонтометричних характеристик є важливим для персоналізованого планування ортодонтичного та ортогнатичного лікування у молодих пацієнтів з фізіологічним прикусом. Мета дослідження – побудувати та провести аналіз регресійних моделей розмірів необхідних для побудови коректної форми зубної дуги в українських юнаків і дівчат із фізіологічним прикусом в залежності від телерентгенометричних показників за методом Schwarz і комп'ютерно-томографічних розмірів зубів. В застосунку OnyxCeph³™, версії 3DPro (компанія Image Instruments GmbH, Німеччина) на отриманих стандартним шляхом телерентгенограмах і створених в програмному забезпеченні 3D Slicer v5.4.0 телерентгенограмах з маркованими на 3D об'єктах точками у 41 українського юнака і 68 дівчат із фізіологічним прикусом проведено вимірювання телерентгенометричних показників за методом Schwarz. Також в юнаків і дівчат в програмних застосунках i-Dixel One Volume Viewer (Ver.1.5.0) J Morita Mfg. Cor та Planmeca Romexis Viewer (ver. 3.8.3.R 15.12.14) Planmeca OY на комп'ютерних томограмах проведено вимірювання розмірів зубів верхньої й нижньої щелеп та лінійних параметрів зубних дуг. За допомогою ліцензійного пакету «Statistica 6.0» побудовані регресійні моделі параметрів коректної форми зубної дуги в залежності від особливостей телерентгенометричних показників і комп'ютерно-томографічних розмірів зубів. Встановлено, що в юнаків побудовані усі 18 можливих достовірних моделей із коефіцієнтом детермінації більшим 0,6 (R^2= від 0,680 до 0,893, p<0,001); а у дівчат – лише 6 достовірних моделей із коефіцієнтом детермінації більшим 0,6 (R^2= від 0,611 до 0,800, p<0,001). При аналізі частоти входження до регресійних рівнянь комп'ютерно-томографічних розмірів зубів і телерентгенометричних показників встановлено: в юнаків найбільш часто до моделей входять ширина коронкової частини зуба у вестибуло-оральній і мезіо-дистальній площині, телерентгенометричні показники та довжина зуба; а у дівчат – телерентгенометричні показники та ширина коронкової частини зуба у мезіо-дистальній і вестибуло-оральній площині. При аналізі частоти входження до регресійних рівнянь відповідних зубів встановлено, що в юнаків до моделей найбільш часто входять верхні різці, нижні різці, верхні малі кутні зуби, нижні малі кутні зуби та верхні ікла; а у дівчат

– верхні різці, нижні різці, нижні ікла та нижні малі кутні зуби.
Ключові слова: *стоматологія, телерентгенометрія за методом Schwarz, комп'ютерно-томографічні розміри зубів і зубних дуг, регресійний аналіз, українськи юнаки та дівчата з фізіологічним прикусом.*

Author's contribution
Spodaruk A. L. – research, methodology and writing of the original draft.
Shinkaruk-Dykovytska M. M. – conceptualization, supervision, project administration.
Valchuk O. G. – review writing and editing.
Pozur T. P. – formal analysis and validation.
Shevchenko V. M. – review writing and editing.
Tykholaz S.I. – software.
Chernysh A. V. – data visualization.

DOI: 10.31393/morphology-journal-2025-31(4)-09 Reports of Morphology, Vol. 31, №4, Pages 69-75

ISSN 1818-1295 eISSN 2616-6194

REPORTS OF MORPHOLOGY

Official Journal of the Scientific Society of Anatomists, Histologists, Embryologists and Topographic Anatomists of Ukraine

journal homepage: https://morphology-journal.com

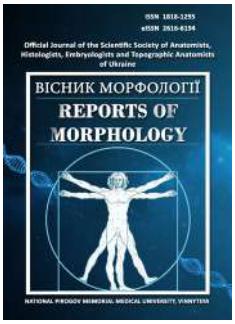

Peculiarities of histological and immunohistochemical changes in the respiratory portion of the white rats' lungs in experimental colon adenocarcinoma *in situ*

Nebesna Z. M.[1], Kulbitska V. V.[1], Ohinska N. V.[1], Dovbush A. V.[1], Lytvynyuk S. O.[1], Rymar A. A.[2]

[1] I. Horbachevsky Ternopil National Medical University, Ternopil, Ukraine

[2] Municipal Institution of Higher Education "Volyn Medical Institute" of the Volyn Oblast Council, Lutsk, Ukraine

ARTICLE INFO

Received: 10 April 2025

Accepted: 3 October 2025

UDC: 616.24-091.8:616-006.6-021.3-092.9(043.3)

CORRESPONDING AUTHOR

e-mail: nebesna_zm@tdmu.edu.ua

Nebesna Z. M.

CONFLICT OF INTEREST

The authors have no conflicts of interest to declare.

FUNDING

Not applicable.

DATA SHARING

Data are available upon reasonable request to corresponding author.

Colorectal cancer is among the most common human malignancies, its pathogenesis is accompanied by the development of endogenous neoplastic intoxication and multi-organ morphofunctional disorders. Among the target organs, the lungs occupy an important place, as they are sensitive to toxic metabolites, oxidative stress and microcirculatory disturbances. The aim of the study was to determine the patterns of morphological and macrophage reactions in the lungs of white rats with N,N-dimethylhydrazine-induced in situ adenocarcinoma of the colon. The study was conducted on 85 adult male white rats, of which 70 animals received N,N-dimethylhydrazine hydrochloride (7.2 mg/kg body weight, subcutaneously, once a week for 30 weeks). Morphological examination of the lungs was performed after fixation in 10 % neutral formalin, followed by embedding in paraffin, preparation of serial sections, and staining with hematoxylin and eosin. For the identification of macrophages, an immunohistochemical method was used with antibodies against CD68 (Abcam, USA) and the PolyVue™ HRP/DAB polymer visualization system. It was established that starting from the fourth stage of the experiment, animals with DMH-induced carcinogenesis developed vascular congestion, aggregation of blood elements, interstitial edema, and histoleukocytic infiltration in the lungs. As the experiment progressed, there was an intensification of destructive-degenerative processes, the development of atelectasis, dystelectasis, emphysematous areas and sclerosis foci were noted. In areas of inflammatory infiltration, in the walls of vessels and bronchi, as well as in zones of atelectasis, a gradual increase in the expression of $CD68^+$ macrophages were observed from moderate to intense with the appearance of foamy forms. At later stages of the experiment, the phenomena of fibroblastic proliferation, the growth of dense oxyphilic collagen fibers and the formation of interstitial fibrosis predominated, indicating the transition of the acute inflammatory reaction to a chronic phase. Thus, a consistent dynamic of alterative-inflammatory and fibrotic changes in the lungs during DMH-induced colon carcinogenesis has been revealed. These changes are accompanied by activation of the macrophage system and remodeling of the respiratory portion of the lungs, reflecting the systemic impact of neoplastic intoxication on the pulmonary parenchyma.

Keywords: *lungs, respiratory portion, colon adenocarcinoma, rats, pan-macrophage marker CD68, histological and immunohistochemical changes.*

Introduction

According to the International Agency for Research on Cancer and the World Health Organization, colorectal cancer remains one of the most common malignancies in the world. In 2022, about 1.9 million new cases and more than 930,000 deaths were registered, accounting for about 10 % of all cancer cases and 9.3 % of cancer related mortality. According to WHO projections, by 2050 the number of new colorectal cancer cases may exceed 3.2 million per year, indicating a steady rise in the global prevalence of this oncological pathology and highlighting the relevance of studying its systemic pathogenetic consequences [19, 27].

Modern oncomorphology considers the tumor process not

only as a local neoplasm, but also as a systemic pathology accompanied by multilevel metabolic and structural rearrangements in the body. One of the leading mechanisms of such changes is endogenous neoplastic intoxication, which develops as a result of prolonged circulation of toxic metabolites, tumor cell destruction products, cytokines and free radicals in the blood. These factors have a multi-organ, damaging effect, promoting the development of morphofunctional disorders in distant organs [10, 11, 12, 29].

The lung tissue has a high level of vascularization, a large diffusion area and intensive metabolic processes, making it extremely sensitive to toxic metabolites and hypoxic ifnluences [7]. In the pathogenesis of lung lesions under tumor growth conditions, crucial roles are played by microcirculatory disturbances, increased vascular wall permeability, activation of inflammatory cells, and secondary destructive-degenerative processes. This leads to remodeling of the respiratory portion of the lungs, development of atelectasis, emphysema, interstitial fibrosis and other pathologies [9, 14, 26].

Particular attention of researchers is drawn to the involvement of the macrophage component of the immune system in shaping the lung tissue response to chronic endogenous intoxication. Alveolar macrophages perform not only a phagocytic functions but also modulate inflammation, regulate apoptosis and stimulate fibrogenesis through the production of proinflammatory cytokines (IL-1β, TNF-α, TGF-β). Their activity is reflected by the level of CD68 expression, a universal marker of the monocyte-macrophage system [2, 6, 21, 28]. Establishing quantitative and topographical changes in $CD68^+$cells in the lungs is essential for understanding the mechanisms of inflammation and parenchymal remodeling during oncogenesis.

At the same time, the available literature lacks comprehensive data that would combine histological and immunohistochemical aspects of the lung respiratory portion during N,N-dimethylhydrazine-induced colon carcinogenesis. This necessitates a more detailed morphological analysis of this process.

The aim of our study was to investigate the dynamics of histological changes and macrophage responses in the lungs of rats with experimental colon adenocarcinoma induced by N,N-dimethylhydrazine.

Materials and methods

The experimental study was conducted on 85 outbred adult white male rats weighing 195±5 g. The experimental animals were kept in standard vivarium conditions with a natural light cycle, constant access to drinking water and *ad libitum* basic diet. Throughout the experiment the general condition, survival, and body weight of the rats were monitored. All experiments were performed in accordance with international bioethical standards [5] and were approved by the Bioethics Committee of the Ivan Horbachevsky Ternopil National Medical University Ministry of Health of Ukraine (Protocol No. 80 of January 10, 2025).

The experimental animals were randomly divided into two separate groups: Group I – control group (15 animals); Group II – animals with DMH-induced colon adenocarcinoma in situ (70 animals).

Colon adenocarcinoma *in situ* was induced by administering of N,N-dimethylhydrazine hydrochloride (DMH) (Sigma-Aldrich Sp. z o.o., Japan, series D161608) for 30 weeks. This model is often used in experimental oncology and most adequately simulates the development of sporadic colorectal cancer in humans [20]. The carcinogen was diluted with an isotonic solution in a ratio of a 1:100 and injected subcutaneously into the interscapular region at a dose of 7.2 mg per 1 kg of animal body weight (in terms of active ingredient) once per week. To simulate potential stress-related effects, animals in the control group received subcutaneous injections of an isotonic solution at a dose of 0.1 ml per 10 g of body weight.

For convenience of data presentation, the entire administration period and tissue sampling process were divided into seven stages (each stage corresponding to 30 days of the experiment). Euthanasia was performed under thiopental sodium anesthesia (intraperitoneally, 10 % thiopental sodium at a dose of 50 mg/kg body weight; Arterium, Ukraine).

The morphology of the structural components of the lungs at the microscopic level was studied using classical histological techniques [23, 25]. Tissue samples were fixed in a 10 % buffered formalin solution, which ensures effective preservation of tissue structure for further analysis. Standard methods were used to process the samples, after which the material was embedded into paraffin blocks. The material was cut on a rotary microtome AMR-400 4-5 μm (Amos, Australia). The resulting sections were stained with hematoxylin and eosin. Photographic documentation was performed using a MICROmed SEO SCAN light microscope with a Vision CCD Camera and a system for displaying images from histological specimens.

To identify macrophage subpopulations in lung tissue, immunohistochemical staining method was used with a panel of specific markers, in particular, CD68 was employed as a pan-macrophage marker. Antigen retrieval was performed by heat-induced epitope retrieval in EnVision FLEX Target Retrieval Solution High pH buffer (pH 9.0), carried out in a KOS histoprocessor (Milestone, Italy) at 98 °C for 20 minutes. To block endogenous peroxidase activity, a 3 % aqueous solution of H_2O_2 was used. Subsequent incubation with specific primary antibodies was conducted for 60 minutes: rabbit polyclonal anti-CD68 antibody (Cat. No. ab125212, Abcam, USA) was used to detect CD68+ cells. The visualization of the resulting immune complexes was performed using the Mouse/Rabbit PolyVue™ HRP/DAB polymer detection system (Diagnostic BioSystems, USA), which provides high sensitivity and specificity due to polymer-conjugated secondary antibodies with peroxidase activity and subsequent chromogenic detection with diaminobenzidine (DAB). Counterstaining of cell nuclei was performed with Mayer's hematoxylin according to the standard protocol.

Results

The results of microscopic examination of the lungs of experimental animals in Group II, in which colon carcinogenesis was modeled, demonstrated initial alterative changes in all structural components of the lungs during the period from 1 to 3 months (i.e., the first three stages).

Starting from the 4th month, microscopic analysis of the lungs of white rats subjected to colon carcinogenesis revealed progressive destructive changes in the vessels, bronchi, and components of the respiratory portion of the lungs.

At this observation point, the blood vessels of the organ were characterized by pronounced congestion, particularly in the venous system. Their walls were often deformed, with pronounced edema of the adventitial tunic and its infiltration with leukocytes. Significant remodeling was observed in the microcirculatory vessels of the lungs. Their lumens contained stasis and erythrocyte sludging (Fig. 1A). Diapedesis of erythrocytes was also noted. The bronchial walls were edematous, with desquamated epithelial fragments present in the lumen; edema and infiltration of the adventitia by histoleukocytic cells were evident. In the respiratory portion of the organ, areas with unchanged histological structure predominate, but areas of dis- and atelectasis, areas of emphysematous altered lung tissue were increasing. The influence of the pathological process was confirmed during this period of observation by an increase in the number of cells of inflammatory genesis, which was immunohistochemically confirmed by the presence of CD68+ cells (++-), both in the interalveolar septa and in the lumen of the alveoli (Fig. 1B).

At the next 5 months of studying histological slides of the lungs of experimental animals with modeled colon carcinogenesis, it was found that the pathological process spread with severe edema and histoleukocyte infiltration of alveolar septa, bronchial adventitia and blood vessels. The areas of emphysematous altered areas, dis- and atelectasis increased and, accordingly, the areas with unchanged histological structure decreased. The circulatory changes were preserved. Pronounced alteration was observed in the bronchi, characterized by epithelial desquamation, edema, and hyperplasia of bronchus-associated lymphoid tissue (BALT) (Fig. 2A).

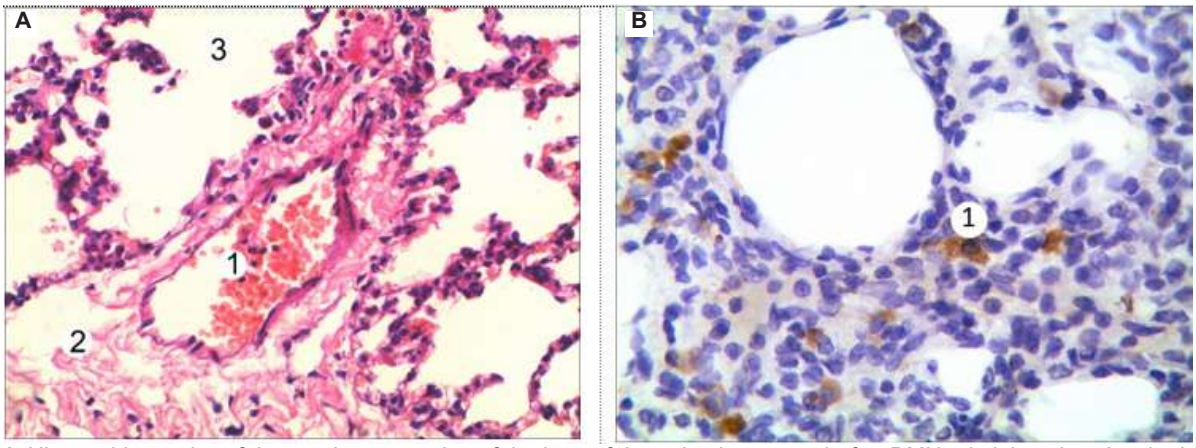

Fig. 1. Histoarchitectonics of the respiratory portion of the lung of the animal at stage 4 after DMH administration. A – the lumen of a small-caliber vein is filled with blood (1), pronounced edema of the adventitial tunic (2), alveoli of the respiratory portion (3). Hematoxylin and eosin staining, ×200. B – moderately expressed CD68+ in interstitial cells (1). Immunohistochemical staining, Mayer's hematoxylin and eosin counterstaining, ×400.

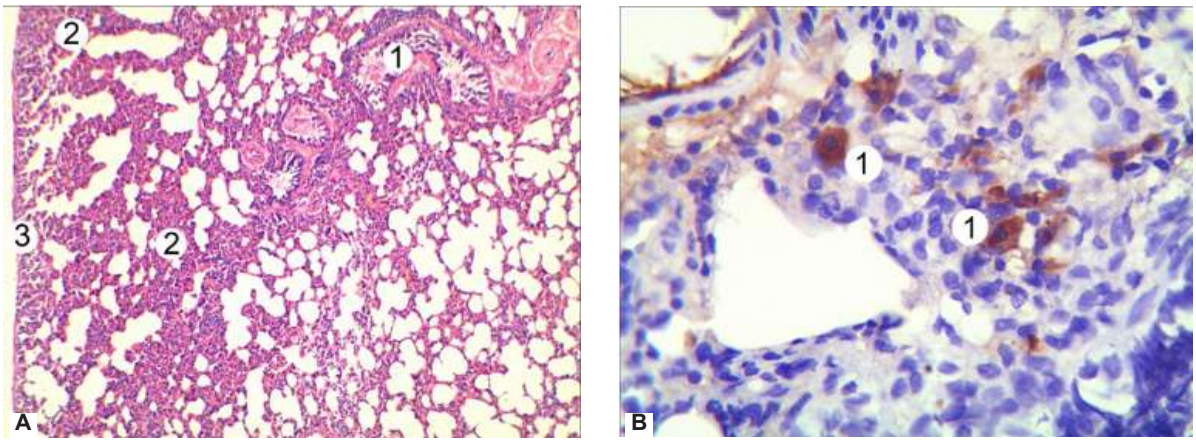

Fig. 2. Morphological changes in the respiratory portion of the animal lung at stage 5 after DMH administration. A – terminal bronchioles with mucous content (1), areas of disatelectasis (2), pleura (3). Hematoxylin and eosin staining, ×100. B – expression of CD68+ cells. Moderately expressed positive reaction in atelectasis cells (1). Immunohistochemical staining, Mayer's hematoxylin and eosin counterstaining, ×400.

Immunohistochemical analysis showed that pulmonary macrophages in the experimental group showed moderate positive CD68 immunoreactivity (++-), they were localized in the adventitia of bronchi and vessels, as well as in areas of atelectasis, disatelectasis and freely in the alveolar lumens (Fig. 2B).

Microscopic analysis of the lungs of white rats six months after induced colon adenocarcinoma revealed distinct alternative changes in all structural elements of the organ, accompanied by deformation of the walls of blood vessels and bronchi, formation of inflammatory cell loci and restructuring of the respiratory portion. In this part of the lungs, there was a significant thickening of the alveolar septa due to leukocyte-histiocyte infiltration. The area of dys- and atelectasis, as well as emphysematous altered zones, increased. Numerous alveolar macrophages, in particular foamy macrophages, were detected in the alveolar lumens and their walls (Fig. 3A). Increased macrophage activity at this stage was confirmed by immunohistochemistry. CD68+ cells with intense immunoreactivity (+++) were detected in the respiratory portion, mainly in the areas of atelectasis (Fig. 3B).

The most pronounced destructive-degenerative changes in the lungs of the laboratory animals were detected 7 months after the completion of the induced colorectal carcinogenesis. The respiratory portion was dominated by voluminous areas of dis- and atelectasis, massive inflammatory infiltrates, emphysematous dilated alveoli, and foci of hemorrhage. Only in relatively small areas was the integrity of the lung histostructure preserved without alteration. Significant accumulations of alveolar macrophages and blood cells, primarily erythrocytes, were found in the alveolar lumen, indicating damage to the alveolar walls. In the areas of atelectasis, there was a significant increase in the number of fibroblasts, fibrocytes and oxyphilic dense fibrous formations, indicating the development of fibrotic changes in the respiratory portion of the lungs (Fig. 4A). Signs of prolonged inflammation 7 months after DMH administration were manifested by an intense positive reaction (+++) in the bronchial walls and areas of atelectasis in the respiratory portion (Fig. 4B).

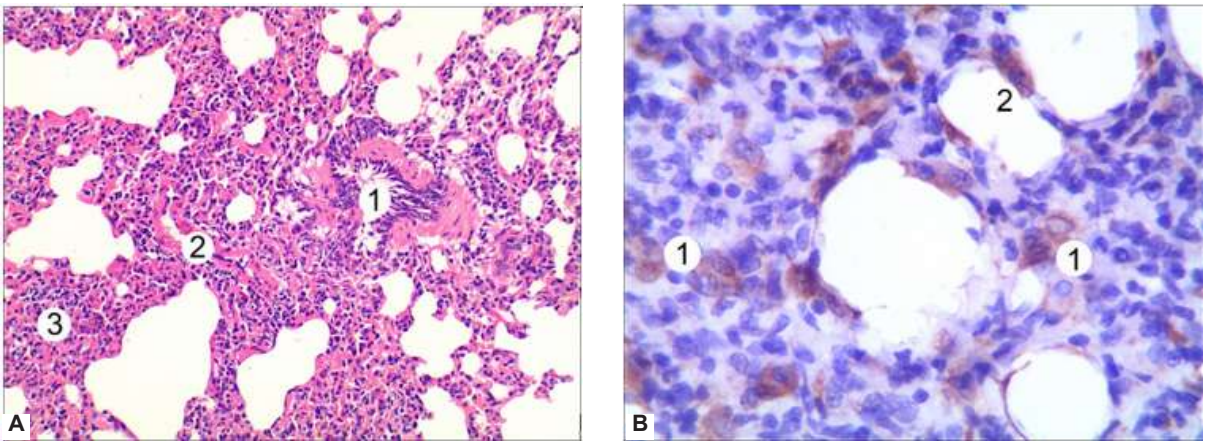

Fig. 3. Histological and immunohistochemical changes in the lung of the animal at stage 6 after DMH administration. A – small bronchus (1), vein (2), area of atelectasis and leukocyte infiltration (3). Hematoxylin and eosin staining, ×200. B – moderate expression of CD68+ interstitial (1) and alveolar cells (2). Immunohistochemical staining, Mayer's hematoxylin and eosin counterstaining, ×400.

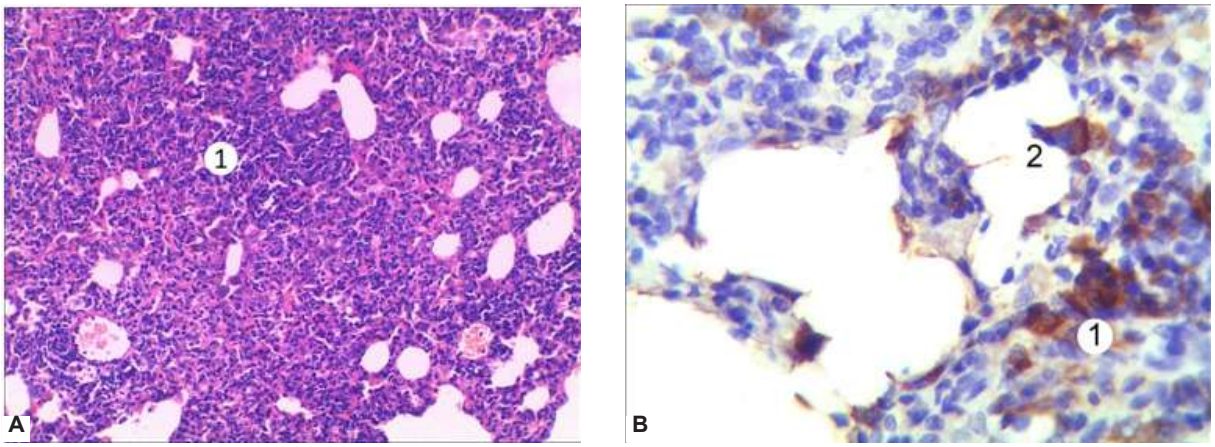

Fig. 4. Remodeling of the structural components of the rat lung at stage 7 after DMH administration. A – areas of dis- and atelectasis and their leukocyte infiltration (1). Hematoxylin and eosin staining, ×200. B – pronounced positive expression of CD68+ in the areas of atelectasis (1) and alveoli (2) of the respiratory portion of the lung. Immunohistochemical staining, Mayer's hematoxylin and eosin (H&E) staining, ×400.

Discussion

Colorectal cancer is one of the leading causes of cancer morbidity and mortality worldwide, which makes it highly relevant to study its etiology and mechanisms of development. The pathogenesis of colorectal cancer is multifactorial and involves the interaction of genetic mutations, epigenetic changes, and the influence of external factors such as nutrition, microbiota, chronic inflammation, and lifestyle. Consistent accumulation of mutations in cell cycle regulatory genes such as APC, KRAS, and TP53 contributes to the formation of adenomatous polyps and their subsequent malignancy. Disorders of the Wnt/β-catenin signaling pathways, MSI (microsatellite instability) and CpG island methylation phenotype, which determine the biological behavior of tumors and response to treatment, also play an important role [16, 27].

An important component of colorectal cancer morphogenesis is dynamic alteration in the stromal component, which largely determine the invasive potential of tumor cells. Activation of cancer-associated fibroblasts, remodeling of the extracellular matrix, and increased expression of metalloproteinases promote invasion of the submucosa and formation of metastatic niches [17, 18]. At the same time, impaired angiogenesis, reflected in increased expression of VEGF and neovascularization in the tumor growth zone, creates a microenvironment favorable for tumor progression. Thus, modern morphological data emphasize that colorectal cancer is a systemic process with a complex interaction of epithelial and stromal components, and its study requires the integration of traditional histological methods with molecular and immunohistochemical technologies for an in-depth understanding of pathogenesis.

Metaplasia remains one of the leading causes of cancer morbidity and mortality worldwide, with an upward trend in both developed countries and Ukraine. Its clinical course is often asymptomatic in the initial stages, which makes timely diagnosis and effective treatment difficult. The study of the systemic impact of the neoplastic process on target organs is gaining special attention [1, 15]. One of these organs is the lung, which is highly sensitive to endogenous intoxication, oxidative stress, and immunoinflammatory changes that manifest themselves at early stages of carcinogenesis. Even in the absence of metastases, tumor intoxication can cause structural and functional disorders in lung tissue that are important for understanding the mechanisms of the body's systemic response to the primary tumor focus [3, 24].

The obtained results of a comprehensive histological and immunohistochemical analysis indicate that under conditions of DMH-induced colon adenocarcinoma, a pronounced syndrome of systemic endogenous intoxication is formed in the lungs of white rats, accompanied by a gradual remodeling of the structures of the respiratory department. Starting from the fourth stage of the experiment, microcirculatory disorders, vascular hemorrhage, stasis, aggregation of blood cells and interstitial edema were observed. These changes probably reflect the early phase of the systemic response to circulating metabolites of neoplastic origin and activation of oxidative stress mechanisms, as reported by other researchers [4].

The increase in the number of $CD68^+$ macrophages in the interstitium of the respiratory tract indicates the activation of the cellular link of nonspecific immunity. Macrophages in such conditions play a dual role: on the one hand, they phagocytose necrosis products and cellular detritus, and on the other hand, they are a source of proinflammatory cytokines (IL-1β, TNF-α) that enhance endothelial damage and stimulate fibroblast proliferation [2, 4]. The detected gradual increase in the expression of $CD68^+$ cells from the 4th to the 7th stage of the experiment correlates with the increase in destructive and sclerotic changes, which allows us to consider this indicator as an immunomorphological marker of the intensity of lung tissue remodeling.

At the later stages of the experiment, destructive-degenerative processes dominated in the alveolar structures, with the formation of zones of atelectasis, dysatelectasis, emphysematous changes, and sclerosis. The presence of expanding oxyphilic collagen fibers and increased numbers of fibroblasts indicates a transition of the inflammatory response to a chronic phase with the development of fibrosis. Similar findings have been described in studies [8, 13, 22, 30], which demonstrated that macrophage infiltration is a key factor in activating TGF-β-dependent mechanisms of pulmonary fibrogenesis.

The identified morphological rearrangements confirm that the lungs function as one of the target organs of systemic neoplastic intoxication during colorectal carcinogenesis. Thus, the observed remodeling of the respiratory portion reflects not only a local reaction to toxic metabolites but also a general homeostatic shift toward chronic inflammation with elements of fibrosis.

The novelty of the study lies in the identification of the stepwise dynamics of morphological and immunohistochemical changes in the lungs under experimental colon adenocarcinoma, which allows us to interpret lung tissue as a sensitive indicator of systemic responses during neoplastic processes. The findings expand current knowledge about the morphological manifestations of chronic endogenous intoxication, enhance understanding of the mechanisms of pulmonary remodeling under oncogenesis, and may be used to further develop morphofunctional criteria for evaluating the effectiveness of therapeutic and preventive approaches.

Conclusions

1. The morphological changes in the lungs under conditions of DMH-induced oncogenesis exhibit a pattern of progressive remodeling of the vascular bed, proliferation of lymphoid elements and the formation of zones of emphysematous transformation, dis- and atelectasis within the respiratory portion. Starting from the fourth stage of the experiment, a gradual intensification of alterative-destructive processes was observed, followed by the formation of polymorphic structural disorders of the pulmonary parenchyma. By the seventh stage, the pathological

changes reach maximal severity, manifested by profound destruction of alveolar walls and the appearance of regions with significant disruption of the lung histoarchitecture.

2. The protective mechanisms in the lungs during DMH-induced oncogenesis are manifested by a gradual activation of the immune response, accompanied by hyperplasia of lymphoid tissue and increased macrophage infiltration. In the dynamics of the experiment, an increase in the number of foamy and $CD68^+$ macrophages was determined, the intensity of which increased in parallel with the intensification of inflammatory-destructive processes in the respiratory portion of the lungs.

References

[1] Acevedo-León, D., Gómez-Abril, S. Á., Sanz-García, P., Estañ-Capell, N., Bañuls, C., & Sáez, G. (2023). The role of oxidative stress, tumor and inflammatory markers in colorectal cancer patients: A one-year follow-up study. *Redox Biol*, *62*, 102662. doi: 10.1016/j.redox.2023.102662

[2] Cardoso, R., Guo, F., Heisser, T., Hackl, M., Ihle, P., De Schutter, H., … & Brenner, H. (2021). Colorectal cancer incidence, mortality, and stage distribution in European countries in the colorectal cancer screening era: an international population-based study. *The Lancet. Oncology*, *22*(7), 1002-1013. doi: 10.1016/S1470-2045(21)00199-6

[3] Carini, F., Mazzola, M., Rappa, F., Jurjus, A., Geagea, A. G., Al Kattar, S., … & Tomasello, G. (2017). Colorectal Carcinogenesis: Role of Oxidative Stress and Antioxidants. *Anticancer research*, *37*(9), 4759-4766. doi: 10.21873/anticanres.11882

[4] Choi, J. P., Park, S. Y., Moon, K. A., Ha, E. H., Woo, Y. D., Chung, D. H., … & Cho, Y. S. (2020). Macrophage-derived progranulin promotes allergen-induced airway inflammation. *Allergy*, *75*(5), 1133-1145. doi: 10.1111/all.14129

[5] de l'Europe, C. (1986). *European Convention for the protection of vertebrate animals used for experimental and other scientific purposes/Convention européenne sur la protection des animaux vertébrés utilisés à des fins expérimentales ou à d'autres fins scientifiques:[Strasbourg, 18. III. 1986]*. Conseil de l'Europe Section des publications.

[6] Fernandez-Gonzalez, A., Mukhia, A., Nadkarni, J., Willis, G. R., Reis, M., Zhumka, K., ... & Kourembanas, S. (2024). Immunoregulatory macrophages modify local pulmonary immunity and ameliorate hypoxic pulmonary hypertension. *bioRxiv [Preprint]*, 2023.07.31.551394. doi: 10.1101/2023.07.31.551394

[7] Frangogiannis, N. (2020). Transforming growth factor-β in tissue fibrosis. *The Journal of experimental medicine*, *217*(3), e20190103. doi: 10.1084/jem.20190103

[8] Greenwald, M. A., & Wolfgang, M. C. (2022). The changing landscape of the cystic fibrosis lung environment: From the perspective of Pseudomonas aeruginosa. *Current opinion in pharmacology*, *65*, 102262. doi: 10.1016/j.coph.2022.102262

[9] He, J., Du, Y., Li, G., Xiao, P., Sun, X., Song, W., … & Wang, Q. (2022). Myeloid Fbxw7 Prevents Pulmonary Fibrosis by Suppressing TGF-β Production. *Frontiers in immunology*, *12*, 760138. doi: 10.3389/fimmu.2021.760138

[10] Johdi, N. A., & Sukor, N. F. (2020). Colorectal Cancer Immunotherapy: Options and Strategies. *Frontiers in immunology*, *11*, 1624. doi: 10.3389/fimmu.2020.01624

[11] Kennedy, L., Sandhu, J. K., Harper, M. E., & Cuperlovic-Culf, M. (2020). Role of Glutathione in Cancer: From Mechanisms to Therapies. *Biomolecules*, *10*(10), 1429. doi: 10.3390/biom10101429

[12] Klimeck, L., Heisser, T., Hoffmeister, M., & Brenner, H. (2023). Colorectal cancer: A health and economic problem. Best practice & research. *Clinical gastroenterology*, *66*, 101839. doi: 10.1016/j.bpg.2023.101839

[13] Lis-López, L., Bauset, C., Seco-Cervera, M., & Cosín-Roger, J. (2021). Is the Macrophage Phenotype Determinant for Fibrosis Development?. *Biomedicines*, *9*(12), 1747. doi: 10.3390/biomedicines9121747

[14] Liu, H., Wang, Y., Zhang, Q., Liu, C., Ma, Y., Huang, P., … & Ma, L. (2023). Macrophage-derived inflammation promotes pulmonary vascular remodeling in hypoxia-induced pulmonary arterial hypertension mice. *Immunology letters*, *263*, 113-122. doi: 10.1016/j.imlet.2023.10.005

[15] Mahmoud, N. N. (2022). Colorectal Cancer: Preoperative Evaluation and Staging. *Surgical oncology clinics of North America*, *31*(2), 127-141. doi: 10.1016/j.soc.2021.12.001

[16] Makena, P., Kikalova, T., Prasad, G. L., & Baxter, S. A. (2023). Oxidative Stress and Lung Fibrosis: Towards an Adverse Outcome Pathway. *International journal of molecular sciences*, *24*(15), 12490. doi: 10.3390/ijms241512490

[17] Mármol, I., Sánchez-de-Diego, C., Pradilla Dieste, A., Cerrada, E., & Rodriguez Yoldi, M. J. (2017). Colorectal Carcinoma: A General Overview and Future Perspectives in Colorectal Cancer. *International journal of molecular sciences*, *18*(1), 197. doi: 10.3390/ijms18010197

[18] Nguyen, L. H., Goel, A., & Chung, D. C. (2020). Pathways of Colorectal Carcinogenesis. *Gastroenterology*, *158*(2), 291-302. doi: 10.1053/j.gastro.2019.08.059

[19] Pernot, S., Terme, M., & Voron, T. (2014). Colorectal cancer and immunity: what we know and perspectives. *World J Gastroenterol*, *20*(14), 3738. doi: 10.3748/wjg.v20.i14.3738

[20] Perše, M., & Cerar, A. (2011). Morphological and molecular alterations in 1,2 dimethylhydrazine and azoxymethane induced colon carcinogenesis in rats. *J. Biomed Biotechnol*, 11, 473-96. doi: 10.1155/2011/473964

[21] Rivera, J. A., Corchuelo, S., Parra, E. A., Meek, E. A., Mercado, M., & Torres-Fernández, O. (2022). Inmunohistochemical detection of pandemic SARSCoV- 2 antigens in lung tissue. Detección inmunohistoquímica de antígenos de SARS-CoV-2 en tejido pulmonar. *Biomedica : revista del Instituto Nacional de Salud*, *42*(Sp. 2), 9-13. doi: 10.7705/biomedica.6132

[22] Sobanski, V., de Vries-Bouwstra, J., Hoffmann-Vold, A. M., Huscher, D., Alves, M., Matucci-Cerinic, M., … & EUSTAR Collaborators (2025). Lung function and skin fibrosis changes as predictors of survival in SSc-associated interstitial lung disease: a EUSTAR study. *Rheumatology (Oxford, England)*, *64*(10), 5344-5353. doi: 10.1093/rheumatology/keaf264

[23] Spaniol, K., Guthoff, R., Schrader, S., Borrelli, M., Kajasi, N., Schramm, M., & Geerling, G. (2016). Diagnostik von Binde- und Hornhauterkrankungen [Histological Techniques]. *Klinische Monatsblatter fur Augenheilkunde*, *233*(6), e17-e28. doi: 10.1055/s-0033-1358232

[24] Sul, O. J., & Ra, S. W. (2021). Quercetin Prevents LPS-Induced Oxidative Stress and Inflammation by Modulating NOX2/ROS/NF-kB in Lung Epithelial Cells. *Molecules*

(Basel, Switzerland), *26*(22), 6949. doi: 10.3390/molecules26226949
[25] Suvarna, S. K., Layton, C., & Bancroft, J. D. (2018). *Bancroft's theory and practice of histological techniques (8th ed.)*. Elsevier. 672 p.
[26] Yamamura, A. (2025). Growth factors involved in vascular remodeling in pulmonary arterial hypertension. *Journal of smooth muscle research=Nihon Heikatsukin Gakkai kikanshi*, *61*, 82-92. doi: 10.1540/jsmr.61.82
[27] Yu, B., Kang, J., Lei, H., Li, Z., Yang, H., & Zhang, M. (2024). Immunotherapy for colorectal cancer. *Frontiers in immunology*, *15*, 1433315. doi: 10.3389/fimmu.2024.1433315
[28] Zaiats, L. M., & Klishch, I. P. (2018). Ultrastructure of alveolar macrophages in case of experimental acute renal failure. *World of medicine and biology*, *1*(63), 130-133. doi: 10.26.724/2079-8334-2018-1-63-130-133
[29] Zhang, C., Stampfl-Mattersberger, M., Ruckser, R., & Sebesta, C. (2023). Kolorektales Karzinom [Colorectal cancer]. *Wiener medizinische Wochenschrift (1946)*, *173*(9-10), 216-220. doi: 10.1007/s10354-022-00975-6
[30] Ziablitsev, D. S., Kozyk, M., Strubchevska, K., Dyadyk, O. O., & Ziablitsev, S. V. (2023). Lung Expression of Macrophage Markers CD68 and CD163, Angiotensin Converting Enzyme 2 (ACE2), and Caspase-3 in COVID-19. *Medicina (Kaunas, Lithuania)*, *59*(4), 714. doi: 10.3390/medicina59040714

ОСОБЛИВОСТІ ГІСТОЛОГІЧНИХ ТА ІМУНОГІСТОХІМІЧНИХ ЗМІН РЕСПІРАТОРНОГО ВІДДІЛУ ЛЕГЕНЬ БІЛИХ ЩУРІВ ПРИ ЕКСПЕРИМЕНТАЛЬНІЙ АДЕНОКАРЦИНОМІ ТОВСТОЇ КИШКИ IN SITU

Небесна З. М., Кульбіцька В. В., Огінська Н. В., Довбуш А. В., Литвинюк С. О., Римар А. А.

Колоректальний рак належить до найпоширеніших злоякісних новоутворень людини, патогенез якого супроводжується розвитком ендогенної неопластичної інтоксикації та поліорганними морфофункціональними порушеннями. Серед органів-мішеней важливе місце посідають легені, чутливі до токсичних метаболітів, оксидативного стресу та порушень мікроциркуляції. Мета дослідження – з'ясувати закономірності морфологічних і макрофагальних реакцій у легенях білих щурів при N,N-диметилгідразин-індукованій аденокарциномі товстої кишки in situ. Дослідження проведено на 85 статевозрілих білих щурах-самцях, з яких 70 тварин отримували N,N-диметилгідразин гідрохлорид (7,2 мг/кг маси тіла, підшкірно, один раз на тиждень протягом 30 тижнів). Морфологічне вивчення легень здійснювали після фіксації у 10 % нейтральному формаліні з подальшим заливанням у парафін, виготовленням серійних зрізів і забарвленням гематоксиліном та еозином. Для ідентифікації макрофагів застосовували імуногістохімічний метод із використанням антитіл до CD68 (Abcam, США) та полімерної системи візуалізації PolyVue™ HRP/DAB. Встановлено, що починаючи з четвертого етапу експерименту в легенях тварин із ДМГ-індукованим канцерогенезом з'являються судинне повнокрів'я, агрегація формених елементів, набряк інтерстицію та гістолейкоцитарна інфільтрація. У подальшій динаміці відмічено посилення деструктивно-дегенеративних процесів, розвиток ателектазів, дисателектазів, емфізематозних зон і фокусів склерозу. У ділянках запальної інфільтрації, стінках судин і бронхів, а також у зонах ателектазів спостерігалося поетапне зростання експресії CD68$^+$ макрофагів від помірної до інтенсивної, із появою пінистих форм. На пізніх етапах досліду домінували явища фібробластичної проліферації, розростання щільних оксифільних колагенових волокон і формування інтерстиціального фіброзу, що свідчить про перехід гострої запальної реакції в хронічну фазу. Таким чином, виявлено закономірну динаміку альтеративно-запальних і фібротичних змін у легенях при ДМГ-індукованому канцерогенезі товстої кишки, що супроводжується активацією макрофагальної ланки та ремоделюванням респіраторного відділу, яке відображає системну дію неопластичної інтоксикації на легеневу паренхіму.

Ключові слова: *легені, респіраторний відділ, аденокарцинома товстої кишки, щури, пан-макрофагальний маркер CD68, гістологічні і імуногістохімічні зміни.*

Author's contribution

Nebesna Z. M. – conceptualization, data curation, formal analysis, funding acquisition, methodology, project administration, supervision, validation, writing – review & editing.
Kulbitska V. V. – formal analysis, investigation, writing – review & editing.
Ohinska N. V. – data curation, investigation, methodology, visualization, conceptualization, writing – original draft.
Dovbush A. V. – methodology, investigation, visualization.
Lytvynyuk S. O. – methodology, investigation, visualization.
Rymar A. A. – data curation, investigation, methodology, visualization, conceptualization.

DOI: 10.31393/morphology-journal-2025-31(4)-10 Reports of Morphology, Vol. 31, №4, Pages 76-81

ISSN 1818-1295 eISSN 2616-6194

REPORTS OF MORPHOLOGY

Official Journal of the Scientific Society of Anatomists, Histologists, Embryologists and Topographic Anatomists of Ukraine

journal homepage: https://morphology-journal.com

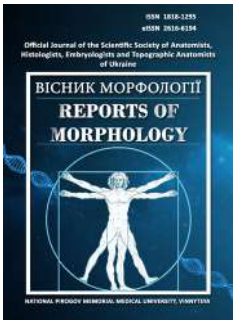

Features of CD20 expression in the kidney tissue of experimental rats three hours after administration of Leiurus macroctenus scorpion venom

Matkivska R. M.[1], Samborska I. A.[2], Mostiuk O. M.[3]

[1] Bogomolets National Medical University, Kyiv, Ukraine, Kyiv, Ukraine

[2] DILA Medical Laboratory, Department of Oncology Diagnostics, Pathomorphology Laboratory, Kyiv, Ukraine

[3] Educational and Scientific Centre "Institute of Biology and Medicine", Taras Shevchenko National University of Kyiv, Kyiv, Ukraine

ARTICLE INFO

Received: 2 April 2025

Accepted: 8 October 2025

UDC: 616-001.43;616-022.912/.913

CORRESPONDING AUTHOR

e-mail: rujena011279@gmail.com

Matkivska R. M.

CONFLICT OF INTEREST

The authors have no conflicts of interest to declare.

FUNDING

Not applicable.

DATA SHARING

Data are available upon reasonable request to corresponding author.

Bites from venomous animals, such as snakes, vipers, and arthropods (particularly scorpions), are a significant public health problem in many countries worldwide. Acute kidney injury is one of the main effects of these venoms and is associated with high morbidity and mortality. The study aims to investigate the features of CD20 expression in the kidney tissue of experimental rats three hours after administration of scorpion Leiurus macroctenus venom. The study used 10 white male laboratory rats weighing 200 g (±10 g). The venom of the scorpion Leiurus macroctenus (Buthidae) was administered to rats once intramuscularly (0.5 ml of a venom solution previously dissolved in saline; 28.8 µg/ml; LD50=0.08 mg/kg). To identify the CD20 cell subpopulation in kidney tissue, rabbit recombinant primary antibodies Anti-CD20 (ab64088, Abcam, USA) were used. Visualisation of the formed immune complexes was performed using the Mouse/Rabbit PolyVue™ HRP/DAB polymer detection system (Diagnostic BioSystems, USA). Counterstaining of cell nuclei was performed with Mayer's hematoxylin according to the standard protocol. The preparations were examined using a MICROmed SEO SCAN light microscope. Administration of the scorpion venom Leiurus macroctenus at an early stage of the study (after 3 hours) induces activation of the immune response in the kidney tissue of rats, as evidenced by the appearance of single CD20⁺ B-lymphocytes in the cortical substance and renal corpuscles. In the control group, CD20 expression is absent, confirming the normal immune status of the kidney and the absence of physiological B-cell infiltration. Thus, the appearance of single CD20⁺cells after venom administration reflects the early phase of the inflammatory reaction and the initiation of B-lymphocyte recruitment in response to toxic injury. However, the intensity of infiltration at this stage remains minimal, not massive.

Keywords: *histology, expression, kidney, inflammation, apoptosis, rats.*

Introduction

Venomous animal bites, including those from snakes, vipers, and arthropods, especially scorpions, are a significant public health problem in many countries worldwide. Acute kidney injury is one of the main consequences of these venoms, leading to high morbidity and mortality [21, 26, 30]. The World Health Organisation recognises venomous animal bites as a neglected public health problem, especially in regions such as Latin America, Asia, and Africa. Estimates range from 421,000 to 1.8 million snakebites occur annually, with 20,000 to 94,000 of these resulting in death. The most vulnerable groups are economically disadvantaged groups and rural residents. However, the actual number of cases is likely much higher, as existing epidemiological data are primarily based on official reports and may not include victims treated in primary care settings [1, 6, 12].

Snake and scorpion venoms have a diverse chemical composition, including proteins, enzymes, carbohydrates, lipids, metals, biogenic amines, and nucleotides [14, 27, 31, 35]. This toxic composition has evolved as a hunting and defence mechanism. However, urbanisation and population growth have led to an increase in the number of animal bites [34]. Clinical manifestations of envenomation depend on

various factors, including the type and dose of venom, the site of the bite, the size of the victim, and the time of medical intervention; symptoms can range from mild local reactions to severe systemic poisoning that develops over several hours [3, 8, 20].

Acute kidney injury is the leading cause of death among patients exposed to snake and scorpion stings. Studies show that snake and scorpion venom can penetrate renal tissue within minutes, appearing in the urine several hours after exposure. Without timely preventive measures, there is a significant risk of acute renal failure, which may require dialysis [4, 19, 32, 33]. Additional clinical manifestations, such as rhabdomyolysis, intravascular hemolysis, coagulopathy, neurotoxic symptoms, hypopituitarism, and systemic inflammatory response syndrome, further worsen the condition of victims. Studies show that histological signs of renal injury from these venoms include acute tubular necrosis and interstitial nephritis. Morphological analysis of kidney tissue biopsies reveals notable changes, including increased glomerular capillary dilation, destructive changes in the basement membrane, oedema of endothelial cells, and focal proliferation of mesangial cells [7, 9, 17].

Since the composition of scorpion venom has not been thoroughly studied to date, and the mechanisms of kidney damage remain an open question, the topic of our study is relevant.

The study aims to study the features of CD20 expression in the kidney tissue of experimental rats three hours after administration of the venom of the scorpion Leiurus macroctenus.

Materials and methods

The study used 10 white male laboratory rats weighing 200 g (±10 g), raised in the vivarium of the Educational and Scientific Centre “Institute of Biology and Medicine” of Taras Shevchenko National University of Kyiv (Agreement on Scientific and Practical Cooperation between Taras Shevchenko National University of Kyiv, National Pirogov Memorial Medical University, Vinnytsya and I. Ya. Horbachevsky Ternopil National Medical University of the Ministry of Health of Ukraine, dated February 1, 2021). Rats were kept on a standard diet in an accredited vivarium in accordance with the “Standard Rules for the Arrangement, Equipment and Maintenance of Experimental Biological Clinics (Vivaria)”. The experiments were conducted in accordance with the current regulatory documents governing the organisation of work with experimental animals and with the principles of the “European Convention for the Protection of Vertebrate Animals Used for Experimental and Other Scientific Purposes” [11]. Also, all work with animals was carried out in accordance with the Law of Ukraine dated February 21, 2006, No. 3447-IV “On the Protection of Animals from Cruelty and Ethical Norms and Rules for Working with Laboratory Animals”.

The venom of scorpions of the Buthidae family of the Leiurus genus of the Leiurus species was administered to rats once intramuscularly (0.5 ml of venom solution previously dissolved in saline; 28.8 μg/ml; LD50=0.08 mg/kg) [16, 23].

The rats selected for the experiment were divided into two groups: control – 5 rats; no venom was administered; material was collected 3 hours after saline administration; experimental – 5 rats; histological material was collected 3 hours after venom administration. The rats were euthanised by inhalation of carbon dioxide. The isolation of rat kidneys was performed at 4 °C immediately after euthanasia.

To identify the subpopulation of CD20+ cells in the kidney tissue, rabbit recombinant primary antibodies Anti-CD20 (ab64088, Abcam, USA) were used.

Antigens were revealed using the temperature-induced reprivation method in the EnVision FLEX Target Retrieval Solution High pH buffer (pH 9.0), which was carried out in a KOS histology processor (Milestone, Italy) at 98 °C for 20 minutes. To block endogenous peroxidase activity, a 3 % aqueous H_2O_2 solution was used. Further incubation with specific primary antibodies was carried out for 60 minutes: to detect $CD20^+$ cells, rabbit polyclonal antibodies Anti-CD20 (Cat. No. ab64088, Abcam, USA) were used [5, 17].

Visualisation of the formed immune complexes was carried out using the Mouse/Rabbit PolyVue™ HRP/DAB polymer detection system (Diagnostic BioSystems, USA), which provides high sensitivity and specificity due to polymer-conjugated secondary antibodies with peroxidase activity and subsequent chromogenic development with diaminobenzidine (DAB). Counterstaining of cell nuclei was performed with Mayer’s hematoxylin according to the standard protocol [18]. The preparations were examined using a MICROmed SEO SCAN light microscope, and a Vision CCD Camera was used for photodocumentation.

Results

In the kidney parenchyma of rats in the control group, the CD20 reaction precipitate is not detected (-). Immunohistochemical staining is negative in all morphological structures, particularly in the renal corpuscles, nephron tubules, and interstitium. The absence of $CD20^+$ cells indicates that, under physiological conditions, there is no infiltration of renal tissue by B-lymphocytes. This confirms the kidney’s stable immune status under normal conditions and serves as a reference point for assessing inflammatory changes under experimental conditions. Thus, the absence of the precipitate can be regarded as an indicator of the baseline level of CD20 expression, which is practically zero, i.e. negative in the control group of animals (Fig. 1).

In rat kidney tissue, 3 hours after the introduction of scorpion venom, a weak immunohistochemical reaction (+--) is detected with the formation of a single brown precipitate in the cytoplasm of cells corresponding to $CD20^+$ B-lymphocytes. These cells are localised mainly in the interstitium of the cortical substance, indicating the initial phase of the immune response and the migration of B cells to the damaged area. There is also a slight immunoprecipitation in the renal corpuscle area. The staining intensity is low, focal, without signs of massive infiltration (Fig. 2).

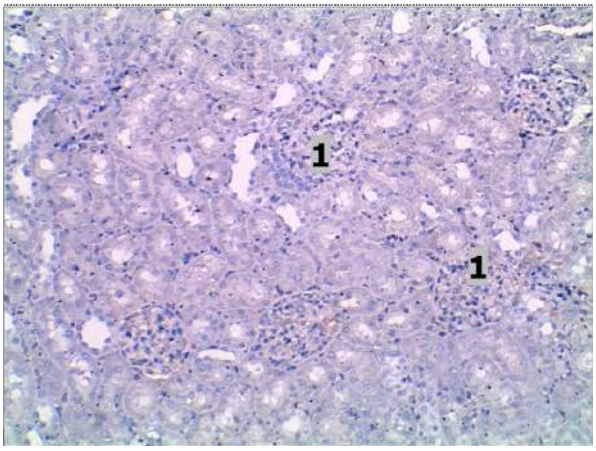

Fig. 1. Expression of CD20+ cells in the parenchyma of the renal cortex of rats in the control group. Absence of precipitate in the structural components of the kidney of rats in the intact group (1). Immunohistochemical staining using an antibody to CD20, counterstaining with Mayer's hematoxylin. ×100.

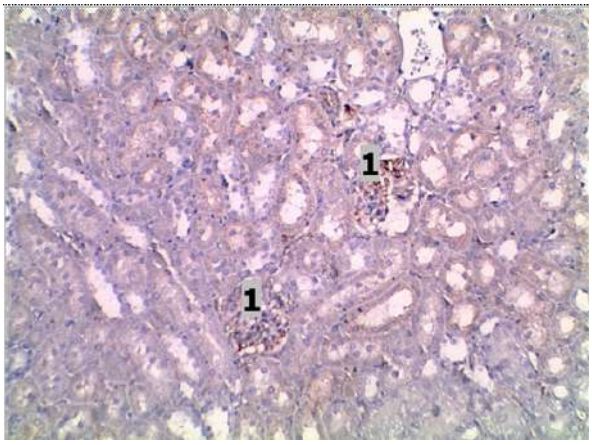

Fig. 2. Expression of CD20+ cells in rat kidneys 3 hours after scorpion venom administration. Immunoprecipitation in the renal corpuscle area (1). Immunohistochemical staining using an antibody to CD20, counterstaining with Mayer's hematoxylin. ×100.

Discussion

Scorpion venom is a mixture of chemical compounds that overactivate the autonomic nervous system, leading to a massive release of vasoactive substances and inflammatory cytokines. Symptoms of scorpion envenomation typically include signs of increased cholinergic and adrenergic activity, cardiovascular dysfunction, and increased neuromuscular excitability. In severe cases, especially in children, there is a risk of pulmonary oedema, multiple organ failure, and even death [22].

Studies have shown that the venom of the scorpion Hemiscorpius lepturus can cause cytotoxicity and hemolysis. The venom is primarily excreted from the body through the kidneys and liver and tends to be highly concentrated in renal tissue. The exact mechanisms of renal injury from scorpion stings are still being investigated, but likely include vascular ischemia due to vasoconstriction, hemodynamic instability, rhabdomyolysis, excessive systemic inflammation, and direct nephrotoxic effects of the venom [15, 24, 28].

Microscopic studies have revealed acute tubular necrosis, destructive changes in the renal glomeruli, interstitial oedema, thrombotic microangiopathy, and cortical necrosis in cases of scorpion stings. Clinical observations suggest that children affected by scorpion stings are at increased risk of developing chronic renal failure. Unfortunately, even with the rapid administration of antivenom, the prognosis for chronic renal dysfunction does not significantly improve [25, 29, 36].

Experimental studies by Zoccal K. F. et al. [37] showed that Tityus silvestris envenomation in mice resulted in severe systemic effects, including hyperglycemia, leukocytosis, cytokine release (IL-6, IL-1β, IL-10), and damage to lung and kidney tissues. In contrast, the venoms of Tityus metuendus and Tityus obscurus resulted in less severe symptoms in animals.

The most significant number of scorpion sting envenomations has been reported in Saudi Arabia, Iraq, and Jordan. The most clinically substantial toxins in Old World scorpion venoms are the α-toxins, which bind to the neurotoxin at three sites on voltage-gated sodium (Nav) channels, leading to sympathetic excitation and the release of endogenous catecholamines, which can cause severe myocardial damage. Most scorpion sting victims experience local lesions, but systemic symptoms, especially in children, are often noted due to the venom of Androctonus and Leiurus scorpions. These systemic manifestations include hemodynamic and respiratory disorders, as well as myocarditis. In addition, other symptoms may include paralysis (from Parabuthus leiosoma), coagulopathy (caused by Nebo hierichonticus and Hemiscorpius species), local tissue damage, hemolysis, and acute kidney injury (associated with Hemiscorpius lepturus). In such cases, early antivenom therapy is crucial, although its effectiveness remains controversial. However, intensive treatment, including the use of vasoactive drugs, is effective in many cases [2].

A. Elmourid et al. [13] observed significant histological and biochemical changes in experimental mice injected with Buthus paris scorpion venom. In the liver, morphological changes included hepatocytes ballooning, haemorrhage, and nuclear pyknosis. Examination of lung tissue showed thickening of the interalveolar septum and pulmonary oedema. In addition, hemorrhagic manifestations were noted after administration of a dose of 450 μg/kg-1 of venom. Examination of the kidneys revealed an expansion of the lumen between the outer and inner layers of Bowman's capsule, as well as destructive changes in the glomeruli. At the same dose, glomeruloneuromas and signs of haemorrhage were also observed. The toxic effect of Buthus paris venom on the heart was characterised by disorganisation and degeneration of myofibrils. Biochemical analysis of the blood serum of poisoned mice showed a significant increase in ALT ($p<0.05$), AST ($p<0.05$) and LDH

(p<0.05). An increase in CPK was also noted.

R. Dizaji et al. [10] found significant changes in biomarkers of acute kidney injury and mitochondrial biogenesis in mice injected with Hemiscorpius lepturus venom. IL-18 expression increased significantly on the first day after administration of 5 and 10 mg/kg doses of venom (p<0.01), indicating early activation of the inflammatory cascade; after 7 days, a significant increase was observed in the 5 mg/kg group compared to the control group. Determination of reactive oxygen species (ROS) production demonstrated a substantial effect of the venom on days 1 and 7 (p<0.05), with post hoc analysis confirming a significant increase in ROS across all groups of poisoned animals (p<0.001). After seven days, ROS levels in the treatment groups were lower than on day 1, indicating a partial restoration of antioxidant status. The venom also induced apoptosis, as evidenced by a significant increase in caspase-9 expression after 1 day in the 10 mg/kg group and after 7 days in the 5 mg/kg group. Caspase-3 expression was significantly increased only 1 day after administration of 5 and 10 mg/kg (p<0.05), with no significant changes in the 7-day group. Studies of regulators of mitochondrial biogenesis showed considerable overexpression of AMPK (AMP-activated protein kinase) in both the 5 and 10 mg/kg groups on day 1 and in the 5 mg/kg group on day 7. Sirt1 expression was significantly increased 24 hours after both doses (p<0.001) and remained elevated in the 5 mg/kg group on day 7 (p<0.01). Sirt3 expression was significantly increased only on day 1 in the 5 mg/kg group (p<0.001), with no significant changes in the 10 mg/kg group. After seven days, a marked increase in expression was also observed in the 5 mg/kg group. Overall, evidence suggests that Hemiscorpius lepturus venom induces a combination of inflammatory, oxidative, and apoptotic pathways, while significantly affecting the regulation of genes involved in mitochondrial biogenesis [10].

Conclusions

The introduction of the venom of the scorpion Leiurus macroctenus at an early stage of the study (after 3 hours) induces the activation of the immune response in the renal tissue of rats, as evidenced by the appearance of single $CD20^+$ B-lymphocytes in the cortical substance and renal corpuscles. In the control group, CD20 expression is absent, which confirms the normal immune status of the kidney and the absence of physiological B-cell infiltration. The appearance of single $CD20^+$ cells following venom introduction reflects the early phase of the inflammatory response and the initiation of B-lymphocyte recruitment in response to toxic damage. However, the intensity of infiltration at this stage remains minimal, not massive.

References

[1] Abd El-Aziz, F. E. A., El Shehaby, D. M., Elghazally, S. A., & Hetta, H. F. (2019). Toxicological and epidemiological studies of scorpion sting cases and morphological characterization of scorpions (Leiurusquin questriatus and Androctonus crassicauda) in Luxor, Egypt. *Toxicol Rep*, *6*, 329-335. doi: 10.1016/j.toxrep.2019.03.004

[2] Amr, Z. S., Abu Baker, M. A., Al-Saraireh, M., & Warrell, D. A. (2021). Scorpions and scorpion sting envenoming (scorpionism) in the Arab Countries of the Middle East. *Toxicon*, *191*, 83-103. doi: 10.1016/j.toxicon.2020.12.017

[3] Avalo, Z., Barrera, M. C., Agudelo-Delgado, M., Tobón, G. J., & Cañas, C. A. (2022). Biological effects of animal venoms on the human immune system. *Toxins (Basel)*, *14*(5), 344. doi: 10.3390/toxins14050344

[4] Bahloul, M., Regaieg, K., Chabchoub, I., Kammoun, M., Chtara, K., & Bouaziz, M. (2017). Severe scorpion envenomation: pathophysiology and the role of inflammation in multiple organ failure. *Med Sante Trop*, *27*(2), 214-221. doi: 10.1684/mst.2017.0688

[5] Bagriy, M. M., Dibrova, V. A., Popadynets, O. G., & Hryschuk, M. I. (2016). *Методики морфологічних досліджень* [*Methods of morphological research*]. Вінниця: Нова книга=Vinnytsia: New Book.

[6] Chan, Y. S., Cheung, R. C. F., Xia, L., Wong, J. H., Ng, T. B., & Chan, W. Y. (2016). Snake venom toxins: toxicity and medicinal applications. *Appl Microbiol Biotechnol*, *100*(14), 6165-6181. doi: 10.1007/s00253-016-7610-9

[7] Chen, N., Xu, S., Zhang, Y., & Wang, F. (2018). Animal protein toxins: origins and therapeutic applications. *Biophys Rep*, *4*(5), 233-242. doi: 10.1007/s41048-018-0067-x

[8] De Oliveira, N. A., Cardoso, S. C., Barbosa, D. A., & da Fonseca, C. D. (2021). Acute kidney injury caused by venomous animals: inflammatory mechanisms. *J Venom Anim Toxins Incl Trop Dis*, *27*, 20200189. doi: 10.1590/1678-9199-JVATITD-2020-0189

[9] Delgado-Prudencio, G., Cid-Uribe, J. I., Morales, J. A., Possani, L. D., Ortiz, E., & Romero-Gutiérrez, T. (2022). The enzymatic core of scorpion venoms. *Toxins (Basel)*, *14*(4), 248. doi: 10.3390/toxins14040248

[10] Dizaji, R., Sharafi, A., Pourahmad, J., Vatanpour, S., Dinmohammadi, H., Vatanpour, H., … & Hosseini, M. J. (2022). Correlation between coenzyme Q_{10} content and the nutrient sensors in AKI induced by *Hemiscorpius lepturus* envenomation. *Bioimpacts*, *12*(5), 431-438. doi: 10.34172/bi.2022.23422

[11] Dobrelia, N. V., Boitsova, L. V. & Danova, I. V. (2015). Правова база для проведення етичної експертизи доклінічних досліджень лікарських засобів з використанням лабораторних тварин [Legal basis for ethical examination of preclinical studies of drugs using laboratory animals]. *Фармакологія та лікарська токсикологія=Pharmacology and drug toxicology*, (2), 95-100.

[12] Echeverría, S., Leiguez, E., Guijas, C., do Nascimento, N. G., Acosta, O., Teixeira, C., … & Rodríguez, J. P. (2018). Evaluation of pro-inflammatory events induced by Bothrops alternatus snake venom. *Chem Biol Interact*, *281*, 24-31. doi: 10.1016/j.cbi.2017.12.022

[13] Elmourid, A., Elhidan, M. A., Boussaa, S., Laaradia, M. A., Bouimeja, B., Amahmid, O., … & Touloun, O. (2024). A Comprehensive Pathophysiologic, Histologic, and Biochemical Analysis of *Buthus paris* (C. L. Koch, 1839) Venom. *Wilderness Environ Med*, *35*(3), 271-277. doi: 10.1177/10806032241249748

[14] Estrada-Gómez, S., Gomez-Rave, L., Vargas-Muñoz, L. J., & van der Meijden, A. (2017). Characterizing the biological and biochemical profile of six different scorpion venoms

from the Buthidae and Scorpionidae family. *Toxicon*, *130*, 104-115. doi: 10.1016/j.toxicon.2017.02.007

[15] Furtado, A. A., Daniele-Silva, A., Silva-Júnior, A. A. D., & Fernandes-Pedrosa, M. F. (2020). Biology, venom composition, and scorpionism induced by brazilian scorpion Tityus stigmurus (Thorell, 1876) (Scorpiones: Buthidae): A mini-review. *Toxicon*, *185*, 36-45. doi: 10.1016/j.toxicon.2020.06.015

[16] Gunas, V., Maievskyi, O., Raksha, N., Vovk, T., Savchuk, O., Shchypanskyi, S., & Gunas, I. (2024). Study of the Acute Toxicity of Scorpion *Leiurus macroctenus* Venom in Rats. *Wiley The Scientific World Journal*, Article ID 9746092. doi: 10.1155/2024/9746092

[17] Herzig, V., Cristofori-Armstrong, B., Israel, M. R., Nixon, S. A., Vetter, I., & King, G. F. (2020). Animal toxins - Nature's evolutionary-refined toolkit for basic research and drug discovery. *Biochem Pharmacol*, *181*, 114096. doi: 10.1016/j.bcp.2020.114096.

[18] Horalskyi, L. P., Khomych, V. T., & Kononskyi, O. I. (2011). *Основи гістологічної техніки і морфофункціональні методи досліджень у нормі та при патології* [*Fundamentals of histological technique and morphofunctional research methods in normal and pathology*]. Житомир, Полісся=Zhytomyr: Polissya.

[19] Júnior, F. A. N., Jorge, A. R. C., Marinho, A. D., Silveira, J. A. M., Alves, N. T. Q., Costa, P. H. S., … & Monteiro, H. S. A. (2019). Bothrops alternatus snake venom induces cytokine expression and oxidative stress on renal function. *Curr Top Med Chem*, *19*(22), 2058-2068. doi: 10.2174/1568026619666190809100319

[20] Mazzeo, A., Sincos, A. P. W. B., Leite, K. R. M., Góes, M. A. Jr., Dos Pavão, O. F. S., & Kaufmann, O. G. (2019). Study of kidney morphologic and structural changes related to different ischemia times and types of clamping of the renal vascular pedicle. *Int Braz J Urol*, *45*(4), 754-762. doi: 10.1590/S1677-5538

[21] Naqvi, R. (2015). Scorpion sting and acute kidney injury: case series from Pakistan. *Br J Med Med Res*, *9*(10), 1-6. doi: 10.9734/BJMMR/2015/19611

[22] Nejati, J., Saghafipour, A., Rafinejad, J., Mozaffari, E., Keyhani, A., Abolhasani, A., … & Kareshk, A. T. (2018). Scorpion composition and scorpionism in a high-risk area, the southwest of Iran. *Electron Physician*, *10*(7), 7138-7145. doi: 10.19082/7138

[23] Özkan, Ö., & Filazi, A. (2004). The determination of acute lethal dose-50 (LD50) levels of venom in mice, obtained by different methods from scorpions, Androctonus crassicauda (Oliver 1807). *Turkiye Parazitol Derg*, *28*(1), 50-53.

[24] Palm, N. W., & Medzhitov, R. (2013). Role of the inflammasome in defense against venoms. *Proc Natl Acad Sci USA*, *110*(5), 1809-1814. doi: 10.1073/pnas.1221476110

[25] Ramírez-Bello, V., Sevcik, C., Peigneur, S., Tytgat, J., & D'Suze, G. (2014). Macrophage alteration induced by inflammatory toxins isolated from Tityus discrepans scorpion venom. The role of $Na^{(+)}/Ca^{(2+)}$ exchangers. *Toxicon*, *82*, 61-75. doi: 10.1016/j.toxicon.2014.02.011

[26] Ranaweera, G. G., Bavanthan, V., Nazar, A. L., & Lokuhetty, M. D. (2015). Acute renal insufficiency after scorpion sting. *Ceylon Med J*, *60*(1), 31-32. doi: 10.4038/cmj.v60i1.7487

[27] Reis, M. B., Rodrigues, F. L., Lautherbach, N., Kanashiro, A., Sorgi, C. A., Meirelles, A. F. G., … & Faccioli, L. H. (2020). Interleukine-1 receptor-induced PGE_2 production controls acetylcholine-mediated cardiac dysfunction and mortality during scorpion envenomation. *Nature communications*, *11*(1), 5433. doi: 10.1038/s41467-020-19232-8

[28] Reis, M. B., Zoccal, K. F., Gardinassi, L. G., & Faccioli, L. H. (2019). Scorpion envenomation and inflammation: Beyond neurotoxic effects. *Toxicon*, *167*, 174-179. doi: 10.1016/j.toxicon.2019.06.219

[29] Ryan, R. Y. M., Seymour, J., Loukas, A., Lopez, J. A., Ikonomopoulou, M. P., & Miles, J. J. (2021). Immunological responses to envenomation. *Front Immunol*, *12*, 661082. doi: 10.3389/fimmu.2021.661082

[30] Saidani, C., Béchohra, L., Laraba-Djebari, F., & Hammoudi-Triki, D. (2019). Kidney inflammation and tissue injury induced by scorpion venom: comparison with a nephrotoxic model. *Toxin Reviews*, *38*(3), 240-247. doi: 10.1080/15569543.2018.1446028

[31] Santhosh, K. N., Pavana, D., & Thippeswamy, N. B. (2016). Impact of scorpion venom as an acute stressor on the neuroendocrine-immunological network. *Toxicon*, *122*, 113-118. doi: 10.1016/j.toxicon.2016.09.021

[32] Santos, M. S., Silva, C. G., Neto, B. S., Grangeiro Júnior, C. R., Lopes, V. H., Teixeira Júnior, A. G., … & Lima, M. A. (2016). Clinical and epidemiological aspects of scorpionism in the world: A systematic review. *Wilderness Environ Med*, *27*(4), 504-518. doi: 10.1016/j.wem.2016.08.003

[33] Stone, S. F., Isbister, G. K., Shahmy, S., Mohamed, F., Abeysinghe, C., Karunathilake, H., … & Brown, S. G. (2013). Immune response to snake envenoming and treatment with antivenom; complement activation, cytokine production and mast cell degranulation. *PLoS Negl Trop Dis*, *7*(7), e2326. doi: 10.1371/journal.pntd.0002326

[34] Tambourgi, D. V., & van den Berg, C. W. (2014). Animal venoms/toxins and the complement system. *Mol Immunol*, *61*(2), 153-62. doi: 10.1016/j.molimm.2014.06.020

[35] Tobassum, S., Tahir, H. M., Arshad, M., Zahid, M. T., Ali, S. & Ahsan, M. M. (2020). Nature and applications of scorpion venom: an overview. *Toxin Reviews*, *39*(3), 214-225. doi: 10.1080/15569543.2018.1530681

[36] Van Baelen, A. C., Robin, P., Kessler, P., Maïga, A., Gilles, N., & Servent, D. (2022). Structural and functional diversity of animal toxins interacting with GPCRs. *Front Mol Biosci*, *9*, 811365. doi: 10.3389/fmolb.2022.811365

[37] Zoccal, K. F., de Castro Figueiredo Bordon, K., Reis, M. B., Rosa Nunes de Souza Chini, P. B., Martins, J. G., Zuanazzi, B. A., … & Arantes, E. C. (2025). Divergent clinical, inflammatory, and histopathological responses induced by Amazonian Tityus venoms: insights and limitations of current antivenom therapy. *Biochimie*, *238*, 159-171. doi: 10.1016/j.biochi.2025.08.004

ОСОБЛИВОСТІ ЕКСПРЕСІЇ CD20 В ТКАНИНІ НИРОК ЕКСПЕРИМЕНТАЛЬНИХ ЩУРІВ ЧЕРЕЗ ТРИ ГОДИНИ ПІСЛЯ ВВЕДЕННЯ ОТРУТИ СКОРПІОНА LEIURUS MACROCTENUS

Матківська Р. М., Самборська І. А., Мостюк О. М.

Укуси отруйних тварин, таких як змії, гадюки та членистоногі (зокрема скорпіони), є суттєвою проблемою громадського здоров'я в багатьох країнах світу. Гостре ураження нирок є одним із головних ефектів дії цих отрут і асоційоване з високим рівнем захворюваності та смертності. Метою дослідження є вивчення особливостей експресії CD20 в тканині

нирок експериментальних щурів через три години після введення отрути скорпіона Leiurus macroctenus. У дослідженні використано 10 білих лабораторних щурів-самців масою 200 г (±10 г). Отруту скорпіонів родини Buthidae роду Leiurus виду Leiurus macroctenus вводили щурам одноразово внутрішньом'язово (0,5 мл розчину отрути попередньо розчиненому у фізіологічному розчині; 28,8 мкг/мл; ЛД50=0,08 мг/кг). Для ідентифікації субпопуляції CD20 клітин в тканині нирок використовували кролячі рекомбінантні первинні антитіла Anti-CD20 (ab64088, Abcam, США). Візуалізацію сформованих імунних комплексів здійснювали з використанням полімерної детекційної системи Mouse/Rabbit PolyVue™ HRP/DAB (Diagnostic BioSystems, США). Контрастне дозабарвлення клітинних ядер виконували гематоксиліном Майєра відповідно до стандартного протоколу. Препарати досліджували за допомогою світлооптичного мікроскопа MICROmed SEO SCAN. Введення отрути скорпіона Leiurus macroctenus вже на ранньому терміні дослідження (через 3 години) індукує активацію імунної відповіді в нирковій тканині щурів, про що свідчить поява поодиноких CD20⁺ В-лімфоцитів у кірковій речовині та ниркових тільцях. У контрольній групі експресія CD20 повністю відсутня, що підтверджує нормальний імунний статус нирки та відсутність фізіологічної В-клітинної інфільтрації. Таким чином, поява поодиноких CD20⁺ клітин після введення отрути відображає ранню фазу запальної реакції та ініціацію рекрутування В-лімфоцитів у відповідь на токсичне ушкодження, хоча інтенсивність інфільтрації на цьому етапі залишається мінімальною та не носить масивного характеру.

Ключові слова: *гістологія, експресія, нирки, запалення, апоптоз, щури.*

Author's contribution

Matkivska R. M. – conceptualization, research, writing of the original draft.
Samborska I. A. – project administration, resources.
Mostiuk O. M. – validation, software

Signed for print 11.12.2025
Format 60x84/8. Printing offset. Order № 9312. Circulation 100.
Vinnytsia. Printing house “TVORY”, Nemyrivske shose St., 62a,
Vinnytsya, 21034
Phone: 0 (800) 33-00-90, (096) 97-30-934, (093) 89-13-852,
(098) 46-98-043
e-mail: tvory2009@gmail.com
http://www.tvoru.com.ua